

## INFORMATION TO USERS

This manuscript has been reproduced from the microfilm master. UMI films the text directly from the original or copy submitted. Thus, some thesis and dissertation copies are in typewriter face, while others may be from any type of computer printer.

**The quality of this reproduction is dependent upon the quality of the copy submitted.** Broken or indistinct print, colored or poor quality illustrations and photographs, print bleedthrough, substandard margins, and improper alignment can adversely affect reproduction.

In the unlikely event that the author did not send UMI a complete manuscript and there are missing pages, these will be noted. Also, if unauthorized copyright material had to be removed, a note will indicate the deletion.

Oversize materials (e.g., maps, drawings, charts) are reproduced by sectioning the original, beginning at the upper left-hand corner and continuing from left to right in equal sections with small overlaps. Each original is also photographed in one exposure and is included in reduced form at the back of the book.

Photographs included in the original manuscript have been reproduced xerographically in this copy. Higher quality 6" x 9" black and white photographic prints are available for any photographs or illustrations appearing in this copy for an additional charge. Contact UMI directly to order.

# UMI

A Bell & Howell Information Company  
300 North Zeeb Road, Ann Arbor, MI 48106-1346 USA  
313/761-4700 800/521-0600



**POLYELECTROLYTE ADSORPTION BY ACTIVATED  
CARBON AND THE EFFECTS OF PRELOADING ON  
TRICHLOROETHYLENE ADSORPTION**

**by**

**James Edward Kilduff**

A dissertation submitted in partial fulfillment  
of the requirements for the degree of  
Doctor of Philosophy  
(Environmental Engineering)  
in The University of Michigan  
1995

Doctoral Committee:

Professor Walter J. Weber, Jr., Chair  
Assistant Professor Avery Demond  
Professor H. Scott Fogler  
Associate Professor Kim F. Hayes

UMI Number: 9610163

Copyright 1995 by  
Kilduff, James Edward  
All rights reserved.

---

UMI Microform 9610163  
Copyright 1996, by UMI Company. All rights reserved.

This microform edition is protected against unauthorized  
copying under Title 17, United States Code.

---

UMI

300 North Zeeb Road  
Ann Arbor, MI 48103



© James Edward Kilduff 1995  
All Rights Reserved

## ACKNOWLEDGMENTS

I gratefully acknowledge the guidance, insight, direction and support provided by my faculty advisor, Professor Walter J. Weber, Jr. I thank Professors Avery Demond, H. Scott Fogler and Kim Hayes for serving on my thesis committee and for contributing their expertise to various aspects of this work. Dr. Timothy Vogel, member ex-officio, provided support, encouragement, and insights into the scientific process. I thank Professor Will Hanson of the Department of Civil and Environmental Engineering for his assistance with nitrogen gas-phase adsorption analysis, and Tom Yavaraski for assistance in developing analytical methods and for sharing his insights into analytical chemistry. I thank technicians Nefise Karanfil, Mary Lynam, Yan Chen, Ping Yuan and Xiu Min Yong, and Work Study students Duane Cook, Guan Ruh Duh, Meredith Wiener and Jae Son for invaluable assistance in collecting laboratory data, and making the lab a pleasant place to work.

It has been a pleasure and a privilege to work with many outstanding colleagues during my years at Michigan. In particular, Lynn Katz has contributed immeasurably to my personal and professional development by providing a critical ear, unconditional encouragement, and an example for commitment to excellence. Dr. Yu-Ping Chin generously shared his expertise of humic substances and provided support, encouragement, and ideas during the initial phases of this work, and invaluable expertise and assistance in making size-exclusion chromatography measurements during the later stages. I have had the pleasure to work directly with Paul McGinley, Rich Gullick, Suparna Mukherji, as Teaching Assistants for Professor Weber's courses. Research is most productive and most fun when treated as a team effort, and I have benefitted from the

contributions of expertise, encouragement, and support of those who have voluntarily subjected themselves to the same fate: I thank Dr. Kevin Olmstead, Dr. Margaret Carter, Dr. Henry Corseuil, Astrid Hillers, Mark Henry, Tom Young and Dr. Mark Schlautmann. A special thanks goes to Dr. Tanju Karanfil who provided many stimulating discussions, a collaborative atmosphere, and who helped make the West-Coast office possible. Life in the laboratory (and out) was made more enjoyable by the friendship, support, and perspectives of Dr. Howard Reeves, Dr. Susan Powers, Dr. Nada Assaf-Anid, Dr. Paul Anid, Dr. Larry Nies, Dr. Pedro Alvarez, Dr. Iara Oliviera, Hildegard Selig, Dr. Eric Petrovskis, John Lang, Yung-Ming Chen, Dr. Mamadou Diallo, and Sanjay Yadav. I thank John Lenard for providing continuing guidance, support, and for his contributions to my development as an engineer.

Last, but certainly not least, I thank my family for providing guidance and unconditional support, and Kathleen, who has helped keep everything in perspective.

Partial financial support for this research was provided by the National Science Foundation, Award Number CES-8702786. I gratefully acknowledge the financial support received from the American Society of Civil Engineers through the 1994 Research Fellowship.



## TABLE OF CONTENTS

<b>ACKNOWLEDGMENTS</b> .....	<b>ii</b>
<b>LIST OF TABLES</b> .....	<b>vii</b>
<b>LIST OF FIGURES</b> .....	<b>x</b>
<b>LIST OF APPENDICES</b> .....	<b>xvi</b>
<b>CHAPTER</b>	
<b>I. INTRODUCTION AND OBJECTIVES</b> .....	<b>1</b>
1.1 Introduction .....	1
1.2 Objectives .....	7
1.3 Significance and Relevance .....	8
<b>II. BACKGROUND AND RELATED RESEARCH</b> .....	<b>9</b>
2.1 Activated Carbon Surface Chemistry and Structure .....	9
Quantification of Adsorbent Surface Properties .....	13
2.2 Humic Substances: A General Characterization .....	15
2.3 Adsorption of Humic Substances and Other Polyelectrolytes .....	18
General Considerations .....	18
Effects of Molecular Weight on Polyelectrolyte Adsorption .....	19
Effects of Ionic Strength on Polyelectrolyte Adsorption .....	21
2.4 Modeling Adsorption Equilibria .....	23
2.5 Site Energy Distributions .....	28
2.6 Mass Transfer Models .....	31
2.7 Implications for GAC Systems .....	37
<b>III. RESEARCH APPROACH AND DATA COLLECTION</b> .....	<b>38</b>
3.1 Research Approach .....	38
Selection of Model Systems .....	41
3.2 Data Collection .....	45
Water .....	45
Macromolecules .....	45
Low-Molecular-Weight Synthetic Organic Chemicals .....	48
Adsorption Isotherms: General Considerations .....	49
Macromolecule Adsorption Isotherms and Rate Studies .....	49
Humic Acid Preloading Supernatant Isotherms .....	51
Humic Substance Preloading .....	52
Measurement of TCE Isotherms .....	53
TCB Preloading of F400 Carbon .....	54
Permeation and Fractionation Experiments .....	54
Size Exclusion Chromatography .....	55

<b>IV. MACROMOLECULE SIZE CHARACTERIZATION AND FRACTIONATION.....</b>	<b>58</b>
4.1 Introduction .....	58
4.2 Ultrafiltration Processes .....	59
4.3 Ultrafiltration System Operation and Characterization .....	62
System Characterization.....	63
4.4 Model Development.....	67
Macroscopic Versus Microscopic Models .....	67
Transport Mechanisms .....	69
Solute Transport .....	69
4.5 Solute Transport Model Verification .....	75
Effects of Operating Mode.....	79
Effects of Macromolecule Structure .....	80
Macromolecule Solution Fractionation .....	83
4.6 Size Exclusion Chromatography System Calibration and Data Analysis .....	95
4.7 Conclusions.....	103
<b>V. MACROMOLECULE ADSORPTION RATE STUDIES .....</b>	<b>104</b>
5.1 Introduction .....	104
5.2 Estimation of Adsorption Rate Parameters .....	104
Estimation of Film Mass-Transfer Coefficient .....	105
Estimation of Intraparticle Diffusion Coefficients.....	109
5.3 Model-Based Criteria for Establishing Time to Equilibrium .....	111
Computation of Biot Number .....	112
Criteria for the Time Required to Reach Equilibrium.....	114
5.4 Equilibration Times Reported in the Literature.....	116
5.5 Laboratory Measurements of Macromolecule Rates.....	117
5.6 Order-of-Magnitude Analysis.....	120
<b>VI. ADSORPTION OF NATURAL AND SYNTHETIC POLYELECTROLYTES.....</b>	<b>125</b>
6.1 Introduction .....	125
6.2 Polyelectrolyte Adsorption on Activated Carbon .....	126
Adsorption of a Model Polyelectrolyte: polystyrene sulfonate.....	126
Adsorption from Mixtures .....	129
6.3 Adsorption of Soil Humic and Fulvic Acids .....	131
Humic Substances as Multicomponent Mixtures.....	131
Preferential Adsorption.....	131
Effects of Macromolecule Size .....	134
Competitive Interactions among Humic Acid Components.....	137
Effect of Ionic Strength on Competitive Interactions Among Humic Acid Components .....	143
Effect of Calcium on the Competitive Interactions among Humic Acid Components.....	152
Effect of Adsorbent Characteristics on Interactions among Humic Acid Components.....	157
Effect of Organic Matter Type on Adsorption of Humic Substances .....	161
6.4 Conclusions.....	163

<b>VII. ADSORPTION OF TCE ON PRELOADED CARBON: MECHANISTIC INTERPRETATIONS.....</b>	<b>167</b>
7.1 Introduction .....	167
7.2 Selection of an Equilibrium Modeling Approach .....	168
7.3 TCE Isotherms on Non-Preloaded Carbon.....	171
7.4 Impacts of Preloading on TCE Adsorption: Theoretical Predictions .....	173
Langmuir-Freundlich Isotherm Sensitivity Analysis .....	174
Composite Isotherm Sensitivity Analysis.....	177
Preloading in a Model Bi-Solute System.....	179
Site Energy Distributions .....	185
7.5 Impacts of Preloading on TCE Adsorption: Experimental Investigations.....	191
7.6 Effects of Preloading on Adsorbent Pore Structure .....	199
7.7 Summary and Conclusions.....	203
<b>VIII. EFFECTS OF HUMIC SUBSTANCE PRELOADING ON TCE ADSORPTION.....</b>	<b>205</b>
8.1 Introduction .....	205
8.2 Single-Solute TCE Adsorption by Non-Preloaded Carbon .....	206
8.3 TCE Adsorption by Carbon Preloaded with Discrete Size Fractions .....	211
Preloading with UF Size Fractions: Effects of Molecular Size.....	211
Preloading with UF Size Fractions: <3K Fraction.....	216
8.4 TCE Adsorption by Carbon Preloaded with Macromolecule Mixtures.....	223
Preloading by Adsorptive Fractionation.....	223
TCE Adsorption by Carbon Preloaded with Mixtures of UF Fractions.....	230
8.5 Effects of Solution Chemistry on TCE Adsorption by Preloaded Carbon .....	235
Effects of Ionic Strength on TCE Adsorption by Preloaded Carbon .....	235
Effects of Calcium on TCE Adsorption by Preloaded Carbon.....	239
8.6 Effects of Adsorbent Characteristics on TCE Adsorption by Preloaded Carbon .....	247
TCE Adsorption on Preloaded Coal-Based Adsorbents.....	249
TCE Adsorption on Preloaded Wood-Based Adsorbents.....	254
TCE Adsorption on BPL and MACRO Adsorbents Preloaded with UF Fractions .....	256
8.7 Conclusions.....	258
<b>IX. CONCLUSIONS AND RECOMMENDATIONS.....</b>	<b>262</b>
9.1 Conclusions.....	262
9.2 Recommendations for Further Research.....	269
<b>APPENDICES.....</b>	<b>272</b>
<b>REFERENCES.....</b>	<b>301</b>

## LIST OF TABLES

### **Table**

---

Table 2-1.	The Generalized Langmuir isotherm and its simplifications.....	27
Table 3-1.	Physical and chemical characteristics of TCE and TCB .....	42
Table 3-2.	Adsorbent structure characterization -- nitrogen adsorption analysis.....	44
Table 3-3.	Adsorbent surface chemistry characterization using surface titration.....	44
Table 3-4.	Chemical characterization of Laurentian humic substances.....	47
Table 3-5.	Conductivity analysis -- preloading stocks.....	47
Table 3-6.	Conditions used in macromolecule adsorption isotherm experiments.....	51
Table 3-7.	Analytical error in TCE and TCB determinations.....	55
Table 4-1.	Permeation factors of ultrafiltration size fractions .....	93
Table 4-2.	Effect of $1/a(t)$ on computed MW .....	101
Table 5-1.	Reynolds number and terminal settling velocity for discrete settling of carbon particles.....	106
Table 5-2.	Free-liquid diffusivities and external "film" mass-transfer coefficients for selected macromolecules .....	108
Table 5-3.	Macromolecule pore diffusion coefficients.....	110
Table 5-4.	Humic substance surface diffusion coefficients by F400 carbon.....	110
Table 5-5.	Surface and pore diffusion Biot numbers .....	115
Table 5-6.	Criteria for time to reach equilibrium in a batch reactor.....	116
Table 5-7.	Equivalent diffusion times for various size carbon particles .....	121
Table 5-8.	Modified Freundlich isotherm parameters for humic and fulvic acid adsorption by F400 carbon: effect of particle size.....	123
Table 6-1.	Adsorption of polystyrene sulfonate by F400 carbon: effects of molecular weight and ionic strength.....	127

Table 6-2.	Adsorption of Laurentian humic acid by F400 carbon: effect of competitive adsorption from a mixture.....	133
Table 6-3.	Adsorption of Laurentian humic acid size fractions prepared by ultrafiltration .....	136
Table 6-4.	Permeation factors determined for humic acid components remaining in solution after adsorptive fractionation.....	140
Table 6-5.	HPSEC analysis of Laurentian humic acid adsorption.....	141
Table 6-6.	Adsorption of Laurentian humic acid: effect of ionic strength .....	144
Table 6-7.	HPSEC analysis of Laurentian humic acid adsorption: effect of ionic strength .....	146
Table 6-8.	Adsorption of Laurentian humic acid by F400 carbon: effect of calcium concentration .....	153
Table 6-9.	HPSEC analysis of humic acid adsorption: effect of calcium concentration.....	153
Table 6-10.	Comparison of Laurentian humic acid and fulvic acid adsorption.....	162
Table 7-1.	TCE single-solute adsorption modeling: comparison of isotherm models .....	170
Table 7-2.	TCE single-solute adsorption data.....	173
Table 7-3.	LF isotherm sensitivity analysis: effect on Freundlich parameters fit to low concentration data (<100 mg/l).....	175
Table 7-4.	LF isotherm sensitivity analysis: composite isotherm.....	179
Table 7-5.	Single-solute adsorption of TCE and TCB by F400 carbon .....	182
Table 7-6.	IAST predictions of TCB displacement in a model bi-solute preloading system .....	183
Table 7-7.	TCB preloading: model bi-solute preloading system.....	192
Table 7-8.	Measured TCB displacement in a model bi-solute preloading system for a TCB loading of 22 mg/g .....	192
Table 7-9.	Adsorption of TCE on TCB-preloaded F400 carbon .....	194
Table 7-10.	The effect of TCB adsorption on adsorbent characteristics.....	200
Table 8-1.	Single-solute TCE adsorption data .....	207
Table 8-2.	Humic acid preloading of F400 carbon with UF size fractions-- experimental conditions.....	212

Table 8-3.	Humic acid preloading of F400 carbon with UF fractions -- isotherm analysis .....	215
Table 8-4.	Humic acid preloading of F400 carbon with the <3K fraction -- experimental conditions.....	217
Table 8-5.	Humic acid preloading of F400 carbon with the <3K fraction -- isotherm analysis .....	219
Table 8-6.	Humic acid preloading of F400 carbon by adsorptive fractionation: isotherm analysis .....	225
Table 8-7.	The effect of initial molecular size distribution: experimental conditions .....	231
Table 8-8.	The effect of initial molecular size distribution: isotherm analysis.....	233
Table 8-9.	Sequential loading experiment: experimental conditions.....	234
Table 8-10.	Sequential loading experiment: isotherm analysis .....	234
Table 8-11.	The effect of ionic strength on humic acid preloading: experimental conditions .....	236
Table 8-12.	The effect of ionic strength on humic acid preloading: isotherm analysis .....	237
Table 8-13.	The effect of calcium content on humic acid preloading: experimental conditions .....	240
Table 8-14.	The effect of calcium content on humic acid preloading: isotherm analysis .....	242
Table 8-15.	The effect of calcium content at constant humic acid preloading: isotherm analysis .....	246
Table 8-16.	The effect of coal-based adsorbent characteristics on humic acid preloading: experimental conditions.....	248
Table 8-17.	The effect of wood-based adsorbent characteristics on humic acid preloading: experimental conditions.....	249
Table 8-18.	The effect of coal-based adsorbent characteristics on humic acid preloading: isotherm analysis .....	250
Table 8-19.	The effect of wood-based adsorbent characteristics on humic acid preloading: isotherm analysis .....	251
Table 8-20.	The effect of molecular size on humic acid preloading: experimental conditions .....	257
Table 8-21.	The effect of molecular size on humic acid preloading: isotherm analysis .....	257

## LIST OF FIGURES

<b>Figure</b>		
Figure 1-1.	Schematic illustration of a fixed bed reactor treating a water containing a target pollutant and DOM.....	3
Figure 1-2.	Breakthrough curves simulated using the HSDM model illustrate the effect of preloading on fixed bed reactor breakthrough curves .....	3
Figure 2-1.	Model macromolecular structures as proposed by Gosh and Schnitzer.....	22
Figure 4-1.	Schematic depiction of the experimental ultrafiltration system illustrating the two different modes of operation .....	62
Figure 4-2.	Characterization of mixing conditions in the experimental ultrafiltration reactor.....	64
Figure 4-3.	The effect of transmembrane pressure on water flux through Amicon Y-series spiral-wound membranes .....	66
Figure 4-4.	The permeation of salt through the 30K membrane .....	66
Figure 4-5.	Model linearization and data normalization for the concentration mode of operation. Representative data for polystyrene sulfonate.....	76
Figure 4-6.	Model linearization and data normalization for the diafiltration mode of operation. Representative data for polystyrene sulfonate.....	77
Figure 4-7.	Model linearization and data normalization for the concentration mode of operation. Representative data for Aldrich humic acid.....	77
Figure 4-8.	The effect of volume throughput on the membrane permeation factor.....	79
Figure 4-9.	Model calibration and permeation factor determination for a sequential mode of operation.....	81
Figure 4-10.	The effects of ionic strength on the dimensionless permeation factors for different polystyrene sulfonate molecular weights .....	82
Figure 4-11.	The effects of ionic strength on the dimensionless permeation factors for purified humic acid.....	82

Figure 4-12.	Molecular weight solute rejection calibration curves for two ultrafiltration membranes and two ionic strengths.....	84
Figure 4-13.	Mass throughput of purified humic acid using a sequential concentration/diafiltration mode of operation (3K membrane).....	86
Figure 4-14.	Schematic depiction of the cascade-type fractionation protocol used to prepare ultrafiltration size fractions.....	87
Figure 4-15.	Ultrafiltration fractionation of Aldrich humic acid showing the effect of initial concentration on the mass distribution. Inorganic matrix: pH = 6.5, 1x10 <sup>-4</sup> -M phosphate buffer.....	88
Figure 4-16.	Ultrafiltration fractionation of Aldrich humic acid showing the effect of initial concentration on the mass distribution. Inorganic matrix: pH = 6.5, 1x10 <sup>-4</sup> -M phosphate buffer, 0.05-M NaCl.....	88
Figure 4-17.	Ultrafiltration fractionation of Aldrich humic acid showing the effect of diafiltration volume on the mass distribution. Inorganic matrix: pH = 6.5, 1x10 <sup>-4</sup> -M phosphate buffer.....	89
Figure 4-18.	Fractionation experiment conducted using sequential concentration/diafiltration on the 3K membrane.....	92
Figure 4-19.	Fractionation experiment conducted using sequential concentration/diafiltration on the 100K membrane.....	92
Figure 4-20.	Mass distribution of Laurentian humic acid size fractions prepared using the sequential concentration/diafiltration technique.....	94
Figure 4-21.	Standardization of a Waters Protein-Pak 125 Å functionalized silica column with polystyrene sulfonates.....	96
Figure 4-22.	Size exclusion chromatogram of Laurentian humic acid.....	97
Figure 4-23.	TOC/UV correlations for Laurentian humic acid size fractions prepared by ultrafiltration.....	99
Figure 4-24.	The effect of molecular weight on the absorptivity of Laurentian humic acid size fractions prepared by ultrafiltration.....	100
Figure 4-25.	Correlation of ultrafiltration permeation factors determined for size fractions with molecular weight as determined by HPSEC.....	102
Figure 4-26.	Size-exclusion chromatograms of ultrafiltration size fractions.....	102
Figure 5-1.	Rate of polystyrene sulfonate adsorption by F400 carbon for two different molecular weights.....	118
Figure 5-2.	Rate of 1.8K polystyrene sulfonate adsorption on BPL and F400 coal-based activated carbons.....	119
Figure 5-3.	Rate of Laurentian humic acid adsorption by F400 carbon: effect of particle size.....	119



Figure 5-4.	Rate of Laurentian fulvic acid adsorption by F400 carbon: effect of particle size.....	120
Figure 5-5.	The effect of particle size on the adsorption of Laurentian humic acid by F400 carbon.....	123
Figure 5-6.	The effect of particle size on the adsorption of Laurentian fulvic acid by F400 carbon.....	124
Figure 6-1.	Adsorption of polystyrene sulfonate by F400 carbon: effect of molecular weight and ionic strength.....	127
Figure 6-2.	Schematic representation of adsorption isotherms obtained for DOM when concentration is expressed in terms of TOC .....	130
Figure 6-3.	The adsorption of Laurentian humic and fulvic acids by F400 carbon at two initial concentrations using the variable-dose methodology .....	132
Figure 6-4.	Adsorption of Laurentian humic acid components remaining in solution after initial equilibration with F400 carbon.....	132
Figure 6-5.	Normalization of Laurentian humic acid adsorption isotherms by F400 carbon at two initial concentrations by $C_e/D_0$ .....	135
Figure 6-6.	Adsorption of Laurentian humic acid size fractions prepared by ultrafiltration .....	135
Figure 6-7.	The effect of humic acid molecular weight, as determined by size exclusion chromatography, on the Freundlich $K_F$ value .....	137
Figure 6-8.	Preloading isotherms of Laurentian humic acid by F400 carbon showing the effect of initial concentration and adsorbent dose .....	139
Figure 6-9.	The effect of adsorptive fractionation on the membrane transport characteristics of Laurentian humic acid supernatant solutions .....	139
Figure 6-10.	The effect of adsorptive fractionation on the size exclusion chromatograms of Laurentian humic acid .....	142
Figure 6-11.	The effect of adsorptive fractionation on the average molecular weight of TOC remaining in solution after adsorption.....	142
Figure 6-12.	The effect of ionic strength on the adsorption of Laurentian humic acid by F400 carbon .....	144
Figure 6-13.	The effect of adsorbent dose on the molecular-weight distribution of Laurentian humic acid remaining in solution after adsorption.....	146
Figure 6-14.	The effect of ionic strength on the fraction of TOC remaining in solution after adsorption by F400 carbon .....	147
Figure 6-15.	The effect of ionic strength on the average molecular weight of TOC remaining in solution after adsorption by F400 carbon.....	147

Figure 6-16.	The effect of ionic strength on the average molecular weight of TOC remaining in solution after adsorption by F400 carbon.....	150
Figure 6-17.	Schematic drawing showing the effect of ionic strength on molecular size, adsorbent dose, TOC removal, and the TOC isotherm .....	151
Figure 6-18.	The effect of calcium content on the molecular-weight distribution of Laurentian humic acid remaining in solution after adsorption.....	154
Figure 6-19.	Calcium removed from solution by association with Laurentian humic acid.....	156
Figure 6-20.	The effect of adsorbent characteristics on the adsorption of Laurentian humic acid.....	158
Figure 6-21.	The molecular-weight distribution of Laurentian humic acid remaining in solution after adsorption: coal-based adsorbents.....	160
Figure 6-22.	The molecular-weight distribution of Laurentian humic acid remaining in solution after adsorption: wood-based adsorbents.....	160
Figure 6-23.	Adsorption of Laurentian humic acid and fulvic acid by F400 carbon illustrating the effect of organic matter type on the DOM adsorption isotherm .....	162
Figure 7-1.	The adsorption of TCE on coal-based carbon, with capacity expressed on a mass basis.....	172
Figure 7-2.	The adsorption of TCE on coal-based carbon, with capacity expressed on a surface area basis.....	172
Figure 7-3.	Sensitivity analysis of the Langmuir-Freundlich model .....	176
Figure 7-4.	TCE adsorption by F400 carbon fit by a composite of four Langmuir isotherms.....	178
Figure 7-5.	Adsorption of TCE and TCB by F400 carbon.....	182
Figure 7-6.	IAST predictions of TCE adsorption on TCB-preloaded carbon for different TCB loadings .....	184
Figure 7-7.	IAST predictions of the effect of TCB preloading on Freundlich isotherm parameters for TCE .....	185
Figure 7-8.	Sensitivity of the approximate site-energy distribution to variations in Langmuir-Freundlich isotherm parameters: effect of $b$ and $n$ .....	188
Figure 7-9.	Sensitivity of the approximate site-energy distribution to variations in Langmuir-Freundlich isotherm parameters: effect of $Q^0$ and $n$ .....	188
Figure 7-10.	Sensitivity of the approximate site-energy distribution calculated for low concentration data to Langmuir-Freundlich isotherm parameters.....	190

Figure 7-11.	Site energy distributions computed from IAST predictions of TCE adsorption on carbon preloaded with different amounts of TCB .....	190
Figure 7-12.	Adsorption of TCB by F400 carbon in the presence of TCE .....	193
Figure 7-13.	Experimental verification of IAST predictions of TCE adsorption by F400 carbon preloaded with TCB.....	193
Figure 7-14.	Site energy distributions computed from TCE adsorption isotherms on F400 carbon preloaded with TCB .....	196
Figure 7-15.	The effect of TCB preloading on total F400 carbon surface area and surface area in pores having widths less than 20 Å .....	200
Figure 7-16.	Effect of TCB preloading on total F400 carbon pore volume.....	201
Figure 7-17.	Linear correlation between micropore surface area and total pore volume for TCB preloaded F400 carbon .....	202
Figure 7-18.	Effect of reduction in F400 carbon micropore surface area as a result of preloading on the Freundlich unit capacity parameter .....	202
Figure 8-1.	The adsorption of TCE on coal-based carbon, with capacity expressed on a mass basis.....	208
Figure 8-2.	The adsorption of TCE on coal-based carbon, with capacity expressed on a surface area basis.....	208
Figure 8-3.	The adsorption of TCE on wood-based carbon, with capacity expressed on a mass basis.....	211
Figure 8-4.	The adsorption of TCE by F400 carbon preloaded with various size fractions of Laurentian humic acid .....	213
Figure 8-5.	The adsorption of TCE by F400 carbon preloaded with the <3K size fraction of Laurentian humic acid (12.1 mg TOC/g) .....	213
Figure 8-6.	Freundlich $K_F$ values for TCE adsorption by F400 carbon preloaded with Laurentian humic acid size fractions .....	214
Figure 8-7.	The effect of preloaded Laurentian humic acid (<3K fraction) on the adsorption of TCE by F400 carbon: effect of TOC loading.....	218
Figure 8-8.	Freundlich $K_F$ and $n$ values for TCE adsorption by F400 carbon preloaded with Laurentian humic acid (<3K fraction) .....	220
Figure 8-9.	Site energy distributions computed from TCE isotherms on F400 carbon preloaded with Laurentian humic acid (<3K fraction).....	221
Figure 8-10.	The adsorption of TCE by F400 preloaded with Laurentian humic acid by adsorptive fractionation.....	225

Figure 8-11.	The effect of humic acid preloading by adsorptive fractionation on the fraction of F400 virgin carbon capacity remaining ( $K_F/K_{F0}$ ) after preloading .....	227
Figure 8-12.	The effect of fulvic acid preloading by adsorptive fractionation on the fraction of F400 virgin carbon capacity remaining ( $K_F/K_{F0}$ ) after preloading .....	227
Figure 8-13.	TCE adsorption by preloaded F400 carbon comparing the effects of preloading with the <3K fraction and the whole humic acid solution using adsorptive fractionation.....	229
Figure 8-14.	TCE adsorption by preloaded F400 carbon comparing the effects of preloading with the <3K fraction and the whole humic acid solution using adsorptive fractionation: effect on site-energy distributions.....	229
Figure 8-15.	The effect of <3K fraction preloading on the fraction of F400 virgin carbon capacity remaining ( $K_F/K_{F0}$ ) after preloading .....	230
Figure 8-16.	Freundlich $K_F$ -values for TCE adsorption on carbon preloaded with mixtures of the <3K and 10-30K UF size fractions.....	233
Figure 8-17.	The effect of ionic strength on humic acid preloading and the fraction of F400 virgin carbon capacity remaining ( $K_F/K_{F0}$ ) after preloading as a function of TOC removal percentage .....	238
Figure 8-18.	The effect of ionic strength on humic acid preloading and the fraction of F400 virgin carbon capacity remaining ( $K_F/K_{F0}$ ) after preloading as a function of adsorbed amount of TOC .....	239
Figure 8-19.	The effect of calcium on humic acid preloading and on the fraction of F400 virgin carbon capacity remaining ( $K_F/K_{F0}$ ) after preloading as a function of TOC removal.....	243
Figure 8-20.	Freundlich $K_F$ -values for TCE adsorption on carbon preloaded with humic acid in the presence of calcium.....	245
Figure 8-21.	The adsorption of TCE by F400 carbon preloaded with Laurentian humic acid, demonstrating the effects of calcium.....	245
Figure 8-22.	Comparison of TCE adsorption by WPLL and BPL carbons preloaded with Laurentian humic acid .....	254
Figure 8-23.	The adsorption of TCE on MICRO carbon preloaded with Laurentian humic acid.....	255
Figure 8-24.	The adsorption of TCE on MACRO carbon preloaded with Laurentian humic acid.....	256

## LIST OF APPENDICES

### **Appendix**

---

Appendix A. Nomenclature: Symbols and Acronyms .....	273
Appendix B. Preloading Data.....	277
Appendix C. Isotherm Regression Analysis .....	285
Appendix D. Size Exclusion Chromatography Analysis .....	299

## CHAPTER I

### INTRODUCTION AND OBJECTIVES

#### 1.1 Introduction

Granular activated carbon (GAC) adsorption has been identified by the Safe Drinking Water Act Amendments of 1986 as the best available technology for removing synthetic organic contaminants (SOCs) from potable water supplies. GAC is particularly suited for water treatment applications because of its ability to remove a wide range of organic compounds effectively, and because it can act as a buffer to protect water supplies from spills of toxic or potentially carcinogenic compounds. A limitation to the more widespread application of GAC treatment systems is the potentially high cost of design and operation. For this reason, it is crucial that adsorption systems are designed and operated efficiently. Presently, the design process involves costly and time consuming pilot studies which may require up to one year to complete.

Activated carbon processes are most efficiently configured as fixed-bed reactors (FBRs), the design of which requires quantifying the shape and velocity of the mass-transfer zone (MTZ) of the contaminants of interest. Mathematical models are particularly suited for this purpose. The optimal design approach involves using a limited amount of pilot plant data to verify a laboratory-calibrated mathematical or physical model which takes into account the fundamental processes of pollutant transport and adsorption. Mass-transfer-based mathematical models have been shown to have wide applicability in describing and predicting the behavior of sorption processes (Crittenden and Weber 1978a,b,c; Liu and Weber 1981, Weber and Pirbazari 1982, Hand et al. 1984, Endicott and Weber 1985, Smith and Weber 1989). A calibrated, predictive model can be used to minimize design and operating costs, and to evaluate system reliability. Thus, models constitute important design tools, which can be used to:

- investigate alternative design and process configurations which may be too costly to investigate at the pilot scale;
- optimize the design for a particular set of treatment objectives;
- investigate the system response to shock loadings or spill scenarios to increase the reliability of the process.

Predictive models have been developed which can accurately describe the removal of pollutants from "clean" (distilled) water at the laboratory scale. However, application of these models to full-scale systems treating natural water has not met with similar success.

A major factor contributing to the complexity of modeling adsorption processes in natural systems is the presence of naturally-occurring, macromolecular, dissolved organic matter (DOM), which is ubiquitous in surface and groundwater supplies. A large component (30 to 50%) of the dissolved organic carbon in natural waters is comprised of humic substances, humic and fulvic acids, which are ill-defined, heterodisperse, hydrophilic mixtures of high molecular weight polyelectrolytic macromolecules and colloids (Thurman 1982). Due to its high molecular weight and polymeric nature, DOM is more slowly adsorbed than most SOCs, and therefore moves more rapidly through fixed-bed adsorbers used in treatment applications, fouling the carbon ahead of the pollutant. This "preloading" phenomenon is illustrated schematically in Figure 1-1.

While DOM may not be specifically targeted for removal in some GAC systems, it has been shown that the fouling or "preloading" phenomena can significantly reduce both the equilibrium capacity of GAC for target contaminants (Endicott and Weber 1985, Smith et al. 1987, Smith and Weber 1989, Speth and Miltner 1989, Speth 1991), and the rate of target compound adsorption (Weber and Pirbazari 1982, Smith et al. 1987, Smith and Weber 1989, Zimmer et al. 1988). The reduction in GAC efficiency may be caused by several factors: i) DOM is generally present in natural waters at much higher concentrations than target pollutants; ii) DOM may compete with pollutants by several mechanisms, including direct competition for adsorption sites and pore blockage; and, iii) DOM does not desorb readily, due to its high molecular weight and polymeric nature.

Simulated TCE breakthrough curves from a fixed bed reactor, illustrating the potential impacts of DOM preloading, are shown in Figure 1-2. The simulations were generated with the Homogeneous Surface Diffusion Model (HSDM) (Crittenden and

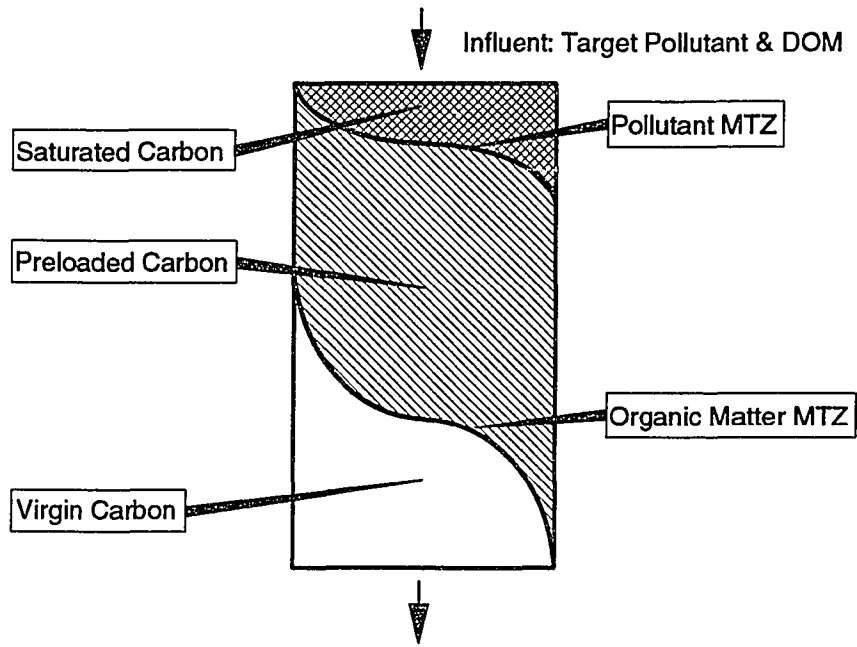


Figure 1-1. Schematic illustration of a fixed bed reactor treating a water containing a target pollutant and DOM. The DOM mass-transfer zone (MTZ) passes through the column ahead of the target pollutant, preloading the virgin carbon and reducing the adsorption capacity for the pollutant.

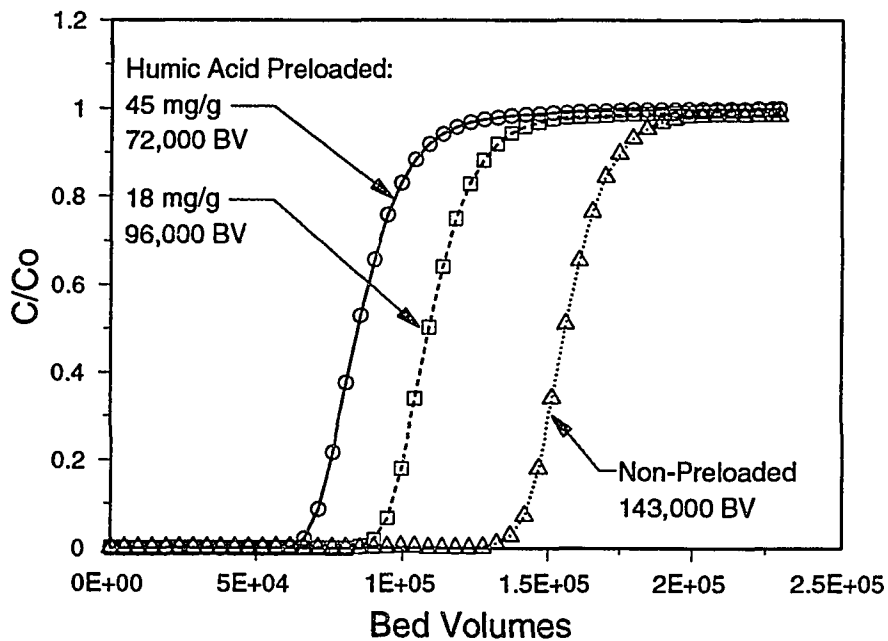


Figure 1-2. Breakthrough curves simulated using the HSDM model illustrate the effect of preloading on fixed bed reactor breakthrough curves. Isotherm parameters for TCE adsorption by carbon preloaded with humic acid were input to the model. Bed volume comparison based on a  $C/C_0 = 0.10$  treatment objective.



Weber 1978a). Input to the model included representative isotherm parameters for TCE adsorption on carbon preloaded with humic acid, literature values for the TCE adsorption rate parameters, and a typical loading rate of 2 gpm/ft<sup>2</sup>. These breakthrough curves illustrate how preloading can cause significant reductions in the ability of an adsorption system to treat a polluted water. To design an efficient carbon adsorption process, therefore, it is necessary to take into account the potential effects of dissolved organic matter. This requires an understanding of the factors which may affect the adsorption of DOM and its subsequent impact on the adsorption process.

Inorganic chemical characteristics of the source water may also influence the impact of DOM on the adsorption process. Solution ionic strength affects the adsorption of DOM substances by screening electrostatic charge and reducing the repulsive forces which occur between like-charged functional groups. Electrostatic forces can influence the size and shape of DOM molecules and the affinity for charged adsorbent surfaces. In general, polyelectrolyte adsorption is enhanced by increasing solution ionic strength (Pefferkorn et al. 1978, Papenhuizen et al. 1985a,b, Cosgrove et al. 1986, Ramachandran and Somasundaran 1987). Increases in ionic strength are known to decrease the effective size and configuration of DOM in solution (Ghosh and Schnitzer 1979, Summers and Roberts 1988, Chin and Weber 1989, 1990), potentially rendering them more adsorbable and hence better able to compete with SOCs for adsorption sites (Weber et al. 1983, Jodellah 1985).

The particular characteristics of microporous GAC which potentially impact system effectiveness include particle size, pore-size distribution and surface chemical properties. Adsorbent characteristics are governed by the source material and activation conditions, and vary among commercially-available products. An important characteristic of GAC with respect to typical water treatment objectives is pore-size distribution, which governs the adsorptive surface area available to a molecule of given size. The impact of pore size distribution on adsorption capacity has been demonstrated for low-molecular weight SOCs (Graham 1955, Hashimoto et al. 1979, Urano et al. 1982, Sontheimer 1988), and high-molecular-weight DOM (Weber et al. 1983, Summers and Roberts 1988a,b, Ogino et al. 1988). In some systems, the chemical properties of the carbon surface -- including surface charge and functionality -- may also influence the adsorption process. Surface charge is an important component of polyelectrolyte/ surface interactions in systems with moderate ionic

strengths. Differences in adsorption capacity for phenol on coconut shell and coal-based activated carbons were attributed to the impact of surface functional groups (Snoeyink et al. 1969). In studies of the adsorption of humic and fulvic acids, Lee et al. (1981) attributed observed adsorption phenomena to both pore-size distribution and the chemical properties of the carbon surface.

The application of mass-transfer-based mathematical models for design requires the estimation and mathematical representation of adsorption capacity and rate for the contaminant of interest. In systems which contain DOM, the effects of preloading on adsorption capacity and rate must be accounted for. Adsorption capacity is estimated by conducting equilibrium experiments in which the amount adsorbed is measured as a function of solution concentration, and is described mathematically by fitting the data with an appropriate isotherm model. The rate of adsorption is generally controlled by two diffusion steps which occur in series -- diffusion across a boundary layer "film" at the particle surface, and diffusion within the particle, which may occur in the pore fluid and in the adsorbed state along the pore surface (Weber and Chakravorti 1974, Crittenden et al. 1986). The rate of adsorption is estimated by conducting dynamic experiments in which the amount adsorbed is measured as a function of time, and is described mathematically by fitting the data with a mass-transfer model appropriate to the conditions (e.g., reactor configuration) of the experiment. The adsorption isotherm is a component of a fully-specified mass-transfer model; therefore, adsorption capacity must be known before adsorption rates can be interpreted.

Fitting isotherm and rate data with appropriate equilibrium and rate models, using statistical procedures to determine optimal model parameters by minimizing the difference between the data and the model, is a process known as model calibration. Adsorption capacity and rate are therefore described by mathematical functions which can be characterized in terms of their calibrated parameters. Comparison of model parameters offers a convenient means of assessing changes in adsorption capacity and rate resulting from DOM preloading.

The design of an adsorption system for a particular contaminant can be accomplished using a mathematical model calibrated for the conditions of a particular system. Model parameters determined in the calibration process must be considered

empirical in the sense that they depend on the contaminant present, the type of adsorbent, and the configuration of the system. However, the relative values of parameters are thought to represent differences in the energetics and dynamics of fundamental adsorption mechanisms. Therefore, calibrated parameters should be constant for a given system. While it is clear that preloaded DOM influences the energetics and dynamics of SOC adsorption, the mechanisms by which this occurs are not well understood. Furthermore, it has been observed that model parameters for SOC adsorption in the presence of DOM are often not constant, and may vary in time or position in the adsorber bed.

There has been no systematic study to identify the mechanisms of DOM preloading, or the factors which contribute to changes in adsorbent characteristics resulting from preloaded organic matter. However, several mechanisms have been proposed to explain the observed changes in SOC adsorption behavior resulting from DOM preloading (Carter et al. 1992). Preloaded organic matter may compete for adsorption sites and block adsorbent pores, reducing the extent of adsorption and changing the isotherm relationship. DOM accumulates in adsorbent pores and on adsorbent surfaces, and may thus create resistance to the diffusion of target compounds, decreasing adsorption rates. In the absence of more fundamental understanding of the impact of preloaded organic matter on subsequent adsorption of SOCs, empirical design approaches incorporating the effects of preloading have been developed.

There have been several attempts to develop protocols for the design of GAC systems which incorporate the effects of DOM. Several researchers have measured how equilibrium and rate parameters vary as a function of column operation time, and have incorporated this time variability into the design model. This approach has proven successful; however, it significantly increases the degree of empiricism inherent in the model calibration process. The time variability of model parameters is often highly system-specific, and cannot be readily applied to other systems. Furthermore, the time-variable models are difficult to calibrate, due to their complexity and their need for extensive laboratory data. There is a need, therefore, for an accurate, conceptually-based predictive model based on a fundamental understanding of the interactions among activated carbon, dissolved organic matter and target pollutants. This research was undertaken to systematically investigate the effects of DOM molecular weight, solution chemistry, and

adsorbent characteristics on the activated carbon adsorption of DOM, and on the subsequent adsorption of low-molecular weight pollutants.

## 1.2 Objectives

To provide the basis for a more fundamental understanding of the preloading phenomenon and how preloading affects subsequently adsorbed SOC<sub>s</sub>, it is necessary to identify the components in a macromolecular solution which compete most effectively with target compounds. Furthermore, it is necessary to understand how i) solution chemistry, including ionic strength and the presence of divalent cations; and ii) adsorbent characteristics, including pore structure and surface charge, influence the adsorption of DOM and the component(s) of DOM which compete most effectively with subsequently adsorbed SOC<sub>s</sub>. Based upon a review of the literature and the research needs identified, several hypotheses were formulated:

- **Hypothesis:** Larger-molecular-weight DOM components are likely to have greater affinities for adsorbent surfaces, which make them better able to compete with low-molecular-weight SOC<sub>s</sub>. However, small molecular weight components have higher mass-transfer rates and may access larger fractions of adsorbent surface area. Competition requires the ability to access the adsorbent surface on which the SOC<sub>s</sub> are adsorbed. Therefore, it was hypothesized that smaller molecular weight components compete most effectively with target compounds.
- **Hypothesis:** Solution ionic strength affects the size and shape of DOM molecules and therefore affects the extent to which they are adsorbed, their ability to access adsorbent surfaces, and the subsequent adsorption of SOC<sub>s</sub> on preloaded carbon.
- **Hypothesis:** Divalent cations, which have been shown to be effective coagulants of DOM, affects the size and shape of DOM molecules, their state of aggregation, and their interactions with adsorbent surfaces. Therefore, the extent to which DOM molecules are adsorbed, their ability to access adsorbent surfaces, and the subsequent adsorption of SOC<sub>s</sub> on preloaded carbon depends on whether divalent cations are present.
- **Hypothesis:** Adsorbent pore structure affects the ability of macromolecular DOM to access adsorbent surfaces and therefore to compete with subsequently adsorbed SOC<sub>s</sub>. Adsorbent surface charge will affect the size and shape of DOM molecules, and their interactions with adsorbent surfaces. Therefore, the extent to which they are adsorbed, their ability to access adsorbent surfaces, and the subsequent adsorption of SOC<sub>s</sub> on preloaded carbon depends on adsorbent characteristics.

A research program was designed to provide a framework for testing these hypotheses. Specific objectives of this program were to:

- Develop techniques to characterize molecular size, molecular size distributions, and to fractionate macromolecular mixtures according to size.
- Characterize the adsorption of DOM, using synthetic model compounds, natural humic materials and size fractions of humic substances, to i) identify the effects of molecular size and size distribution on the extent of adsorption; ii) characterize competitive interactions among humic components in an attempt to identify a reactive fraction; iii) evaluate the effects of ionic strength and the presence of calcium on the extent of adsorption and on competitive interactions among components; and iv) evaluate the effects of adsorbent pore structure and surface charge on the extent of adsorption and on competitive interactions among components.
- Identify mechanisms by which preloaded organic matter competes with subsequently adsorbed low-molecular-weight SOCs.
- Evaluate the impact of preloaded humic substances on the subsequent adsorption of SOCs to identify the effects of i) molecular size and size distribution of preloaded organic matter; ii) solution ionic strength and the presence of calcium during preloading; and iii) adsorbent pore structure and surface charge.

### **1.3 Significance and Relevance**

This work serves as a systematic investigation of the effects of factors currently considered to most significantly impact the adsorption of DOM on the subsequent adsorption of SOCs. The results of this work will contribute to the development of more efficient and cost-effective adsorbent design protocols by providing a more fundamental understanding of the preloading phenomenon and mechanistic insight into the interactions between DOM and low-molecular-weight synthetic organic chemicals in adsorption systems. This work identifies optimum pretreatment objectives required to remove components of DOM which most effectively compete with the adsorption of SOCs, and optimum solution chemistry conditions to mitigate the effects of preloading. This work provides information about adsorbent characteristics which may exacerbate the effects of preloading, which can be used as criteria for adsorbent selection. Further, this work identifies adsorbent properties which may be further tailored in the manufacturing process to mitigate the preloading phenomenon.

## CHAPTER 2

### BACKGROUND AND RELATED RESEARCH

#### 2.1 Activated Carbon Surface Chemistry and Structure

Activated carbon is produced from carbonaceous raw materials such as coal, coconut shells, wood and sugar. First, the raw material is heated to drive off moisture and volatile impurities, resulting in a char. The char is then heated to sufficiently high temperatures (600 °C) to drive off non-carbon impurities, producing a carbonaceous char. Microcrystallites are formed, the structure of which derives from graphite, in the carbonization process. Graphite is comprised of carbon atoms forming ordered, parallel stacks of hexagonal layers. Microcrystallites are about 20-50 Å in diameter and are comprised of 5 to 15 layers of fused hexagonal rings of carbon atoms (Snoeyink and Weber 1967). The interlayer spacing is greater than graphite, about 3.6 Å, and the parallel stacks are not ordered. The microcrystallites are randomly oriented and are extensively cross-linked with tetrahedrally-bonded carbon (Boehm 1966). Heterocyclic rings may be present at the edges of microcrystallite planes. During carbonization, or upon cooling (at temperatures >200 °C), the carbonaceous char is activated by oxidizing gasses (O<sub>2</sub>, CO<sub>2</sub>, or H<sub>2</sub>O) which react with oxidizable portions of the char to create a porous structure. The physical and chemical nature of the activated product, in terms of a pore-size distribution and the chemical reactivity of the surface, depend on the raw material, the composition of the activation atmosphere, and the time and temperature of activation (Mattson and Mark 1971).

Pore-size distribution of activated carbons may be tailored to some extent by controlling the degree of combustion (burnoff) of the raw material by controlling the time and temperature of activation. Hashimoto et al. (1979) studied the evolution of adsorbent surface area and pore structure as a function of activation time (degree of raw material

burnoff) and found that increasing activation increased i) the total pore volume and the volume in pores with diameters less than 200 Å; ii) the BET surface area; and iii) the weight fraction of remaining mineral matter. Cannon and Roberts (1982) found that increasing the activation time increased the surface area and pore volume of a prune pit GAC, and shifted the pore volume distribution to larger sizes. At low levels of activation, surface area may increase due to the opening of closed pores. At higher levels of activation, the coalescence of adjacent pores becomes more important, which results in a relative increase in the fraction of meso- and macropores (Hashimoto et al. 1979).

The activated carbon surface may contain hydrogen groups, inorganic impurities such as metals, and surface oxides. Hydrogen is most likely present as terminal groups on the fused aromatic planes, or as part of hydrocarbon functional groups attached to these planes (Snoeyink and Weber 1967). Inorganic constituents may be present in the raw material or may be added during the activation process. Metals and inorganic salts may influence the adsorbent surface charge, and may participate in a variety of reactions at the surface (i.e. complex formation, precipitation, and electron transfer reactions). It has been reported that a high percentage of the inorganic species present on the adsorbent surface can be removed by acid treatment (Snoeyink and Weber, 1967).

The surface chemistry of activated carbon is, in large part, determined by the types of surface oxides present. The types of oxides that form depend on i) the temperature of activation; ii) the composition of the atmosphere during activation; iii) the composition of the atmosphere upon cooling; and iv) the relative exposure to oxygen at room temperature (aging). Hennig (1962) found that edge atoms which terminate graphite crystal faces are 20 times more reactive than atoms comprising the basal planes; therefore, oxygen-containing functional groups are formed preferentially at the edges of layer planes. Surface oxides can influence the acidity, zeta potential and hydrophobicity of the carbon surface. Exposure to oxygen at some point during the manufacture of activated carbon is necessary for the surface to develop acid/base reactivity. The effect of surface oxides depends on the activation temperature and conditions (Mattson and Mark 1971).

Steenberg (1944) developed a classification of carbon based on activation temperature, gaseous atmosphere during activation and cooling, and surface oxide

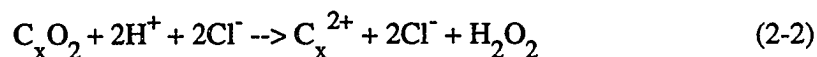
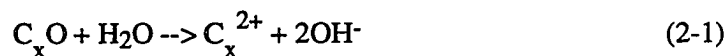
functional group content. H carbons are produced at activation temperatures ranging from about 500 °C to 1200 °C. H character corresponds to a surface composed of primarily basic oxides, which form when the carbon is activated at high temperature in either a pure CO<sub>2</sub> atmosphere or under vacuum, and subsequently cooled in an inert atmosphere followed by exposure to oxygen at room temperature. H carbons have a low density of surface oxygen-containing functional groups, are hydrophobic, exhibit strong acid adsorption, and have a positive zeta potential. L character is created when carbon is activated at low temperature (200 to 400 °C) in an oxygen-containing atmosphere, or in an aqueous oxidizing solution. These materials have a higher density of oxygen-containing functional groups, are hydrophilic, adsorb base, and exhibit a negative zeta potential (Mattson and Mark 1971). H and L classifications represent idealized limiting conditions. Many carbons exhibit both H and L characteristics. For example, cooling a high-temperature activated carbon in an oxygen-containing atmosphere results in an adsorbent which has some L character. Exposure of carbon to oxygen at room temperature, or aging, also tends to slowly increase its L character. Many carbons are activated at intermediate temperatures (500-600 °C) and will neutralize at least small amounts of both acid and base. Activated carbons having a wide range of pore structures and surface functional groups can be manufactured by varying the time and temperature of activation, and the degree of exposure to oxygen during cooling; however, the details of activated carbon manufacture are generally proprietary.

Several techniques have been used to identify oxygen-containing functional groups on carbon surfaces (Mattson and Mark 1971). Examples are: i) titrations with different inorganic bases including HCO<sub>3</sub><sup>-</sup>, CO<sub>3</sub><sup>2-</sup> and NaOH, ii) reaction with diazomethane, iii) reaction with organic functional group reagents including 2,4-dinitrophenyl hydrazine, 2,4-dinitrofluorobenzene, p-nitrobenzoyl chloride, and thionyl chloride, iv) polarographic analysis, and v) infrared transmission and internal reflectance spectroscopic methods. The spectroscopic data indicate i) the presence of carboxylic acid functional groups, probably present as dicarboxylic acids on adjacent sites; ii) the presence of the enolic form of a 1,3-di-ketone; and, iii) the presence of C-O and C-O-C bonds (Mattson and Mark 1971). The presence of carboxylic groups is supported by the results of alkali titrations, reaction with



diazomethane, and reaction with thionyl chloride. The phenolic hydroxy functional group is often suggested, if present, based on NaOH titration data. However, the enolic hydroxy group of a 1,3-di-ketone may result in similar titration behavior, thus definitive identification based on titration data alone is not straightforward. Polarographic analysis suggests the presence of quinone groups, but similar polarographic response could be generated by the  $\beta$ -keto group of an enol (Mattson and Mark 1971).

Mattson and Mark (1971) have summarized several investigations of acid adsorption by activated carbon. They report that carbons activated at high temperatures (1000 °C) in a vacuum and cooled in a vacuum did not adsorb or neutralize any acid from a solution of degassed 0.01 N HCl. Subsequent acid adsorption was found to exhibit an exponential dependence on the partial pressure of O<sub>2</sub> admitted above the solution. It is hypothesized that oxygen is incorporated into surface functional groups, which participate in oxidation-reduction reactions. The following mechanism has been proposed to account for the removal of acid from dilute (<0.01 N) solutions:



The first reaction explains the ability of H carbons to increase the pH of a solution. As a result of the positive charge formed, the reaction also explains the adsorption of anions. The second reaction is supported by the detection of hydrogen peroxide evolution during the adsorption of acid by activated carbon. Some researchers attribute the carbon-oxygen complex to a chromene surface group, however, direct evidence for such a structure is lacking.

An additional mechanism of acid uptake may be important. There is compelling evidence for the specific adsorption of anions, particularly at high anion concentrations (>0.01 M). Anions may be either the conjugate anion of the acid, or may be from another source. Adsorption of anions may cause a corresponding increase in the concentration of

protons and cations in the diffuse layer. This mechanism explains why acid uptake has been shown to depend on the nature of the anion, and on salt concentration.

### Quantification of Adsorbent Surface Properties

Based on the above discussion, it is evident that the charge on the carbon surface is due, in part, to chemical reactions at the surface. During activation, oxygen is incorporated into surface functional groups, which may subsequently ionize and participate in redox reactions. Further, under certain conditions, surface charge may develop due to the specific adsorption of ions onto the surface (unsolvated ions located at the inner Helmholtz plane). In general, the excess surface charge results from the adsorption of  $H^+$ ,  $OH^-$ , and other specifically adsorbed anions and cations,  $A^{z-}$  and  $M^{z+}$ . Muller et al. (1980, 1985) have modeled the activated carbon surface as consisting of acidic and basic groups:



where  $S_A$  and  $S_A^-$  are generalized surface acidic and basic sites. In the absence of specifically adsorbable anions or cations, the excess surface charge is given by:

$$\sigma = F(\Gamma_H - \Gamma_{OH^-}) \quad (2-5)$$

where  $\sigma$  is the surface charge,  $C/m^2$ ,  $F$  is the Faraday constant  $C/mol$ , and  $\Gamma_i$  is the adsorption density,  $mol/m^2$ . At the pH corresponding to the point of zero proton condition ( $pH_{zpc}$ ), the number of positive surface groups is equal to the number of negative surface groups, and the surface carries no net charge. (This pH value is also referred to as the point of zero charge,  $pH_{pzc}$ ). In the absence of specifically adsorbing ions other than  $H^+$  and  $OH^-$ , the  $pH_{zpc}$  is equal to the pH at which the particle is electrokinetically uncharged, the iep or isoelectric point (Stumm and Morgan 1981).

If the surface charge is caused only by the binding of  $H^+$  and  $OH^-$ , the surface charge can be computed from titration data. A system charge balance yields:

$$C_A - C_B + [OH^-] - [H^+] = [S_B^+] - [S_A^-] \quad (2-6)$$

Where  $C_A$  and  $C_B$  are the molar concentrations of acid and base added per liter, and  $[ ]$  indicates concentrations of solute and surface species in moles per liter of solution. The excess surface charge is obtained knowing the specific surface area of the solid, and the solid concentration in solution (Stumm and Morgan 1981):

$$\sigma = \frac{F(C_A - C_B + [OH^-] - [H^+])}{D_0 S} = F(\Gamma_H - \Gamma_{OH}) \quad (2-7)$$

where  $D_0$  is the solids concentration, kg/l and  $S$  is the specific surface,  $m^2/kg$ .

Arico et al. (1989) characterized a variety of adsorbents by KOH/HNO<sub>3</sub> titration. Points of zero charge were determined from excess surface charge curves. Two types of excess surface charge curves were noted; "acidic" carbons showed a regular increase in positive surface charge with decreasing pH, while "basic" carbons displayed an initial increase in surface charge, then a charge reversal. The steady increase in surface charge up to the  $pH_{pzc}$  is due to the protonation of oxygen-containing surface functional groups. Below the  $pH_{pzc}$ , an oxidation-reduction mechanism involving basic surface sites results in a positive surface charge. Upon the addition of more acid, specific adsorption of the anion results in a negative surface charge. The basic carbons, which contain fewer acidic groups to protonate, exhibit charge reversal behavior in the pH range of 3 to 4, while the more acidic carbons do not. Measured  $pH_{pzc}$  values ranged from 3.11 to 9.85 for various carbons.

Muller et al. (1980, 1985) determined the charge density and  $pH_{pzc}$  using two different titration techniques with strong acid and base (HCl/NaOH). The first method involved a batch titration at constant ionic strength. Carbon samples were equilibrated with solutions of varying initial pH, and the  $pH_{pzc}$  was obtained when the initial and equilibrium pH were identical. The second method involved surface titrations at several different concentrations of background electrolyte. While the surface charge should increase with

increasing background electrolyte due to charge screening, the pH at which the surface charge is zero should not change. Thus, in the absence of specifically adsorbing ions, the pH of the common intersection point (cip) of titration curves obtained with different concentrations of background electrolyte should be equal to the  $\text{pH}_{\text{pzc}}$  (Stumm and Morgan 1981). Muller et al. (1985) found good agreement between the two methods for two acidic carbons.

Summers and Roberts (1988) used a batch titration technique at constant ionic strength (0.10 N NaCl) technique to quantify the  $\text{pH}_{\text{pzc}}$  for five activated carbons, four basic carbons ( $\text{pH}_{\text{pzc}} = 9.3$  to  $10.2$ ) and one acidic carbon ( $\text{pH}_{\text{pzc}} = 5.0$ ). The measurements of Summers and Roberts for F300 and F400 carbon agree well with the results of Huang et al. (1985), who used a direct titration method. Arico (1989) has reported that the  $\text{pH}_{\text{pzc}}$  values obtained from electrophoretic mobility measurements were generally lower than values obtained from direct titration methods. Huang and Wu (1977) and Huang (1980) report  $\text{pH}_{\text{pzc}}$  values of 7.0 and 7.1 for F400 carbon based on electrophoretic mobility measurements, in contrast to the value reported by Huang et al. (1985) of 10.4 based on direct titration methods.

To differentiate among acidic groups on the carbon surface, Boehm (1966) studied the neutralization of 0.05 N solutions of bases of different basicities. This was later referred to as to as a multibasic titration technique (Mattson and Mark 1971). Acidic surface oxides with  $\text{pK}_a$  values less than about 4.4, 8.2, and 10 in aqueous solution can be titrated with 0.05 N solutions of  $\text{HCO}_3^-$ ,  $\text{CO}_3^{2-}$ , and  $\text{OH}^-$  respectively. The acidic surface oxide groups which can be identified by this technique include weak and strong carboxylic groups, and the OH group of an enol or lactone (Mattson and Mark 1971).

## **2.2 Humic Substances: A General Characterization**

Humic substances are a whole group of yellow to brown, refractory, macromolecular organic compounds formed in soil, water and sediment. They are defined in a negative sense, i.e. they include all organic compounds found in natural systems except proteins, polysaccharides and lipids (Buffle 1990). However, carbohydrates and proteinaceous materials may be adsorbed or covalently bonded to a humic substance "core"

(Malcolm 1990, Schnitzer 1991, Schulten and Schnitzer 1993). As might be expected from this definition, humic substances comprise the bulk of organic substances in natural systems; estimates range from 30 to 70% (Thurman 1982, Morel 1983, Buffle 1990). Humic substances are generally further categorized operationally into humic and fulvic acids. Humic acids are soluble in dilute alkali, but coagulate upon acidification, while fulvic acids remain in solution under both alkaline and acidic conditions.

Two general theories have been proposed for the formation of humic substances, a process known as humification. The biopolymer degradation theory considers humic substances to derive from the biotic and abiotic degradation of large molecular weight plant-derived biopolymers. The abiotic condensation theory postulates condensation reactions which form large molecular weight humic molecules from reactive, low-molecular-weight precursors which were themselves formed by the enzymatic degradation of large molecular weight biopolymers (Hedges 1988). The key difference between these two theories is whether the processes directly responsible for the genesis of humic substances are "degradative" or "aggregative" in nature. If humification is degradative, then humic acids are precursors to fulvic acids; if the condensation theory is correct, then the opposite is true. It is likely, however, that humification is a dynamic process and both degradation and polymerization processes occur simultaneously (Hatcher and Spiker 1988).

As suggested by their different solubility properties, the chemical and structural characteristics of humic and fulvic acid are different. Fulvic acids tend to have lower molecular weights, generally less than a few thousand, while the molecular weights of humic materials may be much higher (Buffle 1990). Humic acids generally contain more C, H, N and S than the fulvic acids, which contain a greater proportion of oxygen (Schnitzer 1991). Elemental analysis of a variety of humic substances suggests a composition of 45-55% C, 35-50% O, 3-6% H, 1-4% N, and 0-2% S. The carboxylic, phenolic and total acidity of fulvic acids are generally higher than humic acids. The total acidity of a soil fulvic acid reported by Schnitzer (1991) was 12.4 meq/g, a value that is considered representative.

It has been shown that the composition of saccharide, phenolic, methoxyl, aromatic, hydrocarbon, amino acid and nitrogen moieties of each type of humic substance depends,

to some degree, on whether the source was a surface water, marine, or soil environment (Malcolm 1990). Aromaticity increases in the order marine < stream < soil for both humic and fulvic acids. About 50% of the carbon in soil humic acid has been identified as aromatic and phenolic (Schnitzer 1991).

The molecular size and weight of humic substances has been estimated using a variety of techniques, including gel-permeation chromatography, high-performance size-exclusion chromatography, vapor pressure osmometry, x-ray scattering, field-flow fractionation, ultrafiltration, and diffusion measurements. The measured molecular weight may depend on the methods used to extract or isolate the humic material, and to some degree, most measurement techniques introduce some bias. Bias may result from the type of solvent the humic material is dissolved in, and the type of molecules chosen to standardize the analytical system. Nevertheless, the measurements recently reported in several different studies are fairly consistent and have identified useful trends. It has been found that weight-averaged molecular weights for stream humic substances generally range from 1500 to 5000 g/mol for humic acids and from 600 to 2000 for fulvic acids (Beckett et al. 1987, Reid et al. 1990, Chin and Gschwend 1991, Chin et al. 1994). This compares to a range of 1000 to 5000 for soil fulvic acids (Malcolm 1990). The upper molecular weight range for soil humic acids may be larger, ranging from 50,000 to 500,000. In general, number-averaged molecular weights are smaller than weight-averaged. Based on x-ray scattering measurements, Thurman et al. (1982) estimated the size of humic substances (radius of gyration) to range from about 5 to 33 Å, corresponding to molecular weights ranging from 500 to 10,000. Cornel et al. (1986) estimated the hydrodynamic radius of a commercial humic acid using diffusion measurements, and reported values ranging from 0.80 to 80 Å, depending upon temperature and ionic strength. These results suggest that at least some components of humic substances are small enough to access a significant fraction of activated carbon surfaces, while some appear to be an appropriate size to lodge at the entrance of larger mesopores, possibly preventing smaller molecules from accessing otherwise vacant surfaces.

## 2.3 Adsorption of Humic Substances and Other Polyelectrolytes

### General Considerations

The adsorption properties of organic macromolecules are governed by their high molecular weights, their molecular charge, and the fact that they normally occur as mixtures of components. Natural humic molecules are charged because they contain ionizable functional groups, including carboxylic and phenolic moieties, and for this reason they are classified as polyelectrolytes. This section begins with a discussion of how the distinguishing features of polyelectrolytes influence their adsorption behavior, which may be quite different from the adsorption of low-molecular-weight compounds.

In general, the adsorption of any molecule is governed by interactions between the adsorbate and the adsorbent, and between the adsorbate and the solvent. Interactions may include hydrogen bonding, ion-ion and ion-dipole electrostatic (Coulombic) interactions, and attractive forces resulting from interaction between permanent and induced dipoles (including Debye, Keesom and London dispersion forces). For polyelectrolytes, these interactions are governed, in large part, by the molecular charge. For example, molecular charge and charge on adsorbent surface sites may result in strong attractive or repulsive Coulombic forces, depending on the magnitude and sign of the charge. Molecular charge facilitates hydrogen bonding with water, causing a high affinity for the solvent. For this reason, charged macromolecules having molecular weights on the order of  $10^6$  may remain soluble (Ramachandran and Somasundaran 1985).

Repulsive forces between like-charged functional groups on the same molecule is a feature of polyelectrolyte adsorption which differentiates it from the adsorption of neutral polymers, and may influence both adsorbate/adsorbent and adsorbate/solvent interactions.

The impact of surface affinity, molecular weight and ionic strength on polyelectrolyte adsorption depends on the relative importance of sorbate/sorbent and sorbate/solvent interactions. For example, if a strong attraction or repulsion between the sorbate and the surface exists, small changes in the affinity of the sorbate for the solvent will have little effect on the overall adsorption. Additionally, the equilibrium partitioning of macromolecules may be strongly influenced by two physical factors -- the ability of a macromolecule to access adsorbent surface area, and diffusion-controlled adsorption

kinetics. Therefore, when considering the impact of molecular weight and solution composition on the adsorption of polyelectrolytes, it is necessary to account for both chemical and physical factors.

#### Effects of Molecular Weight on Polyelectrolyte Adsorption

The impact of molecular weight on polyelectrolyte adsorption has been shown to depend on i) the importance of sorbate/solute and sorbate/solvent affinities; ii) the ability of the adsorbate to access adsorbent surface area; iii) the polydispersity of the mixture; and, iv) adsorption kinetics. For low-molecular-weight solutes, in general, adsorption increases as molecular weight increases due to a reduction in the affinity for the solvent reflected in reduced solubility. This is the basis of Lundelius' Rule, which states that an inverse relationship is expected between the extent of adsorption and solubility, and Traube's Rule, which states that adsorption increases as a homologous series is ascended. This effect is also observed for the adsorption of polyelectrolytes, if access to adsorbent surfaces is not restricted (i.e., for non-porous adsorbents), and if the solution contains electrolyte. A strong dependence on molecular weight is an indication of weak adsorbate-adsorbent affinity, since variations in adsorbate/solvent affinity have a significant effect on the adsorbed amount. This behavior is generally observed in systems with low-energy, low-charge-density surfaces at high ionic strength (Papenhuijzen et al. 1985, Ramachandran and Somasundaran 1987).

The adsorption from polyelectrolyte mixtures which contain little or no electrolyte may exhibit an inverse dependence on molecular weight -- low-molecular-weight components are adsorbed to a greater extent (Bain et al. 1982, Cosgrove et al. 1986, Ramachandran and Somasundaran 1987). These results are explained on the basis of kinetics and electrostatic repulsion between adsorbed and dissolved molecules. The kinetics of low-molecular-weight components are faster, and therefore these components populate the surface initially. Under conditions of low ionic strength, the high-molecular-weight components are prevented from approaching the surface as a result of electrostatic repulsion. At higher electrolyte concentrations, however, electrostatic repulsion is



suppressed, and higher molecular weight components can approach the surface and displace the low-molecular-weight components.

The ability of an adsorbate to access adsorbent surfaces may have a significant impact on polyelectrolyte adsorption, which may occur when the adsorbent exhibits internal porosity. As suggested by studies of polyelectrolyte adsorption by porous adsorbents such as activated carbon, macromolecule size (or size distribution) relative to the adsorbent pore size distribution can have a dramatic impact on the extent of adsorption. Lee et al. (1981) observed that the extent of humic acid adsorption was greatest for adsorbents with a large volume of mesopores, defined here as pores having widths between 20 and 500 Å (Gregg and Sing 1982). Cannon and Roberts (1982) found that increasing GAC activation time increased the pore volume and shifted the pore volume distribution to larger pore sizes, which increased the extent of filtered secondary effluent adsorption on both a mass and surface area basis. Weber et al. (1983) found that the extent of humic substance adsorption increased with increasing predominant pore size, but this effect diminished with increasing molecule size. Ogino et al. (1988) found that a peat humic acid adsorbed to a greater extent on a mesoporous GAC than microporous carbon fiber or carbon black. Similar results were obtained for the adsorption of a commercial humic acid on a microporous activated carbon cloth and a GAC having a significant mesopore volume (Starek et al. 1994). For adsorption on ion-exchange resins, Fu and Symons (1990) found that for a given hydrophobicity and structure (macroporous versus gel), resin effectiveness was directly related to adsorbent pore size.

The exclusion of adsorbate on the basis of molecular size may result in the preferential adsorption of low-molecular-weight components, even at relatively high electrolyte concentrations. Preferential adsorption of low-molecular-weight fractions of a humic acid solution was demonstrated by Summers and Roberts (1988a,b) who showed that the liquid phase molecular weight distribution of the supernatant was shifted to larger molecular weights after equilibration with activated carbon. When isotherms were expressed on an available surface area basis, carbon capacity exhibited a direct dependence on molecular weight, while an inverse dependence on molecular weight was exhibited when the isotherm was expressed in terms of adsorbent mass. It is evident that two

factors, adsorbent structure (porous versus non-porous) and solution composition, may have a significant impact on the adsorption of polyelectrolytes.

#### Effects of Ionic Strength on Polyelectrolyte Adsorption

Electrolyte concentration, characterized by ionic strength, may have a significant impact on electrostatic interactions, and may thereby influence adsorbate/adsorbent, adsorbate/solvent and adsorbate/adsorbate affinity. Increases in ionic strength result in an increase in the concentrations of counterions which can shield electrostatic charge. For example, positively charged sodium ions are attracted to a negatively charged sulfonate functional group, partially "neutralizing" the charge.

Increases in solution ionic strength may increase the extent of polyelectrolyte adsorption by reducing the repulsive forces between different segments of the polyelectrolyte molecule, thus making it less favorable to be dissolved in a polar solvent such as water. This enhancement can be significant if the attraction between the polyelectrolyte and the surface is relatively weak (Pefferkorn et al. 1978, Papenhuizen et al. 1985a,b, Cosgrove 1986, Ramachandran and Somasundaran 1987). If the surface carries the same charge as that of the polyelectrolyte, increases in solution ionic strength can also reduce the repulsive forces between the surface and the polyelectrolyte, thus increasing the extent of adsorption. However, if the surface carries the opposite charge as that of the polyelectrolyte, increases in ionic strength can shield the charge, reduce the electrostatic attraction between the polyelectrolyte and the surface, and thereby reduce the amount adsorbed.

The influence of ionic strength on the repulsive forces between different segments of the polyelectrolyte molecule can change the size and configuration of the polyelectrolyte. There is considerable evidence to suggest that ions in solution shield charged functional groups on the humic molecule, reducing the electrostatic repulsion forces between like-charged functional groups, thus facilitating coiling, compression, or folding of the humic structure. Figure 2-1 shows features of a conceptual model of humic structure proposed by Gosh and Schnitzer (1980). They characterized the structure of humic and fulvic acids as flexible linear colloids at concentrations and ionic strengths typical of natural waters, and as

spherical colloids at higher concentrations and ionic strengths. The decrease in molecular size with increasing ionic strength has been documented by Cornel et al. (1986), who showed that macromolecule diffusion coefficients increased significantly in response to higher ionic strengths, and by Kilduff and Weber (1992) who showed that increases in ionic strength resulted in increased mass transfer through ultrafiltration membranes. Therefore, the effective size of a humic molecule may be controlled to some extent by solution ionic strength.



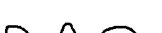







Sample Conc.	NaCl Concentration, M				
	0.001	0.005	0.010	0.050	0.100
Low					
High					

Figure 2-1. Model macromolecular structures as proposed by Gosh and Schnitzer (1980). Humic and fulvic acids behave as linear colloids at low concentrations and ionic strengths, and rigid spherocolloids at high concentrations and ionic strengths.

Decreases in polyelectrolyte size due to coiling or compression may make surface area in a microporous adsorbent more accessible. Increases in humic substance adsorption with increasing ionic strength has been demonstrated (Randtke and Jepsen 1982, Weber et al. 1983, Summers and Roberts 1988b, Lafrance and Mazet 1989).

It is evident that many factors may influence the adsorption of polyelectrolytes, and the relative impacts of molecular size and solution chemistry. Equilibrium partitioning may depend on the type, source, and size distribution of the DOM, the surface chemistry and pore-size distribution of the adsorbent, and the solution electrolyte composition. Because adsorption measurements can be so system specific, it is important to carefully characterize the adsorption characteristics of a particular system.

## 2.4 Modeling Adsorption Equilibria

The partitioning of sorbates from the aqueous phase onto activated carbon is expressed in terms of an adsorption isotherm, which is a function which relates the amount of solute adsorbed ( $q_e$ ) to the aqueous-phase concentration ( $C_e$ ) at equilibrium. In this research, isotherms were measured in completely mixed batch reactors (CMBRs). Each point on the isotherm is determined from an individual reactor containing a known mass of solute to which a known mass of adsorbent is added. After a suitable equilibration period, the aqueous phase concentration of solute is measured, and the amount adsorbed is calculated from a mass-balance on the liquid phase:

$$q_e = \frac{C_0 - C_e}{D_0} \quad (2-8)$$

where  $C_0$  is the initial sorbate concentration, and  $D_0$  is the adsorbent concentration, or adsorbent dose ( $ML^{-3}$ ). By varying either the initial solute concentration or the adsorbent dose, equilibrium conditions may be obtained for a wide range of aqueous concentrations. The isotherm data are generally fitted with an isotherm model, which is a mathematical function characterized by one or more parameters. In this way, the solute partitioning can be quantified, and results from different experiments can be compared.

Activated carbon is a chemically and physically heterogeneous surface. To accurately correlate isotherm data, a model which can account for this heterogeneity must be chosen. In many applications, the two-parameter Freundlich isotherm model has been used successfully. The Freundlich model accurately describes data which is linear when plotted on log-log coordinates:

$$q_e = K_F C_e^n \quad (2-9)$$

where  $K_F$  is a unit-capacity parameter, equal to the amount adsorbed at a value of  $C_e$  equal to unity (in whatever concentration units chosen), and  $n$  is a dimensionless parameter related to the site energy distribution.

When data is collected over a wide range of concentration, or when the compound adsorbs strongly, evidence of surface saturation is reflected in data which is non-linear on log-log coordinates. To model this type of data, researchers have employed multiple Freundlich isotherms (Snoeyink and Weber 1969) and isotherms which contain additional parameters. A family of such isotherms has been derived from the theory of adsorption by heterogeneous surfaces. These isotherms are derived from characteristic site energy distributions, and contain parameters which relate to properties of the distributions.

The basis for the theory of adsorption by heterogeneous surfaces is the dimensionless integral representation of the overall adsorption isotherm for a surface with non-interacting sites proposed by Halsey and Taylor (1947):

$$\theta_t(C_e, T) = \frac{q(C_e, T)}{Q^0(T)} = \int_0^{\infty} \theta(C_e, E, T) F(E) dE \quad (2-10)$$

where  $\theta_t(C_e)$  is the dimensionless overall adsorption isotherm, representing the total amount adsorbed as a function of the equilibrium solute concentration, for a given temperature,  $T$ . The parameter  $q(C_e)$  is the amount adsorbed (usually normalized to adsorbent surface area or mass),  $Q^0$  is the maximum adsorption capacity,  $\theta(C_e, E)$  is the local adsorption isotherm representing the amount adsorbed on sites with a given adsorption energy  $E$ , and  $F(E)$  is the site energy distribution function. For a given site,  $E$  represents the difference between the adsorption energies of the solute and the solvent (Marczewska et al. 1984). While the limits on the integral should be based on minimum and maximum adsorption energies known *a priori* (Misra 1970) these limits are generally not known, and it is generally assumed that the adsorption energies range from zero to infinity (Jaroniec 1975). The function  $\theta_t(C, T)$  is subject to the conditions:

$$\theta_t(C_e = 0, T) = 0, \text{ and } \theta(C_e = \infty, T) = 1 \quad (2-11)$$

where the second condition implies that:

$$\int_0^{\infty} F(E) dE = 1 \quad (2-12)$$

Commonly, it is assumed that the local isotherm takes a Langmuir form:

$$\theta(C_e) = \frac{q_e}{Q^0} = \frac{b_1 C_e}{1 + b_1 C_e} \quad (2-13)$$

Where  $b_1$  is a temperature-dependent parameter related to the energy of adsorption:

$$b_1 = b_{10} e^{(E/RT)} \quad (2-14)$$

and  $b_{10}$  is essentially a frequency factor (Adamson 1982).

Theoretically, if the local adsorption isotherm and the site-energy distribution function are known, the integral representation of the overall isotherm may be solved to yield a corresponding form for the overall adsorption isotherm; this approach was taken by Halsey and Taylor (1947) to derive the Freundlich isotherm based on a Langmuir local isotherm and an exponential site-energy distribution. Conversely, the mathematical forms of the local and overall isotherm models may be selected, and the integral equation may be solved to derive the corresponding site-energy distribution; this approach has been taken by Sips (1948, 1950), Misra (1970) and Toth (1974). It has been shown that the isotherms derived by both of these analytical approaches all represent simplifications of a more general isotherm equation, the Generalized Langmuir (GL) isotherm, which can be written (Jaroniec 1983):

$$q_e = Q^0 \left[ \frac{(b C_e)^m}{1 + (b C_e)^m} \right]^{(n/m)} \quad (2-15)$$

where  $b$  now represents a Langmuir-type constant which incorporates a characteristic site energy  $E_0$ , and  $b_0$  is essentially a frequency factor:

$$b = b_0 e^{(E_0/RT)} \quad (2-16)$$

The constant  $E_0$  is the energy corresponding to the maximum site frequency, and determines the position of the energy distribution function on the energy axis. For a symmetric, quasi-Gaussian distribution,  $E_0$  represents the mean site energy, while for an exponential distribution,  $E_0$  represents the minimum site energy. The parameters  $m$  and  $n$  are heterogeneity parameters -- the parameter  $m$  characterizes the shape of the site energy

distribution in the direction of lower values of  $E$  while the parameter  $n$  characterizes the shape of the site energy distribution in the direction of higher values of  $E$  (Marczewska et al. 1984). For various combinations of limiting values of  $m$  and  $n$ , the Langmuir (L), Langmuir-Freundlich (LF), Toth (T), and Generalized Freundlich (GF) isotherms can be derived. The classical Freundlich equation can be shown to be a low-concentration limit of the LF, GF and GL isotherm equations. The various isotherm forms are shown in Table 2-1. For completeness, the Redlich-Peterson equation is included, because it is similar in form, and can be derived from the generalized Langmuir equation by expanding the denominator with a Taylor series with respect to  $C_e^m$  about the point  $C_e^m = 0$  (Marczewska et al. 1984).

The values of  $m$  and  $n$  listed in the table designate the values or range of values of these parameters that, when substituted into the Generalized Langmuir model, result in the isotherm equation shown in the corresponding row. The column labeled "high conc. behavior" shows the isotherm form which results when  $bC_e \gg 1$ , and the column labeled "low conc. behavior" shows the isotherm form which results when  $bC_e \ll 1$ . All of the isotherms in Table 2-1 satisfy the condition  $\theta_t(C_e = 0, T) = 0$ , and all of the direct simplifications of the generalized Langmuir equation (LF, GF and T isotherms) satisfy the condition  $\theta(C_e = \infty, T) = 1$ . The behavior of the three-parameter isotherms differ significantly from the local Langmuir isotherm. The Toth equation predicts linear partitioning at low concentration (Henry's region), and exhibits a limiting capacity. The Redlich-Peterson isotherm also predicts a Henry's region, but exhibits an infinite adsorption capacity at high concentrations, behavior which is physically unrealistic. The Generalized Langmuir, Langmuir-Freundlich and Generalized Freundlich isotherms all exhibit a limiting capacity, but none predict a Henry's region. The classical Freundlich equation exhibits neither a linear region at low concentration or a limiting capacity; nevertheless, it has proven successful in describing adsorption data over ranges of concentration of interest in engineering applications. Concentrations of interest commonly range from typical drinking water limits (low  $\mu\text{g/L}$  for many regulated compounds) to several orders of magnitude higher. In this range, adsorption data for many compounds are linear on log-log coordinates and exhibit neither a Henry's region or saturation

**Table 2-1. The Generalized Langmuir Isotherm and Its Simplifications**

Code	Isotherm Equation	m	n	Low Conc. Behavior	High Conc. Behavior
GL	$q_e = Q^0 \left[ \frac{(bC_e)^m}{1+(bC_e)^m} \right]^{(n/m)}$	(0,1)	(0,1)	$Q^0(bC_e)^n$	$Q^0$
L	$q_e = \frac{Q^0 b C_e}{1+bC_e}$	(0,1)	(0,1)	$Q^0 b C_e$	$Q^0$
LF	$q_e = \frac{Q^0 (bC_e)^n}{1+(bC_e)^n}$	m = n	(0,1)	$Q^0 (bC_e)^n$	$Q^0$
GF	$q_e = Q^0 \left[ \frac{bC_e}{1+bC_e} \right]^n$	1	(0,1)	$Q^0 (bC_e)^n$	$Q^0$
T	$q_e = \frac{Q^0 b C_e}{(1+(bC_e)^m)^{(1/m)}}$	(0,1)	1	$Q^0 b C_e$	$Q^0$
F	$Q^0 (bC_e)^n$	(0,1)	---	$Q^0 (bC_e)^n$	$\infty$
RP	$q_e = \frac{Q^0 b C_e}{1+(bC_e)^m}$	(0,1)	---	$Q^0 b C_e$	$\infty$

behavior. The Freundlich isotherm is less successful, however, when the concentration range is broadened significantly.

The behavior of the various isotherm equations relates, in part, to their underlying site energy distributions. The Toth and Langmuir-Freundlich equations both have quasi-Gaussian distributions. The Langmuir-Freundlich distribution is symmetrical, while the Toth distribution is widened toward lower energy values. The Generalized Freundlich, Freundlich and Redlich-Peterson isotherm equations have exponential distributions. When both heterogeneity parameters are equal to unity, all of the isotherms in Table 2-1 reduce to



the Langmuir equation. When the Freundlich  $n$ -value is equal to unity, the resulting isotherm corresponds to the linear (Henry) region of the Langmuir isotherm.

In many cases, several of the isotherm equations shown in Table 2-1 will describe experimental data equally well, even though the shapes of the site energy distributions are different. In large part, this is due to the fact that over the concentration ranges commonly examined in engineering applications, the distribution functions, and therefore the isotherm equations, are similar. This is one reason why the Freundlich isotherm has enjoyed such widespread application for describing adsorption data. However, when experimental data are collected over a wider range of concentrations, the choice of isotherm equation becomes more critical, and a more detailed evaluation must be performed.

## 2.5 Site Energy Distributions

In this section, the theory of site energy distributions is developed. Observed changes in experimentally measured isotherms resulting from preloading can be related to changes in the energetic characteristics of sorbent surfaces by characterizing adsorbent site energy distributions. In turn, observed changes in site energy distributions determined from experimental data can verify hypotheses regarding specific preloading mechanisms. Changes in site energy distributions account for changes in the numbers, diversity and average energy of surface sites. The effects of changes in the adsorbent structure are included implicitly, because these effects are reflected phenomenologically in the adsorption isotherm. Pore blockage by preloaded solutes and restricted access to micropores are examples of potential structural changes.

There are two general techniques for obtaining site energy distributions. The first method involves assuming a form for the local and overall isotherms, and solving the integral adsorption equation for  $F(E)$ . The Stieltjes integral transform has been used in this regard to derive exact site energy distributions for the general Langmuir isotherm and its simplifications (Sips 1948, 1950, Misra 1970, Marczewska et al. 1984). The exact distributions are normalized, and their shape is determined by the values of the applicable heterogeneity parameters, while their position on the energy axis is determined by the choice of a reference energy ( $E_0$ ).

A second general technique for generating approximate site energy distribution functions uses specific approximations of the local isotherm. These methods result in stable, analytical expressions which do not require any *a priori* assumptions about the shape of the distribution. In contrast to more complex numerical techniques, their application to the limited data sets characteristic of environmental studies is straightforward (Nederlof et al. 1990).

The simplest of the approximate methods is the condensation approximation, as illustrated by Cerofolini (20), which assumes that the local isotherm is a step function. The condensation approximation results in a specific relationship between the energy parameter of the local isotherm and solute mole fraction. Alternatively, as done by Marczevska et al. (1984), the equilibrium liquid phase concentration can be related to the energy of adsorption by the following relationship:

$$C_e = C_s \exp\left(\frac{-(E-E_s)}{RT}\right) = C_s \exp\left(\frac{-E^*}{RT}\right) \quad (2-17)$$

where  $C_s$  is the maximum solubility of the solute in the solvent,  $E_s$  is the energy corresponding to  $C_e = C_s$ ,  $R$  is the universal gas constant,  $T$  is absolute temperature and  $E^* = E - E_s$  (Cerofolini, 1974; Derylo-Marczevska et al., 1984; Seidel and Carl, 1989). Equation 2-17 may also be obtained from Polanyi theory (Manes and Hofer, 1969). The  $E_s$  reference state for  $E$  represents the lowest physically realizable sorption energy, and its magnitude depends only on the solute; i.e., it is independent of the sorbent (Derylo-Marczevska et al., 1984). The parameter  $E_s$  is analogous to  $E_0$  (Eq. 2-16) in that it determines the position of the distribution on the energy axis.

Because the overall sorption isotherm is defined in terms of  $C_e$ , substitution of Equation 2-17 into any isotherm expression results in a sorption equation written in terms of a net energy,  $E^*$ . By incorporating Equation 2-17 into Equation 2-10, it can be shown that an approximate site energy distribution,  $F(E^*)$ , is obtained by differentiating the isotherm,  $q_e(E^*)$ , with respect to  $E^*$ :

$$F(E^*) = \frac{-dq_e(E^*)}{dE^*} \quad (2-18)$$

The resulting site energy distributions are expressed in terms of isotherm model parameters and are therefore not normalized. The area under the distribution is equal to the adsorption capacity for the chosen range of concentration.

A smoothing function may be applied to the experimental data before differentiating the isotherm to eliminate variability which may cause spurious or negative peaks when derivatives are taken (Nederlof et al 1990). While any function could be chosen to smooth the data, the Langmuir-Freundlich model, and where appropriate, the Freundlich model, were chosen as smoothing functions because they describe the data accurately. Specifying a functional form for the isotherm is not required to apply the method, and the use of an isotherm function to fit the data does not make any *a priori* assumption about the shape of the site energy distribution. Therefore, computed site energy distributions are independent of both the isotherm model used to fit the data and its underlying distribution. However, because isotherm models are used as smoothing functions, the approximate site energy distributions are functions written in terms of isotherm parameters.

The Langmuir-Freundlich Isotherm and Approximate Energy Distribution. In terms of adsorption energy, the Langmuir-Freundlich isotherm can be written:

$$\frac{q_e}{Q^0} = \frac{(bC_s)^n e^{-nE/RT}}{1 + (bC_s)^n e^{-nE/RT}} \quad (2-19)$$

In accordance with the condensation approximation (Equation 2-18), the first derivative yields an approximate site energy distribution in terms of isotherm model parameters  $Q^0$ ,  $b$ , and  $n$ :

$$F(E) = - \frac{dq_e(E)}{d(E)} = \frac{Q^0 n (bC_s)^n}{RT} e^{(-nE/RT)} [1 + (bC_s)^n e^{(-nE/RT)}]^{-2} \quad (2-20)$$

The Freundlich Isotherm and Approximate Energy Distribution. In terms of adsorption energy, the Freundlich isotherm can be written:

$$q_e = Q^0 (bC_s)^n e^{-nE/RT} \quad (2-21)$$

The first derivative yields the approximate site energy distribution in terms of Langmuir Freundlich adsorption parameters  $Q^0$ ,  $b$  and  $n$ , or in terms of Freundlich parameters  $K_F$  and  $n$ :

$$F(E) = \frac{dq_e(E)}{dE} = \frac{Q^0 n (b C_s)^n}{RT} e^{(-nE/RT)} = \frac{K_F n C_s^n}{RT} e^{(-nE/RT)} \quad (2-22)$$

## 2.6 Mass Transfer Models

Pilot testing has traditionally been the primary design tool for large GAC systems. While this method provides for close similarity to full-scale operations, it is costly, time-consuming, and offers no convenient means for evaluating alternative reactor configurations or operational scenarios. Over the past two decades, investigators have developed design procedures using computer-based mathematical models which may be used as alternatives or adjuncts to pilot column tests (Crittenden and Weber 1978a,b,c, Liu and Weber 1981, Hand et al. 1984, Crittenden et al. 1987, Weber and Wang 1987, Smith and Weber 1988, 1989, Crittenden et al. 1991). Two predictive models which have been validated over an extensive range of conditions are the homogeneous surface diffusion model (HSDM) and the pore-surface diffusion model (PSDM) (Crittenden and Weber 1978a,b,c, Thacker et al. 1984, Weber and Smith 1987, Smith and Weber 1988, Smith and Weber 1989, Hand et al. 1989, Summers et al. 1989).

The HSDM and PSDM both incorporate a mathematical description of the major physicochemical mechanisms recognized to occur in fixed-bed systems: axial flow with dispersion, mass transfer across a hydrodynamic boundary layer surrounding the particle, local equilibrium at the surface of the particle, and intraparticle diffusion. Rate processes are modeled as two resistances in series, are characterized by an external mass transfer coefficient,  $k_f$ , and an intraparticle diffusion coefficient(s). The PSDM models intraparticle diffusion as diffusion along pore surfaces in parallel with diffusion through pore liquid (Weber and Smith 1987). The HSDM is identical to the PSDM except that diffusion through pore liquid is considered negligible compared to surface diffusion. Mathematical representation of both models is based on liquid- and solid-phase mass balance equations

written for each solute of interest. The one-dimensional liquid-phase mass balance equation is written (Weber and Smith 1987):

$$\frac{\partial C}{\partial t} = -v_z \frac{\partial C}{\partial z} + D_h \frac{\partial^2 C}{\partial z^2} - \rho_p \frac{(1-\epsilon_r)}{\epsilon_r} \frac{\partial q}{\partial t} \quad (2-23)$$

with the corresponding boundary conditions:

$$C = C_0 + \frac{D_h}{v_z} \frac{\partial C}{\partial z} \text{ at } z = 0 \quad (2-24)$$

$$\frac{\partial C}{\partial z} = 0 \text{ at } z = L \quad (2-25)$$

and the initial condition:

$$C = 0 \text{ at } 0 \leq z \leq L \text{ when } t = 0 \quad (2-26)$$

where  $C$  and  $q$  are liquid- and solid-phase concentrations, respectively;  $t$  is time;  $v_z$  is the interstitial fluid velocity in the direction of flow,  $z$ , along the fixed-bed reactor axis;  $D_h$  is the coefficient of hydrodynamic dispersion,  $\rho_p$  is the apparent particle density, and  $\epsilon_r$  is the reactor (bed) void fraction. The liquid-phase mass balance equation is coupled with the solid-phase mass balance equation, which incorporates, in general, both pore and surface intraparticle diffusion mechanisms. In spherical coordinates, this equation is written (Sonthheimer et al. 1989):

$$\rho_p \frac{\partial q}{\partial t} + \epsilon_p \frac{\partial C_p}{\partial t} = \frac{1}{r^2} \frac{\partial}{\partial r} \left[ r^2 \rho_p D_s \frac{\partial q}{\partial r} + r^2 \epsilon_p D_p \frac{\partial C_p}{\partial r} \right] \quad (2-27)$$

with the corresponding boundary conditions:

$$\rho_p \frac{\partial q}{\partial r} = \epsilon_p \frac{\partial C_p}{\partial r} = 0 \text{ at } r = 0 \quad (2-28)$$

$$k_f (C - C_{\text{surf}}) = \rho_p D_s \frac{\partial q}{\partial r} + \varepsilon_p D_p \frac{\partial C_p}{\partial r} \text{ at } r = R_p \quad (2-29)$$

$$C_{\text{surf}} = C_p \text{ at } r = R_p \quad (2-30)$$

and the initial conditions:

$$q = C_p = 0 \text{ at } t = 0 \quad (2-31)$$

where  $\varepsilon_p$  is the particle void fraction,  $C_p$  is the intraparticle pore concentration,  $r$  is the particle radius variable,  $R_p$  is the particle radius,  $D_s$  is the surface diffusion coefficient,  $D_p$  is the pore diffusion coefficient,  $k_f$  is the film mass transfer coefficient, and  $C_{\text{surf}}$  is the liquid concentration at the particle surface.

Equation 2-28 expresses radial symmetry at the particle center, and Equation 2-29 equates external mass-flux from the bulk liquid to the particle surface with the intraparticle flux, which is equivalent to assuming that no mass accumulates at the particle surface. Equation 2-30 expresses liquid-phase continuity from the particle surface to the internal pore. The amount adsorbed,  $q$ , is related to  $C_p$  and  $C_s$  through the adsorption isotherm relationship, which is equivalent to assuming local equilibrium at the particle surface and along the pore walls.

It is generally not possible to predict, *a priori*, which intraparticle diffusion mechanism will dominate; furthermore, when the PSDM is used to describe dynamic adsorption data, it is often not possible to determine both diffusion coefficients,  $D_s$  and  $D_p$ , uniquely (Sontheimer et al. 1989). However, attempts at modeling adsorption rates using only a pore diffusion mechanism has yielded  $D_p$  values in excess of free-liquid diffusivities, implying that an additional intraparticle transport mechanism was operative. This additional mechanism has been attributed to surface diffusion (Sontheimer et al. 1989).

Regardless of whether the PSDM or HSDM is selected to describe dynamic adsorption data, model input parameters consist of reactor characteristics which can be controlled or measured experimentally ( $v_z$ ,  $D_h$ , and  $\varepsilon_r$ ), adsorbent properties which can be

measured experimentally ( $\rho_p$ ,  $\varepsilon_p$ , and  $R_p$ ), phenomenological rate coefficients ( $k_f$ ,  $D_s$ , and/or  $D_p$ ) and parameters which characterize the equilibrium phase-distribution relationship (adsorption isotherm).

The effects of background DOM on adsorption processes and process modeling have been investigated (Lee et al. 1983, Pirbazari and Weber 1984, Fettig and Sontheimer 1987, Zimmer et al. 1988, Smith et al. 1987, Smith and Weber 1988, Smith and Weber 1989, Summers et al. 1989, Wilmanski 1990, Speth 1991, Carter et al. 1991). Because of their prevalence and relative stability, humic substances are thought to be the DOM component which most significantly affects SOC adsorption (Morel 1983, Fettig and Sontheimer 1987, Summers et al. 1989). The extent and rate of adsorption of SOCs on activated carbon preloaded with humic substances can be reduced significantly in comparison with non-preloaded carbon (Zimmer et al. 1988, Hand et al. 1989, Summers et al. 1989, Sontheimer et al. 1989, Carter et al. 1991). When both DOM and target SOCs are present and adsorbing simultaneously, DOM can compete with the target compound for adsorption sites (Pirbazari and Weber 1984, Smith et al. 1987, Smith and Weber 1989, Speth and Miltner 1989). SOCs have also been shown to associate with the dissolved organic matter in the solution phase and hence enhance the solubility of the target compound (Callaway et al. 1984, Chin and Weber 1989, 1990), reducing its affinity for adsorption from solution. The presence of DOM in adsorbent pores is also thought to reduce the intraparticle diffusion rate of target compounds (Zimmer et al. 1988, Pirbazari and Weber 1984, Smith et al. 1987, Smith and Weber 1988). Some researchers, however, have observed no effect of dissolved organic matter on equilibrium adsorption (Baldauf 1986).

Various approaches have been developed to incorporate the effects of DOM into the mathematical modeling methodology. Weber and Pirbazari (1982) determined rate and equilibrium parameters for the homogeneous surface diffusion model for numerous organic contaminants of environmental concern in waters containing various degrees of background organic matter. Model predictions which incorporated these parameters in the solution algorithm resulted in adequate prediction of fixed-bed performance for the compounds and conditions studied. Pirbazari et al. (1983) demonstrated that a similar methodology could

be employed to obtain reasonable predictions of breakthrough behavior for 1,2-dichloroethane in Ohio River water. Smith et al. (1987) used homogeneous surface diffusion model parameters determined in a background of uncharacterized commercial humic acid to obtain good predictions of the breakthrough of the pesticide lindane in pilot-scale studies. Smith and Weber (1988) adopted the same approach to successfully predict the removal of trichloroethylene and p-dichlorobenzene from a complex leachate-contaminated groundwater and from a laboratory-prepared water containing a mixture of known organic contaminants and uncharacterized commercial humic acids (Smith and Weber 1989).

While such approaches adequately predict adsorber performance for the system under study, they provide only limited insight into the detailed nature of interactions between target solutes, background dissolved organic matter, inorganic solution constituents, and adsorbent materials. Moreover, a general predictive methodology which applies to systems in which preloading occurs has not been developed, primarily because changes in adsorbent characteristics and adsorbent/adsorbate interactions which occur after preloading with DOM cannot be accounted for.

Some researchers have attempted to predict adsorber breakthrough using the Rapid Small-Scale Column Test, or RSSCT (Speth and Miltner 1989, Summers et al. 1989). The RSSCT method employs a physical, rather than mathematical model, to predict large-scale breakthrough profiles. Dimensions and operating conditions of small GAC columns are derived from dimensional analysis of the pore surface diffusion model. Data obtained in the resulting small column system are hypothesized to produce a breakthrough curve equivalent to the large column. The RSSCT method was not able to accurately reproduce breakthrough curves of large-scale systems in which preloading occurred. In other words, the effects of preloading could not be accurately scaled (Speth and Miltner 1989, Summers et al. 1989, Crittenden et al. 1991). Zimmer et al. (1988) incorporated an expression for a time-variable isotherm capacity into the pore surface diffusion model for adsorption of several SOCs from a groundwater based on isotherms conducted with preloaded GAC. The method predicted large-column behavior with reasonable success; however, due to the heterogeneous composition of natural waters, the time-variable capacity expression



developed in one application will not likely be transferable to any other. Speth and Miltner (1989) were able to obtain an adequate large column prediction of dichloroethene breakthrough in an Ohio groundwater using the pore surface diffusion model and parameter estimation techniques developed for simultaneously adsorbing systems, even though isotherm studies conducted with preloaded carbon indicated large decreases in equilibrium capacity due to preloading. Because the large column was run for a significantly shorter period of time than the preloading studies, however, the capacity of the large column was much closer to that obtained with fresh carbon than to that using preloaded carbon, and no direct comparison could be made. Carter et al. (1991) examined the preloading effect on activated carbon exposed to DOM in Huron River Water. Initially, a statistically significant decrease in overall GAC capacity for trichloroethylene with preloading time was observed. The decrease leveled off somewhat at the longest preloading times examined, suggesting a limiting effect. From these data, they concluded that at early preloading times, reductions in GAC capacity for the target compound were primarily due to direct competition with the DOM for adsorption sites. However, they found evidence that pore blockage may be the most significant mechanism of capacity reduction at extended preloading times. Similar trends were observed for carbon preloaded with polymaleic acid (unpublished data), a polymer which has been shown to exhibit elemental analyses, IR spectra, and acid hydrolysis products similar to naturally-occurring soil fulvic acids (Spiteller and Schnitzer, 1983).

The ultimate goal of GAC system modeling is to aid in the design of a full scale system. However, if the full-scale system is to treat a water containing DOM, it is certain that some amount of preloading will occur. Current methods used to model systems in which preloading occurs have not been generally reliable. It is clear that the methods currently employed do not properly account for factors critical to the accurate description of large column systems in which preloading is occurring. Clearly, research is needed to identify the key factors which must be addressed in modeling efforts to provide satisfactory predictions in preloading systems.

## 2.7 Implications for GAC Systems

Successful design of GAC systems in drinking water treatment hinges upon accurate representation of the impacts of DOM in the design process. Dissolved organic matter is comprised of compounds having a wide range of molecular weights, chemical moieties, and adsorption affinities that, when pre-adsorbed by GAC, may significantly alter the adsorption characteristics of target chemicals. Design protocols need to be developed which account for preloading phenomena. Critical to the development of any such design approach is a reasonable understanding of the mechanisms involved in the process, and a rational model on which to base design procedures. As yet, however, research has done little to illuminate the mechanistic basis for the preloading effect, nor has it provided any clear indication of what may be the most appropriate design approach.

The premise of this research is that a more fundamental understanding of preloading phenomena may be found by understanding the effects of DOM molecular weight distribution, adsorbent pore size distribution, and solution chemistry on DOM adsorption and the effect of preloaded organic matter on the subsequent adsorption of SOCs. Once the basic role each of these factors plays in heterogeneous adsorption is understood, the development of fundamentally-based GAC system design procedures can follow.

## CHAPTER III

### RESEARCH APPROACH AND DATA COLLECTION

#### 3.1 Research Approach

This Chapter is composed of two main sections. In the first section, Research Approach, the research approach and rationale are outlined briefly to provide an overall scope of the research and the methods of investigation. This section also discusses the selection of the model experimental systems studied. In the second section, Data Collection, specific details of experimental procedures and protocols are described. Approaches used to analyze data, and equations used to model and interpret data are developed in subsequent Chapters. In particular, Chapter 4 is devoted entirely to the development and application of methods for characterizing macromolecular size.

The overall objectives of the research were to investigate the adsorption of DOM and the effect of preloaded DOM on the subsequent adsorption of target contaminants. The goal was to provide information that could be incorporated into design protocols, mathematical models, and model parameter estimation methods. A literature review identified several areas of investigation that offered the most promise for furthering our understanding of DOM sorption and preloading phenomena. This research focuses on the chemical and physical polydispersity of DOM, the chemical and physical heterogeneity of adsorbent materials, and solution composition. Understanding how these factors affect preloading and the subsequent adsorption of target contaminants will form the basis for: i) the rational selection of pretreatment technologies; ii) the specification of optimal adsorbent properties, and iii) the development of appropriate modeling approaches.

Corresponding to these objectives, research was conducted at a level detailed enough to permit mechanistic interpretation of the data. Such an approach required that each component of the system—target species, background organic matter, and

adsorbate—be known and quantifiable. The research was divided into three phases; each phase is developed in detail in a separate chapter of this thesis. Pursuant to the hypothesis that molecular size and size distribution are critical factors governing the adsorption of DOM and hence the subsequent adsorption of SOCs on preloaded carbon, the first phase of this research was devoted to molecular size characterization and size fractionation. Ultrafiltration was developed as a technique for characterizing molecular size and for fractionating polydisperse mixtures of macromolecules. A single-parameter permeation model was verified using polystyrene sulfonate (PSS), a random-coil polymer available commercially in narrow molecular weight ranges. The model was used to characterize macromolecule size, and to design fractionation procedures. A natural humic material extracted from soil (Laurentian) was fractionated according to size. High-Performance Size-Exclusion Chromatography (HPSEC) was used to further characterize molecular size and size distributions of whole humic solutions and humic fractions. It was shown that size measurements made by the two different techniques were consistent, and the permeation factor determined from ultrafiltration measurements could be correlated with the weight-averaged molecular weight determined from the HPSEC chromatograms.

The second phase of the research investigated the adsorption of polyelectrolytes on activated carbon. Polystyrene sulfonate was selected as a model compound to investigate the impact of molecular weight and ionic strength for a molecule with a known and molecular-weight-invariant structure. Certain properties of PSS, however, may not accurately represent natural DOM. The sulfonate functional group, the high degree of charge on the molecule, and the linear structure of the molecule are probably not representative of natural materials. Therefore, PSS adsorption was studied to provide insight for interpreting the macromolecular nature of DOM adsorption behavior, not to mimic the effects of natural DOM.

The adsorption of humic acid size fractions prepared by ultrafiltration was measured to investigate the effect of macromolecule size, and to compare the trends exhibited by a natural material with those exhibited by polystyrene sulfonate. The adsorption of whole soil humic and fulvic acids was measured under a range of conditions to investigate the effects of solution polydispersity, ionic strength, divalent metal concentration, and adsorbent characteristics. The effects of polydispersity were investigated using an

"adsorptive fractionation" technique. Humic substances are comprised of a mixture of components having different adsorbabilities, which results in competitive interactions among components (Weber et al. 1983). Differences in the adsorbability of mixture components can be exploited to fractionate the mixture. Adsorptive fractionation is accomplished by conducting equilibrium experiments with different mass ratios of humic substance and adsorbent -- by contacting various amounts of adsorbent with humic acid solutions of varying initial concentration. Systems with low carbon concentrations (doses) or high initial concentrations will selectively remove the more preferentially-adsorbed components, thereby fractionating the DOM mixture (Summers and Roberts 1988a).

Humic acid isotherms were measured at different solution ionic strengths and with different divalent metal ion concentrations. The presence of inorganic ions can influence the structural configuration of humic macromolecules. Increases in ionic strength are known to decrease the effective size of macromolecular DOM in solution, potentially rendering it more adsorbable and hence better able to compete with specifically targeted pollutants for adsorption sites (Gosh and Schnitzer 1980, Jodellah and Weber 1985, Cornel et al. 1986, Chin et al. 1990). Ultrafiltration size measurements and HPSEC chromatograms were used to characterize and interpret polyelectrolyte adsorption behavior, and to identify reactive components of the humic mixture based on molecular size. Humic acid isotherms were measured using several different activated carbons exhibiting a range of pore-size distributions and surface charge to investigate the effects of adsorbent characteristics on macromolecule adsorption.

The third phase of the research consisted of i) assessing the mechanisms by which preloaded organic matter reduces the equilibrium extent of adsorption of SOCs, as reflected in the adsorption isotherm; and ii) measuring the effects of preloading on the adsorption of trichloroethylene (TCE), a widespread environmental pollutant. Preloading mechanisms were assessed by i) performing theoretical analyses using isotherm models developed from the theory of adsorption on heterogeneous surfaces, ii) making predictions of preloading effects in a model bi-solute system using the Ideal Adsorbed Solution Theory (IAST), and iii) verifying the theoretical prediction experimentally.

The effects of preloading on TCE adsorption were investigated by preloading activated carbon with humic and fulvic acids, humic acid fractions, and mixtures of humic

acid fractions. The effects of organic matter type, molecular size, initial molecular size distribution, extent of preloading, and preloading time were investigated. For these experiments, a representative ionic strength of 0.01-M was chosen. Whole humic solutions were preloaded on a representative water treatment carbon, under a variety of conditions to investigate the effects of solution ionic strength and calcium concentration. Whole humic solutions were also preloaded onto several different activated carbons exhibiting a range of pore-size distributions and surface chemistries to investigate the effects of adsorbent characteristics. Adsorbents were characterized by nitrogen gas adsorption at 77 K, acid and base neutralization techniques, and determination of the point of zero charge.

### Selection of Model Systems

The effects of dissolved organic matter on adsorption processes have been discussed in some detail. Based on the fact that a high percentage of natural organic matter is comprised of humic and fulvic acids, these substances were chosen as representative models of DOM in natural water. Recently, humic and fulvic substances extracted from Laurentian soil have become commercially available (Fredrik's Research Products, Amsterdam, The Netherlands). These materials were chosen to provide a reproducible reference point and to ensure experimental consistency. In addition, adsorption experiments were conducted with polystyrene sulfonate to provide a basis for interpreting the adsorption of humic substances. PSS was chosen because it is commercially available in environmentally-relevant molecular weights having narrow molecular-weight distributions. Furthermore, it is comprised of repeating units of known structure; therefore, chemical reactivity does not depend on molecular size. Concentrations of both PSS and humic substances used in adsorption experiments were generally representative of those found in natural systems, on the order of 2 to 15 mg/L dissolved total organic carbon (TOC); however, some experiments extended the adsorption isotherms to higher concentrations to obtain more mechanistic information.

Trichloroethylene (TCE, Mallinckrodt, Paris, KN) was chosen as the primary target pollutant employed in this work. TCE is used for metal degreasing, and in the paint and ink, electronic components, and rubber processing industries. It was selected because

it is a widespread contaminant, it has been designated as a priority pollutant by the USEPA, and it is a regulated compound under the Safe Drinking Water Act. Further, TCE can be analyzed accurately using liquid-liquid extraction into hexane followed by capillary column gas chromatography with electron capture detection. In one series of experiments, TCE adsorption on carbon preloaded with 1,2,4 trichlorobenzene (TCB, Aldrich Chemical, Milwaukee, WI) was studied.

TCB is used as a dye carrier, in degreasing agents, is an intermediate in the manufacture of herbicides, higher chlorinated benzenes, and dielectric fluids. TCB was chosen for these experiments because it is strongly adsorbing and because it is not displaced to a significant degree by TCE. It therefore mimics an important feature of preloading by natural humic substances. Studying a system containing two molecularly discrete solutes made it possible to make theoretical predictions of the impacts of non-displaceable preloaded organic matter on TCE adsorption. Single solute isotherms for TCE and TCB were measured and predictions of TCE adsorption in the bi-solute system were made using the Ideal Adsorbed Solution Theory. Theoretical predictions were verified with experimental results. Both TCE and TCB are expected to remain stable under the conditions of this research and do not hydrolyze significantly, or biodegrade at an appreciable rate under aerobic conditions (Howard 1990). Relevant physicochemical properties of TCE and TCB, including Henry's Constant,  $K_H$ , Log octanol-water partition coefficient,  $K_{oc}$ , and vapor pressure,  $P_v$ , are tabulated in Table 3-1 (Howard 1990).

**Table 3-1. Physical and Chemical Characteristics of TCE and TCB**

Solute	Molecular Weight	Solubility mg/L	$K_H$ atm- m <sup>3</sup> /mol	Log $K_{oc}$	$P_v$ , mm Hg (25°C)
TCE	131.40	1100.0 (25°C)	0.0103	2.42	69.0
TCB	181.46	48.8 (20°C)	0.0014	4.02	0.29

In this research, most experiments were conducted using a bituminous-coal based, granular activated carbon (F400, Calgon, Pittsburgh PA). F400 was chosen because it is widely used in water treatment applications, and because it has been studied extensively by researchers in our laboratory and elsewhere. However, in recognition of the fact that

adsorbent pore-size distribution and surface chemistry may affect the adsorption of humic substances and the subsequent adsorption of target compounds, a series of carbons which were manufactured from different raw materials, and were activated to different degrees were also examined. To some extent, differences in adsorbent characteristics relate to differences in the internal structures of the raw material (Hashimoto et al, 1979). One group of adsorbents (Calgon), was manufactured from bituminous coal, and included the F400, WPLL, FS100, and BPL carbons. A second group of adsorbents was manufactured from wood, and included the MICRO, MESO and MACRO carbons (Westvaco Chemical Co., Covington, VA). These are research adsorbents whose names signify their relative pore-size distributions.

In addition to the raw material type, the method and degree of activation also determines adsorbent characteristics. For the coal-based carbons, which were thermally activated, the differences in pore-size distribution are due to increased combustion (burnoff) of the raw material as a result of increased activation. The coal-based carbons selected for this study exhibit a range of microporosity (percentage of surface area in pores less than 10 Å radius) from 73.6 to 91.1 percent, and the range of surface area in pores of 10 to 50 Å radius is 8.5 to 25.6 percent. The degree of mesoporosity increases in the order WPLL < FS100 < F400 < BPL.

In contrast to the coal adsorbents, the wood-based adsorbents are chemically activated. By choosing appropriate acid mixtures and catalysts, different pore-size distributions can be developed while keeping the surface area relatively constant. The wood-based carbons selected for this study exhibit a range of microporosity from 52.5 to 83.3 percent, and the range of surface area in pores of 10 to 50 Å radius is 16.6 to 43.8 percent. The degree of mesoporosity increases in the order MICRO < MESO < MACRO. The structural characteristics of the different carbons, determined with a nitrogen adsorption analyzer (Quantachrome, Syosset, NY) at 77 K, are tabulated in Table 3-2.

The raw material and type of activation used to manufacture the carbon also has a significant impact on surface chemistry. The wood-based carbons have a more acidic character exemplified by a  $pH_{pzc}$  well below that of a neutral solution, while the coal-based carbons have a more basic character. At the pH of the adsorption experiments, the coal



**Table 3-2. Adsorbent Structure Characterization -- Nitrogen Adsorption Analysis**

Carbon Type	Surface Area, m <sup>2</sup> /g	Avg. Pore Radius, Å	Pore Volume, cm <sup>3</sup> /g	Percent Surface Area in Stated Range of Pore Widths			
				< 20 Å	20-100 Å	100 - 200 Å	> 200 Å
WPLL	294	11.58	0.171	91.1	8.5	0.25	0.15
FS100	751	11.33	0.433	86.6	12.5	0.60	0.30
BPLF3	1200	11.84	0.710	73.6	25.6	0.59	0.21
F400	948	12.00	0.566	83.7	15.0	0.90	0.40
MICRO	1593	9.95	0.793	83.3	16.6	0.09	0.01
MESO	1664	13.50	1.10	52.5	46.6	0.81	0.09
MACRO	1644	16.20	1.26	52.5	43.8	3.1	0.60

**Table 3-3. Adsorbent Surface Chemistry Characterization: Multibasic Surface Titration**

Carbon	HCl C <sub>0</sub> = 0.048 N meq/ 1000 m <sup>2</sup>	NaHCO <sub>3</sub> C <sub>0</sub> = 0.054 N meq/ 1000 m <sup>2</sup>	Na <sub>2</sub> CO <sub>3</sub> C <sub>0</sub> = 0.051 N meq/ 1000 m <sup>2</sup>	NaOH C <sub>0</sub> = 0.058 N meq/ 1000 m <sup>2</sup>	pH <sub>pzc</sub>
WPLL	1.26	0.44	0.54	0.85	9.20
FS100	0.61	0.23	0.27	0.47	9.25
F400	0.57	0.11	0.15	0.23	9.5
BPL	0.40	0.09	0.13	0.24	9.15
MICRO	0.31	0.20	0.38	0.65	5.35
MESO	0.26	0.17	0.31	0.52	5.05
MACRO	0.13	0.20	0.43	0.57	3.45

based carbons carry a net positive charge, while the surface of the wood-based carbons are negatively charged. The values for pH<sub>pzc</sub> measured in this study, and the trends in acidity with carbon source type, are in good agreement with those reported by Summers and Roberts (1988a) for similar carbons. Adsorbent surface chemistry, including the pH<sub>pzc</sub>,

was characterized by acid and base neutralization. The results of this characterization are tabulated in Table 3-3.

### 3.2 Data Collection

#### Water

Water used in all experiments was municipal (tap) water that was de-ionized, distilled, and filtered through a Milli-Q system (MQ-water; Millipore, Bedford MA). MQ-water was also used as a final rinse for all glassware used in experimental work.

#### Macromolecules

Polystyrene sulfonate was obtained in narrow molecular weight fractions from either Polysciences (Warrington, PA) or Pressure Chemical (Pittsburgh, PA). A major determinant in selection of the synthetic polymer, polystyrene sulfonate, was its availability in relatively narrow molecular weight fractions. Weight fractions used for adsorption and ultrafiltration studies included 1.8K, 5.4K, 8K, 18K, 35K, and 72K. (Molecular weights will be referred to using K to symbolize 1,000 daltons, i.e. 1.8K represents 1,800 daltons). The 1.8K molecular weight has a weight to number average molecular weight of 1.25 while the other sizes all have an  $M_w/M_n$  ratio of 1.10, indicating low polydispersity. The chemicals were used as received and stored in a desiccator. Stock solutions of PSS were made up in  $1 \times 10^{-3}$  phosphate buffer prior to each experiment, and solution ionic strength was adjusted with reagent-grade NaCl. Experiments were conducted at a pH of 7.0 +/- 0.20 unless otherwise indicated. Conductivity measurements confirmed that the PSS did not measurably contribute to the solution ionic strength at the PSS concentrations used in this study.

The bulk of the experimentation done in this research used soil humic and fulvic acids extracted from a Laurentian soil, which were obtained from Fredrik's Research Products. Various physical and chemical properties of these materials are tabulated in Table 3-4. The properties of these materials are consistent with representative values and trends reported in the literature, as discussed in Chapter 2 (Section 2.2). The humic acid has a higher carbon content and lower oxygen content than the fulvic acid. Further, the

fulvic acid exhibits a higher total and carboxylic acidity, although the humic acid has a higher phenolic acidity.

Humic substances used in this research were received as a dry powder. To solubilize the powder, about 0.5 g were weighed, dissolved into one liter of MQ-water adjusted to pH 10 (using NaOH), and stirred for a minimum of one hour. The solution pH was then adjusted to about 7.0 (using HCl), after which inorganic constituents were added and the solution was diluted to a stock concentration, generally 60 to 100 mg total organic carbon (TOC) per liter. Unless otherwise noted, the inorganic matrix consisted of  $10^{-3}$  M phosphate buffer, 100 mg/L (0.0015 M) sodium azide (a bacteriostat), and NaCl to yield an ionic strength of 0.01 M. In experiments which contained calcium, the phosphate buffer was omitted, and the solution pH was adjusted with either HCl or NaOH as required. As reported in Table 3-5, conductivity measurements confirmed that the humic substances prepared in this way did not measurably contribute to the solution ionic strength at the concentrations used in this study.

Humic acids obtained from Aldrich Chemical (Milwaukee, WI) were used in some ultrafiltration fractionation experiments. Aldrich humic acids were purified before use to reduce the high ash content of these materials as received from the manufacturer. The humic acids were received as a dry powder, and were solubilized as described above. The humic acid solution was purified by repeated: i) centrifugation of filtered humic solution at pH 11 to separate humic solution from a light-colored precipitate which was discarded; ii) precipitation of the humic material in 1.0-N HCl; and, iii) re-solubilization of the precipitate in 0.010-M NaOH. This process was repeated until no further light-colored precipitate was formed in the high-pH step. Purified humic material was lyophilized and stored in a desiccator until use.

To remove undissolved particulate matter, the stock solution was sequentially filtered through a 10-micron polyethylene filter, a 1-micron glass fiber filter and a 0.45-micron polysulfone (Gelman Sciences, Ann Arbor, MI) filter in a 122-mm diameter stainless-steel filter holder. Stock solutions were kept in refrigerated storage, in the dark, until use. The solution pH was checked prior to adsorption experiments and adjusted to  $7.0 \pm .1$  with HCl or NaOH as necessary.

**Table 3-4. Chemical Characterization of Laurentian Humic Substances**

Parameter	Fulvic Acid	Humic Acid
<u>Acidity, mmol/g</u>		
Total	11.6	7.6
Total Carboxyl	8.6	2.5
Carboxyl Type A	5.1	
Carboxyl Type B	3.5	
Phenolic	3.0	5.1
<u>Bidentate complexing capacity</u>		
	5.8	2.5
<u>Elemental Composition</u>		
C, wt %	45.1	51.9
H	4.1	5.5
N	1.1	2.3
O	49.7	39.9
Na, ppm	<1	6
K	<0.1	0.5
Ca	<0.1	4
Mg	<0.1	ND
Fe	<1	2
Data reported by manufacturer, from Sojo-Lopez, L.E. (1988) Ph.D. Dissertation, Department of Chemistry, Concordia University, Montreal, Canada.		

**Table 3-5. Conductivity Analysis -- Preloading Stocks**

Sample	I.S., M as NaCl	Cond, mS/cm
NaCl Standards	0.005	566
	0.01	1155
	0.05	5195
	0.10	9905
HA Stock 57 mg TOC/L	0.01	1068
FA Stock 47 mg TOC/L	0.01	1111
Note: Conductivity data represents an average of 3 trials obtained after stabilization of reading, which generally took three to four rinses of the conductivity probe.		

### Low-Molecular-Weight Synthetic Organic Chemicals

TCE (Mallinckrodt Specialty Chemical, Paris, KN) and TCB (Aldrich Chemical, Milwaukee, WI) used in this research was reagent grade (pesticide free) and was used without further purification. Stock solutions were prepared in 50 ml serum vials sealed with Teflon-lined rubber septa and aluminum crimp-seals. A microliter quantity of TCE or TCB was injected into spectrophotometric-grade methanol (Mallinckrodt Specialty Chemical, Paris, KN) and quantified gravimetrically. Stock concentrations ranged from 400 to 5000 mg/L. Working solutions were prepared by spiking background water with a desired amount of stock solution to achieve the desired initial concentration of solute. Stock concentrations and spike volumes were designed to maintain methanol concentrations below  $10^{-3}$  mole fraction; below this concentration methanol as a co-solvent does not have a significant effect on adsorption (Wauchope and Koskinen 1983, Curtis 1984). This conclusion is consistent with estimates of co-solvent effects made using the model proposed by Nkedi-Kizza et al. (1985).

Background solutions consisted of  $10^{-3}$  M phosphate (Mallinckrodt Specialty Chemical, Paris, KN) to buffer pH, , 100 mg/L sodium azide (Fluka AG, Fuchs, Switzerland, purum p.a. grade) to control biological activity, and sodium chloride to achieve an ionic strength of 0.01 M. All chemicals were reagent grade and were used as received from the manufacturer. Experiments were conducted at room temperature ( $23 \pm 3$  °C) at pH  $7 \pm 0.2$  with pH adjustment by either HCl or NaOH as required.

### Activated Carbon Adsorbents

Activated carbons obtained from the manufacturer were crushed using a three-blade blender and were mechanically sieved to uniform particle sizes using U.S. standard sieves on a rota-tap mechanical shaker. Two particle sizes were used in this research. The 58-micron particles (geometric mean diameter) include those that passed the #200 and were retained on the #325 sieve; the 165-micron particles include those that passed the #80 and were retained on the #100 sieve. Size fractions were washed with Milli-Q water, oven dried at 105 °C to constant weight, and stored in a desiccator until use. Prior to using, an aliquot of carbon (generally 1 to 2 g) was retrieved from the desiccator, sonicated for 30

sec in Milli-Q water, washed free of fines, and oven dried at 105 °C to constant weight. The sonication procedure has been recommended by Summers et al. (1992) to reduce the amount of fines produced during the adsorption experiment.

#### Adsorption Isotherms: General Considerations

While an isotherm is defined on the basis of equilibrium partitioning, in systems exhibiting very slow adsorption rates, such as macromolecule adsorption by activated carbon, it may be desirable to define an "operational" equilibrium. Long equilibration times may result in only marginal increases in amount adsorbed, and may compromise solute stability. Of particular concern are volatility losses from the reactor, partitioning into reactor components, and hydrolysis and biodegradation reactions. To assure that the operational equilibrium is close to a true equilibrium, a common practice is to reduce the necessary equilibration time required by using a particle size smaller than what would normally be used in a full-scale system. This approach exploits the fact that adsorption rates increase with decreasing particle size. In this study, two particle sizes, 58 and 165 micron, were chosen. To determine a suitable operational equilibration period, adsorption rate studies, conducted by observing the amount adsorbed as a function of time, were performed. Based on several rate studies, operational equilibration periods for PSS, humic substances, and TCE were chosen. The experimental methods for rate data collection are discussed in the following section, while the theoretical basis for choosing equilibration periods and experimental verification of the theoretical analysis will be discussed in detail in Chapter 5.

#### Macromolecule Adsorption Isotherms and Rate Studies

Isotherms and rate studies were conducted using the bottle-point method in either 20, 50 or 100 ml vials sealed with Teflon-lined rubber septa. The 20-ml vials were a screw-cap type while the 50 and 100 ml vials were serum vials which used aluminum crimp-seals. Activated carbon, prepared as outlined above, was weighed into individual vials using an analytical balance. Diluted stock solution (generally 12 to 60 mg TOC/L) was pipetted into each vial, which was immediately capped, wrapped in bubble-wrap and

placed on a rotary tumbler for the desired equilibration time. After the equilibration period, reactors were sampled with glass syringes, and the solution was filtered through 0.45-micron polysulfone filter (Supor, Gelman Sciences). Macromolecule concentrations were quantified by total organic carbon (TOC) analysis and UV spectrophotometry (Varian Optical, Victoria, Australia). PSS was quantified at 224 nm while humic solutions, which contained azide, were quantified at 300 nm; in both cases, a solution which contained the identical inorganic composition as the macromolecule solution was used as a reference blank. The range of conditions used in adsorption experiments is tabulated in Table 3-6.

TOC measurements were made on a TOC analyzer (Model TOC-500, Shimadzu, Japan); TOC was determined as the difference between total carbon and inorganic carbon. Total carbon was determined by combustion of the sample on a platinum-coated alumina catalyst at 650 °C and infrared detection of the evolved CO<sub>2</sub>. External standards were prepared with potassium hydrogen phthalate, KH<sub>2</sub>P<sub>2</sub>O<sub>7</sub> (Fluka AG, Fuchs, Switzerland). A 200 mg/L stock solution was prepared in MQ water adjusted to pH 2 to inhibit microbial activity and contamination from inorganic carbon. The stock solution was diluted down to a working stock solution with MQ water which was further diluted for standards. Standards were prepared fresh daily, and two sets of standards were run for each isotherm determination. Inorganic carbon was determined by passing the sample over an acid-treated quartz bed reactor at 150 °C, and infrared detection of the evolved CO<sub>2</sub>. Experiments were performed to compare the instrument response to inorganic and organic carbon. Using potassium hydrogen phthalate (Fluka AG, Fuchs, Switzerland) and carbonate solutions, it was found that an equivalent mass of either type of carbon would produce an identical machine response. Therefore, a separate calibration curve for inorganic carbon was not developed.

MQ-water was run as a TOC blank, and the area counts of phthalate standard were corrected by subtracting blank area counts. The TOC of the MQ-water consistently ranged from 0.1 to 0.3 mg TOC/L.

One isotherm experiment generally consisted of 10 to 15 different conditions, with duplicates and several vials without carbon to serve as blank controls. Stock solutions were sampled for immediate UV and TOC analysis and these results were compared to the

**Table 3-6. Conditions Used in Macromolecule Adsorption Isotherm Experiments**

Isotherm Experiment	$D_0$ , g/L	$q_e/C_0$ , mg/g	$C_e/C_0$	Particle Size	Time, days
PSS	0.10 - 3.15	0.05 - 6.0	0.001 - 0.904	200/325	14 - 22
PSS	0.10 - 3.15	0.05 - 6.0	0.001 - 0.904	80/100	90
HA/FA	0.10 - 2.00	0.39 - 2.9	0.042 - 0.768	200/325	27 - 30
HA/FA	0.10 - 2.00	0.39 - 2.9	0.042 - 0.768	80/100	27 - 30
HA Preloading	0.25 - 4.00	0.31 - 1.4	0.473 - 0.785	80/100	30
HA Fractions	0.15 - 1.30	0.49 - 4.8	0.007 - 0.898	80/100	30
UF Supernatant	0.10 - 1.30	0.64 - 3.2	0.160 - 0.677	200/325	27 - 30

blank controls after equilibration. Based on the results of control vials, there was no measurable loss of macromolecular substances from the reactors, and all changes in concentration in the aqueous-phase of reactors containing carbon was attributed to adsorption.

#### HA Preloading Supernatant Isotherms

Activated carbon (165-micron particle size F400) was preloaded for 30 days according to the conditions listed in Table 3-6. After obtaining samples from the preloading reactors for TOC and UV measurements, supernatant solutions were filtered on a 47-mm diameter membrane filter having a 0.45-micron pore size ( Type HA, Millipore, Bedford, MA,). Filtered solutions were then diluted to approximately 6.5 mg/L prior to conducting variable-dose isotherms on 58-micron F400 carbon. The nominal pH and ionic strength values for both the preloading and the preloading supernatant isotherms were 6.8 and 0.01 M respectively. Preloading supernatant isotherm parameters were obtained by regressing the amount adsorbed,  $q_e$  (mg/g) against the liquid phase concentration normalized by the adsorbent dose,  $C_e/D_0$  (mg/g) using the log-linearized form of the Freundlich isotherm equation. The dose normalization was done to control for slight differences in the initial concentration and the competitive effects of humic acid components. For each isotherm, both UV and TOC measurements were obtained for every sample. A UV/TOC correlation was established for each isotherm, and was used to



compute TOC values from measured absorbances. This procedure was used to take advantage of the greater precision of UV measurements while accounting for differences in the UV/TOC relationships resulting from variations in supernatant solution composition.

#### Humic Substance Preloading

Activated carbon was preloaded with humic acid by two different methods. Most of the preloading was conducted in 1-liter amber-colored glass bottles sealed with poly-seal liners. The large reactor volume provided ample supernatant solution and a large sample of preloaded adsorbent which was used for further experiments. Reactors were mixed on a rotary tumbler for an operational equilibration period of 30 days. Supernatant solution was filtered through a 0.45-micron filter and stored for further analysis by ultrafiltration and size-exclusion chromatography. Activated carbon was recovered from these reactors by vacuum filtration on a 0.2-micron filter and washed. Speth (1991) found that washing or mechanically scouring the GAC surface did not in any way mitigate the impacts of preloading. The carbon was dried under vacuum in a desiccator for a period of 14 days; preliminary experiments demonstrated that this time was sufficient to reduce the moisture content to below measurable levels. Samples were stored in a desiccator under vacuum.

A second method of preloading was necessitated because the supply of material available from some ultrafiltration fractionation experiments was not sufficient to conduct preloading in large-scale reactors. Therefore, some carbon was preloaded directly in the 250-ml bottles used for the TCE isotherm. First, the adsorbent was contacted with a humic acid solution for a period of several weeks. After the preloading period, TCE was spiked into the reactor, and allowed to equilibrate for an additional two weeks. Speth (1991) measured preloading isotherms for dichloroethene, and compared these two different techniques for preparing preloaded carbon. Identical isotherms were measured regardless of whether the carbon was used in a wet state or vacuum and desiccant dried.

A common approach in many preloading studies is to preload a large particle size carbon, which is subsequently crushed prior to conducting the target compound isotherm. The carbon is crushed to reduce the time required to reach equilibrium. However, Carter et al. (1992) showed that crushing preloaded carbons tends to restore some of the virgin carbon capacity, probably as a result of opening blocked or otherwise previously

inaccessible micropores. Therefore, to avoid the need to crush the carbon, the approach taken in this study was to preload the particle size selected for the TCE isotherm.

### Measurement of TCE Isotherms

Isotherm experiments were conducted using the completely mixed batch reactor (CMBR) method, in which each point on an adsorption isotherm is obtained from an independent experiment conducted in one of a set of individual CMBRs. The reactors consisted of 250-ml amber-colored glass bottles sealed with screw caps and Teflon-lined silicone septa. A predetermined mass of carbon was weighed on an analytical balance and added to each batch reactor, which was then partially filled with buffer solution. The batch reactor was then spiked with a microliter aliquot of stock solution to obtain the desired initial concentration. The reactor was then filled completely and sealed with no headspace. The reactors were kept well mixed by tumbling end-over-end on a rotary tumbler for a period of two weeks. Preliminary rate studies indicated that this time was sufficient to reach equilibrium.

After the equilibration period, reactors were sampled with glass pipettes, and extracted into hexane for quantification by a gas chromatograph with a large-bore column, and an electron capture detector (Model 5890, Hewlett Packard, Palo Alto, CA). The detector signal was integrated electronically using the HPCHEM software (Hewlett Packard, Palo Alto, CA). The gas chromatograph was calibrated using external standards which were prepared in aqueous solution using a spiking technique similar to that used in the isotherm experiments, and were extracted into hexane using the same procedure as for the samples.

The mass adsorbed was calculated by the difference between the initial ( $C_0V$ ) and final ( $C_eV$ ) solution phase solute mass; reactor volume ( $V$ ) was determined for each CMBR by weighing the reactor empty and filled with MQ water.

Potential losses resulting from volatilization, sorption onto reactor components, or bacterial activity, were assessed with control reactors which did not contain adsorbent. Losses in these experiments were consistently less than 5%. Because these losses were low, and because the percentage of initial mass adsorbed was high, no attempt at correction for losses was made.

### TCB Preloading of F400 Carbon

TCB was preloaded onto aliquots of activated carbon using the TCE isotherm procedure outlined above. Individual batch reactors were spiked with a 10,000 mg/L trichlorobenzene stock solution. A microliter quantity of TCB stock was injected to yield an initial concentration calculated to result in a predetermined amount adsorbed based on preliminary isotherm experiments. The batch reactor was then filled completely and sealed free of headspace. The batch reactors were kept well mixed by tumbling end-over-end on a rotary tumbler for a period of two weeks. Preliminary rate studies indicated that this time was sufficient to reach equilibrium for TCB.

After the carbon equilibrated with TCB, the reactors were carefully opened and spiked with TCE from either a 400 or 5,000 mg/L stock prepared in methanol. A range of initial concentrations were chosen to yield equilibrium concentrations ranging from about 2 to about 2,000 µg/L. The reactors were then tumbled for two weeks, after which the reactor contents were sampled. Aqueous samples were withdrawn from each reactor using a glass pipette, and were extracted into pesticide-free hexane (Ultra resi-analyzed, J. T. Baker). The TCE and TCB concentrations in the hexane were determined by gas chromatography with electron capture detection as described above. The combined analytical accuracy for the extraction and GC determination of TCE and TCB was determined by repeated measurements of known concentrations (standards). The results of this analysis are shown in Table 3-7.

### Permeation and Fractionation Experiments

The macromolecular solutions used in the permeation and fractionation experiments were prepared as previously described. The solutions were fractionated in a pumped ultrafiltration system (Model CH2RPS, Amicon, Danvers, MA) incorporating hydrophilic, neutral, cellulosic-type spiral-wound membranes having nominal molecular-weight cutoffs of 100K, 30K, 10K and 3K. At the beginning and end of each run, the membranes were washed with a 0.01-M solution of NaOH and thoroughly rinsed with MQ-water until no change in the MQ-water pH was detected. At the conclusion of each run, membranes were

**Table 3-7. Analytical Error in TCE and TCB Determinations**

Concentration	Number of Samples	95% C.I.	% Error
<u>TCE</u>			
12.4	26	0.4	3
98.7	44	0.7	<1
398	10	6	2
1043	32	5	<1
<u>TCB</u>			
10.8	24	0.3	3
977	30	3	<1
2009	24	4	<1

rinsed with MQ-water, washed with a 0.01-M solution of NaOH and rinsed with MQ-water, per manufacturers recommendations. Membranes were stored in a refrigerator when not in use. Recirculation flowrate was 0.833 L/min and applied membrane pressure was 30 psig for all permeation factor determinations, although preliminary experiments indicated that permeation factor values determined using an applied pressure of 20 psig were not statistically different. Therefore, pressure affects the rate of volume throughput but not intrinsic solute permeation. Fractionation experiments were conducted at applied pressures of either 20 or 30 psig.

Solution concentrations of polystyrene sulfonate polymer were measured by ultraviolet spectroscopy at a wavelength of 224 nm, and humic substances were measured at either 224 or 300 nm, using a U.V./Visible spectrophotometer (Varian Optical, Victoria, Australia), as described previously. Theoretical development of models used to characterize solute transport in ultrafiltration systems, and approaches used for data analysis and interpretation, are fully developed in Chapter 4.

#### Size Exclusion Chromatography

High-Performance Size Exclusion Chromatography (HPSEC) was carried out on a glycol-functionalized silica column with a 125 Å pore size (Protein-Pak 125, Waters,

Milford, MA). This column packing exhibits low residual hydrophobicity and minimal ion-exchange capacity (Chin et al. 1994). Instrumentation included a solvent pump (Model 510, Waters, Milford, MA), a tunable absorbance detector (Model 486, Waters, Milford, MA), and a rotary injection valve equipped with a 20  $\mu$ L sample loop. A flowrate of 1 ml/min. was used for all experiments. All compounds except acetone were detected at a wavelength of 224 nm, and acetone was detected at 280 nm. Data were collected by Maxima GPC computer software (Waters, Milford, MA), and data manipulation and peak integrations were done using spreadsheet software (123, Lotus Development, Cambridge, MA).

Ideally, HPSEC systems should be calibrated with compounds having identical structure as the samples being analyzed. When the samples are polyelectrolytes, their structure and potential interactions with the stationary phase may depend, in part, on solution pH and ionic strength. Despite recent advances in bonded stationary phases, a number of researchers have noted that chromatograms determined using size exclusion chromatography may depend on the eluent composition (Miles and Brezonik 1983, Knuutinen et al. 1988). A number of researchers studying different molecular size characterization techniques have observed that systems calibrated with globular proteins may significantly overestimate the molecular weights of humic substances and other polymers (Beckett et al. 1987, Reid et al. 1990, Chin and Gshwend 1991, Kilduff and Weber 1992). To overcome this limitation, several investigators have calibrated their systems with polymers, including polysaccharides (Rausa et al. 1991) and polystyrene sulfonates (Beckett et al. 1990, Chin et al 1991, Kilduff and Weber 1992). Chin and Gschwend (1991) found that the coiled configuration of polystyrene sulfonate standards and Suwanee fulvic acid (an International Humic Substance Society (IHSS) standard) were nearly identical when a mobile-phase ionic strength equivalent to 0.10 M NaCl and pH of 6.8 was used. Saito and Hayano (1979) used the same mobile phase composition and found that chromatograms of humic and fulvic acids were independent of flowrate and mass-injected. Therefore, in this research, a mobile phase with an ionic strength of 0.10 M buffered to pH 6.8 was used. The salt composition of all samples was adjusted to yield an ionic strength of 0.10 M prior to chromatographic analysis to eliminate artifacts arising from dynamic coiling phenomena during sample transport through the chromatographic

system (Chin and Gshwend 1991). Theoretical development of models used to characterize molecular size distributions, and approaches used for data analysis and interpretation, are fully developed in Chapter 4.

## CHAPTER IV

### MACROMOLECULE SIZE CHARACTERIZATION AND FRACTIONATION

#### 4.1 Introduction

The objectives of this research required techniques to fractionate polydisperse mixtures of macromolecules (natural humic substances), characterize molecular size under environmentally-relevant conditions, and measure molecular-weight distributions. Ultrafiltration was chosen to fractionate solutions of macromolecules because it is a relatively inexpensive, versatile, expedient, simple, non-destructive and a reagent-free technique (Buffle et al. 1978, Logan and Jiang 1990). Advantages of ultrafiltration in this regard include the ability to process large volumes of sample (Logan and Jiang 1990) without having to modify solution chemistry (i.e., ionic strength) or pre-concentrate the macromolecular analyte. Ultrafiltration was also used to characterize macromolecule size under environmental conditions by modeling solute flux with a permeation model based on membrane flux equations. Macromolecule transport behavior was characterized by a single semi-empirical model parameter, the membrane permeation factor.

Methods for characterizing the size of macromolecules in solution include size exclusion chromatography (Chin and Gschwend 1991), ultrafiltration (Amy et al. 1987), field flow fractionation (Beckett et al. 1987), analytical UV scanning ultracentrifugation (Reid et al. 1990), vapor pressure osmometry (Reuter and Perdue 1981), pressure area isotherms (Hayase 1992), and measurements of macromolecule diffusion (Cornel et al. 1986). A detailed comparative assessment of these techniques is beyond the scope of this work. Despite the many advantages of the ultrafiltration technique, the method is poorly suited to measuring well-resolved molecular size or weight distributions. After a

preliminary assessment of the other methods available, high-performance size-exclusion chromatography (HPSEC) was chosen to characterize molecular-weight distributions.

HPSEC was used to measure molecular-weight distributions relative to polystyrene sulfonate standards, and the distributions were characterized in terms of weight-averaged molecular weights. Recent developments in this technique have resulted in improved resolution and have eliminated the need for sample pre-concentration. Sample ionic strengths were adjusted to a relatively high value (0.10 M) to minimize interaction between macromolecules in solution and the column packing. High ionic strengths also promote more compact macromolecular structures, thus providing a more consistent basis for molecular weight measurements. As a result, however, the technique is not useful for characterizing macromolecule size under ambient (environmental) conditions. HPSEC provides a fundamental measure of molecular weight, therefore, while ultrafiltration provides operational, system specific measure of molecular size. The two techniques provide a complementary and comprehensive characterization of macromolecule size.

In this chapter, the development and application of ultrafiltration as a process for characterizing macromolecule size will be presented. The permeation model was validated for describing the transport of random-coil polymers in ultrafiltration systems, and the effects of system operating variables and solution ionic strength were systematically investigated. The model was used to characterize macromolecule size in terms of the permeation factor, to measure membrane cutoff values applicable to charged macromolecules, and to design fractionation protocols. The application of HPSEC to characterize molecular-weight distributions of natural humic substances and size fractions prepared using ultrafiltration is demonstrated, and size characterizations made by the two techniques are compared.

## **4.2 Ultrafiltration Processes**

Ultrafiltration membranes are typically characterized by molecular weight cutoff (MWC) values established by calibrating a membrane using molecules of known molecular weight. Membrane manufacturers generally calibrate membranes and specify cutoff values based on the rejection characteristics of globular molecules. The accuracy of a specified



molecular weight cutoff depends primarily on how closely the fractionated molecules resemble the molecules used to calibrate the membrane. Gosh and Schnitzer (1980) characterized the structure of humic and fulvic acids as flexible linear colloids under conditions of pH and ionic strength typical of natural waters; changes in configuration ("coiling") in response to changes in ionic strength or pH were observed. It would therefore seem most logical that membranes used for the ultrafiltration of natural organic matter be calibrated with molecules which exhibit similar behavior. Molecules which exhibit this behavior include charged random-coil polymers, macromolecules which have sufficient flexibility to take on random configurations under the influence of thermal energy, and which coil in response to changes in solution pH or ionic strength.

The reports of many ultrafiltration separations of natural organic polymers detailed in the literature indicate that results may depend, to varying degrees, on several physicochemical parameters including concentration, ionic strength, and pH. High solute concentrations promote the accumulation of solute at the membrane surface, which induces upgradient diffusive transport of solute away from the membrane in a direction opposite to permeate flow. This phenomenon, referred to as concentration polarization, may affect the measurement of solute rejection and corresponding molecular-weight distributions (Buffle et al. 1978, Woerner and McCarthy 1986). Logan (1990) states that mass accumulation at a membrane surface is minimized at dissolved organic levels below 100 mg/L, a criterion satisfied for most natural waters and pretreated wastewaters.

An increase in solution ionic strength causes charged macromolecules to coil, compress or otherwise reduce their size in solution, reducing their retention on a given membrane (Brown 1975, Kwak and Nelson 1977, Woerner and McCarthy 1986). As a result, molecular-weight distributions measured for polyelectrolytes depend, in part, on solution ionic strength (Cornel et al. 1986, Kwak and Nelson 1977). The retention characteristics of neutral macromolecules (i.e., polyethylene glycol), however, are not influenced significantly by ionic strength (Cornel et al. 1986). It is expected that solution pH may influence macromolecule configuration depending on the pK values of functional groups present on the macromolecules and on the solution ionic strength.

Because solute transport in ultrafiltration systems may depend on many different physicochemical parameters and operating variables, membrane rejection must be explicitly accounted for to derive meaningful values of molecular size from ultrafiltration measurements (Logan and Jiang 1990). If membrane rejection is not accounted for, the results of molecular weight determinations are dependent upon the degree of sample concentration or diafiltration used in a particular experiment, which makes it difficult to compare results obtained under different conditions. As a result, application of the technique as an analytical tool has been limited to process monitoring and natural water characterization based on relative differences in measured molecular-weight distributions (Amy et al. 1987). Ultrafiltration systems have also been used to preparatively fractionate humic solutions for a variety of research applications. However, if the rejection characteristics of a particular membrane/solute system are not well characterized, incomplete separations may result, leading to apparently anomalous results (Cornel et al. 1986).

Single-parameter transport models, which incorporate macromolecule rejection in terms of a model coefficient, have been shown to provide a basis for characterizing macromolecule size, determining molecular-weight distributions and for designing fractionation procedures that are independent of the mode of operation or of such operational variables as the degree of sample concentration or diafiltration. Equations have been developed for determining rejection factors ( $R$ ) from ultrafiltration data for both continuous batch operation (diafiltration) and discontinuous batch operation (concentration) (Porter and Nelson 1972, Blatt 1976). Buffle et al. (1978) used a permeation model to characterize the ultrafiltration of glycine, citric acid and natural water samples. More recently, Logan and Jiang (1990) developed a method for determining molecular-weight distributions based on fitting a permeation model to ultrafiltration membrane permeation data. This method quantifies membrane rejection and initial concentration of solutes smaller than the membrane cutoff value independent of the volume of sample filtered. While application of the permeation model is increasing, there has been no effort to validate the model for describing the transport of random-coil polymers, or to investigate the effects of system operating variables and solution ionic strength. In doing so, this work expands

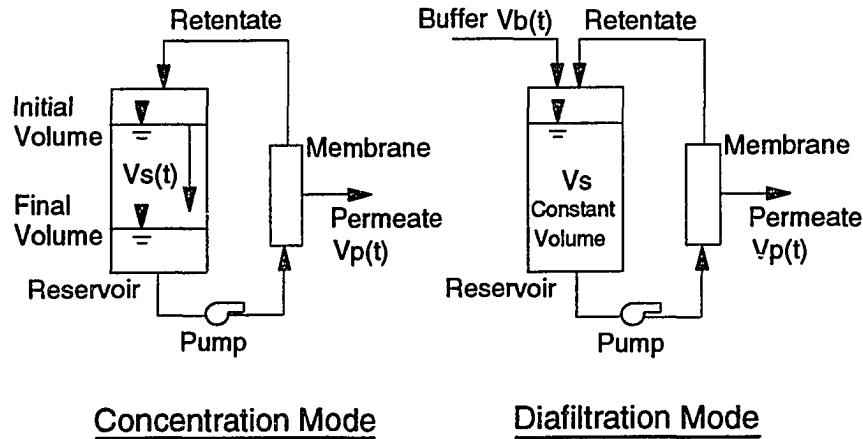


Figure 4-1. Schematic depiction of the experimental ultrafiltration system illustrating the two different modes of operation.

the usefulness of the ultrafiltration process and furthers the development of permeation factor models.

### 4.3 Ultrafiltration System Operation and Characterization

The ultrafiltration system employed in this study consists of a reservoir, a peristaltic pump, and a spiral-wound membrane cartridge, as indicated schematically in Figure 4-1. Process solution is pumped from the reservoir into the membrane cartridge; permeate flow is diverted to a collection line, and the flow which does not permeate the membrane (retentate) is recycled back to the reservoir. Pressure drop across the membrane is controlled by a valve on the retentate line and by the pump speed (flowrate). The flowrate is maintained as high as possible within the manufacturer's recommendations to maximize cross-flow velocity, and thus minimize concentration gradients at the membrane surface.

As also illustrated in Figure 4-1, the ultrafiltration process can be operated in two distinct modes, diafiltration and concentration. Each operating mode has different operating characteristics. In the diafiltration mode, the system volume ( $V_s$ ) is maintained

constant by replacing the volume lost as permeate with solute-free buffer solution. Because the system volume is constant, the concentration of retained macromolecules -- solutes with a permeation factor of zero -- remains constant. The concentration of permeating molecules -- solutes with a permeation factor greater than zero -- decreases over time in both the reservoir and the permeate. The ultrafiltration system is operated until a chosen filtration volume,  $V_f$ , has permeated the membrane.

In the concentration mode, the system volume is not held constant; the initial solution volume,  $V_0$ , is concentrated to a final retentate volume,  $V_r$ . In this mode, the concentrations of all molecules having permeation factors less than unity increase over time, in both the reservoir and the permeate.

### System Characterization

The semi-batch ultrafiltration system was characterized in terms of mixing conditions, solvent flux characteristics, and salt rejection. Simplifying assumptions applied to subsequent model development were based on the results of this characterization. The recycle configuration of the semi-batch system configuration allows operational flexibility to obtain backmixing conditions which approximate completely mixed flow, thereby simplifying the system mass-balance equations. A macroscopic modeling approach was used, primarily because the cartridge-type membrane configuration does not facilitate a more mechanistic approach, and because the resulting model equations are more readily solved and implemented. A tracer study was performed with the 3K and 100K MWC membranes to verify that the mass distribution within the reactor system approached well-mixed conditions. The reservoir was filled with a UV-absorbing tracer solute, sodium azide, which was then diafiltered with several liters of tracer-free water. Under the assumption of complete mixing, the integrated mass-balance equation for these conditions has the form:

$$-\ln\left(\frac{C}{C_0}\right) = \frac{Q}{V_s} t = \frac{V_p}{V_s} \quad (4-1)$$

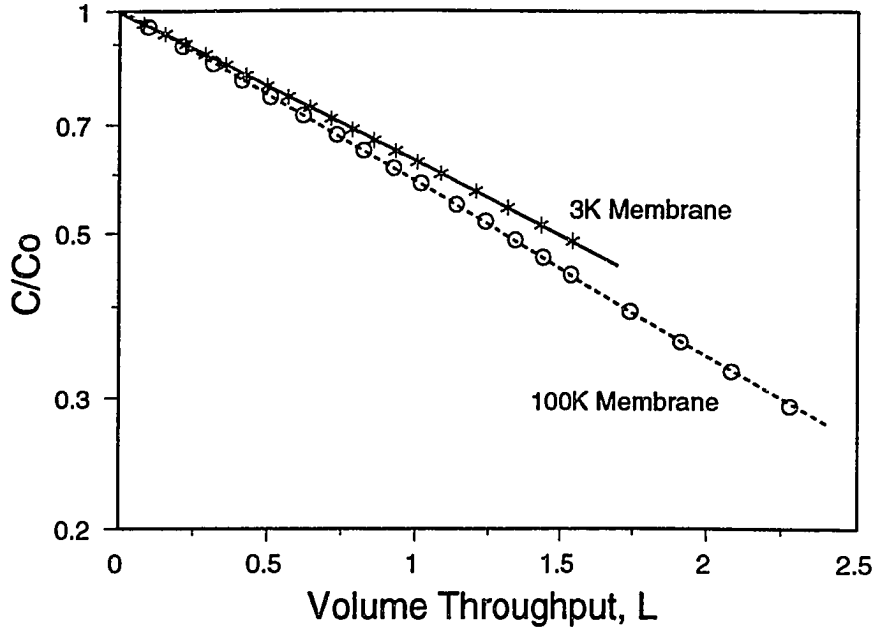


Figure 4-2. Characterization of mixing conditions in the experimental ultrafiltration reactor. Data are normalized by the linearized mass-balance model which assumes completely mixed conditions.

where  $C$  is the tracer concentration in the ultrafiltration system at any time  $t$ ,  $C_0$  is the initial tracer concentration,  $Q$  is the volumetric permeate flow, and  $V_p$  is the permeate volume throughput at any time  $t$ . A plot of  $\ln C/C_0$  versus  $V_p$ , therefore, should be linear with a slope equal to  $-1/V_s$ . Tracer study results are plotted in Figure 4-2. The linearity of the data plotted in the form of Equation 4-1 demonstrates that the behavior of the system closely approaches completely mixed conditions.

The primary driving force for solvent flux across an ultrafiltration membrane is a net pressure gradient,  $\Delta p_n$ . The total volumetric flux,  $J_v$ , of solvent (water) across the membrane is given by Soltanieh and Gill (1981):

$$J_v = L_p \Delta p_n = L_p (\Delta p_a - \sigma \Delta \Pi) \quad (4-2)$$

where  $L_p$  is the "filtration coefficient" or coefficient of hydraulic conductivity,  $\Delta p_a$  is the applied pressure,  $\Delta \Pi$  is the osmotic pressure (equal to zero in the absence of a retained solute), and  $\sigma$  is a solute "reflection coefficient." The value of  $\sigma$  is equal to zero if the

membrane is equally permeable to both solute and solvent, and equal to unity if the solute is completely rejected. The coefficient of hydraulic conductivity is directly proportional to the membrane porosity,  $\epsilon$ , the square of the pore radius,  $r$ , and the liquid density ( $\rho_l$ ); and is inversely proportional to the membrane thickness,  $\delta$ , liquid viscosity,  $\mu$ , and the square of the tortuosity factor,  $\tau$  (Weber 1972):

$$L_p = \frac{\epsilon r^2 \rho_l}{8 \tau^2 \mu \delta} \quad (4-3)$$

The hydraulic conductivity of each membrane studied was determined as the slope of a plot of water flux as a function of applied pressure, as shown in Figure 4-3. A linear relationship is predicted from theory, and such a relationship was observed for the 3K and 10K MWC membranes at pressures up to 50 psig. However, the 30K and 100K MWC membranes showed linear behavior only up to 30 and 20 psig, respectively. The non-linearity of the larger MWC membranes at high pressures may be due to some degree of membrane compression, influencing the membrane pore structure (Michaels 1968). Only the 100K MWC membrane exhibited slight non-linear behavior at 30 psig; therefore, this pressure was chosen as a reasonable compromise between high flux rates and low membrane distortion.

The exclusion of ions by the membrane and subsequent accumulation at the membrane surface could influence the transport of charged macromolecules and could result in a time-dependent ionic strength effect. Retentate and permeate conductivities were monitored for several fractionation runs to assess whether ions were accumulating at the membrane surface. The rejection of sodium chloride,  $R$ , determined as the ratio of retentate and permeate conductivity, was found to be negligible. Representative data, plotted in terms of permeation ( $1 - R$ ), are shown in Figure 4-4 as a function of dimensionless throughput ( $V_p/V_0$ ) for the 30K-MWC membrane operated in the concentration mode.

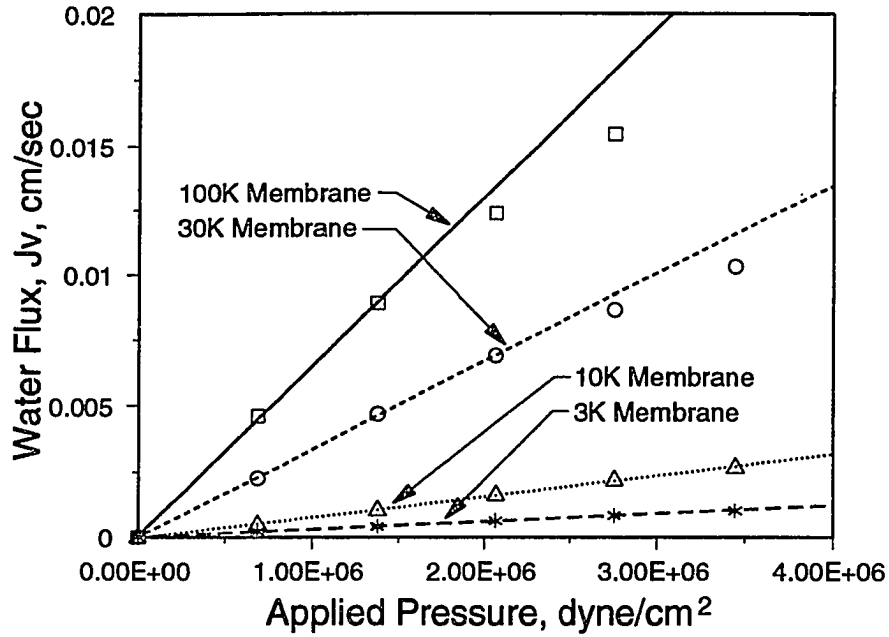


Figure 4-3. The effect of transmembrane pressure on water flux through Amicon Y-series spiral-wound membranes. The coefficient of hydraulic conductivity,  $L_p$ , is determined by the slope of the curve. 3K membrane,  $L_p = 3.1E-10$  cm<sup>3</sup>/dyne-sec, 10K membrane,  $L_p = 7.83E-10$  cm<sup>3</sup>/dyne-sec, 30K membrane,  $L_p = 3.36E-9$  cm<sup>3</sup>/dyne-sec, 100K membrane,  $L_p = 4.74E-9$  cm<sup>3</sup>/dyne-sec.

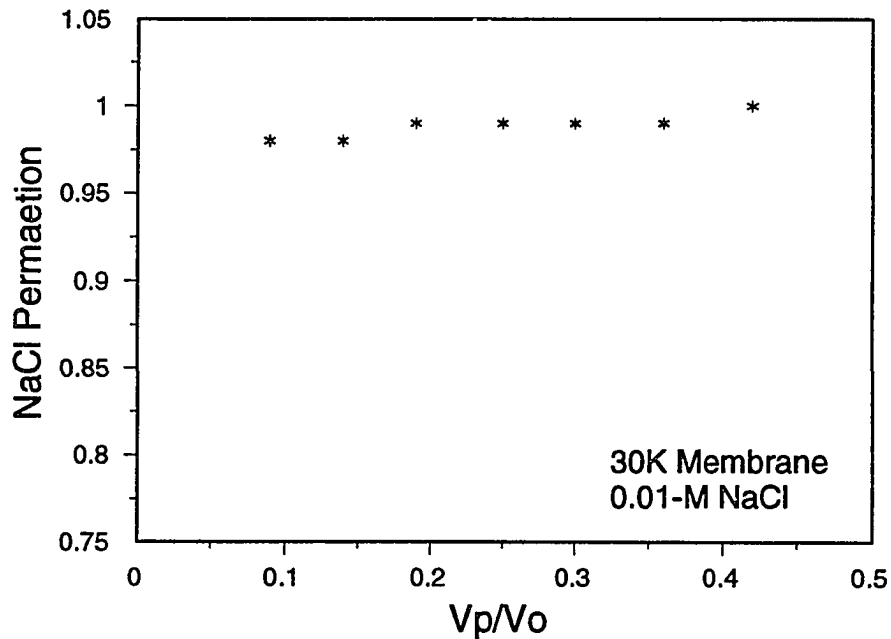


Figure 4-4. The permeation of salt through the 30K membrane, illustrating negligible salt rejection by the membrane. NaCl = 0.01-M.

#### 4.4 Model Development

##### Macroscopic Versus Microscopic Models

Mass distribution within the reactor and the transport of both solute and solvent across the membrane must be characterized to model ultrafiltration systems. The scale over which the mass distribution within the reactor system is characterized establishes the distinction between "microscopic" and "macroscopic" models. In this research, a macroscopic model is developed and validated. Macroscopic models make several implicit assumptions and are therefore characterized by certain inherent limitations. The type of assumptions that are made, and how they represent potential limitations, can best be illustrated by contrasting microscopic and macroscopic models. The development of microscopic modeling concepts will be reviewed briefly.

Microscopic models apply the fundamental equations of change (mass and momentum) to differential elements within the reactor system to develop differential equations which are solved to yield profiles of velocity, pressure, and concentration as a function of time and space. Lebrun et al. (1989) modeled solute transport in a thin channel with two porous walls. The x-direction was taken along the channel length, and the y-direction normal to the porous walls. At the channel inlet,  $x = 0$ , and  $y = 0$  at the channel centerline. The porous walls were separated by a thickness equal to  $2b$ . The general (microscopic) mass balance equation for this geometry, neglecting axial dispersion, takes the form:

$$\frac{\partial C}{\partial t} + v_x \frac{\partial C}{\partial x} + v_y \frac{\partial C}{\partial y} = D \left[ \frac{\partial^2 C}{\partial y^2} \right] \quad (4-4)$$

with an initial condition specifying the concentration in the reactor at  $t=0$ :

$$C(t=0, x, y) = C_0 \quad (4-5)$$

and boundary conditions:

$$C(t, x=0, y) = C_0 \quad (4-6)$$



$$\left[ \frac{\partial C}{\partial y} \right]_{y=0} = 0 \quad (4-7)$$

$$v_y C - \left[ D \frac{\partial C}{\partial y} \right]_{y=b} = J_s \quad (4-8)$$

Equation 4-6 specifies a constant inlet concentration, Equation 4-7 specifies flux symmetry normal to the porous walls (i.e., flux normal to the walls equals zero at the channel centerline), and Equation 4-8 constitutes a mass-balance at the surface of the porous walls, where  $J_s$  the solute flux through the membrane. Unless the concentration boundary layer is much smaller than the momentum boundary layer, this equation must be coupled with the equation of motion and solvent flux relationships to develop expressions for the fluid velocity and pressure profiles as a function of time and space. The solution of the system of equations requires a numerical approach. Solutions are available in the literature for various flow geometries under the restrictions of steady-state ( $\partial C/\partial t = 0$ ) with perfect membrane rejection,  $J_s = 0$  (Weisner and Chellam 1992), non-steady-state with perfect membrane rejection (Ma et al. 1985), and steady-state with solute permeation (Lebrun et al. 1989). The significant advantage of microscopic models is that they yield transport parameters which have a mechanistic basis. However, in comparison with macroscopic models, they require the estimation of more model coefficients, they are difficult to apply to the complex geometrical configurations of practical laboratory-scale ultrafiltration systems, and they are not readily amenable to non-steady-state analysis. For these reasons, a macroscopic modeling approach was chosen in this research.

The macroscopic modeling approach makes no attempt to characterize the distribution of mass as a function of position along the membrane. Transport is characterized using effective model coefficients based on readily measured macroscopic concentrations, such as the reactor inlet concentration. The advantages of macroscopic modeling is that fewer model coefficients are required, and the resulting mass-balance equations can be solved analytically. However, the transport parameters measured depend on operating conditions, and must be considered phenomenological. Regardless of

whether a macroscopic or microscopic modeling approach is used, similar expressions for solvent and solute flux across the membrane must be employed.

### Transport Mechanisms

In general, the flux of both solvent and solute in membrane systems involves coupled transport processes. In some ultrafiltration membranes, depending on the pore sizes involved, solvent may be transported by viscous flow. In membranes having smaller pore sizes, the flux of mass is due primarily to the contribution of concentration diffusion (c), pressure diffusion (p), forced diffusion (g), and thermal diffusion (T) (Bird et al. 1960):

$$J_{s,i} = J_{s,i}(c) + J_{s,i}(p) + J_{s,i}(g) + J_{s,i}(T) \quad (4-9)$$

In addition to inducing the flux of solvent, pressure drop also makes a contribution to the flux of solute in the direction of decreasing pressure. The buildup of rejected solute at the membrane surface creates a concentration gradient which transports solute by diffusion away from the membrane surface, in the direction of decreasing pressure. However, osmotic forces induce a flux of solvent in opposition to the diffusive flux. Forced diffusion, resulting in electroosmotic and electrophoretic effects, and thermal diffusion, the transport of mass due to gradients in temperature, are probably unimportant in most ultrafiltration systems.

### Solute Transport

Flux of solute occurs as a result of viscous and diffusional flow in response to an applied pressure gradient, the predominant driving force for flux across an ultrafiltration membrane (Lakshminarayanaiah 1965). The predominant mechanism for macromolecular separation is selective sieving through membrane pores, and solute rejection behavior is thus governed by: i) molecular size, shape, and flexibility; ii) diffusional behavior within the bulk fluid and within the membrane pores; and, iii) electrostatic and/or Van der Waals forces between solute molecules and the membrane (Weber 1972). Various mechanisms

have been proposed to model the transport of solutes and solvents in membranes, resulting in the so-called solution-diffusion, solution-diffusion-imperfection, finely-porous, and preferential sorption-capillary flow models (Soltanieh and Gill 1981).

Solute rejection is an important property of any membrane, whether used for water treatment or macromolecule characterization. Solute rejection (or rejection *factor*) is quantified in terms of the percentage reduction in the feed concentration across the membrane, and is defined as

$$R = 1 - \frac{C_p}{C_f} \quad (4-10)$$

where  $C_f$  is the concentration at the upstream side of the membrane (feed), and  $C_p$  is the concentration at the downstream side of the membrane (permeate). The quantity  $1 - R$  is defined as the solute permeation factor,  $P_F$ . The permeate concentration is given by the ratio of the solute and the volumetric flux:

$$R = 1 - \frac{J_s}{J_v C_f} \quad (4-11)$$

Therefore, solute flux is given by:

$$J_s = P_F J_v C_f \quad (4-12)$$

The rejection factor,  $R$ , has been theoretically related to either phenomenological coefficients -- in the case of models derived from irreversible thermodynamics -- or to physicochemical properties of the membrane system, including membrane pore size, porosity, tortuosity, and solute and solvent diffusivity and solubility in the membrane (Soltanieh and Gill 1981). The mathematical *form* for solute rejection is the same for all models which treat the membrane as a continuous phase, whether the model is derived from irreversible thermodynamics or from an assumed transport mechanism. For systems in which the solvent flux is constant, the intrinsic membrane rejection theoretically depends only on the physicochemical properties of the membrane system (Soltanieh and Gill 1981).

This concept will be demonstrated by considering two different theoretical approaches for developing expressions for the rejection (or permeation) factor.

Solute flux equations can be derived from the Kedem-Katchalsky model, which has been widely applied to membrane transport (Blatt 1976, Soltanieh and Gill 1981, Cussler 1984). This model, derived from irreversible thermodynamics, expresses solvent and solute flux in terms of phenomenological transport coefficients and osmotic, diffusive and pressure driving forces (Cussler 1984). The volumetric flux,  $J_v$ , of solvent across the membrane is given by the product of a coefficient of hydraulic conductivity,  $L_p$ , and the net pressure drop,  $\Delta p_n$ , across the membrane, as given in Equation 4-2. The total flux of solute,  $J_s$ , across the membrane is the sum of contributions from diffusion and convection:

$$J_s = \omega \Delta \Pi + (1 - \sigma) C_f J_v \quad (4-13)$$

The diffusive transport coefficient,  $\omega$ , the solute permeability at zero volume flux, incorporates the free-liquid diffusivity of the solute, the membrane partition coefficient, and the membrane thickness. The convective transport coefficient,  $(1 - \sigma)$ , can be interpreted as the fraction of the solvent flux carried by pores large enough to pass solute molecules (Blatt 1976). Rigorously,  $C_f$  represents a logarithmic mean concentration within the membrane (Soltanieh and Gill 1981). In most practical membrane systems, however, the log-mean concentration cannot be determined because the concentration at the membrane surface cannot be measured. It therefore becomes necessary to operationally define the convective transport coefficient in terms of the bulk feed concentration,  $C_f$ , which can be measured experimentally (Blatt 1976, Logan and Jiang 1990). Insofar as the true surface concentration depends on the hydrodynamic conditions at the membrane surface, measured transport coefficients are specific to the particular flow conditions and membrane configuration of the system under consideration.

In systems characterized by moderate concentrations of relatively high-molecular-weight solutes, such as most natural waters, the osmotic pressure is small, and Equations 4-2 and 4-13 may be simplified by neglecting the associated terms, yielding, respectively:

$$J_v = L_p \Delta p_a \quad (4-14)$$

$$J_s = (1-\sigma)C_f J_v \quad (4-15)$$

The solute permeation factor can be related to the convective transport coefficient  $(1-\sigma)$  by expressing the permeate concentration as the ratio of the solute mass flux and the solvent volumetric flux, and combining equations 4-11, 4-14, and 4-15 to yield:

$$P_F = 1-R = \frac{C_p}{C_f} = \frac{J_s}{C_f J_v} = \frac{(1-\sigma)C_f J_v}{C_f J_v} = (1-\sigma) \quad (4-16)$$

An alternative approach to developing theoretical expressions for the permeation factor is to solve the solute transport equation within the membrane. The form of this equation is consistent with models based on irreversible thermodynamics, multicomponent diffusion and hydrodynamic transport theories (Opong and Zydney 1991):

$$J_s = J_v C_p = K_c J_v C_s - K_d D \frac{dC_s}{dz} \quad (4-17)$$

Where  $J_s$  is the total flux of solute. The first term ( $K_c J_v C_s$ ) represents the solute transport at the volume averaged velocity,  $J_v$ , and the second term represents diffusive transport. The coefficients  $K_c$  and  $K_d$  are "hindrance factors", and  $D$  is the effective pore diffusion coefficient. The integration is performed subject to the boundary conditions:

$$C_s(z=0) = \phi C_f \text{ and } C_s(z=\delta) = \phi C_p \quad (4-18)$$

where  $\phi$  is the membrane partition coefficient, and  $z=0$  is taken at the membrane surface. The integrated form yields an expression for the permeation factor:

$$P_F = \frac{C_p}{C_f} = \frac{\phi \exp(N_{Pe})}{\phi + \frac{\exp(N_{Pe})}{K_c} - \frac{1}{K_c}} \quad (4-19)$$

where  $N_{Pe}$  is the membrane Peclet number:

$$N_{Pe} = \frac{K_c J_v \delta}{K_d D} \quad (4-20)$$

All models which treat the membrane as a continuous phase have the same mathematical form for the permeation factor; differences arise only in the interpretation of their respective coefficients (Soltanieh and Gill 1981). The general form of the permeation factor is:

$$P_F = \frac{1}{A_1 - A_2 e^{(-A_3 X)}} \quad (4-21)$$

where  $X$  is a function of  $J_v$ , and  $A_1$ ,  $A_2$ , and  $A_3$  are empirical coefficients which must be determined experimentally.

The foregoing discussion demonstrates that the permeation factor can be theoretically related to a variety of phenomenological constants such as the transport coefficient ( $1-\sigma$ ), hindrance factors ( $K_c$  and  $K_d$ ), and effective pore diffusion coefficient ( $D$ ). It is beyond the scope of this work to characterize these various constants, but it is important to recognize that the permeation factor represents a function of constants which relates solute and membrane characteristics. For a given membrane and volumetric flux, the flux of solute can be related to the permeation factor, which can be interpreted as a measure of molecular size, shape, and flexibility.

Equations describing solute transport in batch ultrafiltration systems can be developed by incorporating the solute flux expression into a system mass balance relationship; this approach has been employed by Logan and Jiang (1990). It should be noted that while the macroscopic system is modeled as a completely mixed reactor, the microscopic hydrodynamic conditions at the membrane surface are not known. Equating mass accumulation within the system to the rate of mass permeation through the membrane, the general differential mass-balance can be written:

$$V_s \frac{dC_f}{dt} + C_f \frac{dV_s}{dt} = J_s A_m = Q C_p = J_v A_m C_p \quad (4-22)$$

where  $A_m$  is the superficial membrane area and other terms are as defined previously. To solve this differential equation, the permeate concentration,  $C_p$ , must be functionally related

to the feed concentration,  $C_f$ . This is accomplished by invoking the expression for the membrane permeation factor, Equation 4-10:

$$C_p = (1-R)C_f = (P_F)C_f \quad (4-23)$$

The integrated form of the differential mass-balance equation has been referred to as a "permeation coefficient model" (Logan and Jiang 1990).

It has been shown theoretically that  $P_F$  is a constant for constant  $J_v$  and constant membrane characteristics. It is assumed that both  $J_v$  and membrane characteristics remain constant in the systems studied here, which requires that the dilute macromolecule solutions studied here do not give rise to significant concentration polarization effects. It is further assumed that the solute does not undergo transformation and that adsorption to the membrane surface is negligible. These assumptions will be subsequently discussed. In the diafiltration mode, the system volume is maintained constant and equal to  $V_0$ ; therefore, the volume derivative in Equation 4-22 is equal to zero. The differential mass-balance equation can be integrated with the initial condition  $C_f = C_{f0}$  when  $t = 0$ . Making the substitution  $J_v A_m t = V_p$ , the permeate volume throughput, the transport equation takes the form:

$$C_f = C_{f0} e^{(P_F \frac{V_p}{V_0})} \quad (4-24)$$

If the ultrafiltration system is operated in the concentration mode, the system volume,  $V_s$ , is a function of time, or permeate volume throughput,  $V_p$ :

$$V_s = V_0 - J_v A_m t = V_0 - V_p \quad (4-25)$$

and the time derivative of the system volume is equal to  $J_v A_m$ . Separation of variables and integration for the initial condition  $C_f = C_{f0}$  when  $t = 0$  yields the transport equation for the concentration mode:

$$C_f = C_{f0} \left[ \frac{V_0}{(V_0 - V_p)} \right]^{(1-P_F)} \quad (4-26)$$

The permeation factor may be determined from the log-linearized forms of the integrated mass-balance equations. For the diafiltration mode, a plot of  $\ln(C_f/C_{fo})$  vs.  $V_p/V_o$  yields a slope equal to  $(-P_F)$ , and for the concentration mode, a plot of  $\ln(C_f/C_{fo})$  vs.  $\ln[V_o/(V_o-V_p)]$  yields a slope equal to  $(1-P_F)$ . Alternative linearization forms which allow the determination of  $C_{fo}$  from the intercept of the linearized plot can also be employed.

#### 4.5 Solute Transport Model Verification

The applicability of the macromolecule transport models developed above were evaluated for both the concentration and diafiltration modes of operation by plotting the log-linearized forms of the integrated mass-balance equations:

$$\text{Concentration Mode:} \quad \ln\left(\frac{C_f}{C_{fo}}\right) = (1-P_F) \ln\left(\frac{V_o}{V_o-V_p}\right) \quad (4-27)$$

$$\text{Diafiltration Mode:} \quad \ln\left(\frac{C_f}{C_{fo}}\right) = -P_F \left(\frac{V_p}{V_o}\right) \quad (4-28)$$

Representative results for the corresponding modes of operation are shown respectively in Figures 4-5 and 4-6 for a range of polystyrene sulfonate molecular weights and several different membranes. Representative results for purified Aldrich humic acid at several different ionic strengths are shown in Figure 4-7. For all cases, the squared correlation coefficient is greater than 0.99. It is apparent that the mass-balance models are able to describe the permeation data for charged macromolecules accurately; however, the linearity of the permeation data does not in and of itself validate the assumption of a constant permeation factor made during the model formulation. Nevertheless, these results confirm that the permeation factor is a solute transport parameter related to macromolecule size and membrane pore size (molecular weight cutoff), and thereby validate the permeation factor model for describing the transport of charged macromolecules.

Some runs exhibited slight non-linearity at high volume throughputs, indicating an apparent decrease in the permeation factor at high concentration ratios. This effect could be due to solute accumulation at the membrane surface, or to some degree of polydispersity of



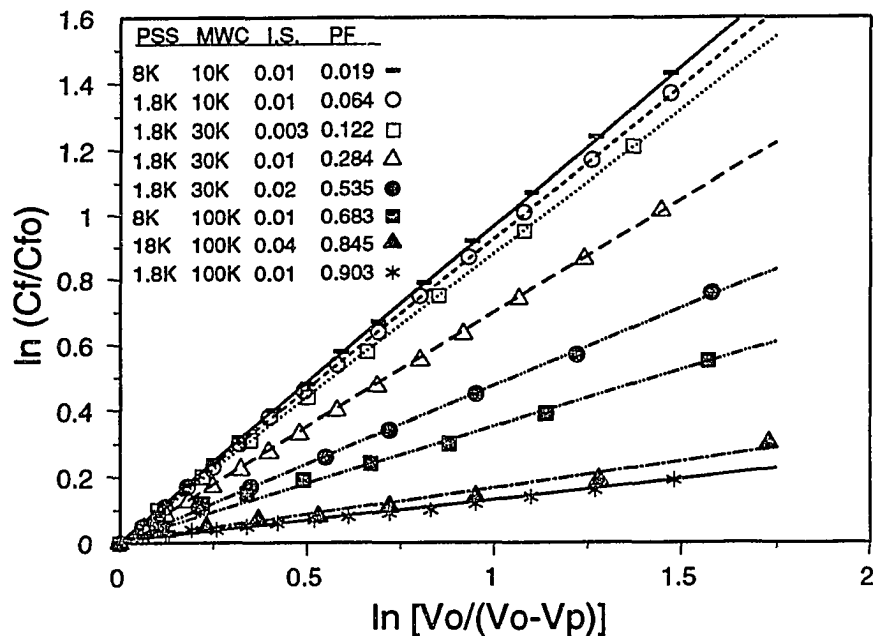


Figure 4-5. Model linearization and data normalization for the concentration mode of operation. Representative data and computed permeation factors ( $P_F$ ) are shown for various PSS molecular weights, membrane molecular weight cutoffs (MWC) and solution ionic strengths (IS).

the solute molecular weight or membrane pore-size distributions.

If the model assumptions are valid, and the transport behavior of a particular macromolecule with respect to a particular membrane can in fact be accurately characterized by a single coefficient, the value of  $C_{f0}$  computed from the intercept of the log-linearized plot of  $\ln(C_f)$  vs.  $\ln[V_o/(V_o-V_p)]$  should, within the limits of experimental error, equal the known starting value. The average error involved in computing  $C_{f0}$  values from the log-linearized plots was 0.72%, with a standard deviation of 0.57%, indicating that under the conditions studied, the model accurately characterizes the transport of random-coil polymers in the recirculating batch ultrafiltration system.

An important assumption in the model development was that adsorption of solute to the membrane surface was negligible. This validity of this assumption was determined by computing an overall mass-balance for each ultrafiltration run, based on a comparison of the initial mass of solute in solution ( $V_o C_{f0}$ ) and the mass in solution at the end of the experiment [ $C_r V_r + \sum(C_p V_i)$ ]. For 44 ultrafiltration runs, losses averaged 3.17% with a

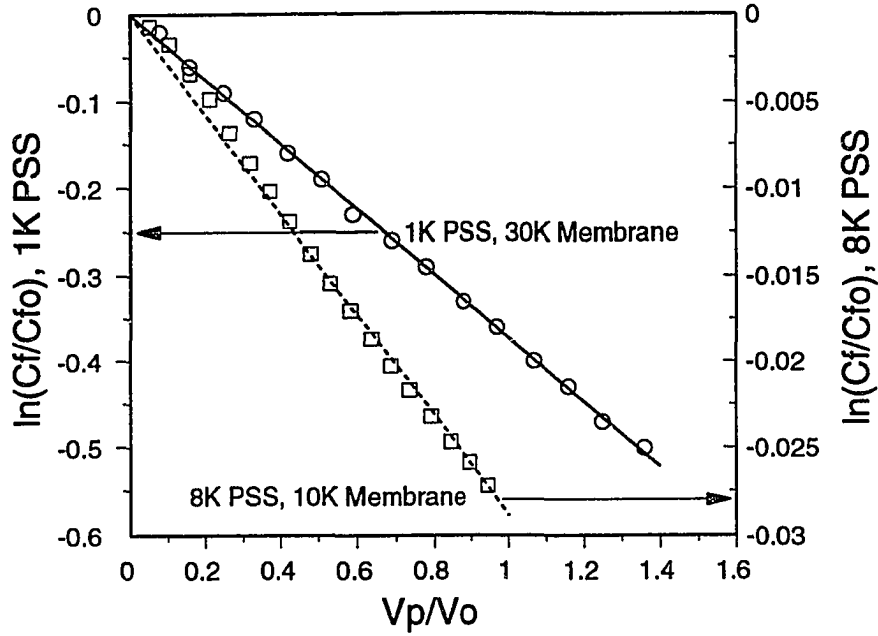


Figure 4-6. Model linearization and data normalization for the diafiltration mode of operation.

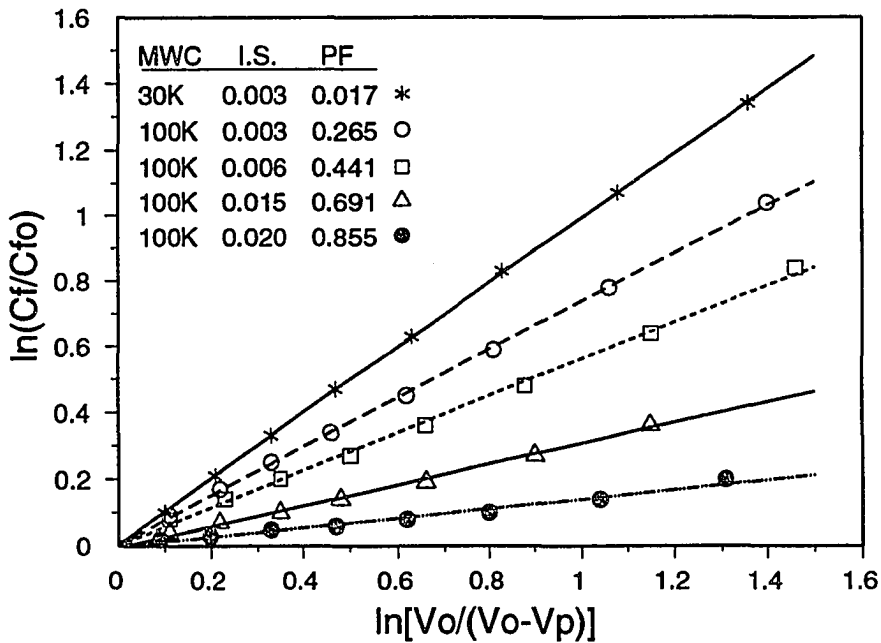


Figure 4-7. Model linearization and data normalization for the concentration mode of operation. Representative data and computed permeation factors ( $P_F$ ) are shown for purified Aldrich humic acid for two membrane molecular weight cutoffs (MWC) for various ionic strengths.

standard deviation of 2.46%. These losses are quite low, and it is believed that the assumption of negligible solute uptake by the membrane surface is valid. Although it might be anticipated that such losses could exhibit a relationship to solution ionic strength, no statistically significant trends were observed.

While the above analysis suggests that the assumptions inherent in the transport model development are met satisfactorily, a more detailed examination of the assumption of a singular and constant permeation factor was performed by plotting the values for the measured permeation factors as a function of the dimensionless volume throughput ( $V_p/V_o$ ); representative data are shown in Figure 4-8. Regions of nearly constant behavior are observed in most cases for early periods of operation. However, significant decreases in permeation factors are noted at high volumetric throughputs, corresponding to high concentration factors. Therefore, model assumptions of a constant permeation factor are most closely met at low volumetric throughputs.

It is well documented, experimentally and theoretically, that concentration polarization resulting from the accumulation of solute at membrane surfaces may significantly affect the mass transfer properties of solutes in membrane separation processes (Lebrun et al. 1989). The mechanical properties of the solute "layer" at the membrane surface, having a greater concentration,  $C_m$ , than the bulk solution,  $C_f$ , govern the transport of hydrophilic macromolecules (Porter and Nelson 1972, Cussler 1984). If the molecules within the layer are relatively mobile, the concentration polarization should result in an increase in solute flux, an effect similar to that observed for low molecular weight solutes. However, if the polarized layer is coherent, so that the molecules are relatively immobile, a highly viscous or gelatinous sublayer may develop. This sublayer will provide an additional resistance to mass-transfer, thereby reducing solvent flux, and increasing the apparent rejection efficiency of the membrane (Porter and Nelson 1972). A true gel layer is expected to form only at high concentrations, on the order of several weight-percent. Logan and Jiang (1990) assume that the low concentrations of dissolved organic matter typical of waters and wastewaters lead to minimal solute accumulation at membrane surfaces, and long periods of operation before the onset of concentration polarization, resulting in nearly constant solvent fluxes.

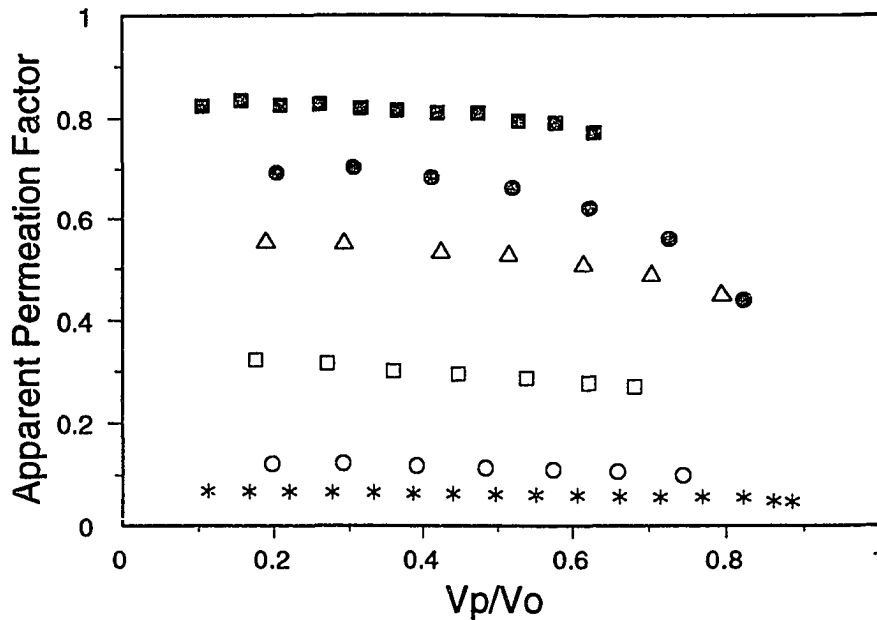


Figure 4-8. The effect of volume throughput on the membrane permeation factor. Conditions (molecular weight, membrane MWC, ionic strength): solid square: 1.8K, 30K, 0.10 M; solid circle: 18K, 100K, 0.01 M; open triangle: 1.8K, 30K, 0.02 M; open square: 1.8K, 30K, 0.01 M; open circle: 1.8K, 30K, 0.003-M; asterisk: 1.8K, 10K, 0.01 M.

The findings of this study support the conclusion that solvent flux remains essentially constant during batch ultrafiltration separations; no measurable decrease was detected. However, the observed variations in measured permeation factors as a function of volume throughput illustrated in Figure 4-8 provide evidence of both enhanced (early time) and hindered (later time) solute mass transfer, suggesting that solute accumulation at the membrane surface may occur in batch systems with low concentrations of the relatively high-molecular-weight organic matter used in these experiments.

#### Effects of Operating Mode

Since fractionation methodologies are often most efficient when concentration and diafiltration modes are used in conjunction, an experiment was conducted to determine whether the mode of operation had an effect on macromolecule transport characteristics. Figure 4-9 illustrates the results of model calibration to a set of data from an experiment in which the ultrafiltration system was operated in a sequential mode. The initial solution was

first diafiltered, using a filtration volume of 1.3 L, after which the buffer feed was stopped, allowing the operation to continue in the concentration mode. The permeation factor for each mode was determined independently, yielding similar values. These results suggest that the mode of operation, for the range of volume throughputs used in this experiment, does not significantly affect solute transport characteristics. It can be noted, however, that the value for the permeation factor for the diafiltration mode was slightly higher than that measured for the concentration mode. This trend was observed in all experiments in which different modes of operation were compared. This is consistent with the fact that the concentration of retained solute remains constant in the diafiltration mode, in contrast to the concentration mode, in which it increases. This difference may relate to the development and subsequent effects of a concentration polarization layer. The implications of this result as it relates to the design of fractionation protocols will be discussed in greater detail in subsequent sections.

#### Effects of Macromolecule Structure

The data shown in Figures 4-5 and 4-7 suggest that solution ionic strength has a significant impact on transport in ultrafiltration systems. To investigate this phenomenon in more detail, PSS permeation factors were measured for a wide range of ionic strengths. To determine whether the effect of ionic strength showed a dependence on molecular weight, two PSS molecular weights were studied, 1.8K and 18K, bracketing a range of molecular weights typical of natural systems. The concentration mode of operation was used for all permeation factor measurements. The results are shown in Figure 4-10. The increase in the permeation factor with ionic strength is dramatic over a range of ionic strengths characteristic of natural waters. The effect of ionic strength is similar over the order of magnitude difference in PSS molecular weights, a range which encompasses the predominant size range expected of aquatic dissolved organic matter. Figure 4-11 presents similar results for a solution of purified Aldrich humic acid representing a total organic carbon (TOC) content of 4 mg/L. These findings may have significant implications for the removal efficiency of membrane processes used in water treatment applications, and for the effective MWC of a given membrane in a particular application.

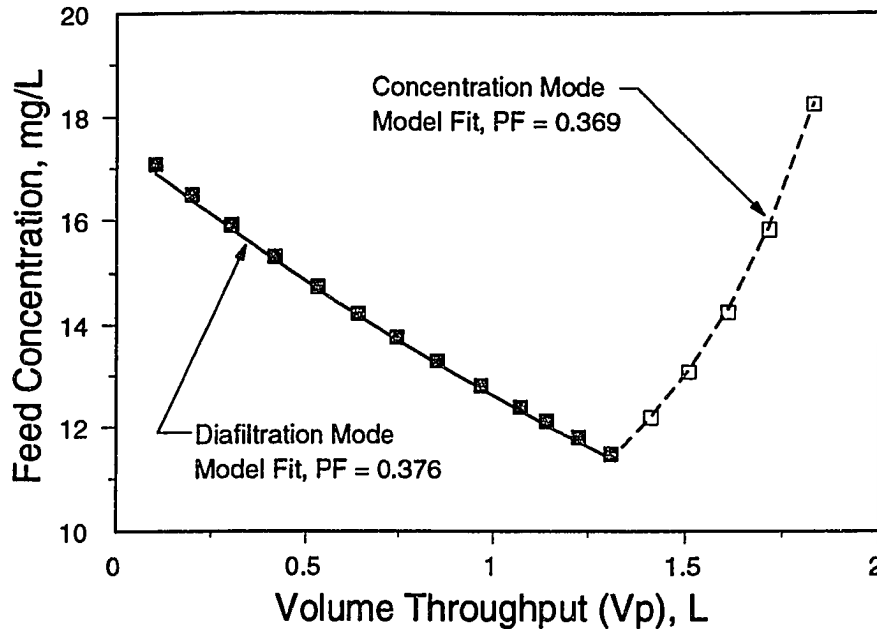


Figure 4-9. Model calibration and permeation factor determination for a sequential mode of operation. Conditions: 1.8K PSS, 30K MWC membrane, I.S. = 0.01 M. Lines represent model fits to the experimental data: concentration mode  $P_F = 0.369$ ; diafiltration mode  $P_F = 0.376$ .

The effect of ionic strength is interpreted as the result of changes in macromolecular configuration which occur in solution. This is consistent with the conceptual model of Gosh and Schnitzer (1980) and can be attributed to the ability of salts to shield charge and compress the electrical double layer which exists between adjacent charged structural units. The ionic strength effect is not attributed to the accumulation of ions at the membrane surface, because control experiments indicated negligible ion exclusion. The curves are strikingly similar to membrane calibration curves generated with a series of solutes exhibiting a wide range of molecular weights, indicating that the effect of ionic strength on solute permeation characteristics for random-coiled polymers is to change the "effective" size in solution. In contrast to membrane calibration curves, the ionic strength profiles exhibit upper bounds less than unity, and lower bounds greater than zero, presumably corresponding to fully coiled and fully uncoiled configurations.

The impact of ionic strength on permeation factors illustrates the utility of using ultrafiltration to characterize macromolecule size. A charged macromolecule may have a

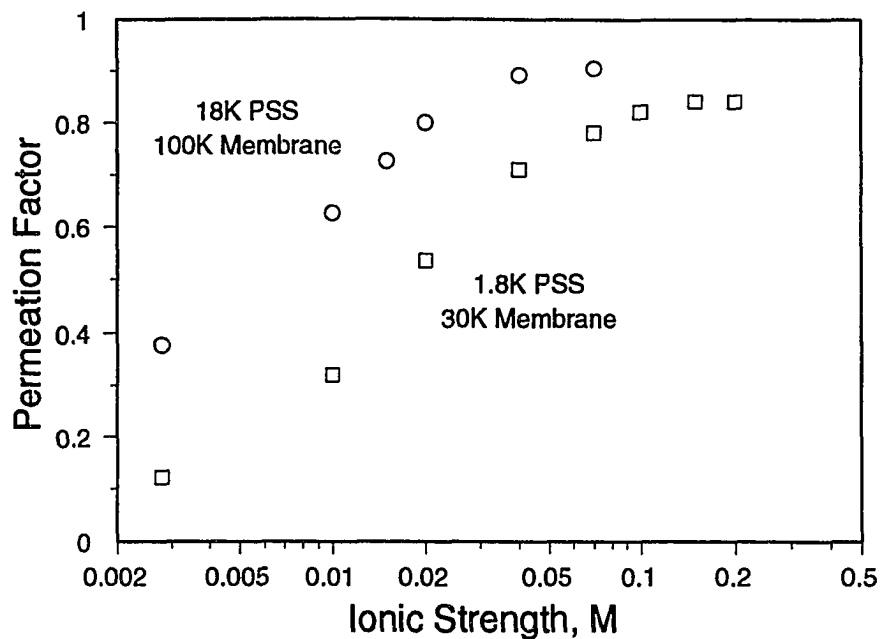


Figure 4-10. Effects of ionic strength on the dimensionless permeation factors for different PSS molecular weights determined using the concentration mode of operation.

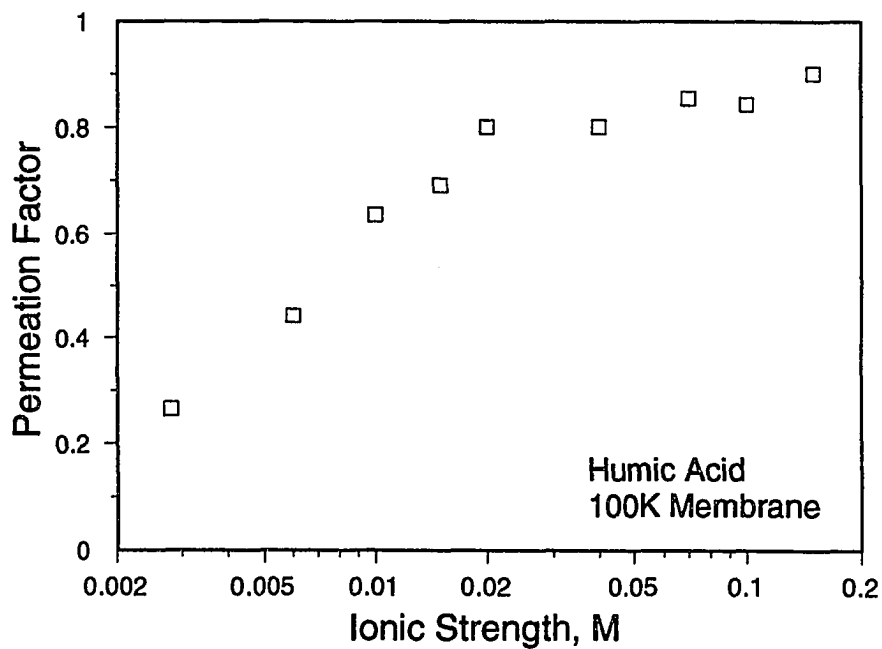


Figure 4-11. Effects of ionic strength on the dimensionless permeation factors for purified humic acid determined using the concentration mode of operation.

wide range of sizes in solution, depending on the solution chemistry. The activated carbon adsorption behavior of macromolecules may depend on macromolecule size, because molecule size and adsorbent pore-size distribution determine the fraction of the adsorbent surface area which can be accessed. Therefore, adsorption behavior should relate, in part, to the membrane permeation factor of a given macromolecule. These results also point out the difficulty of using ultrafiltration to characterize absolute values of molecular weight, since a single molecular weight component may have a spectrum of sizes and permeation factors.

The observed effect of ionic strength on the permeation characteristics of charged macromolecules suggests that: i) calibration curves provided by membrane manufacturers may not be generally applicable to natural waters with different ionic strengths; and, ii) effective membrane molecular weight cutoff values depend on the specific chemistry of a particular water sample. Manufacturers generally specify a molecular weight cutoff corresponding to a measured rejection somewhat less than 100%. For the 3K, 10K, 30K and 100K membranes used in this study, the molecular weight cutoff is specified for rejections of 88%, 95%, 95% and 92%, respectively. Figure 4-12 illustrates that at low ionic strengths, specified molecular weight cutoff values may be significantly higher than the effective cutoff values for charged macromolecules, and that membrane calibration profiles show an ionic strength dependence. These results suggest that ultrafiltration membranes used for the characterization of natural waters should in each case be calibrated with random-coil polymers in standard solutions having inorganic compositions similar to those of the natural water of interest. Inadequate membrane calibration may result in overestimates of molecular weights based on ultrafiltration measurements (Brown 1975).

#### Macromolecule Solution Fractionation

The permeation model was used to evaluate alternative fractionation procedures for preparing different size fractions of natural organic macromolecules, to identify an optimal fractionation procedure. Expressions for the mass throughput were derived by integrating the permeation model appropriate for a particular mode of operation, written in terms of the permeate concentration, with respect to permeate volume throughput,  $V_p$ , yielding:



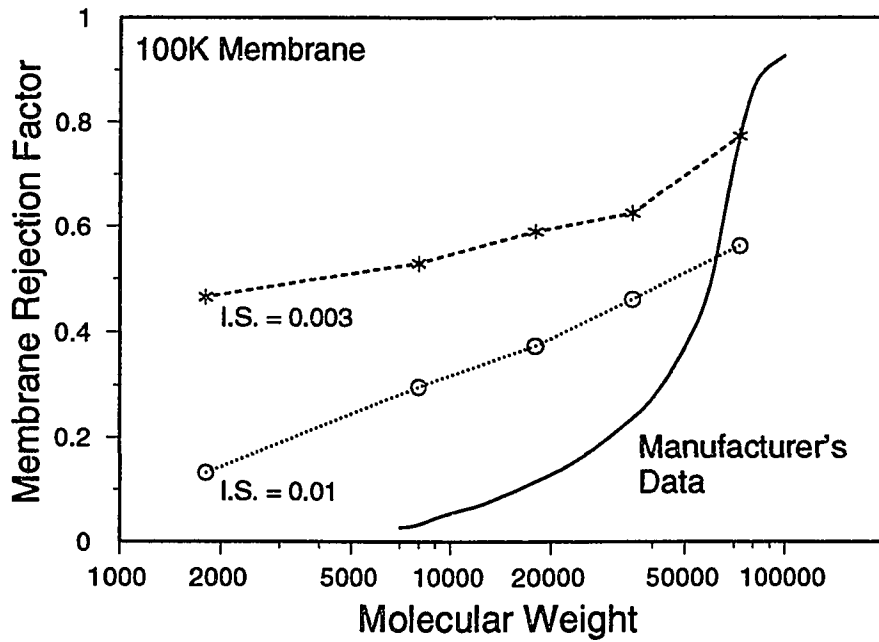
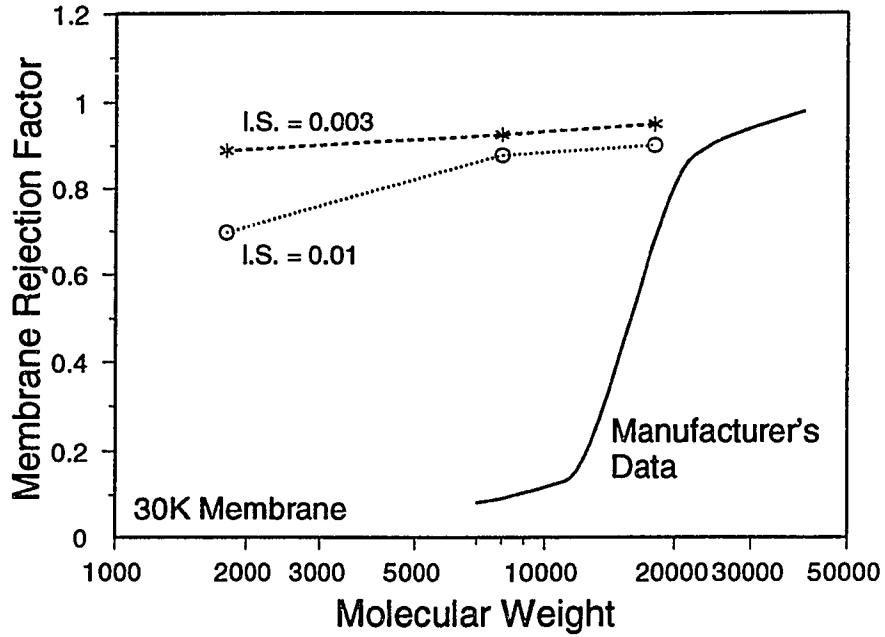


Figure 4-12. Molecular weight solute rejection calibration curves for two ultrafiltration membranes and two ionic strengths. Manufacturer's data from Technical Data publication 744, Amicon Division, W.R. Grace & Company, 1987.

Diafiltration Mode Mass Throughput:

$$C_{fo}V_o \left[ 1 - e^{-\left(\frac{P_F V_p}{V_o}\right)} \right] \quad (4-29)$$

Concentration Mode Mass Throughput :

$$C_{fo}V_o - C_{fo}V_o^{(1-P_F)}(V_o - V_p)^{(P_F)} \quad (4-30)$$

The mass throughput model was verified in several experiments using purified Aldrich humic acid by operating the ultrafiltration system in a sequential concentration/diafiltration mode. Representative data are shown in Figure 4-13. The model successfully describes trends in the data and was therefore subsequently used to design fractionation procedures.

For a given initial volume, the mass throughput depends on the initial mass present,  $C_{fo}V_o$ , the permeation factor, and the permeate volume throughput,  $V_p$ . Model calculations demonstrate that the most efficient mass throughput is achieved i) at high feed concentrations, and ii) in the concentration mode. However, an important objective of any fractionation procedure is to minimize the effects of concentration polarization and variation in the permeation factor. There are practical limitations, therefore, to both of these strategies.

The diafiltration mode has several advantages over the concentration mode from an operational point of view. The original sample volume is kept constant by the continuous addition of buffer solution containing the same inorganic matrix as the sample. The effects of concentration polarization are minimized, therefore, because the concentrations of retained molecules is kept constant, while the concentrations of permeating molecules decrease as a function of permeate volume throughput. Further, as a matter of operational convenience, the diafiltration mode can be operated continuously. Model calculations indicated that the efficiency of the concentration mode and the operational benefits of the diafiltration mode could be combined by employing a sequential mode of operation. Under this scenario, the sample is first concentrated to enhance mass-throughput efficiency and reduce sample volume. The concentration mode is followed by a period of operation in the diafiltration mode; the smaller sample volume maximizes the value of  $V_p/V_o$  for a given

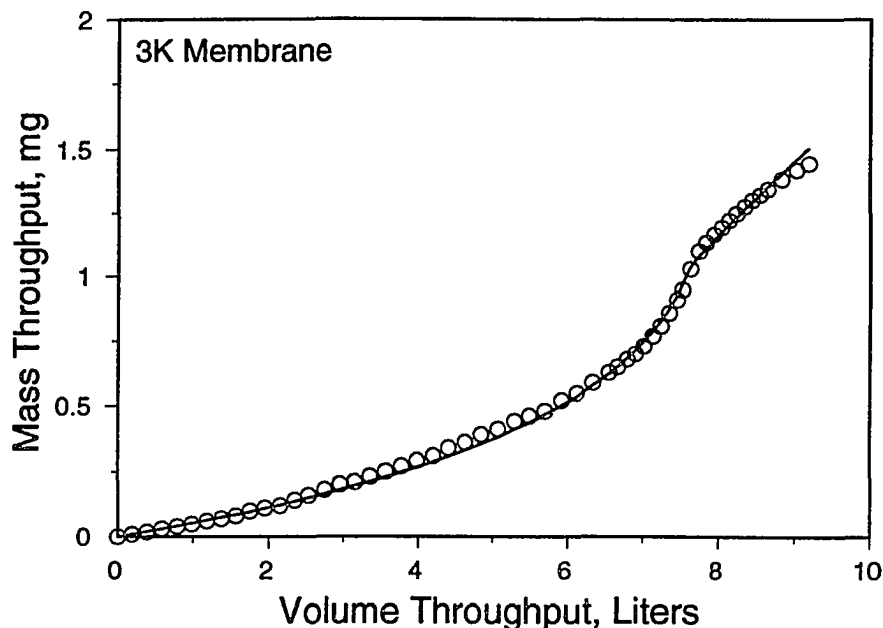


Figure 4-13. Mass throughput of purified humic acid measured for the 3K membrane using a sequential concentration/diafiltration mode of operation. Line represents permeation model fit to the experimental data.

total throughput volume. Based on these considerations, a general cascade-type fractionation protocol was designed. A schematic depiction of the protocol is illustrated in Figure 4-14.

As shown in Figure 4-14, the whole HA solution is first applied to the 3K membrane, which has the smallest MWC. The whole solution is concentrated, then diafiltered with buffer solution, yielding the <3K fraction. The retentate is then fractionated on the 10K membrane, using the same concentration/diafiltration technique. This yields a dilute solution of the 3-10K fraction. This solution is concentrated on the 3K membrane to reduce the fraction volume and to further remove any <3K fraction remaining as a result of incomplete separation. The retentate from the fractionation on the 10K membrane is then applied to the next larger membrane and the process is repeated.

Starting the cascade process with the smallest membrane has several advantages. In general, the fraction which passes the smallest MWC membrane is necessarily the most dilute, because there are no smaller membranes on which to concentrate this fraction. By starting with the smallest membrane, the degree of dilution is minimized.

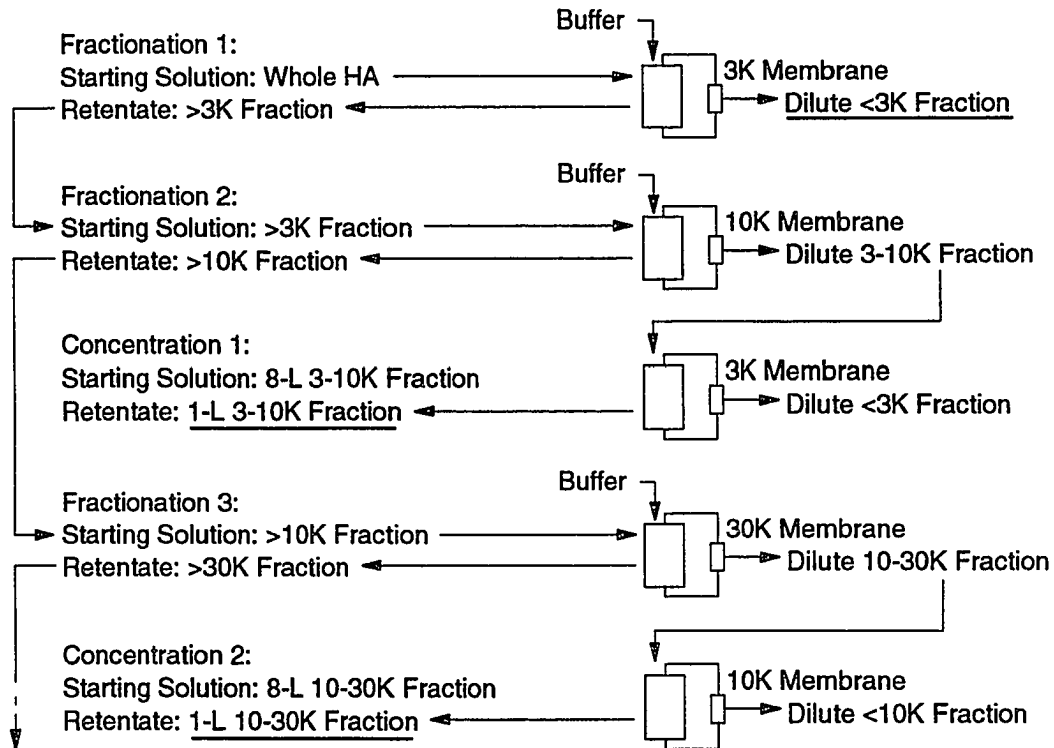


Figure 4-14. Schematic depiction of the cascade-type fractionation protocol used to prepare ultrafiltration size fractions for subsequent use in adsorption experiments. Underlined fractions represent final product.

Furthermore, as a result of subsequent concentration steps, the likelihood of low-molecular size fractions contaminating larger size fractions is minimal. Each fraction is concentrated on the next lower membrane size (i.e., the 30-100K fraction is concentrated on the 30K membrane) which allows smaller molecules to pass freely, thus enhancing the separation efficiency.

Preliminary fractionation experiments were conducted under various conditions to investigate the effects of solute concentration, ionic strength and diafiltration volume. These experiments were conducted with Aldrich humic acid. The results of these experiments are shown in Figures 4-15, 4-16 and 4-17. All experiments were conducted at pH 6.5 in a  $1 \times 10^{-4}$ -M phosphate buffer unless otherwise noted. The ionic strength of one set of experiments was increased by the addition of 0.05-M NaCl; these data are shown in Figure 4-16. The ultrafiltration system was operated in the concentration mode using a 9:1 volume reduction followed by a 4-L diafiltration volume with the exception of one

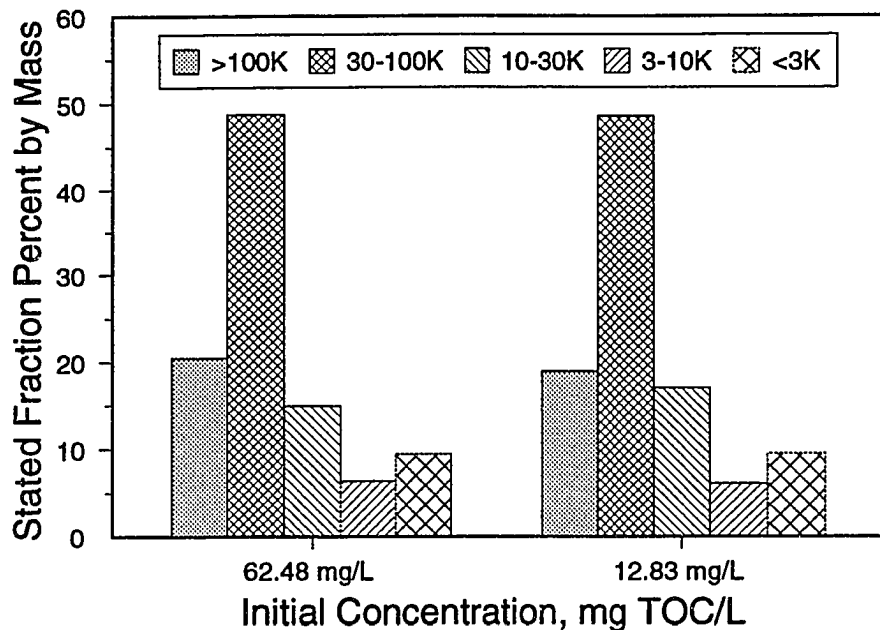


Figure 4-15 Ultrafiltration fractionation of Aldrich humic acid showing the effect of initial concentration on the mass distribution. Inorganic matrix: pH = 6.5,  $1 \times 10^{-4}$ -M phosphate buffer.

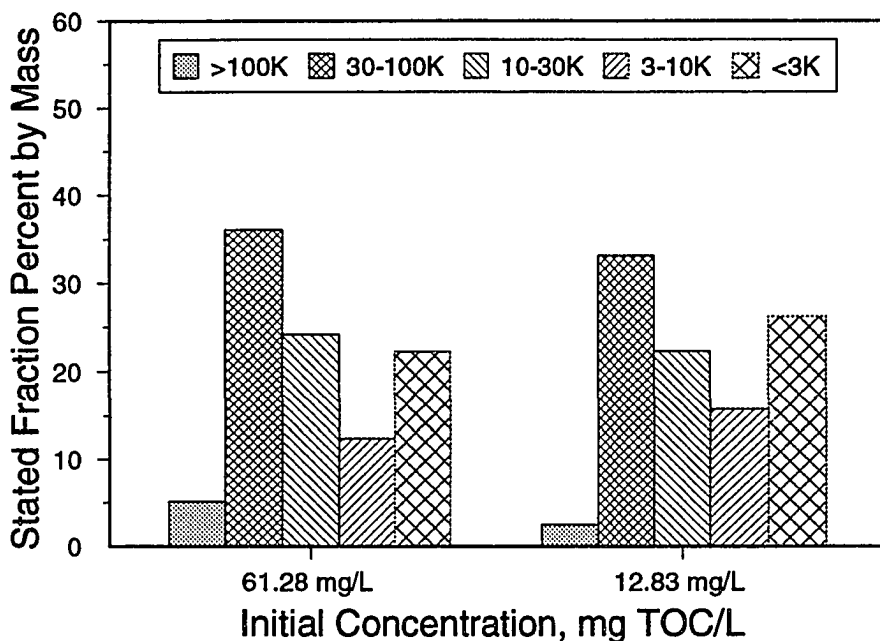


Figure 4-16 Ultrafiltration fractionation of Aldrich humic acid showing the effect of initial concentration on the mass distribution. Inorganic matrix: pH = 6.5,  $1 \times 10^{-4}$ -M phosphate buffer, 0.05-M NaCl.

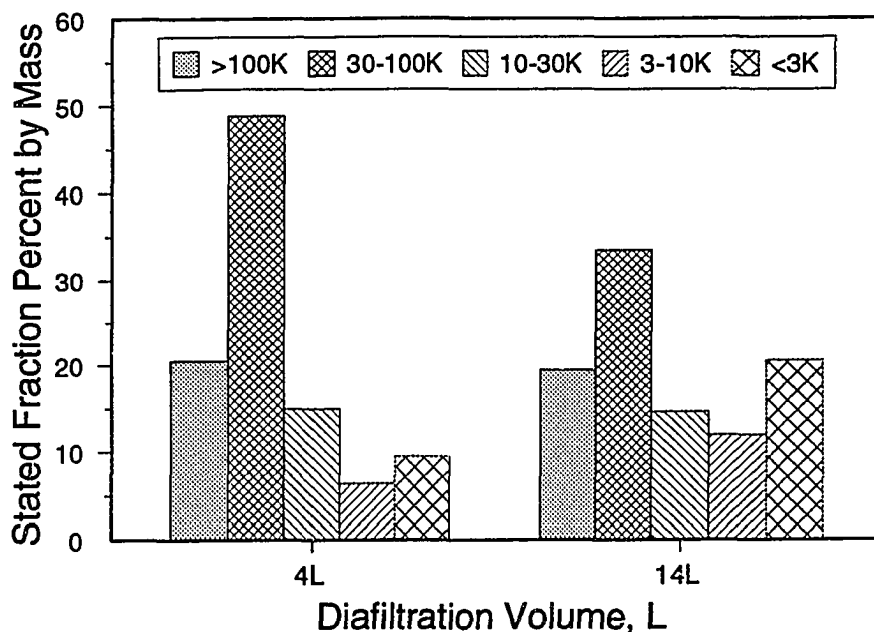


Figure 4-17 Ultrafiltration fractionation of Aldrich humic acid showing the effect of diafiltration volume on the mass distribution. Inorganic matrix: pH = 6.5,  $1 \times 10^{-4}$ -M phosphate buffer.

fractionation experiment, shown in Figure 4-17, in which a 14-L diafiltration volume was evaluated.

Nearly identical distributions for initial concentrations of 13 and 62 mg/L, indicating that there is no significant effect of initial solute concentration over this range, as shown in Figure 4-15. The effect of ionic strength has a significant effect on how mass is distributed among different fractions, as shown by comparing Figures 4-15 and 4-16. The results are consistent with the effects of ionic strength on membrane permeation coefficients, and indicate a significant change in macromolecule structure as a function of ionic strength. At higher ionic strength values, the molecules adopt a more compact or coiled configuration, and permeation through each membrane is increased, shifting the distribution to lower molecular weights. A slight effect of initial concentration is observed at the higher ionic strength, evidenced by a shifted in the distribution to lower molecular sizes with decreasing concentration. A slight loss of the <100K, 30-100K and 10-30K fractions corresponds to an increase in the two smaller fractions.

A significant shift in the distribution to lower molecular sizes is observed with an increase in the diafiltration volume, as shown in Figure 4-17. The greatest decrease is observed for the 30-100K fraction, while the two lower fractions exhibit significant increases. There is little change in the mass of the >100K and 3-10K fractions. It is possible that the mass fraction of the 3-10K fraction remained constant while the composition changed. These results suggest that at low ionic strengths, the separation is incomplete when a diafiltration volume of 4 liters is used, illustrating the exponential nature of the diafiltration process. While not tested, it is likely that better separation could be achieved for a given diafiltration volume at higher ionic strengths.

The results of the preliminary fractionation experiments and permeation factor measurements were used as a basis for designing the final fractionation protocol and fractionation conditions used to prepare size fractions for adsorption experiments. The fractionation was started with 2-liter initial volume of whole HA having a nominal TOC concentration of 60 mg/L. The solution which was first concentrated to 0.5 liters and then diafiltered with 4 liters on the 3K membrane. On subsequent membranes, an initial volume of 1 liter was concentrated to 0.5 liter and diafiltered with 8 liters. A relatively small volume reduction ratio was used in the concentration mode to reduce the potential for concentration polarization. For membranes larger than the 3K, a diafiltration volume of 8 liters was chosen as a compromise between achieving complete separation and maintaining solution concentration sufficiently high to sustain analytical accuracy. As mentioned previously, the cascade-type fractionation protocol was designed to enhance separation efficiency in the concentration step, minimizing the likelihood of small molecular-size fractions contaminating larger size fractions. A diafiltration volume of 4 liters was used with the 3K membrane to minimize sample dilution.

An ionic strength of 0.01 was chosen for both fractionation and adsorption experiments. This value is representative of many natural and engineered systems, and based on the data collected from preliminary fractionation experiments, should minimize the impact of differences in solute concentration while assuring that the smaller sizes represent a significant mass-fraction of the whole mixture.

Solute permeation data from representative fractionation experiments for the 3K and the 100K membranes are shown in Figures 4-18 and 4-19. The solid lines represent permeation factor model (Equations 4-27 and 4-28) fits to the data. Model parameters ( $C_{fo}$  and  $P_F$ ) were estimated by nonlinear regression. A sufficient number of data points to estimate model parameters for the concentration mode was collected for the 3K membrane only, while the model was fit to data from the diafiltration mode for all membranes. Although the model describes the data adequately, a single permeation factor cannot describe the data over the entire range of volume throughput.

The model also exhibits some deviation from the data at volume throughput values corresponding to the transition from the concentration to the diafiltration mode. This can be seen in Figure 4-18 at a throughput volume of just under 2000 mL and in Figure 4-19 at a throughput volume of just under 1000 mL. This behavior is observed because the experimental transition between the two modes is not sharp. The diafiltration mode is started by sealing the reservoir and connecting it to a buffer source. Sealing the reservoir establishes a vacuum which causes the flow of buffer. During the period over which the vacuum develops, there is a gradual transition from the concentration mode to the diafiltration mode. This transition introduces uncertainty into the model parameter estimation procedure. It is for this reason that a sequential concentration/ diafiltration mode is not recommended for measuring molecular-size distributions using techniques which rely on accurate estimates of  $C_{fo}$ . It should be noted that the transition from the diafiltration mode to the concentration mode is much sharper, because once the vacuum is released from the reservoir, concentration will commence. This procedure was used to collect the data shown in Figure 4-9.

Loss of mass to reactor or membrane surfaces during the fractionation experiments was evaluated as described previously, by computing an overall mass-balance for each ultrafiltration run, based on a comparison of the initial mass of solute in solution ( $V_o C_{fo}$ ) and the mass in solution at the end of the experiment [ $C_r V_r + \Sigma(C_p V_i)$ ]. Mass balances were closed to within 1.5% for all fractionation experiments.

The discrete mass distribution of the Laurentian HA, as determined by fractionation, is shown in Figure 4-20. The values shown represent the average of two



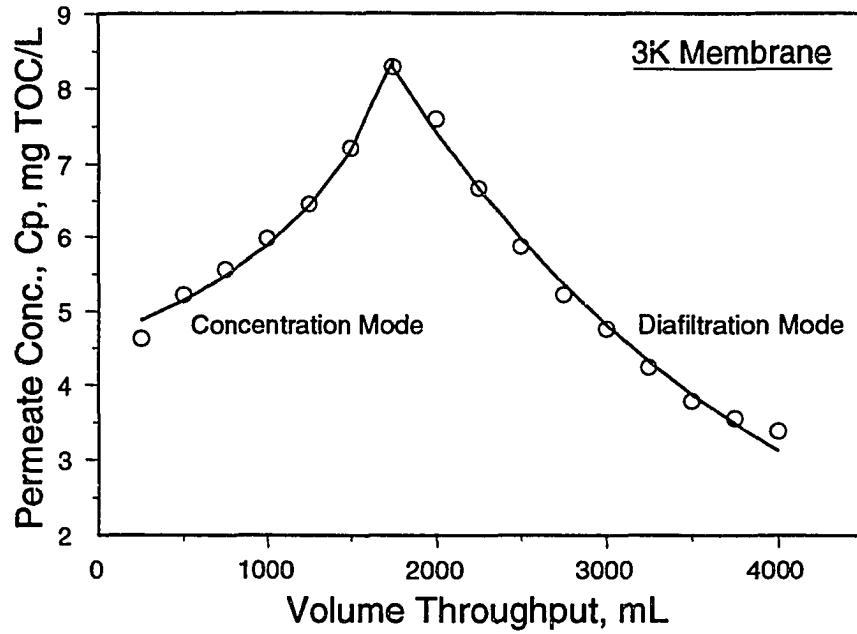


Figure 4-18. Fractionation experiment conducted using sequential concentration/diafiltration on the 3K membrane. Lines represent permeation factor model fits to the experimental data.

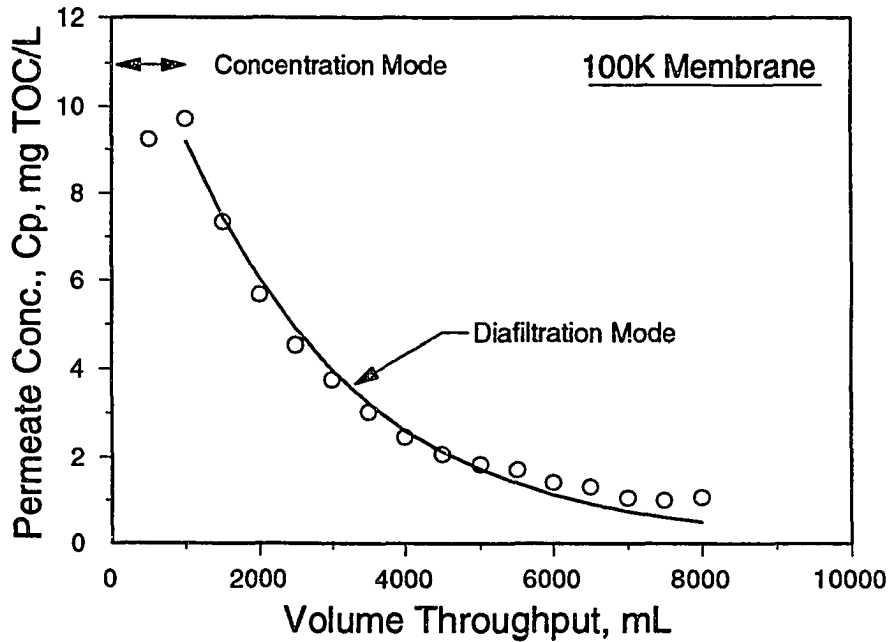


Figure 4-19. Fractionation experiment conducted using sequential concentration/diafiltration on the 100K membrane. Lines represent permeation factor model fits to the experimental data.

independent fractionation experiments. The distribution appears relatively uniform, although the <3K fraction may be underestimated because only 4 liters of diafiltration volume were used. The uniform appearance of the distribution may be due to the relatively few number of discrete fractions which could be prepared. Considering the possibility of incomplete fractionation and the development of concentration polarization layers at the membrane surface, it is difficult to assess how closely this distribution approaches the true distribution. The objective of providing reproducible size fractions, however, was met. Mass fractions determined in different fraction runs generally differed by less than 5%. Permeation factors of each fraction were measured on the 100K membrane in the concentration mode and are reported in Table 4-1. The differences between adjacent fractions are all statistically significant, providing a measure of the separation efficiency attained in the fractionation procedure. The permeation factor measured for the >100K should theoretically be zero. The value obtained is small, indicating that the protocol and fractionation conditions result in nearly complete separations.

**Table 4-1. Permeation Factors of Ultrafiltration Size Fractions.**

Fraction	$P_F$	95% C.I.
<3K	0.901	0.897, 0.905
3-10K	0.822	0.817, 0.827
10-30K	0.756	0.751, 0.761
30-100K	0.581	0.572, 0.590
>100K	0.094	0.088, 0.100

The efficacy of using ultrafiltration to characterize molecular size and to fractionate polydisperse solutions has been demonstrated. While ultrafiltration has also been used to measure molecular-size distributions (Reinhard 1984, Amy et al. 1987, Logan and Jiang 1990), there are significant limitations inherent in such an approach. Molecular weight distributions can be estimated by two different techniques: i) complete fractionation, which requires no modeling (Reinhard 1984), and ii) and partial fractionation accompanied by

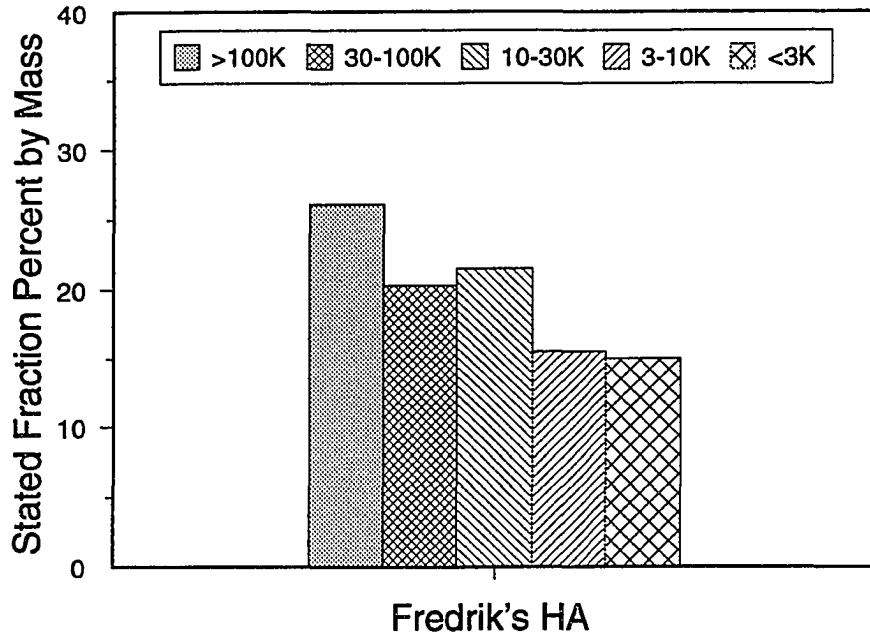


Figure 4-20. Mass distribution of Laurentian HA size fractions prepared using the sequential concentration/diafiltration technique.

solute flux modeling to estimate  $C_{f0}$  (Logan and Jiang 1990). In either case, resolution of the technique is limited by the small number of available membranes on which to fractionate the solution. Complete fractionation requires a relatively large sample size, is labor intensive, and the potential effects of concentration polarization add uncertainty to the results. Accurate estimation of  $C_{f0}$  using the permeation model is possible; however, it was found that the form of the model required for this analysis is sensitive to variations in the permeation factor. In controlled experiments in which the value of  $C_{f0}$  was known, it was found that computed values of  $C_{f0}$  using the permeation factor model were significantly lower than actual values, yielding an erroneous shift in the apparent molecular size distributions to larger molecular sizes. To overcome the inherent limitations of ultrafiltration for measuring size distributions, high-performance size-exclusion chromatography (HPSEC) was used.

#### 4.6 Size Exclusion Chromatography System Calibration and Data Analysis

HPSEC separations are based on the ability of differently sized molecules to access pore volume within the porous column packing material. There are two distinct void volumes in an SEC column -- the bed void volume,  $V_b$ , which is the volume created between the external surfaces of the packing material and the reactor walls, and the intraparticle void volume,  $V_i$ , which can be considered the stationary phase volume. The upper molecular weight cutoff of a HPSEC column is defined by the molecular size which is completely rejected from the particle void volume. Molecules larger than the upper cutoff value reside entirely within the column bed volume, and have a retention time equal to  $V_b/Q$ , where  $Q$  is the flowrate. The lower molecular weight cutoff is defined as the molecular size which can completely access the particle void volume. The retention time of molecules smaller than the low-molecular weight cutoff is  $(V_b+V_i)/Q$ . Molecules larger than the upper molecular weight cutoff or smaller than the lower molecular weight cutoff cannot be resolved, while molecules of intermediate size, which can access a fraction of the particle void volume, have retention times between these limits.

The HPSEC system was calibrated with four different monodisperse PSS fractions, and the void volume was determined with acetone. Standard curves were prepared daily, and an excellent linear correlation was found between the  $\log_{10}$  of the molecular weight and the elution time,  $t$ . Typical standard curve data, described by the regression equation:  $\log_{10}(\text{MW}) = -0.37582(t) + 6.738$  ( $r^2 > 0.998$ ), are shown in Figure 4-21.

Chromatography data were processed by first establishing a baseline. The detector response was generally stable for the first 5.5 minutes. A horizontal line was constructed through the early time data prior to sample elution, and the point where the chromatogram deviated from this line was taken as the beginning of sample elution. The baseline was drawn from the point just prior to sample elution to the chromatogram at 13.33 minutes, which represented the lower limit of the standard curve. The baseline was subtracted from the detector response to yield a corrected chromatogram. In all cases, baseline drift, and therefore the baseline correction applied, was small. The detector response at 13.33 minutes was generally less than 1% of the maximum detector response, and was less than 2% in all chromatograms. Where necessary, chromatograms were corrected for the

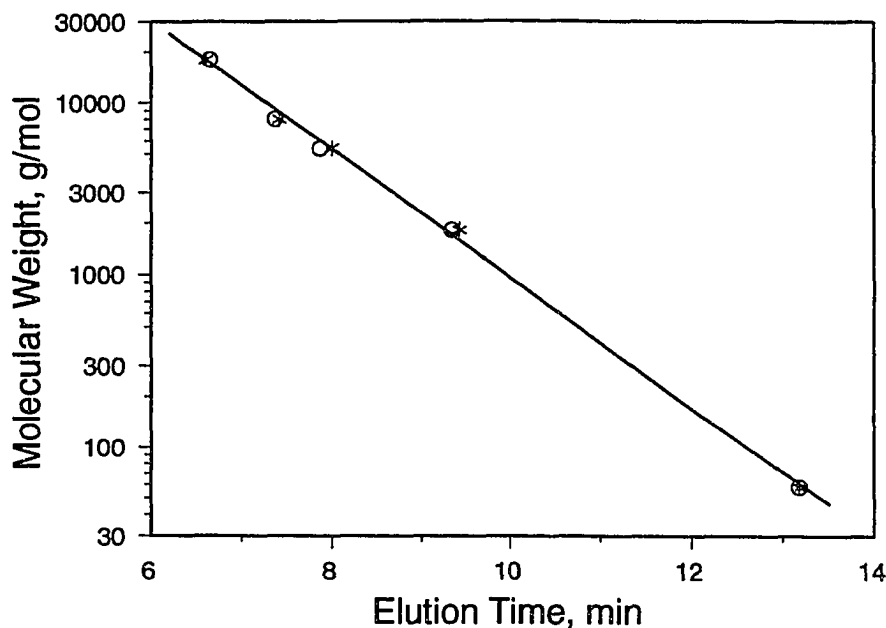


Figure 4-21. Standardization of a Waters Protein-Pak 125 Å functionalized silica column with polystyrene sulfonates; void volume determined with acetone. Mobile phase: pH 6.8 phosphate buffer, 0.10-M NaCl. Flow rate: 1 ml/min. Different symbols represent independently-determined standard curves.

presence of sodium azide by subtracting the azide spectrum. The size-exclusion chromatogram for whole Laurentian humic acid is shown in Figure 4-22. The distribution is generally symmetric with a distinct high-molecular weight peak. The chromatogram is described quantitatively in terms of the first moment of the distribution.

The first moments of the chromatograms were determined by numerically integrating the detector response as a function of elution time from the first point of sample elution to 13.33 minutes. Approximately five hundred data points were integrated in each chromatogram, corresponding to a time interval of 0.0167 min.

The weight-averaged molecular weight,  $M_w$ , was determined by the equation:

$$M_w = \frac{\sum_{i=1}^N MW_i(t)M_i(t)}{M_T} \quad (4-31)$$

where  $MW_i(t)$  is the molecular weight as a function of elution time, determined from the calibration curve;  $M_i$  is the sample mass determined as a function of elution time from the

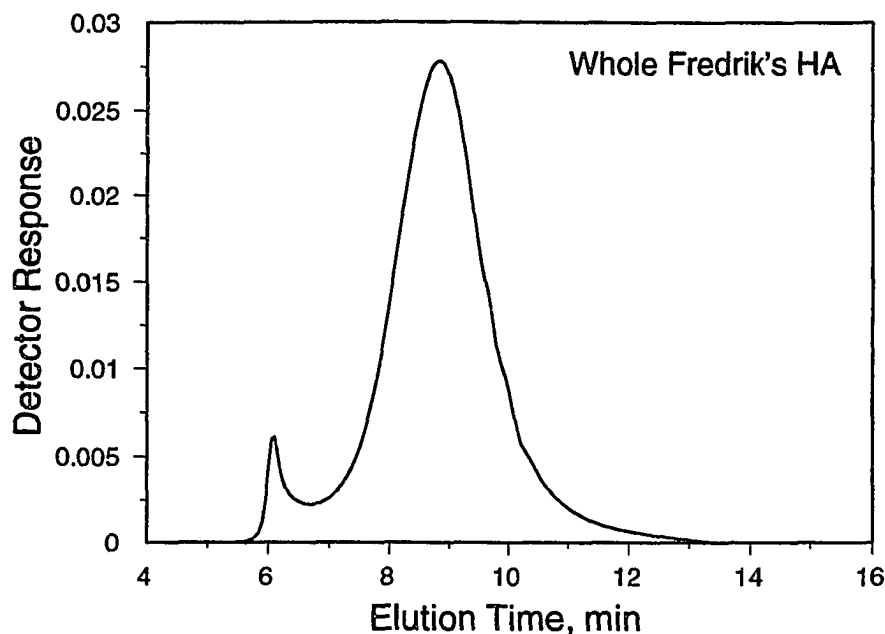


Figure 4-22. Size exclusion chromatogram of Laurentian humic acid.

detector response; and  $M_T$  is the total mass of the sample. The number averaged molecular weight,  $M_N$ , was determined by the equation:

$$M_N = \frac{\sum_{i=1}^N M_i(t)}{\sum_{i=1}^N M_i(t)/MW_i(t)} \quad (4-32)$$

where summations are taken over  $N$  components or sampled fractions designated by the subscript  $i$ . The mass of the sample is given by:

$$M_i(t) = Q \times h_i(t) \times \Delta t \times 1/a(t) \quad (4-33)$$

where  $Q$  is the flowrate,  $h_i(t)$  is the UV detector response,  $\Delta t$  is the time interval, and  $a(t)$  is the sample absorptivity (mass-basis) as a function of elution time.  $M_T$  was determined by integrating  $M_i(t)$  over the entire chromatogram. If the flowrate does not vary with time, the weight-averaged molecular weight can be determined by:

$$M_w = \frac{\sum_{i=1}^N MW_i(t) \times h_i(t) \times \Delta t \times 1/a(t)}{\sum_{i=1}^N h_i(t) \times \Delta t \times 1/a(t)} \quad (4-34)$$

And the number-averaged molecular weight can be determined by:

$$M_N = \frac{\sum_{i=1}^N h_i(t) \times \Delta t \times 1/a(t)}{\sum_{i=1}^N h_i(t) \times \Delta t \times 1/a(t) \times 1/MW_i(t)} \quad (4-35)$$

Sample polydispersity is determined from the ratio of the weight- to number-averaged molecular weights.

If the time interval is constant, and the sample absorbivity does not vary with molecular weight, Equations 4-34 and 4-35 reduce to the expressions given by Yau et al. (1979) and used by Chin et al. (1994). To apply these equations, an estimate of  $1/a(t)$  is needed. The function  $1/a(t)$  can be calculated from the standard curve if  $1/a$  as a function of molecular weight is known:  $1/a(t) = 1/a(MW) \times MW(t)$ . The following approach was taken to estimate  $1/a(t)$ . First,  $1/a$  (TOC/UV, mg-cm/L) was determined as a function of molecular size by measuring the absorbivity of ultrafiltration size fractions. Absorbivity was measured as the slope of a linear correlation between TOC and UV absorbance. A stock solution of FHA was diluted, and TOC was measured for several values of UV absorbance. TOC/UV correlations, shown in Figure 4-23, were linear over the range of concentrations investigated, with  $r^2$  values  $>0.99$ . This finding is consistent with the results of other research (Weber et al. 1980, Weber et al. 1983, Summers and Roberts 1988a). Because the molecular weight of different size fractions were not known *a priori*, the determination of  $1/a(MW)$  and hence  $1/a(t)$  was an iterative process: molecular weight information was needed to calculate  $1/a(MW)$ , but  $1/a(MW)$  was needed to calculate molecular weights.

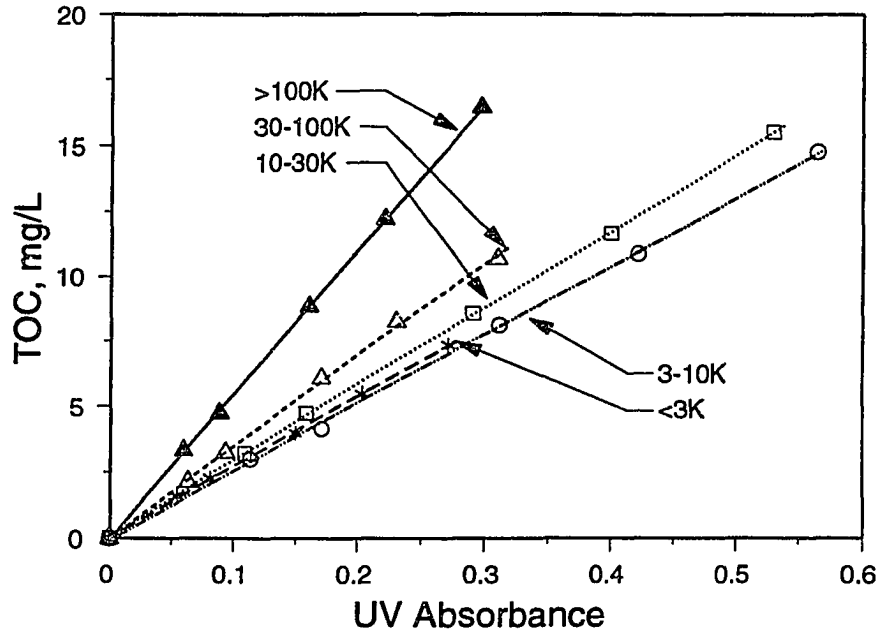


Figure 4-23. TOC/UV correlations for Laurentian humic acid size fractions prepared by ultrafiltration.

The iterative procedure was started by estimating the molecular weight of the size fractions assuming that  $1/a(t)$  was constant. Then,  $1/a$  was regressed as a function of  $\log_{10}(M_W)$  using a second-order polynomial. The choice of this regression function was purely empirical. This regression equation and the standard curve were used in Equations 4-34 and 4-35 to determine new estimates of the molecular weight of the size fractions. This process was repeated until the molecular weight estimates converged, which took only four iterations. The final relationship between  $1/a$  and  $\log_{10}(M_W)$  is shown in Figure 4-24, where  $\beta_0 = 281.31$ ,  $\beta_1 = -156.96$ , and  $\beta_2 = 24.15$ . The trend of decreasing absorptivity (increasing  $1/a$ ) with increasing molecular weight observed in this study is consistent with the findings of several researchers (Ladd 1969, Butler and Ladd 1969, Swift et al. 1970, Stewart and Wetzel 1981, Swift et al. 1992). However, this cannot be considered a general trend because other research has found either no trend or an increase in absorptivity with an increase in molecular weight (Buffle et al. 1978, Chin et al. 1994).

The error associated with assuming a constant sample absorptivity for Laurentian humic acid can be estimated by comparing the molecular weight estimates determined assuming a constant  $a(t)$  and those made using an empirically determined function. The



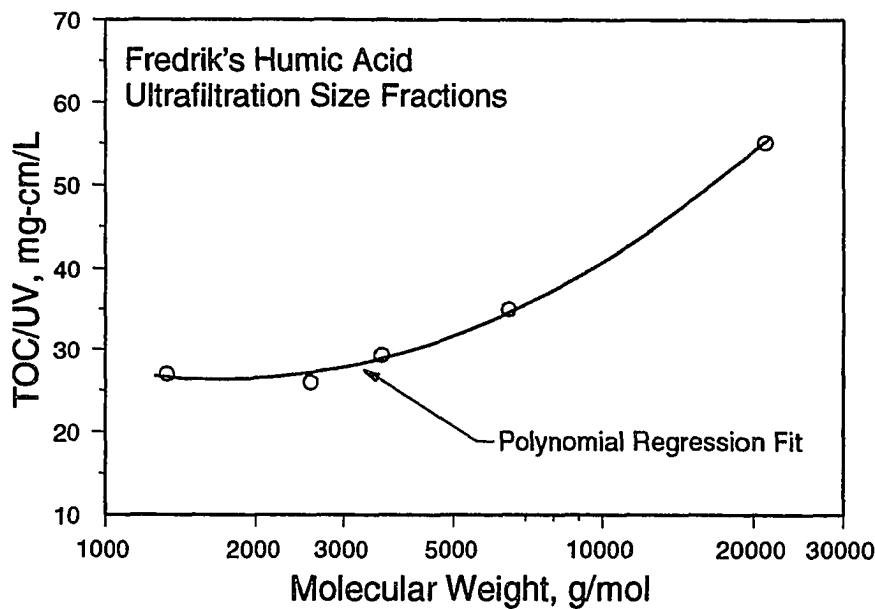


Figure 4-24. The effect of molecular weight on the absorptivity of Laurentian HA size fractions prepared by ultrafiltration. Solid line represents an empirical second-order polynomial fit to the data.

results of this analysis are tabulated in Table 4-2. The assumption of a constant  $a(t)$  results in an underestimation of the molecular weight, and the relative error generally increases with molecular weight.

The molecular sizes of humic substances determined by HPSEC are significantly smaller than the nominal cutoff sizes of the ultrafiltration membranes used to prepare the size fractions, shown by the data in Table 4-2. As discussed previously, this results from the determination of nominal membrane cutoff values using globular proteins, the structures of which are quite dissimilar to humic and fulvic acids. This finding is consistent with previous results reported in the literature (Beckett et al. 1987, Reid et al. 1990, Chin and Gshwend 1991, Kilduff and Weber 1992).

The ultrafiltration permeation factors for the ultrafiltration size fractions were correlated with the average molecular weights determined by HPSEC to verify that the methods of molecular size characterization are consistent. While the two processes are based on exclusion phenomena, different molecular size and shape factors may control macromolecule behavior differently in each system. The HPSEC measurements are

**Table 4-2. Effect of  $1/a(t)$  on Computed  $M_w$** 

Nominal UF Size Fraction	Constant $1/a(t)$	Empirical $1/a(t)$	Percent Error
<3K	1320	1383	4.56
3-10K	2522	2696	6.45
10-30K	3398	3747	9.31
30-100K	5820	6792	14.3
>100K	19563	22033	11.2

conducted at higher ionic strengths than the permeation factor measurements, which may affect degree of hydration and conformation. As discussed previously, the potential effects of concentration polarization are difficult to assess. Nevertheless, the correlation, shown in Figure 4-25, is linear, and suggests a strong relationship between macromolecule size characterized by the two techniques. The linear relationship observed should be regarded as an empirical finding which validates the consistency of interpreting molecular size using either ultrafiltration or size-exclusion chromatography.

The molecular-weight distributions determined for the ultrafiltration size fractions are shown in Figure 4-26. A scaling factor was applied to each distribution to normalize the peak height. The distributions are generally symmetric, with the exception of the >100 and <3K fractions which are skewed towards lower molecular weights. The >100K fraction appears to isolate the high-molecular weight peak found in the whole-HA chromatogram. Some overlap between adjacent fractions can be observed; however, permeation factor measurements confirm that the fractions have significantly different permeation characteristics. Overlap of the distributions of adjacent fractions may occur as a result of i) incomplete separation during the ultrafiltration fractionation; ii) diffuse separation resulting from a wide membrane pore-size distribution; and iii) concentration polarization effects causing variations in membrane rejection. With the exception of the >100K fraction, the polydispersity values ( $M_w/M_N$  ratio) for each fraction are fairly low, however, ranging from 1.44 to 1.63. This compares to a range of 1.1 to 1.25 for commercial polystyrene sulfonates. Band spreading of HPSEC chromatograms may occur as a result of dispersion, mass-transfer limitations between the mobile fluid and the

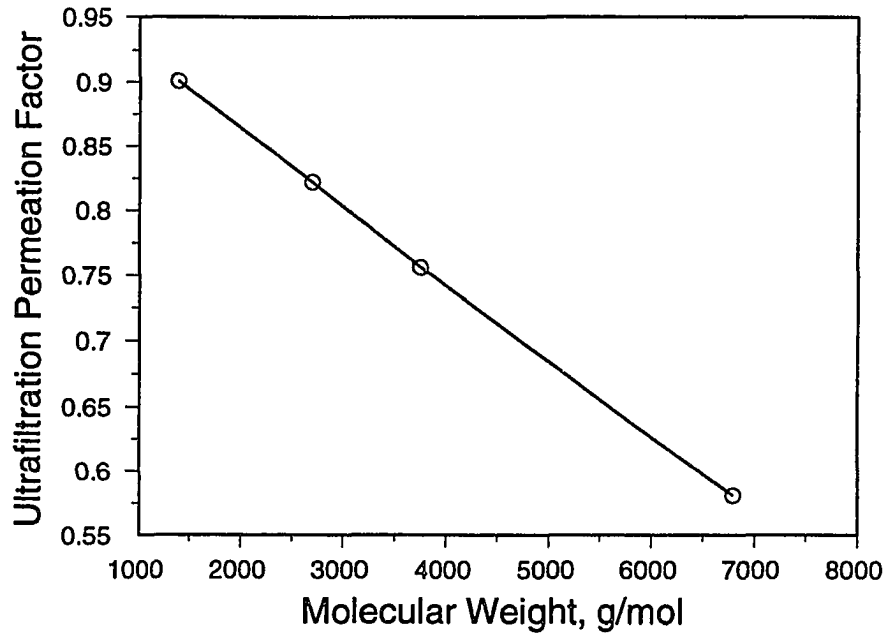


Figure 4-25. Correlation of ultrafiltration permeation factors determined for ultrafiltration size fractions with molecular weight as determined by HPSEC.

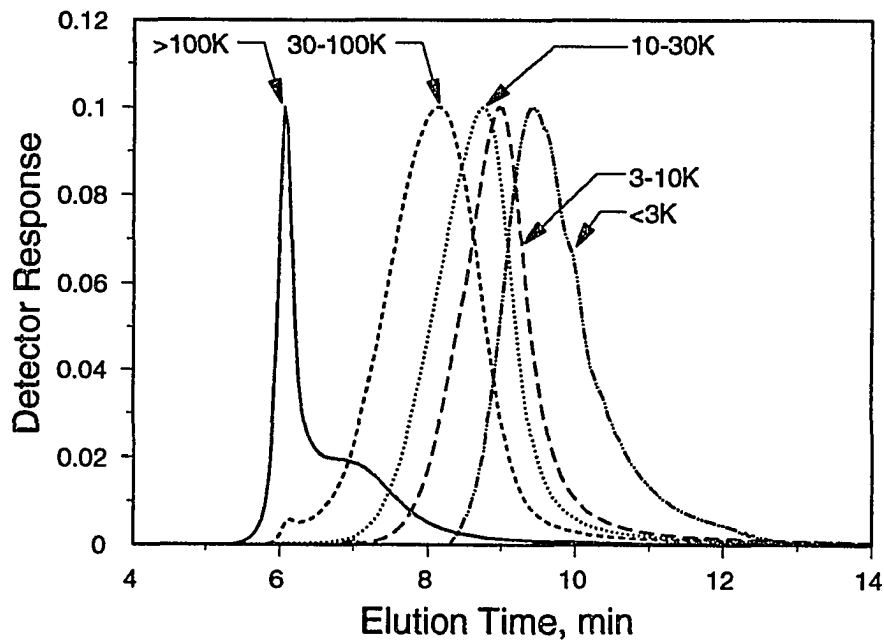


Figure 4-26. Size-exclusion chromatograms of ultrafiltration size fractions.

intraparticle fluid, and hindered diffusion (Gooding and Regnier 1990). Dispersion effects were evaluated by Chin et al. (1994) and were found to be negligible. Hindered diffusion of the >100K fraction may contribute to its higher polydispersity value of 1.80.

#### **4.7 Conclusions**

The single-parameter permeation model presented here can accurately characterize the permeation of organic, random-coil macromolecules in ultrafiltration systems. Solute uptake by membrane surfaces appeared negligible, however, under certain experimental conditions, it was found that the permeation factor decreased with increasing volume throughput, presumably due to the onset of concentration polarization phenomena. Care must therefore be taken to design experimental systems to minimize these variations.

Permeation behavior in ultrafiltration systems depends strongly on macromolecular structure, which is governed by solution ionic strength. Membranes should be calibrated with random-coil polymers of known molecular weight, in inorganic background matrices similar to the water sample to be fractionated. Polystyrene sulfonate was found to have coiling characteristics similar to that found for natural humic and fulvic acids, and may be useful for membrane calibration.

Sample chemistry must be taken into consideration even when using ultrafiltration on a comparative basis for characterization of different natural waters, because membrane permeation behavior of organic macromolecules depends strongly on ionic strength.

The permeation factor model accurately described mass throughput in fractionation experiments and was used to design a protocol to prepare size fractions reproducibly .

Size exclusion chromatography was used to measure molecular-weight distributions, and average molecular weights determined from the first moment of the HPSEC distribution correlated linearly with the permeation factors of the size fractions.

## CHAPTER V

### MACROMOLECULE ADSORPTION RATE STUDIES

#### 5.1 Introduction

By rigorous definition, the phase distribution represented by an adsorption isotherm represents an equilibrium condition. However, when the sorbate is macromolecular and the sorbent is micro-porous, very slow adsorption rates may be observed. In such systems, it may not be possible or desirable to conduct experiments over the time period required for true thermodynamic equilibrium to obtain. Long equilibration times may result in only marginal increases in amount adsorbed, and may introduce error resulting from solute volatilization, partitioning onto reactor components, and biodegradation. Therefore, it is necessary to define an "operational" equilibrium. To select an appropriate operational equilibrium period, it is necessary to consider, in detail, the rate at which equilibrium is approached. In this study, we analyze adsorption rate in the context of: 1) criteria developed on the basis of mathematical models of the adsorption process; 2) equilibration times reported in the literature; and, 3) adsorption rate studies conducted in this study.

#### 5.2 Estimation of Adsorption Rate Parameters

It is commonly assumed in adsorption modeling that activated carbon particles are roughly spherical, and that two diffusion steps occur in series: i) diffusion from the bulk solution, across a hydrodynamic boundary layer ("film"), to the particle surface; and ii) intraparticle diffusion from the surface toward the center of the particle. Since these two mechanisms act in series, the overall rate will be controlled by the slower step. To develop criteria for evaluating the time needed to reach equilibrium, it is first necessary to determine which adsorption mechanism controls the adsorption rate; it is therefore necessary to know or estimate the following adsorption rate parameters: 1) the particle size; 2) the film mass-

transfer coefficient, which incorporates the free-liquid diffusivity and the hydrodynamic boundary layer thickness; and 3) the intraparticle diffusion coefficient. Intraparticle diffusion may be modeled as pore diffusion, surface diffusion, or both. Pore diffusion refers to the diffusion of dissolved solute in the adsorbent pore space, while surface diffusion refers to diffusion of adsorbed solute along the pore surface. The rate of diffusion depends on the magnitude of the diffusion coefficient and on the spatial scale over which diffusion occurs.

#### Estimation of Film Mass-Transfer Coefficient

To estimate the film mass-transfer coefficient,  $k_f$ , for the particle sizes used in this research, a mass-transfer correlation developed by Ohashi et al. (1981) for single particles was used. The value of  $k_f$  depends on the free-liquid diffusivity and the thickness of the hydrodynamic boundary layer. The boundary layer thickness is governed by the particle size, the relative velocity between the particle and the bulk fluid, and the fluid viscosity. The four parameters which govern  $k_f$  are generally incorporated in two dimensionless numbers, the Reynolds number,  $N_{Re}$ , which is used to characterize hydrodynamic conditions, and the Schmidt number,  $N_{Sc}$ , which is used to characterize the relative importance of mass and momentum diffusivity.

The Reynolds number is computed from:

$$N_{Re} = \frac{v_s d_p}{\nu} \quad (5-1)$$

where  $v_s$  is the relative velocity between the particle and the bulk fluid,  $d_p$  is the particle diameter, and  $\nu$  is the kinematic viscosity. For the end-over-end tumbler system,  $N_{Re}$  was computed based on the unhindered terminal settling velocity of a carbon particle, an approach used by Randtke and Snoeyink (1983). The settling velocity calculation was based on Stoke's Law (Metcalf and Eddy 1972). The settling velocity of the carbon particle is:

$$v_s = \left[ \frac{4(\rho_s - \rho) g d_p}{3C_D \rho} \right]^{0.5} \quad (5-2)$$

where  $(\rho_s - \rho)$  is the difference in density between the particle and the fluid,  $d_p$  is the particle diameter,  $g$  is the gravitational acceleration, and  $C_D$  is the drag coefficient. The wetted particle density of  $1.42 \text{ g/cm}^3$  was estimated using data for the skeletal density ( $2.1 \text{ g/cm}^3$ ) and particle porosity (0.614) from Carter (1992). The drag coefficient was computed from the following relationship, valid for  $N_{Re} < 10^4$  (Metcalf and Eddy 1972):

$$C_D = \frac{24}{N_{Re}} + \frac{3}{(N_{Re})^{0.5}} + 0.34 \quad (5-3)$$

The solution requires an iterative determination of  $v_s$ ,  $N_{Re}$ , and  $C_D$ . The calculation was done on a spreadsheet, and the results are tabulated in Table 5-1.

**Table 5-1. Reynolds Number and Terminal Settling Velocity for Discrete Settling of Carbon Particles**

Particle Size	Diameter, cm	$N_{Re}$	$C_D$	$v_s$ , cm/s
58 micron	$58 \times 10^{-4}$	0.048	512.6	0.079
165 micron	$165 \times 10^{-4}$	1.00	27.34	0.576

The Schmidt number,  $N_{Sc}$ , is the ratio of momentum to mass diffusivity, and is defined as:

$$N_{Sc} = \frac{v}{D_1} \quad (5-4)$$

Computation of  $N_{Sc}$  requires estimates of  $D_1$ , the free-liquid diffusivity. Estimates were obtained from Cornel et al. (1986), who measured the diffusivity of PSS, Aldrich humic acid, and HA fractions using a short-bed adsorber technique. Film mass-transfer coefficients were determined from early-time breakthrough profiles from a short-bed

adsorber. Free-liquid diffusivities were computed from measured  $k_f$  values by a correlation appropriate for fixed-bed reactor systems.

The film mass-transfer coefficient,  $k_f$ , for the completely-mixed-batch reactors used in this research were computed using a correlation developed by Ohashi et al. (1981). This correlation was based on the energy dissipation rate defined for a particle. Ohashi et al. showed that many mass-transfer correlations published in the literature collapsed onto a single curve when expressed in terms of the energy dissipated instead of the Reynolds number. The Ohashi correlation incorporated and extended the correlation of Ranz and Marshall (1952) used by Randtke and Snoeyink (1983). This correlation was chosen because i) it was developed explicitly for single particles; and ii) it is valid at the low Reynolds numbers characteristic of the hydrodynamic conditions in the end-over-end tumbler system used in this research to mix individual batch reactors. Ohashi et al. (1981) derived their correlation in terms of the energy dissipation rate per unit mass of liquid flowing around a particle, and expressed their results in terms of a "specific power" dimensionless group. The specific power group can be related to the Reynolds number and the particle drag coefficient; therefore, the correlation can be expressed in terms of more familiar dimensionless numbers:

$$N_{Sh} = \frac{k_f d_p}{D_l} = 2 + 0.517 C_D^{0.19} N_{Re}^{0.57} N_{Sc}^{(1/3)} \quad (5-5)$$

where  $N_{Sh}$  is the Sherwood number. The Ohashi correlation is only strictly valid for  $0.5 < N_{Re} < 100,000$ . Therefore, the results for the 165-micron particle size must be considered the most reliable. The solute/solvent combinations used to develop the correlation have Schmidt numbers less than 1420, while aqueous macromolecules, with low free-liquid diffusivities, have much higher Schmidt numbers. Since the diffusion coefficient also appears in the Sherwood number, and since the diffusion mechanism is not expected to change with increasing molecular weight, the correlation is expected to remain accurate at high Schmidt numbers. This was the finding of Wilson and Geankopolis (1966) who found that Schmidt numbers up to 70,600 did not affect their correlation for mass-



transfer in fixed beds. Finally, no other correlation is available for single particles which is valid over a greater range of Schmidt numbers.

In Table 5-2 shows representative values for macromolecule diffusivities at pH 7 are shown, with corresponding values of  $N_{Sc}$ , and mass-transfer coefficients computed using the Ohashi et al. correlation.

**Table 5-2. Free-Liquid Diffusivities and External "Film" Mass-Transfer Coefficients for Selected Macromolecules**

Compound	Ionic Strength	$D_l$ , m <sup>2</sup> /s	$N_{Sc}$	$k_f$ , m/s 58 micron	$k_f$ , m/s 165 micron
Frac. HA	0.01 M	$8.0 \times 10^{-11}$	11,875	$1.22 \times 10^{-5}$	$1.17 \times 10^{-5}$
Frac. HA	0.10 M	$1.7 \times 10^{-10}$	5,588	$2.15 \times 10^{-5}$	$1.98 \times 10^{-5}$
PSS 1.6K	0.01 M	$6.4 \times 10^{-11}$	14,844	$1.03 \times 10^{-5}$	$1.00 \times 10^{-5}$
PSS 6.5K	0.01 M	$2.4 \times 10^{-11}$	39,583	$5.06 \times 10^{-6}$	$5.10 \times 10^{-6}$
PSS 31K	0.01 M	$1.3 \times 10^{-11}$	73,077	$3.26 \times 10^{-6}$	$3.35 \times 10^{-6}$
PSS 1.6K	0.10 M	$1.4 \times 10^{-10}$	67,857	$1.85 \times 10^{-5}$	$1.73 \times 10^{-5}$
PSS 6.5K	0.10 M	$9.0 \times 10^{-11}$	10,556	$1.33 \times 10^{-5}$	$1.27 \times 10^{-5}$
PSS 31K	0.10 M	$4.6 \times 10^{-11}$	20,652	$8.12 \times 10^{-6}$	$7.97 \times 10^{-6}$

Note: Frac HA is the 50-100K fraction of Aldrich HA fractionated on Amicon ultrafiltration membranes.  $N_{Sc}$  was computed using a value of  $0.0095 \text{ cm}^2/\text{s}$  for the kinematic viscosity, which corresponds to a typical laboratory temperature of 22 °C.

The estimated values of  $k_f$  are consistent with those measured by Lee et al. (1981), who report values ranging from  $1.8 \times 10^{-5}$  to  $2.5 \times 10^{-5}$  m/s for adsorption of humic acid, fulvic acid, and fulvic acid fractionated by ultrafiltration by GAC (600-micron-particles) in a stirred batch reactor. Summers (1986) conducted rate experiments in a differential batch reactor; therefore, the film mass transfer coefficients obtained in that research are not comparable. Fettig and Sontheimer (1987a,c) measured lower values ranging from  $0.72 \times 10^{-5}$  to  $0.89 \times 10^{-5}$  m/s for a fulvic acid, perhaps due, in part, to the larger particles (1.18 mm) used.

The estimated values of  $k_f$  computed for macromolecules in tumbler-type batch systems are lower than values normally observed for low-molecular-weight target pollutants in fixed-bed adsorbers. Smith (1987) reports values for trichloroethylene and p-

dichlorobenzene ranging from  $4.5 \times 10^{-5}$  to  $8.0 \times 10^{-5}$  m/s for 505-micron particles and a velocity of about 1.9 cm/s. Carter (1993) reports a value for trichloroethylene of  $1.6 \times 10^{-4}$  m/s for 165-micron particles and a velocity of 0.51 cm/s. The higher mass-transfer coefficients for low molecular weight pollutants in fixed-bed systems can be attributed to two factors: i) SOCs have lower molecular weights, and thus higher free-liquid diffusivities (on the order of  $1 \times 10^{-9}$  m<sup>2</sup>/s) than macromolecules; and ii) relative velocities between the bulk liquid and the particle surface are generally higher in fixed bed systems. Most fixed-bed systems are designed for loading rates on the order of 2 to 10 gpm per ft<sup>2</sup>; assuming a bed porosity of about 0.35, these loading rates correspond to relative velocities ranging from 0.5 to 2.0 cm/s.

#### Estimation of Intraparticle Diffusion Coefficients

In contrast to the film mass-transfer coefficient, intraparticle diffusion coefficients are intrinsic characteristics of the adsorbate and the adsorbent, and do not depend on the hydrodynamic conditions at the particle surface. Insofar as pore size restrictions and chemical interactions between adsorbate and adsorbent may affect the measured intraparticle diffusion rate, reliable correlations for estimating intraparticle diffusivities are not available. Therefore, estimates for these parameters were taken from macromolecule diffusion measurements reported in the literature.

To determine an intraparticle diffusion coefficient, rate data were fit with a mathematical mass-transfer based rate model. Inherent in the choice of rate model is an assumption of an intraparticle diffusion mechanism. When data is fit with a pore diffusion model and the diffusion coefficient required to fit the data is greater than the free-liquid diffusivity, it is generally assumed that surface diffusion makes a contribution to intraparticle flux. The fact that a particular model fits measured data cannot be interpreted as proof that the assumed mechanism is correct; in fact, Summers (1986) reports that either the Pore Diffusion Model (PDM) or the Homogeneous Surface Diffusion Model (HSDM) fit the rate of the initial 50% of Aldrich humic acid uptake equally well. Therefore, both intraparticle mechanisms were considered. Tables 5-3 and 5-4 summarize results from several studies that investigated macromolecule adsorption rates by activated carbon.

**Table 5-3. Macromolecule Pore Diffusion Coefficients**

Reference	Organic Matter	Background	pH	$D_p, m^2/s$	Conditions
S	Aldrich HA	$10^{-3} PO_4$	7.0	$2.5 \times 10^{-12}$	0.10 M NaCl
S	1K-5K Aldrich HA	$10^{-3} PO_4$	7.0	$3.1 \times 10^{-12}$	0.10 M NaCl
S	50K-100K Aldrich HA	$10^{-3} PO_4$	7.0	$2.0 \times 10^{-15}$	0.10 M NaCl
S	50K-100K Aldrich HA	$10^{-3} PO_4$	7.0	$0.85 \times 10^{-12}$	0.0 M NaCl

Note: Data from Summers 1986 (S).

**Table 5-4. Humic Substance Surface Diffusion Coefficients on F400 Carbon**

Reference	Organic Matter	Background	pH	$D_s, m^2/s$	Conditions
L	Pfaltz & Bauer HA	$10^{-3} PO_4$	6.0	$1.7 \times 10^{-15}$	NS
L	Houghton Peat FA	$10^{-3} PO_4$	6.0	$2.7 \times 10^{-15}$	NS
L	Frac. Peat FA	$10^{-3} PO_4$	6.0	$6.0 \times 10^{-15}$	NS
L	Coag Peat FA	$10^{-3} PO_4$	6.0	$3.0 \times 10^{-15}$	NS
RS	Humic Acid	$10^{-3} CO_3$	8.3	$6.0 \times 10^{-16}$	NS
RS	Fulvic Acid	$10^{-3} CO_3$	8.3	$2.7 \times 10^{-15}$	NS
J	Aldrich HA	$10^{-3} PO_4$	7.0	$1.2 \times 10^{-14}$	NS
J	Aldrich HA	River Water	7.0	$1.2 \times 10^{-14}$	IS = 0.005 M
J	Coag. Aldrich HA	River Water	7.0	$2.3 \times 10^{-14}$	IS = 0.005 M
J	Fulvic Acid	River Water	7.0	$1.5 \times 10^{-14}$	IS = 0.005 M
J	River Water	Natural	7.0	$1.0 \times 10^{-14}$	IS = 0.005 M
S	Aldrich HA	$10^{-3} PO_4$	7.0	$1.3 \times 10^{-15}$	0.10 M NaCl
S	50K-100K Aldrich HA	$10^{-3} PO_4$	7.0	$2.3 \times 10^{-15}$	0.10 M NaCl

Notes: Citations are from Lee et al. 1981 (L), Randtke and Snoeyink 1983 (RS), Jodella 1985 (J) and Summers 1986 (S). Frac. Peat FA refers to Fulvic Acid fractionated on a 50K molecular-weight-cutoff Amicon ultrafiltration membrane. Coag. refers to FA or HA coagulated with alum. NS means that the ionic strength (IS) was not specified.

The pore diffusion coefficients of Aldrich HA measured by Summers (1986) show some variability depending on molecular weight and ionic strength, but differences are not dramatic. A value of about  $1.0 \times 10^{-12}$  m<sup>2</sup>/s appears to be a reasonable value for ionic strengths characteristic of most natural waters.

The reported surface diffusion coefficients are remarkably similar, considering the differences in the materials studied, and the conditions used. The values reported by Jodellah (1985) are about one order of magnitude higher than other values reported, which may be due to the relatively high concentrations of divalent metals in the solutions studied. It is known that Aldrich HA has a high ash content -- some researchers, including Summers (1986), purify the Aldrich material to remove metals. The Huron river water studied by Jodellah (1985) is also known to contain high calcium concentrations, which has been shown to effect humic adsorption rate and capacity. Among the remaining values reported, an average value of about  $2.5 \times 10^{-15}$  seems to be a reasonable surface diffusion coefficient estimate for humic substance adsorption on F400 carbon.

The intraparticle diffusion coefficients reported in the literature were obtained from relatively short-term studies. Summers conducted several longer-term studies, and reports that only the first 50% of solute uptake can be accurately described by a single-component, single-domain diffusion model. Slower diffusivities of less preferentially adsorbed components, or hindered diffusion in micropores, may reduce the apparent intraparticle diffusion coefficient as equilibrium is approached. This possibility could be addressed by performing a sensitivity analysis on the intraparticle diffusion coefficient when assessing equilibrium criteria.

### **5.3 Model-Based Criteria for Establishing Time to Equilibrium**

Several investigators have published mathematical adsorption model simulations, applicable to batch systems, which can be used to develop criteria for the time required to reach equilibrium. For example, Suzuki and Kawazoe (1974, 1975) developed analytical expressions assuming various combinations of intraparticle transport mechanism (surface and pore diffusion) and isotherm type (irreversible, linear and Freundlich). For pore diffusion with an irreversible isotherm, they also provided solutions which illustrate the effect of external mass-transfer resistance. Neretnieks (1976) presented solutions to the

pore/surface diffusion model (PSDM) for both Langmuir and Freundlich isotherms. Hand et al. (1983) presented Homogeneous Surface Diffusion Model (HSDM) simulations assuming a Freundlich isotherm. Randtke and Snoeyink (1983) performed HSDM calculations to examine the effects of particle size, intraparticle diffusivity, initial solute concentration ( $C_0$ ) and adsorbent dose on the time required to reach a specified ratio of either  $q/q_e$  or  $C_e/C_0$ .

If external mass-transfer resistance is significant, the time required to reach equilibrium is lengthened. This phenomena is illustrated by the results of Suzuki and Kawazoe (1975) and Neretnieks (1976), which demonstrated the impact of external mass transfer resistance on the time required to reach equilibrium for the cases of pore diffusion with an irreversible isotherm and pore diffusion with a Freundlich isotherm, respectively. In some cases, the effects of external mass-transfer resistance are not important. The analysis of Randtke and Snoeyink (1983) included mass-transfer at the particle surface; however, they found that their model results were insensitive to the film mass-transfer coefficient because mass-transfer was controlled by intraparticle diffusion. In the case of stirred batch reactors, the experimenter has considerable control over experimental conditions, and can often eliminate the effects of external mass-transfer. This assumption was made by Hand et al. (1983). In the end-over-end tumbler system used in this research, mixing intensity cannot be controlled. To apply the time to equilibrium criteria, it was therefore necessary to determine which mass-transfer mechanism controls the adsorption rate. This was done by evaluating the Biot number, a dimensionless number which reflects the relative importance of film and intraparticle mass-transfer. The computation of the Biot number, in turn, requires the estimation of several physicochemical parameters. The parameters and their estimation techniques are discussed in subsequent sections.

#### Computation of Biot Number

The definition of the Biot number depends on the reactor configuration and the assumed intraparticle diffusion mechanism. For a completely-mixed-batch reactor system in which surface diffusion is the intraparticle mechanism, the Biot number is defined as (Hand et al. 1983):

$$N_{Bi, SURFACE} = \frac{k_f r_p (1-\epsilon_r)}{N_{Dg} D_s \epsilon_r \phi} \left[ 1 - \frac{C_e}{C_o} \right] \quad (5-6)$$

where  $k_f$  is the film mass-transfer coefficient,  $r_p$  is the particle radius,  $\epsilon_r$  is the *reactor* void fraction (the fraction of volumetric space unoccupied by adsorbent),  $N_{Dg}$  is the solute distribution parameter,  $D_s$  is the surface diffusion coefficient, and  $\phi$  is the particle sphericity (the ratio of the surface area of an equivalent volume sphere to the actual particle surface area). The term in brackets represents the percentage of TOC removal from the liquid phase in the reactor at equilibrium. The void fraction,  $\epsilon_r$ , can be computed knowing the adsorbent dose,  $D_o$ , and the particle density,  $\rho_p$ :

$$\epsilon_r = 1 - \frac{D_o}{\rho_p} \quad (5-7)$$

The solid to solution volume ratio can be written as:

$$\frac{(1-\epsilon_r)}{\epsilon_r} = \frac{1}{\frac{\rho_p}{D_o} - 1} \quad (5-8)$$

and the solute distribution parameter is computed from:

$$N_{Dg} = \frac{D_o q_e^*}{\epsilon_r C_o} \quad (5-9)$$

where  $q_e^*$  is the adsorbent phase concentration in equilibrium with the initial liquid phase concentration,  $C_o$ . Estimates of the solute distribution parameter, reactor void fraction and fractional removal required to compute  $N_{Bi, SURFACE}$  were obtained from preliminary HA adsorption data generated using a 58-micron particle size and an equilibration period of 30 days, because it is thought that equilibrium conditions were closely approximated under these conditions.

For a completely-mixed-batch reactor in which pore diffusion is the intraparticle mechanism, the Biot number is defined as (Suzuki and Kawazoe 1974):

$$N_{\text{Bi, PORE}} = \frac{k_f r_p}{D_p} \quad (5-10)$$

where  $D_p$  is the pore diffusion coefficient and is defined by:

$$D_p = \frac{D_l \epsilon_p}{\tau} \quad (5-11)$$

where  $D_l$  is the free liquid diffusivity,  $\epsilon_p$  is the *particle* void fraction, and  $\tau$  is the tortuosity, which ranges from 2 to 6 for microporous adsorbents (Satterfield 1970, Suzuki and Kawazoe 1974).

Computed Biot numbers for both surface and pore diffusion intraparticle transport mechanisms are tabulated in Table 5-5. To compute the Biot numbers, representative values of  $k_f = 1.2 \times 10^{-5}$  m/s,  $D_s = 2.5 \times 10^{-15}$  m<sup>2</sup>/s and  $D_p = 1.0 \times 10^{-12}$  m<sup>2</sup>/s were used.

When pore diffusion is the dominant intraparticle transport mechanism, Biot numbers above about 100 represent essentially complete intraparticle diffusion control (Suzuki and Kawazoe 1974), and the effects of external mass-transfer are insignificant. However, when surface diffusion is the dominant intraparticle diffusion mechanism, adsorption rates are completely controlled by intraparticle diffusion only when the Biot number is above 300 for Freundlich *n*-values ranging from 0.2 to 1.0 (Hand et al. 1983). Under conditions characterized by lower Biot numbers, film mass-transfer resistance plays a role in determining adsorption rate, and becomes increasingly important with decreasing particle size and decreasing adsorbent dose. Low doses corresponds to large amounts adsorbed, and therefore higher surface diffusion fluxes.

#### Criteria for the Time Required to Reach Equilibrium

Criteria for the time required to reach equilibrium, based on model simulations reported in the literature, are tabulated in Table 5-6. The application of each criterion

**Table 5-5. Surface and Pore Diffusion Biot Numbers**

Dose, $D_0$ , g/L	58-micron Carbon		165-micron Carbon	
	$N_{\text{Biot, surface}}$	$N_{\text{Biot, pore}}$	$N_{\text{Biot, surface}}$	$N_{\text{Biot, pore}}$
0.1	15	348	44	990
0.3	42	348	120	990
0.5	65	348	186	990
0.7	87	348	249	990
0.9	106	348	301	990
1.1	123	348	349	990
1.3	136	348	387	990
1.5	145	348	413	990
1.7	150	348	428	990
2.0	160	348	456	990

requires assuming either pore and surface diffusion is the dominant intraparticle transport mechanism. Further, each criterion is strictly valid for a particular isotherm model. In addition, each criterion is subject to specified Biot number constraints. The Biot number analysis summarized in Table 5-5 identifies the conditions under which various constraints may be met for the end-over-end tumbler-type batch systems used in this research.

For all isotherm types and Biot numbers, when intraparticle diffusion is the rate-limiting mechanism, the time to reach equilibrium depends on the square of the adsorbent particle size; this result emphasizes the importance of this parameter in controlling adsorption rate. The time to reach equilibrium has a weak dependence on the value of  $C_e/C_0$  -- as  $C_e/C_0$  decreases, corresponding to larger adsorbent doses, the time to equilibrium is increased, over a range of  $C_e/C_0$  from 0.2 to 0.9 (Suzuki and Kawazoe 1974 & 1975, Randtke and Snoeyink 1983). There is also a weak dependence on the Freundlich exponent (n-value) for the case of surface diffusion; as the exponent increases, the time to equilibrium decreases, over a range of 0.01 to 2.0 (Suzuki and Kawazoe 1974 & 1975, Hand et al. 1983). Based on estimates of adsorption rate parameters and model-based time to equilibrium criteria, the estimated time required for the humic substances studied in this research to reach equilibrium is one week or less for the 58-micron particle size and on the order of 20 to 40 days for the larger 165-micron particle size.



**Table 5-6. Criteria for Time to Reach Equilibrium in a Batch Reactor**

Ref.	Diffusion Mechanism	Isotherm	$N_{Biot}$	$t_e$ Criteria	$t_e$ , days 58 micron	$t_e$ , days 165 micron
S K	Surface	Linear	Large	$t_e > \frac{0.4r_p^2}{D_s}$	4	32
S K	Surface	Freundlich	Large	$t_e > \frac{0.5r_p^2}{D_s}$	5	39
H	Surface	Freundlich	> 300	$t_e > \frac{0.5r_p^2}{D_s}$	5	39
S K	Surface	Irreversible	Large	$t_e > \frac{0.6r_p^2}{D_s}$	6	47
S K	Pore	Irreversible	> 0.75	$t_e > \frac{r_p^2 \rho_p q_0}{C_0 D_p}$	18	50
S K	Pore	Irreversible	> 5	$t_e > \frac{0.4r_p^2 \rho_p q_0}{C_0 D_p}$	7	20
N	Pore	Freundlich	Large	$t_e > \frac{0.4R^2 \rho_p q_0}{C_0 D_p}$	7	20

Notes: Citations are from Suzuki and Kawazoe 1974, 1975 (SK), Hand et al. 1983 (H), and Neretnieks 1976 (N). Criterion from Hand is valid for Freundlich exponent values less than 1.0. Surface diffusion criteria are for  $C_e/C_0$  less than 0.9, pore diffusion criteria for  $C_e/C_0 \approx 0.5$ .

#### 5.4 Equilibration Times Reported in the Literature

The estimated times required for humic substances to reach equilibrium tabulated in Table 5-6 are consistent with the findings of other researchers. Lee et al. (1981) found that the adsorption of a commercial humic acid and a peat fulvic acid reached equilibrium in a rotary shaker-type batch reactor in five days if the carbon was "pulverized," and in 60 days if it was not. The particle sizes of the non-pulverized carbon ranged from 600-micron to 1.67 mm, but the particle sizes of the pulverized carbon was not specified, although they were probably as small or smaller than the 58-micron size used in this research. Randtke and Snoeyink (1983) proposed a relationship for the time required (days) for  $C(t)$  to decrease to within  $1.01C_e$ :

$$t_{1.01} = 93778(d_p^2) \quad (5-12)$$

where  $d_p$  is the particle diameter expressed in centimeters. This relationship was developed using the HSDM for a humic acid with a surface diffusion coefficient of  $6.0 \times 10^{-16} \text{ m}^2/\text{s}$ , a value slightly smaller than the value used in the calculations made in this Chapter. This relationship yields a time-to-equilibrium estimate of three days for 58-micron particle size and 26 days for the 165-micron particle size. A time to equilibrium of five days was used by Summers (1986) for the adsorption of several humic substances, both commercial and natural, on 50-micron particle size carbon. However, Summers also showed that removal still occurred after 21 days; therefore, the five-day period did not represent a true time to equilibrium.

### 5.5 Laboratory Measurements of Macromolecule Rates

The rates of PSS, humic acid, and fulvic acid adsorption were examined experimentally and compared to theoretical predictions. The model-based equilibrium criteria were used to design experiments and interpret experimental results. The rate study data are shown in Figures 5-1 through 5-4. The rate of PSS adsorption was investigated to identify the effects of molecular weight and adsorbent pore structure on adsorption rate. Results for PSS adsorption on 165-micron F400 carbon are shown in Figures 5-1 and 5-2. In addition to having a greater adsorption capacity on F400 carbon, the smaller 1.8K PSS system exhibited a faster approach to equilibrium than the 8K PSS system. The 1.8K PSS system appeared to reach equilibrium in about 20 days, while it took the 8K PSS system about 35 days, or fifteen days longer. The times to reach equilibrium determined experimentally for the PSS systems are consistent with the estimates tabulated in Table 5-6. The trend observed as a function of molecular weight is consistent with the expected impact of molecular weight on both the surface or pore diffusion coefficient (Suzuki et al. 1976). While the extrapolation of these results to natural systems may not be strictly valid, the range of molecular weight studied here (1.8K to 8K) was chosen to be representative of the range found in many natural systems.

As Figure 5-2 illustrates, the type of carbon appears to have a significant influence on the adsorption capacity, but a less dramatic impact on the adsorption rate. The BPLF3 adsorbent has a higher adsorption capacity than the F400 carbon, perhaps due to its larger pore-size distribution. It also appears as though equilibrium is reached before 20 days on

the BPLF3 carbon, an observation which is consistent with the carbon's larger pores and less restrictive intraparticle diffusion.

Figures 5-3 and 5-4 show the rate of humic and fulvic acid adsorption onto F400 carbon for two particle sizes, 165-micron and 58-micron. These rate curves suggest that a near-equilibrium condition is achieved after about 50 days for both particle sizes. The smaller particle size exhibits a slightly greater adsorption capacity for the first 30 days, but the capacities of the different particle sizes appear to converge at longer times. These findings are also consistent with the estimates for time to reach equilibrium tabulated in Table 5-6. While the rate curve appears to reach a plateau, suggesting that the adsorption is near completion, it is difficult to say with certainty that equilibrium has been achieved; these data do not rule out the possibility that slow adsorption may continue for extended periods of time. However, these data suggest that the majority of the adsorption capacity is reached within about four weeks, which is consistent with other studies reported in the literature (Summers 1986, Carter et al. 1991).

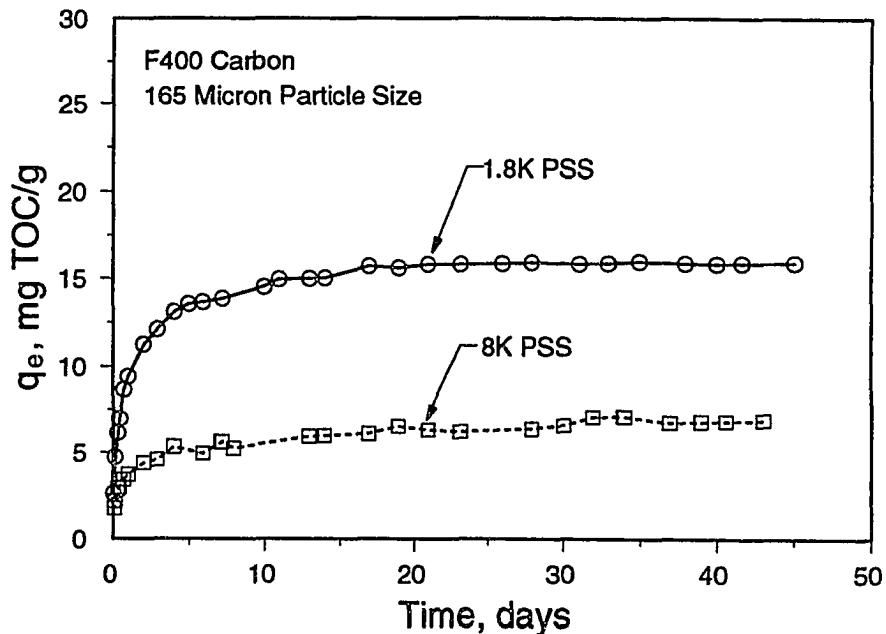


Figure 5-1. Adsorption of PSS on F400 carbon for two different molecular weights.  $C_0 = 20$  mg PSS/L;  $D_0$  (1.8K) = 1250 mg/L;  $D_0$  (8K) = 1500 mg/L.

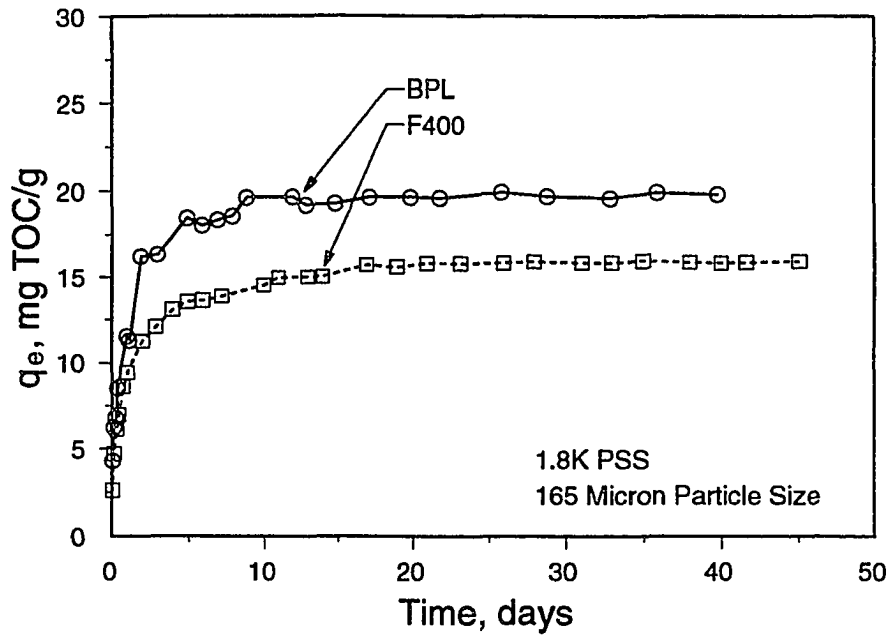


Figure 5-2. Adsorption of 1.8K PSS on two coal-based activated carbons having similar starting materials and activation conditions but different activation times. F400:  $C_o = 20$  mg PSS/L,  $D_o = 1250$  mg/L; BPLF3:  $C_o = 20$  mg PSS/L,  $D_o = 1000$  mg/L.

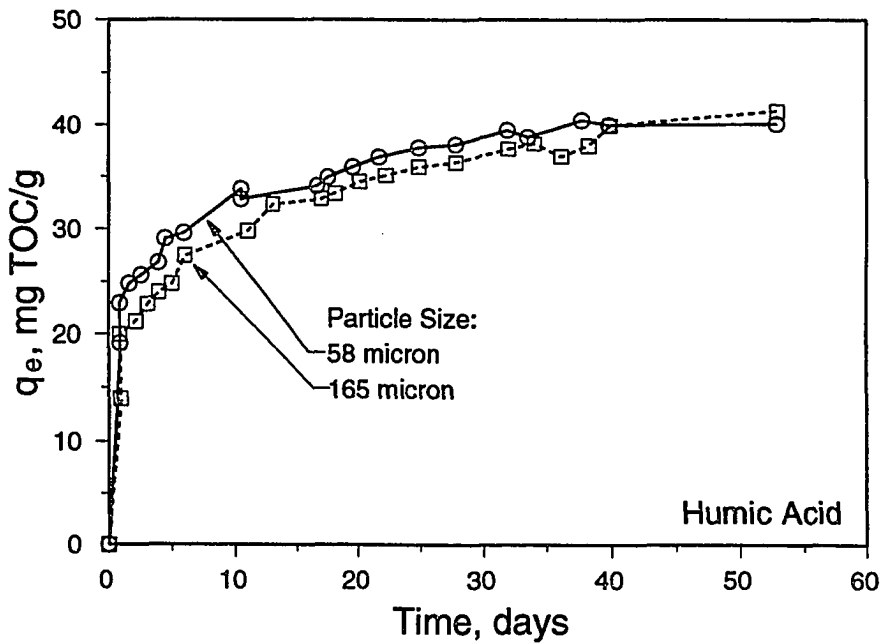


Figure 5-3. Adsorption of Laurentian HA on F400 carbon for two different particle sizes.  $C_o = 21.6$  mg TOC/L,  $D_o = 300$  mg/L.

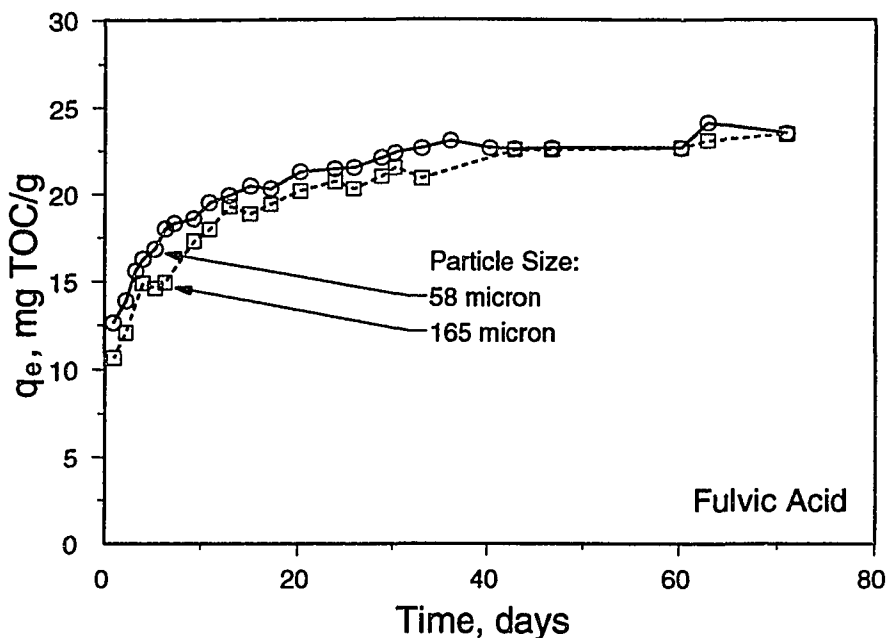


Figure 5-4. Adsorption of Laurentian FA on F400 carbon for two different particle sizes.  $C_o = 9.1$  mg TOC/L,  $D_o = 300$  mg/L.

## 5.6 Order-of-Magnitude Analysis

One approach to determining an operational equilibration period is to equate the effective time of exposure of carbon in a full-scale system to that in the laboratory systems. Full-scale systems, which use carbon particle sizes on the order of 1 to 2 mm in diameter, may operate for periods of months or years before regeneration of carbon is required. Effective exposure times for different particle sizes will be the same when they have been equilibrated for the same dimensionless time. An expression for the dimensionless time was obtained from the dimensionless form of the solid-phase mass balance relationship (Equation 2-27) (Sontheimer et al. 1989). The dimensionless time,  $T^*$ , assuming that surface diffusion dominates intraparticle transport, is written:

$$T^* = \frac{D_s t}{R_p^2} \quad (5-13)$$

a similar expression is obtained assuming pore-diffusion as the controlling intraparticle transport mechanism:

$$T^* = \frac{D_p C_o t}{R_p^2 \rho_p q_o} \quad (5-14)$$

Under the assumption that the intraparticle diffusion coefficient and particle density do not vary with particle size, equating the dimensionless time for different particle sizes yields the relationship:

$$t_1 = t_2 \left( \frac{R_{p1}}{R_{p2}} \right)^2 \quad (5-15)$$

This relationship was used to find equivalent diffusion times for various particle size ranges commonly encountered in adsorption studies; the results of the computation are tabulated in Table 5-7.

**Table 5-7. Equivalent Diffusion Times for Various Size Carbon Particles.**

Particle Size Range, mm or US Std Sieve	Geometric Mean Diameter, mm	Diffusion Time, days
1.3 mm	1.30	2000
30/40	0.505	300
80/100	0.165	30
200/325	0.058	4

This analysis suggests that a four-day isotherm conducted with a 58-micron particle size carbon is equivalent to a 30-day isotherm conducted with an 165-micron particle size carbon, which represents nearly one year or more for the 505-micron particle size and larger particles. Although solutes of interest (particularly macromolecules) may not reach a true equilibrium state in the times tabulated in Table 5-7, under a single domain diffusion assumption, all particle sizes would receive the same effective exposure time. Therefore,

similar reductions in the liquid phase concentration and amount of solute adsorbed should be exhibited. It can be seen that exposure times common in full-scale systems can be scaled to relatively short exposure times in the laboratory by using smaller particle sizes.

The foregoing analysis may provide a convenient means of developing operational equilibrium criteria, but a rather critical assumption is that the diffusion coefficient remains constant in time and space. In fact, there is evidence that the diffusion of macromolecules in microporous adsorbents is not a single-domain process. The presence of micropores may result in hindered diffusion, causing the diffusion coefficient to change over time. Thus, it is probably not strictly valid to assume that the diffusion coefficient remains constant. However, if the pore size distribution of the different particle sizes is similar, then changes in the diffusion coefficient should be similar, rendering the foregoing analysis a reasonable approximation.

Based on the foregoing results and analyses, an operational equilibration time of 30 days was chosen for all isotherm and preloading experiments conducted with natural humic substances. This choice of conditions results in the attainment of a near-equilibrium condition, while reducing the potential of biological activity, and allowing for comparison with previous research. To make a further assessment of how closely equilibrium conditions are approached with the larger 165-micron particle size carbon, 30-day isotherms were measured for both humic and fulvic acid on 58-micron and 165-micron F400 carbon. These results, which provide a working definition of "operational equilibrium," are shown in Figures 5-5 and 5-6. In these experiments, it is assumed that the 58-micron particle size is near a true equilibrium condition. Since the slopes of these isotherms appear relatively independent of particle size, it is reasonable to compare isotherm capacities throughout the range of concentration measured by directly comparing the Freundlich unit capacity parameter,  $K_F$ , of each isotherm. Based on the relative  $K_F$  values tabulated in Table 5-8, the humic acid reaches about 90.2% and the fulvic acid reaches about 74.1% of the equilibrium capacity in the 30 day operational equilibrium period.

**Table 5-8. Modified Freundlich Isotherm Parameters for Humic and Fulvic Acid Adsorption on F400 Carbon. Effect of particle size.**

Solute/ Particle Size	$C_0$ , mg TOC/L	N	$K_F$ (95% C.I.)	n (95% C.I.)
<b>Humic Acid</b>				
58 micron	23.8	14	6.50 (6.28, 6.73)	0.404 (0.389, 0.418)
165 micron	23.4	13	5.86 (5.65, 6.07)	0.391 (0.376, 0.405)
<b>Fulvic Acid</b>				
58 micron	31.0	23	12.02 (11.68, 12.37)	0.275 (0.264, 0.285)
165 micron	23.3	14	8.91 (8.57, 9.27)	0.300 (0.284, 0.317)

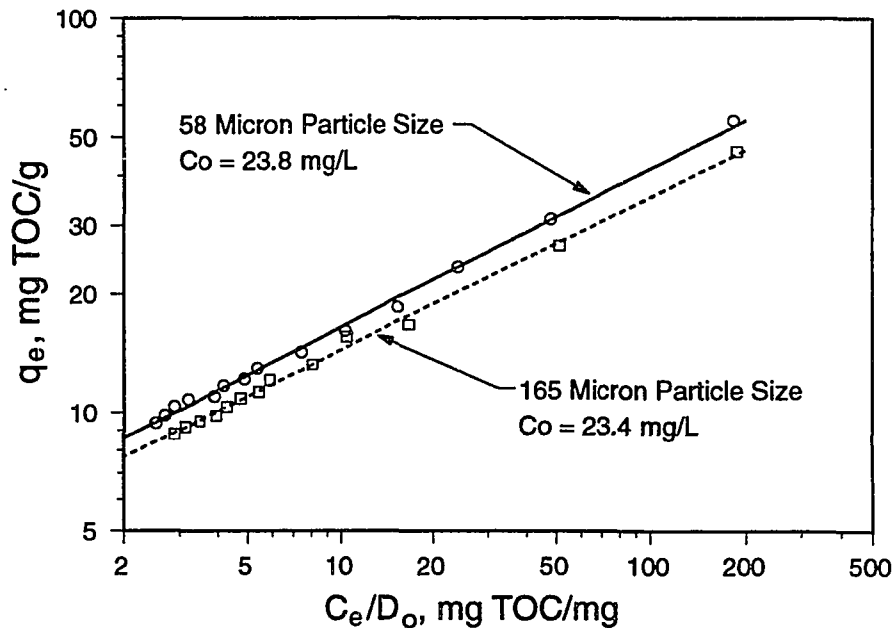


Figure 5-5. The effect of particle size on the adsorption isotherm of Laurentian HA on F400 carbon. A 30-day contact time was used for both particle sizes.  $C_0$  (165-micron) = 23.4 mg TOC/L;  $C_0$  (58-micron) = 23.4 mg TOC/L.



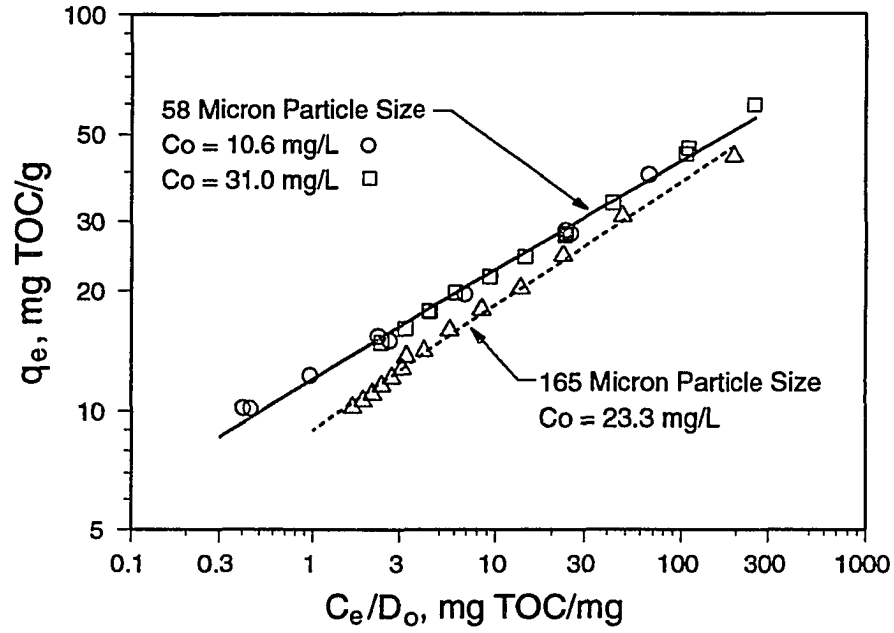


Figure 5-6. The effect of particle size on the adsorption isotherm of Laurentian FA on F400 carbon. A 30-day contact time was used for both particle sizes.  $C_o$  (165-micron) = 23.3 mg TOC/L;  $C_o$  (58-micron) = 30.9 mg TOC/L.

## CHAPTER VI

### ADSORPTION OF NATURAL AND SYNTHETIC POLYELECTROLYTES

#### 6.1 Introduction

The objective of this chapter is to characterize the adsorption of natural humic acids on activated carbon, to better understand the mechanisms of macromolecule adsorption, and to provide insight into the impacts of adsorbed dissolved organic matter on the subsequent adsorption of low-molecular-weight target compounds. In particular, the effects of molecular size (which contributes to adsorbate heterogeneity), solution ionic strength, and calcium concentration on macromolecule adsorption were investigated.

The adsorption of a synthetic polyelectrolyte, polystyrene sulfonate (PSS), was studied as a model compound to isolate important factors governing the adsorption behavior of natural humic materials. The adsorption of well-characterized synthetic polymers onto microporous adsorbents has not received wide attention. There has been no systematic study of the effects of molecular weight and molecular size on the adsorption of narrow molecular-weight-distribution polyelectrolytes in microporous adsorbents such as activated carbon. The adsorption of PSS was studied to investigate i) how size-exclusion phenomena affect the adsorption of macromolecules having known, narrow, molecular-weight distributions; and ii) the effects of ionic strength on the adsorption of well-characterized polyelectrolytes, and on the size exclusion phenomena.

Adsorption isotherms of soil humic and fulvic acids were measured to examine the competitive interactions among components of natural organic matter. The adsorption of soil humic acid size fractions prepared by ultrafiltration fractionation, and narrow molecular weight fractions of polystyrene sulfonate was measured to demonstrate the effect of macromolecule size on the extent of adsorption. Finally, the effects of solution ionic strength, calcium concentration at constant ionic strength, and adsorbent type on the extent

of humic adsorption and on the competitive interactions among humic components were investigated. High Performance Size Exclusion Chromatography (HPSEC) was used to measure molecular size distributions of organic polyelectrolytes remaining in solution after equilibrating with activated carbon to provide information about how different size fractions compete when adsorbed from a mixture. The use of HPSEC made it possible to study natural humic materials and dissolved organic matter at environmentally relevant concentrations. HPSEC chromatograms and first moments of the size distribution are reported as a function of the humic to adsorbent concentration ratio.

## 6.2 Polyelectrolyte Adsorption on Activated Carbon

### Adsorption of a Model Polyelectrolyte: PSS

Adsorption isotherms were measured for different PSS molecular weights, at different solution ionic strengths, to study the effects of macromolecule size and solution chemistry on the extent of adsorption. PSS was chosen as a model compound because it is commercially available in narrow molecular-weight ranges. In contrast to natural organic macromolecules, the effect of molecule size may be studied while maintaining a known, constant, molecular structure.

PSS adsorption isotherms were developed for 1.8K and 18K molecular weights, chosen as representative of molecular weights of natural organic matter. Isotherms were measured at ionic strengths of 0.01, 0.02 and 0.07-M, representative of values found in natural waters and water treatment processes. These isotherms were measured with 200/325 (58 micron) particle size F400 carbon and were equilibrated for two weeks. Isotherm data and modified Freundlich isotherm model fits are shown in Figure 6-1, and isotherm parameters with corresponding 95% confidence intervals are tabulated in Table 6-1. The rationale for plotting the amount adsorbed versus the equilibrium concentration divided by the adsorbent dose,  $C_e/D_0$ , will be demonstrated in subsequent sections. While this equilibration period was shorter than that employed for the natural humic materials, the PSS rate data presented in Chapter 5 (Section 5.5) confirm that the significant differences observed in the extent of adsorption among different PSS molecular weights and solution ionic strengths cannot be attributed to kinetic effects. Rather, these isotherms illustrate the

**Table 6-1. Adsorption of PSS by F400 Carbon: Effects of Molecular Weight and Ionic Strength.**

Experiment	Ionic Strength, M	MW, g/mol	N	$K_F$ (95% C.I.)	$n$ (95% C.I.)
FF2PA7VI	0.07	1.8K	4	38.44 (34.65, 42.64)	0.058 (0, 0.147)
FF2PA2VI	0.02	1.8K	8	28.57 (27.62, 29.54)	0.051 (0.031, 0.070)
FF2PA1VI	0.01	1.8K	5	20.21 (19.03, 21.46)	0.056 (0.033, 0.078)
FF2PD7VI	0.07	18K	7	10.96 (10.53, 11.41)	0.061 (0.041, 0.081)
FF2PD2VI	0.02	18K	8	5.74 (5.41, 6.09)	0.023 (0, 0.054)
FF2PD1VI	0.01	18K	8	2.93 (2.88, 2.98)	0.064 (0.047, 0.081)

Conditions: Isotherms conducted with 58 micron F400 carbon,  $C_0 = 20$  mg PSS/L, 14-day equilibration.

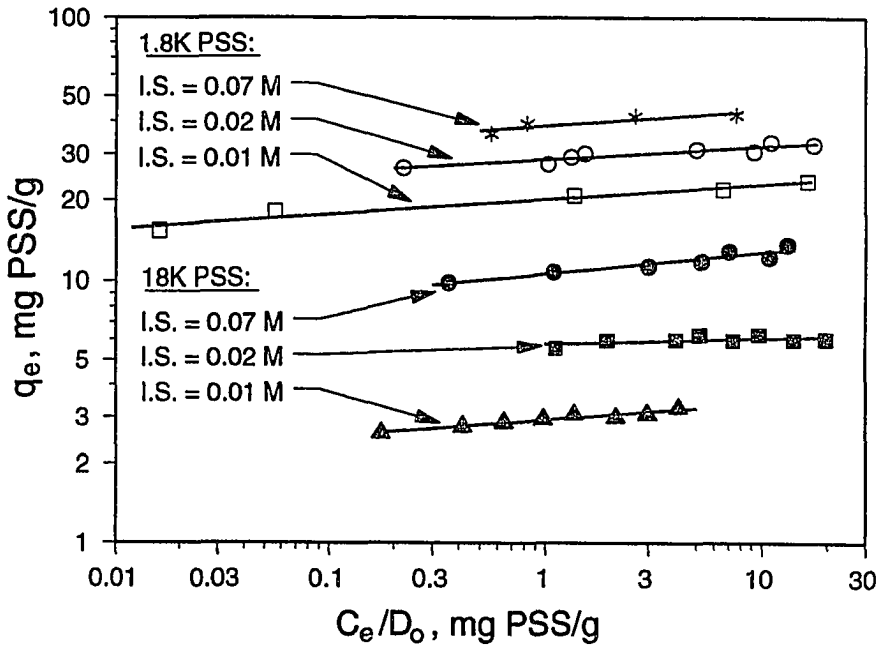


Figure 6-1. Adsorption of polystyrene sulfonate on 58-micron F400 carbon illustrating the effect of molecular weight and ionic strength on the adsorption isotherm.  $C_0 = 20$  mg PSS/L for all solutions.

size exclusion of macromolecules that occurs in microporous adsorbents, and the impacts of ionic strength on molecular size and subsequent adsorption capacity.

For a given ionic strength, the amount adsorbed increases with decreasing molecular weight. The affinity of PSS for the solvent should decrease with increasing molecular weight, resulting in a greater extent of adsorption for higher molecular weight PSS, in accordance with polyelectrolyte adsorption theory (Papenhuijzen et al. 1985b). Since the chemical structure of the different molecular weight fractions is the same, the chemical affinity for the surface should not vary significantly. Therefore, these results suggest that although the high-molecular-weight components may have a greater adsorption affinity than low-molecular-weight components, a smaller fraction of the adsorbent surface area is accessible to them.

For a given molecular weight, a significant increase in adsorption capacity is observed with increasing ionic strength. These results are consistent with observations of the effects of ionic strength on humic substance adsorption by activated carbon reported in the literature (McCreary and Snoeyink 1980, Randtke and Jepson 1982, Weber et al. 1983, Summers and Roberts 1988a, Lafrance and Mazet 1989). There may be some increase in adsorption due to a reduction in the affinity between the PSS and the aqueous phase; however, over the range of ionic strengths studied, this effect is not expected to be important. An increase in ionic strength may enhance hydrophobic bonding by screening electrostatic charge on polymer segments. However, the adsorption experiment was conducted at pH 7, below the pH<sub>pzc</sub> of the F400 carbon. Since the adsorbate and the surface carry opposite charges, the surface affinity is expected to be fairly strong. This suggests that increases in ionic strength, over the range studied here, would not have a significant effect on the surface affinity. This conclusion is supported by the observation that the Freundlich *n* value, the heterogeneity parameter of the surface site energy distribution, remains relatively constant over the range of ionic strengths examined. Therefore, the effects of ionic strength were interpreted primarily in terms of changes in macromolecule configuration. This interpretation is consistent with the model of humic structure proposed by Gosh and Schnitzer (1980).

An increase in the solution ionic strength causes the macromolecule to coil and reduce its effective size, thereby enabling it to access a greater fraction of the adsorbent

surface area. It is important to note that while molecular weight is a fundamental molecular property, molecular size, which may change in response to changes in solution chemistry, is the property which governs adsorption behavior. Similar trends are observed whether the PSS molecular weight is decreased or whether the solution ionic strength is increased, decreasing molecular size. An implication of this finding is that molecular size is a controlling factor in humic substance adsorption. Further, the manipulation of solution ionic strength may be a useful approach to studying the effects of molecular size on the adsorption of natural organic macromolecules.

### Adsorption from Mixtures

The adsorption of humic substances falls under the general category of adsorption from polydisperse mixtures. The polydisperse nature of a mixture may result from components with different adsorption affinities for the surface, or different abilities to access adsorbent surfaces. Weber et al. (1983) demonstrated that humic acid solutions are a polydisperse mixture of components with different adsorption properties. Typically, the components of the mixture cannot be identified or quantified uniquely; therefore, a lumped concentration parameter such as total organic carbon (TOC), must be used. If adsorption from a polydisperse mixture is quantified by a lumped parameter, then the isotherm for the system depends on the experimental conditions used. If variable dose isotherms are measured, different isotherms will be obtained for different initial TOC concentrations. Similarly, if constant dose isotherms are measured, different isotherms will be obtained for each dose. In general, each test condition represents "a set of equilibrium states to which each component in a mixture will be driven and a set of pathways by which the reaction can proceed" (Weber et al. 1983). This behavior results from competitive interactions between mixture components, and occurs whenever mixture components have different adsorbabilities.

When mixture components compete for adsorption sites, the fraction of the mixture removed from solution depends on the initial solution concentration and the adsorbent dose,  $D_0$ . Figure 6-2 illustrates these concepts in schematic form, based on data reported by Summers and Roberts (1988a) and Sontheimer et al. (1989). When isotherms are measured using a constant adsorbent dose and variable initial adsorbate concentration,

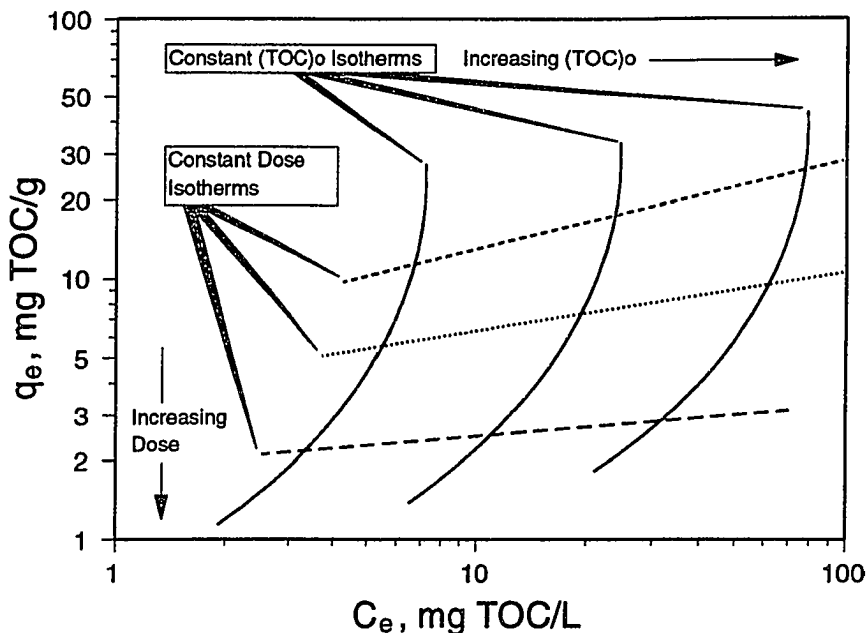


Figure 6-2. Schematic representation of adsorption isotherms obtained for DOM when concentration is expressed in terms of TOC. Equilibrium distribution depends on the fraction of the mixture adsorbed; therefore, the isotherm depends on methodology (constant vs. variable dose) and experimental conditions.

nearly linear isotherms are generally observed when the data are plotted on  $\log(q_e)$  versus  $\log(C_e)$  coordinates. However, constant-dose isotherms conducted at different doses are shifted on the  $\log(q_e)$ -axis. When the adsorbent dose is low, adsorption sites are limited and only the most adsorbable components of the mixture are removed from solution. When the adsorbent dose is high, more adsorption sites are available, and more of the components with lower adsorbabilities are removed from solution. Therefore, for a given equilibrium solution phase concentration, the extent of adsorption decreases with increasing adsorbent dose.

When isotherms are measured using a constant initial adsorbate concentration and a variable adsorbent dose, isotherm data are generally not linear on  $\log(q_e)$  versus  $\log(C_e)$  coordinates. Regardless of the isotherm methodology, however, the amount adsorbed is greatest when only the most adsorbable component is removed from solution, which occurs when the adsorbent dose is low relative to the initial adsorbate concentration. Therefore, for a given equilibrium adsorbate concentration, the amount adsorbed will be

greatest for a smaller initial adsorbate concentration. Thus, adsorption capacity increases upon dilution.

### **6.3 Adsorption of Soil Humic and Fulvic Acids**

#### Humic Substances as Multicomponent Mixtures

Variable-dose isotherms were conducted at two different initial concentrations to show that the Laurentian humic and fulvic acids are comprised of a mixture of components with different adsorbabilities. The isotherms, shown in Figure 6-3, depend on the initial TOC concentration, and isotherm capacity increases with decreasing TOC<sub>0</sub>. This result demonstrates that the humic substances are mixtures of components with different adsorbabilities, which exhibit competitive adsorption.

A second set of experiments, similar to the "skimming" experiment done by Weber et al. (1983), was done to directly show that the Laurentian humic acid was comprised of components with different adsorbabilities which exhibit competitive adsorption. First, the whole humic acid was equilibrated with F400 carbon for an operational equilibrium period of 30 days. The carbon was then removed, and the adsorption of components remaining in the supernatant solution was measured on fresh carbon. The data were fit with the modified Freundlich isotherm; best fit parameters and associated 95% confidence intervals are shown in Table 6-2. The extent of adsorption of components remaining in solution after the first equilibration was significantly lower than the whole humic acid, as shown in Figure 6-4, demonstrating that the most adsorbable components were preferentially removed during the initial equilibration period. Further, as the percentage of TOC removal during the initial equilibration increased, the fraction of more adsorbable components removed from solution increased, resulting in a concomitant reduction in the extent of adsorption of remaining components.

#### Preferential Adsorption

It is evident from Figures 6-2 and 6-3 that the adsorption behavior of a mixture cannot be uniquely described as a function of the equilibrium concentration of a lumped concentration parameter. However, a unique isotherm may be obtained using a simple



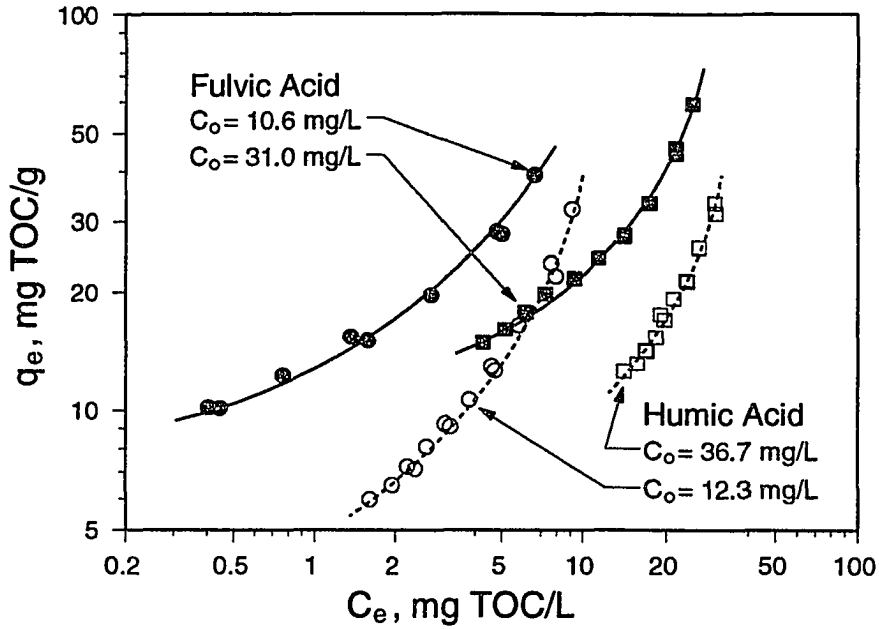


Figure 6-3. The adsorption of Laurentian humic and fulvic acids on F400 58-micron carbon at two initial concentrations using the variable-dose methodology. Isotherms confirm that HA is a mixture of components with different adsorbabilities. Lines illustrate parametric trends.

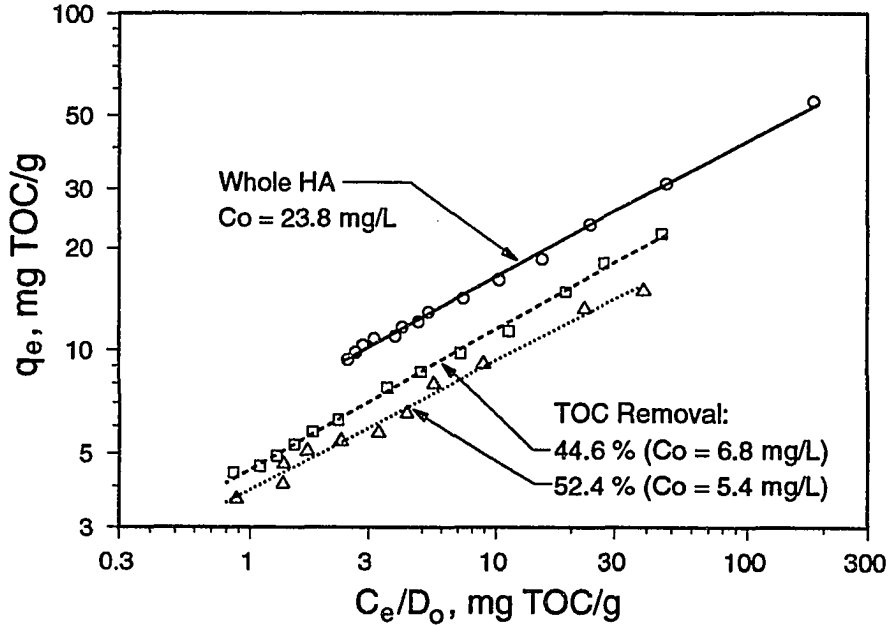


Figure 6-4. Adsorption of Laurentian HA components remaining in solution after initial equilibration with F400 carbon for two different TOC removal percentages.

**Table 6-2. Adsorption of Laurentian HA on F400 Carbon: Effects of Competitive Adsorption from a Mixture**

TOC Removal	$C_0$ , mg/L	N	$K_F$ (95% C.I.)	n (95% C.I.)
0% (Whole HA)	23.8	14	6.50 (6.28, 6.73)	0.404 (0.389, 0.418)
44.6%	6.8	13	4.47 (4.34, 4.60)	0.411 (0.396, 0.425)
52.4%	5.4	11	3.88 (3.66, 4.11)	0.380 (0.348, 0.412)

Conditions: Isotherms conducted with 58-micron F400 carbon, I.S. = 0.01 M, 30-day equilibration.

transformation, if components in the mixture exhibit preferential adsorption.

Preferential adsorption can be considered a special case of competitive adsorption. When components adsorb preferentially, their maximum extent of adsorption is obtained before any other component can gain access to the surface. As adsorbent capacity is exhausted, therefore, progressively less preferentially adsorbed components are excluded from the adsorbent surface. If a solution is comprised of components having adsorption affinities distributed over some range, the components having the highest affinity will always be removed first, and will be removed completely. If isotherms are measured under different conditions, the amount adsorbed will be the same only when the same subset of the distribution is removed from solution. Thus, the amount adsorbed depends on the fraction of the solution adsorbed. That is, the composition of the solution at equilibrium, not the solute concentration, determines the extent of adsorption.

When components adsorb preferentially, the distribution of solution components depends on the adsorbent mass ( $M$ ) and solution volume ( $V$ ), and therefore adsorbent dose ( $D_0 = M/V$ ) of the system (Koopal 1981, Hlady et al. 1982). A unique isotherm may be obtained when the amount adsorbed is expressed in terms of a quantity which characterizes the solution composition. One such parameter is the non-adsorbed amount of solute per unit mass of adsorbent, computed by normalizing the equilibrium concentration by the adsorbent dose ( $C_e/D_0$ ). As shown by Koopal (1981) normalization of isotherms in this way accounts for the polydispersity of the mixture. Therefore, parameters obtained in this

manner may be compared directly regardless of the experimental conditions employed to measure isotherm data.

It has been shown that this technique of normalizing isotherms could be applied to commercial and natural humic materials (Summers and Roberts 1988a) and to natural humics after coagulation and ozonation (Harrington and DiGiano 1989). The normalized isotherm data were described by a modified Freundlich isotherm model:

$$q_e = K_F(C_e/D_0)^n \quad (6-1)$$

where  $q_e$  is the amount adsorbed per unit mass of adsorbent (mg TOC/g);  $C_e$  is the equilibrium liquid-phase concentration (mg TOC/L);  $D_0$  is the adsorbent dose (mg/L); and  $K_F$  and  $n$  are empirical constants. Using this technique, the variable-dose isotherms of Laurentian humic acid, shown by the open symbols in Figure 6-3, were normalized. The results are shown in Figure 6-5. The normalization technique is also applicable to the Laurentian fulvic acid, as illustrated by the data shown in Figure 5-6. These results imply that i) Laurentian humic acid is a polydisperse mixture of components having different adsorption properties; ii) the components of the mixture exhibit competitive adsorption; and iii) more adsorbable components exhibit near-complete preference over less adsorbable components.

#### Effects of Macromolecule Size

The PSS adsorption studies identified macromolecule size as an important factor governing the extent of adsorption of polyelectrolytes on activated carbon. To test the hypothesis that macromolecule size also plays a central role in the adsorption of Laurentian humic acid, adsorption isotherms of ultrafiltration size fractions were measured. Adsorption data was fitted with the modified Freundlich isotherm model; model parameters and associated 95% confidence intervals are reported in Table 6-3.

The isotherms, shown in Figure 6-6, demonstrate that each fraction exhibits significantly different adsorption properties. These results confirm that i) Laurentian HA is a polydisperse mixture of different molecular size components; and ii) macromolecule size

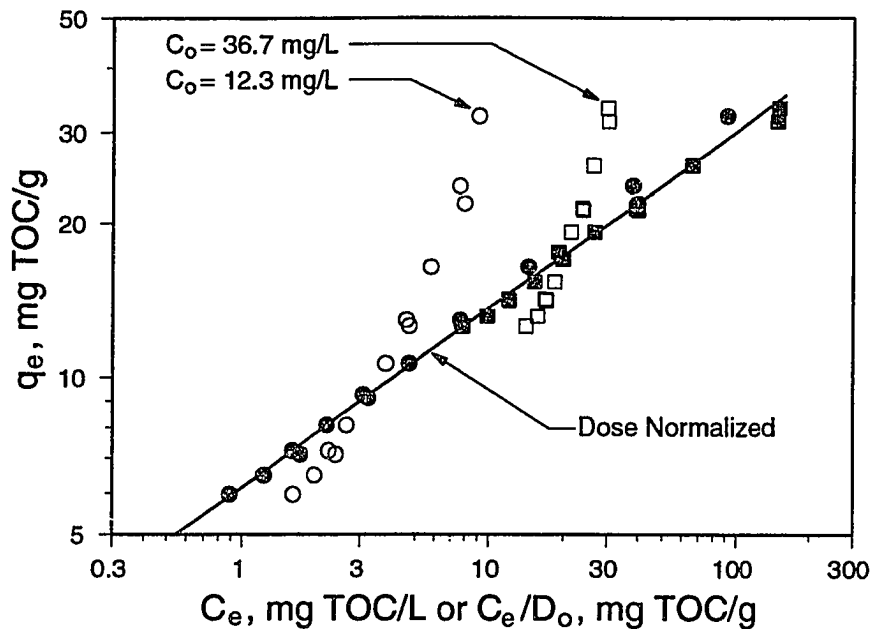


Figure 6-5. Adsorption of Laurentian HA on 58-micron F400 carbon at two initial concentrations using the variable-dose methodology (open symbols). Isotherms are normalized in log-log space when expressed in terms of non-adsorbed DOM per adsorbent mass,  $C_e/D_o$  (closed symbols).

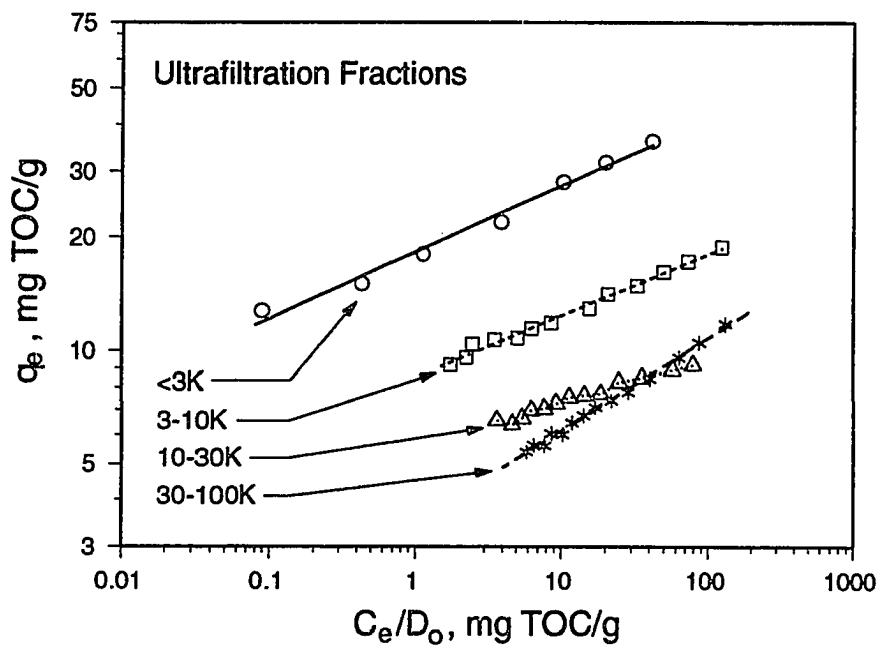


Figure 6-6. Adsorption of Laurentian HA size fractions prepared by ultrafiltration, illustrating the impact of macromolecule size on DOM isotherms.

**Table 6-3. Adsorption of Laurentian HA Size Fractions Prepared by Ultrafiltration**

Fraction	$C_0$ , mg/L	N	$K_F$ (95% C.I.)	n (95% C.I.)
<3K	8.0	7	18.93 (17.82, 20.10)	0.182 (0.156, 0.208)
3-10K	14.2	13	8.48 (8.24, 8.73)	0.163 (0.152, 0.173)
10-30K	13.2	13	5.53 (5.35, 5.72)	0.118 (0.106, 0.130)
30-100K	14.6	14	3.48 (3.36, 3.60)	0.245 (0.234, 0.256)

Conditions: Isotherms conducted with 165-micron F400 carbon, I.S. = 0.01 M, 30-day equilibration.

plays a central role in HA adsorption. As discussed in Chapter 4 (Section 4.6), the molecular weight of each fraction was characterized by high performance size-exclusion chromatography (HPSEC) standardized using narrow molecular weight fractions of sodium polystyrene sulfonate. The adsorbability of each size fraction was characterized in terms of the Freundlich Capacity Factor ( $K_F$ ), determined from linear regression analysis of the log-linearized form of the dose-normalized Freundlich isotherm equation. In this analysis,  $K_F$  is determined from the regression intercept ( $C_e/D_0 = 1$  thus  $\log(C_e/D_0) = 0$ ). In Figure 6-7, the  $K_F$  value is plotted as a function of HA molecular weight. Nearly an order-of-magnitude increase in the amount of TOC adsorbed corresponds to a similar range in the average molecular weight; the greatest capacities were observed for fractions having molecular weights less than 4,000.

These results conclusively verify that the Laurentian HA is comprised of a mixture of molecular sizes, and that the smaller molecular sizes exhibit a greater adsorbability based on the amount adsorbed per unit mass of adsorbent. The effect of molecular size on adsorption capacity observed with natural HA is consistent with the results obtained with synthetic PSS, suggesting that larger molecular sizes do not access a portion of the adsorbent surface area which is available to smaller sized molecules. These results do not necessarily indicate, however, that the larger molecules have a lower adsorption affinity. To compare the affinities of different molecular size components for the carbon surface, it is necessary to determine the surface area accessible to each molecular size, then express isotherm measurements in terms of the amount adsorbed per unit accessible surface

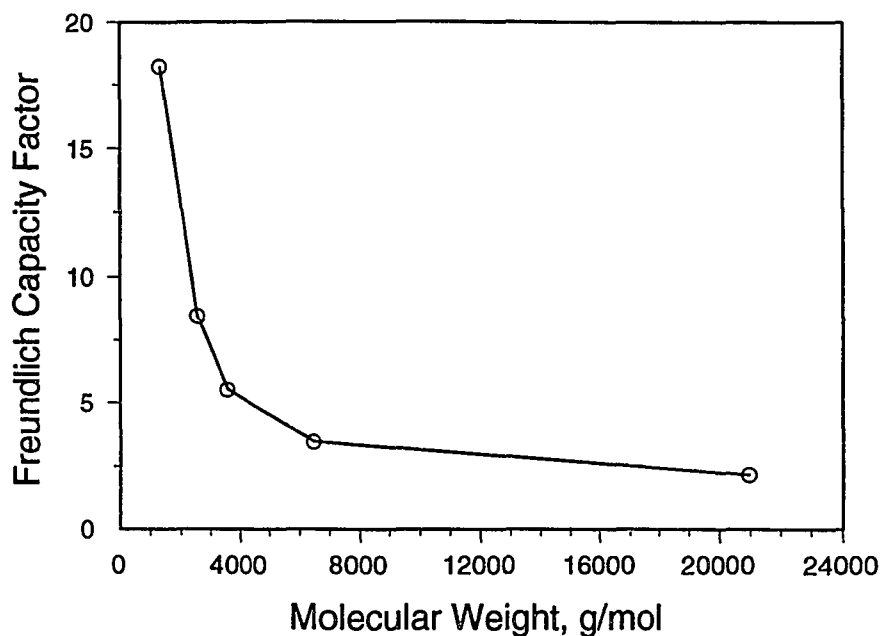


Figure 6-7. The effect of HA molecular weight, as determined by size exclusion chromatography, on the Freundlich  $K_F$  value of dose-normalized HA isotherms of size fractions prepared by ultrafiltration.

area. This was accomplished by Summers and Roberts (1988b), who confirmed that on the basis of accessible surface area, larger molecules indeed have a greater extent of adsorption.

From a practical point of view, these result suggests that molecular weight measurements of natural organic matter can be used to predict their adsorbability, at least as a first approximation. Furthermore, ultrafiltration permeation factor measurements may provide a rapid, inexpensive screening technique for assessment of natural humic substances adsorbability, because ultrafiltration permeation factors were linearly related to average molecular weights determined by HPSEC.

#### Competitive Interactions among HA Components

Results presented thus far have shown that Laurentian HA is i) comprised of a mixture of components with different adsorbabilities which exhibit preferential competition; and, ii) comprised of a mixture of molecules of various sizes, the smaller of which are

more adsorbable on an adsorbent mass basis. A logical extension of these results is the hypothesis that the observed competition occurs between HA components having different molecular sizes. To test this hypothesis, the size of HA components remaining in solution after equilibrating with activated carbon was characterized by measuring ultrafiltration permeation factors and HPSEC molecular-weight distributions.

Adsorptive fractionation of the whole humic solution was demonstrated in Figure 6-5. Under the hypothesis that competition between HA components occurs on the basis of molecular size, adsorptive fractionation will result in changes in the size of molecules remaining in solution after equilibration with activated carbon. As the dose of adsorbent is increased, corresponding to decreasing  $C_e/D_0$  values, an increased fraction of the initial TOC is removed from solution. If small molecules are adsorbed preferentially, the size of the HA components remaining in solution must also increase.

To fractionate solutions by adsorption, different amounts of 80/100 (165 micron) activated carbon were equilibrated in large 1L reactors. The purpose of these experiments was two-fold -- to prepare a large quantity of adsorbent for subsequent TCE adsorption experiments, and to provide a volume of supernatant large enough for further characterization. The results of the preparative fractionation are shown in Figure 6-8. Three adsorbent doses, 0.26, 0.53 and 1.05 g/L and three nominal initial TOC concentrations of 15, 30 and 60 mg/L were used.

The permeation factor is theoretically related to the ratio of solute diameter to the membrane pore diameter; as the molecular size decreases, the permeation factor increases. Therefore, if solutions are fractionated on the basis of molecule size, the permeation factor of HA components remaining in solution should decrease as the adsorbent dose increases. Similarly, an increase in the permeation factor should be observed with increasing  $C_e/D_0$  ratios. As the adsorbent dose approaches zero, the size distribution of components remaining in solution approaches that of the original solution. Therefore, the permeation factor should asymptotically approach that of the original solution. Permeation factors were determined as described in Chapter 4 (Section 4.5). The best-fit permeation factors and the corresponding 95% confidence intervals are tabulated in Table 6-4. The permeation factors are plotted in Figure 6-9; the asymptotically increasing values with increasing  $C_e/D_0$  verify the expected trends in molecular size. This result confirms that adsorptive

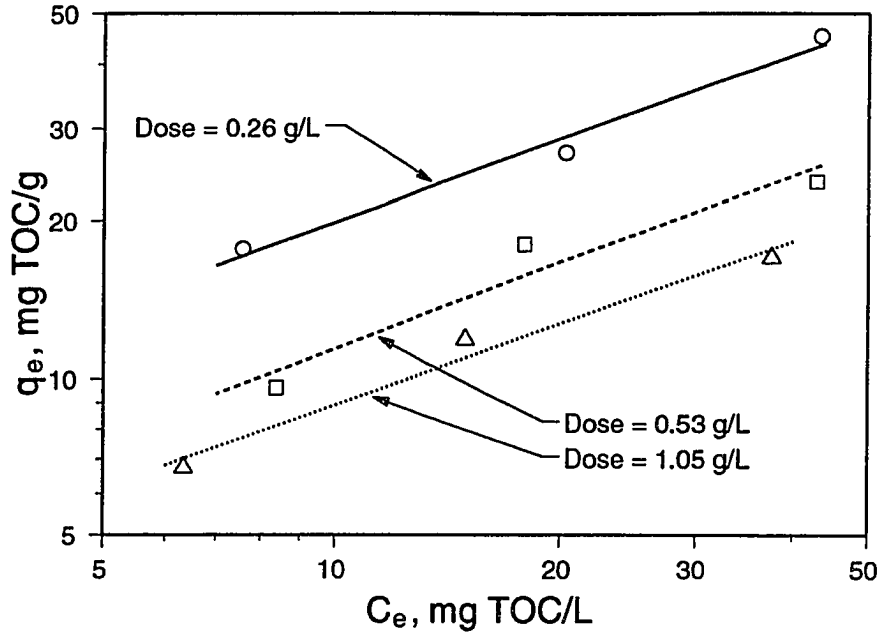


Figure 6-8. Adsorption of Laurentian HA on 165-micron F400 carbon showing the effect of initial concentration and adsorbent dose.  $C_0 = 13.4, 27.4$  and  $55.4$  mg/L. Adsorption experiments were conducted in 1-liter reactors to prepare preloaded carbon and supernatant for subsequent characterization.

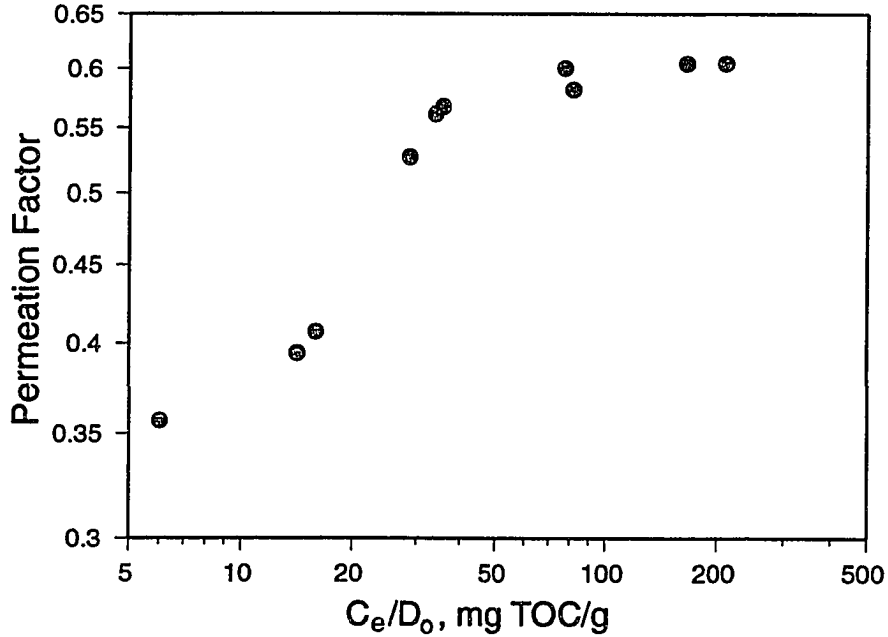


Figure 6-9. Effect of adsorptive fractionation on the membrane transport characteristics of Laurentian HA supernatant solutions from F400 carbon preloading reactors.



**Table 6-4. Permeation Factors Determined for HA Components Remaining in Solution After Adsorptive Fractionation.**

$C_e/D_0$	$C_e/C_0$	$P_F$ (95% C.I.)
6.03	0.47	0.357 (0.341, 0.373)
14.21	0.55	0.394 (0.381, 0.407)
15.93	0.62	0.407 (0.390, 0.424)
28.76	0.62	0.527 (0.514, 0.539)
34.13	0.66	0.561 (0.544, 0.578)
35.72	0.68	0.567 (0.558, 0.576)
77.22	0.74	0.600 (0.591, 0.610)
81.60	0.77	0.581 (0.562, 0.599)
165.32	0.79	0.604 (0.594, 0.613)
Whole HA	1.00	0.618 (0.606, 0.629)

fractionation occurs on the basis of molecule size.

An advantage of the ultrafiltration technique is that it characterizes molecule size under the exact solution conditions used in the isotherm experiment. However, it does not give molecular-weight distributions directly. Therefore, in addition to ultrafiltration experiments, HPSEC was employed to provide direct evidence that adsorptive fractionation occurs on the basis of molecular size. HPSEC measures the MWD directly, while the UF permeation factor provides a single value which can only be interpreted as some effective characteristic of the MWD. A disadvantage of HPSEC is that the MWD must be measured at an ionic strength of 0.10 M, to reduce interactions between the charged analyte molecules and the chromatography column packing. Therefore, the sizes of molecules in the HPSEC system are not necessarily the same as in environmental samples.

Samples obtained from an HA adsorption isotherm were analyzed using HPSEC. Detailed results of isotherm conditions, weight- and number-averaged molecular weights determined from HPSEC chromatograms, and chromatogram polydispersity are tabulated in Table 6-5. The  $C_e/D_0$  ratios for this experiment ranged from about 2.5 to 182 mg/g, corresponding to  $q_e$  values ranging from 9.4 to 55.1 mg/g. This compares to a  $C_e/D_0$  range of about 6 to 165 mg/g for the supernatant solution analyzed by UF, corresponding to  $q_e$  values ranging from 6.7 to 45.3 mg/g. HPSEC chromatograms are shown in Figure

**Table 6-5. HPSEC Analysis of Laurentian Humic Acid Adsorption**

Sample	D <sub>0</sub> , mg/L	C <sub>e</sub> , mg/L	q <sub>e</sub> , mg/g	M <sub>w</sub>	M <sub>N</sub>	M <sub>w</sub> /M <sub>N</sub>
Whole HA	0.0	23.37	0.0	5465	1861	2.94
HA1	100.0	18.77	46.0	6143	2065	2.98
HA2	500.0	14.78	16.9	7312	2444	2.99
HA3	800.0	10.55	16.1	8414	2656	3.17
HA4	1350.0	7.62	11.7	9896	3084	3.21
HA5	1650.0	6.78	10.1	10878	2970	3.66
HA6	1950.0	5.86	9.0	11955	3028	3.95

Experimental conditions: Isotherm conducted with 165-micron F400 carbon; I.S. = 0.01 M, C<sub>0</sub> = 23.4 mg TOC/L, 30-day equilibration time.

6-10, and clearly illustrate the preferential adsorption of the lower molecular size components from the HA mixture. As the adsorbent dose is increased, a greater mass of HA is removed from solution, and the molecular-weight distribution shifts to larger sizes. This trend is shown in terms of average molecular weights in Figure 6-11. These results provide confirmation of the findings of the ultrafiltration analysis, and demonstrate conclusively that small molecular size components are adsorbed preferentially from an HA mixture -- adsorptive fractionation occurs on the basis of molecular size. The data presented in this study for natural organic polyelectrolytes corroborate the results of El-Rehaili and Weber (1987) and Summers and Roberts (1988a), and suggest that the preferential adsorption of low-molecular weight components is a general feature of the adsorption of polyelectrolyte mixtures from solution on activated carbon.

The impact of adsorption on the molecular size distribution of components remaining in solution is expected to depend on the solute size distribution relative to that of the adsorbent. The findings presented in this work suggest that for a given adsorbent pore-size distribution and percentage reduction in total organic carbon, the effect of adsorption on the size of organic matter left in solution depends primarily on the solute molecular size distribution. The basis for preferential adsorption of smaller molecular sizes is most likely due to a combination of factors. Smaller molecular sizes have higher diffusion coefficients, and reach the adsorbent surface ahead of the larger molecules. Once they have reached the

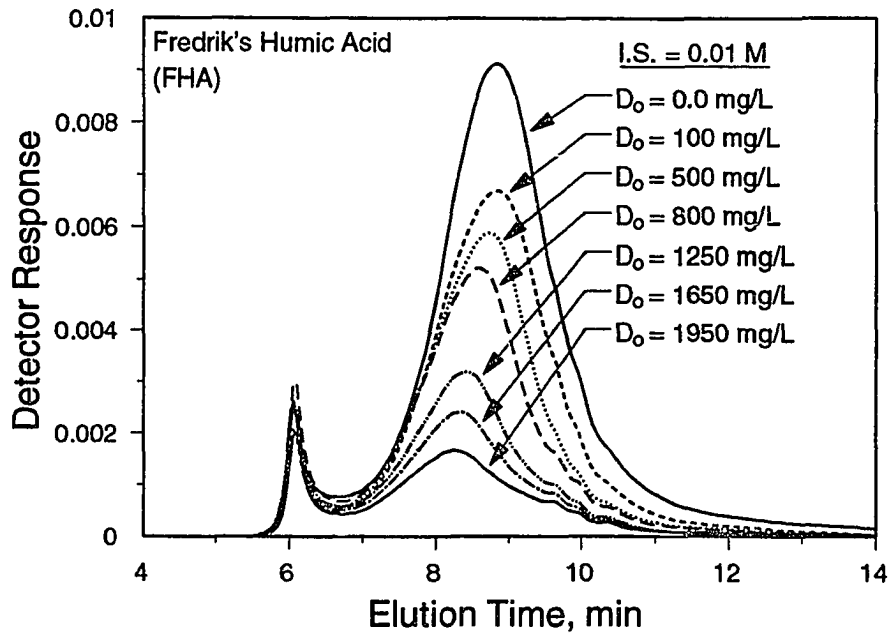


Figure 6-10. The effect of adsorptive fractionation on the size exclusion chromatograms of Laurentian HA. Chromatograms of supernatant solutions from a variable dose isotherm at an ionic strength of 0.01 M on 58-micron F400 carbon.  $C_o = 23.8$  mg TOC/L.

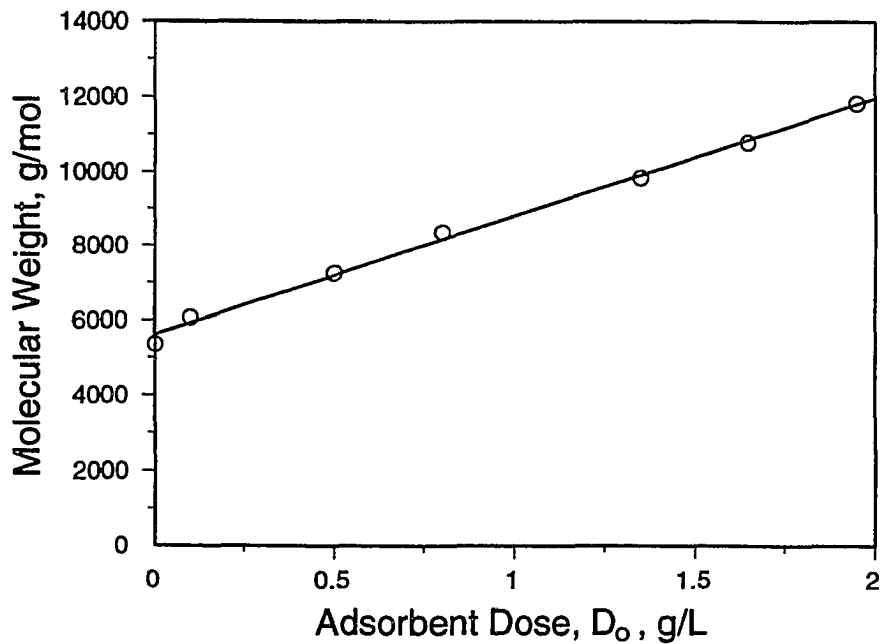


Figure 6-11. The effect of adsorptive fractionation on the average molecular weight of TOC remaining in solution after adsorption at an ionic strength of 0.01 M on 58-micron F400 carbon.  $C_o = 23.8$  mg TOC/L.

particle surface, they can more easily diffuse into the adsorbent pore structure, where they can access a greater adsorbent surface area. Displacement of the small molecules by larger ones may be difficult because of electrostatic repulsion between charged segments on the polyelectrolyte molecule (Ramachandran and Somasundaran 1987), and their exclusion from a portion of the intraparticle adsorbent surface.

These findings, as suggested earlier, have implications for the molecular size distribution of *adsorbed* HA components. Small  $C_e/D_0$  ratios correspond to a large removal of HA from solution, thus, the adsorbed MWD approaches that of the original solution. Large  $C_e/D_0$  ratios correspond to the removal of only the smallest molecules from solution; therefore, the MWD of adsorbed components is shifted to smaller sizes. The HPSEC chromatograms provide dramatic verification that adsorptive fractionation governs the MWD of adsorbed HA components.

#### Effect of Ionic Strength on Competitive Interactions Among HA Components

The extent of adsorption is expected to increase with increasing ionic strength, as a result of a decrease in macromolecular size, in accordance with experimental results for PSS adsorption, and the model of humic structure proposed by Gosh and Schnitzer (1980). Humic acid isotherms were measured at two different ionic strengths, 0.01 M and 0.10 M, to test this hypothesis. Isotherm data were fit with the modified Freundlich isotherm model; model parameters and corresponding 95% confidence intervals are tabulated in Table 6-6. Figure 6-12 illustrates the isotherm data and modified Freundlich model fits. Isotherm data from both experiments were linearized on log-log coordinates when the amount adsorbed was plotted versus the non-adsorbed amount of TOC per unit adsorbent mass,  $C_e/D_0$ . An increase in the ionic strength from 0.01 M to 0.10 M results in a significant increase in the extent of adsorption, which is reflected in the empirically-determined parameters in the modified Freundlich model. Increasing the ionic strength results in a concomitant increase in the value of  $K_F$  from 6.50 to 18.0. In contrast to the PSS adsorption isotherms, the isotherms at different ionic strengths are not parallel --the Freundlich exponent,  $n$ , measured at an ionic strength of 0.10 M is significantly less than the value obtained at 0.01 M. This observation provides additional evidence that the

**Table 6-6. Adsorption of Laurentian HA: Effect of Ionic Strength**

Ionic Strength, M	$C_0$ , mg/L	N	$K_F$ (95% C.I.)	n (95% C.I.)
0.01 M	23.4	14	6.50 (6.28, 6.73)	0.404 (0.389, 0.418)
0.10 M	23.3	14	17.96 (17.24, 18.72)	0.244 (0.227, 0.261)

Conditions: Isotherms conducted with 58-micron F400 carbon, 30-day equilibration.

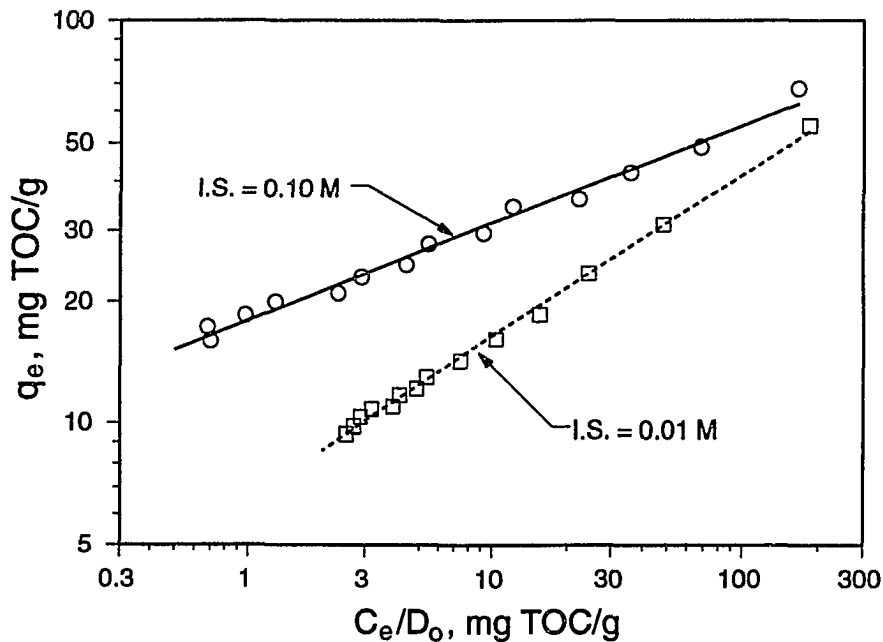


Figure 6-12. Effect of ionic strength on the adsorption of Laurentian HA on 58-micron F400 carbon. I.S. = 0.10:  $C_0 = 23.3$  mg TOC/L; I.S. = 0.01:  $C_0 = 23.8$  mg TOC/L

adsorption is not dominated by sorbate/sorbent interactions -- a higher ionic strength would tend to decrease the adsorption of a negatively-charged molecule on a surface with a net positive charge. It is likely that the change in isotherm slope is due to a differential response of solution components to an increase in ionic strength. The response to ionic strength is significant for high adsorbent doses, corresponding to low  $C_e$  values, when a significant fraction of the less-preferentially adsorbed components are removed from solution. In contrast, the response to ionic strength is much less significant for low

adsorbent dose conditions, corresponding to high  $C_e$  values, when only the most preferentially adsorbed solution components are removed from solution. This observation will be discussed in greater detail below.

To gain insight into the mechanisms of increased adsorbability with increasing ionic strength, samples obtained from the HA adsorption isotherm were analyzed using HPSEC, and isotherm results were interpreted in the context of changes in molecular-weight distributions. Detailed results of isotherm conditions, weight- and number-averaged molecular weights determined from HPSEC chromatograms, and chromatogram polydispersity are tabulated in Table 6-7. Size exclusion chromatograms of Laurentian HA components remaining in solution after equilibration with F400 carbon are shown in Figure 6-13. The preferential adsorption of low-molecular-weight components from the humic mixture is clearly illustrated, and is consistent with the findings at an order of magnitude lower ionic strength shown in Figure 6-10. The impact of ionic strength on the fraction of TOC remaining in solution after equilibrating with a given adsorbent dose is shown by comparing the curves shown in Figure 6-14. The corresponding impact on the average molecular weight is shown in Figure 6-15. For a given adsorbent dose, a greater fraction of the original TOC in solution is removed at the higher ionic strength. The increase in average molecular weight per unit increase in adsorbent dose is greater at the higher ionic strength -- for a given adsorbent dose, the average molecular weight of TOC remaining in solution is higher at higher ionic strength.

The average molecular weight of TOC in solution can be related to the average molecular weight of adsorbed TOC. The molecular-weight distribution of adsorbed TOC is equal to the difference between the initial distribution and the distribution remaining in solution. Since the low-molecular-weight components are adsorbed preferentially, when the distribution of TOC remaining in solution is shifted to higher molecular weights, the distribution of adsorbed TOC must be shifted in the same direction. Therefore, for a given adsorbent dose, the molecular-weight distribution of adsorbed TOC increases with increasing ionic strength. Under high ionic strength conditions, the fraction of the original TOC adsorbed per unit mass of adsorbent is increased, and this increase is obtained by removing a greater fraction of higher molecular weight components from solution.

**Table 6-7. HPSEC Analysis of Laurentian Humic Acid Adsorption: Effect of Ionic Strength**

Sample	Dose, mg/L	$C_e$ , mg/L	$q_e$ , mg/g	$M_w$	$M_N$	$M_w/M_N$
Whole HA	0.0	23.37	0.0	5465	1861	2.94
HAIS 1	100.0	16.50	68.0	7337	2403	3.05
HAIS 2	300.0	10.65	42.2	8803	2863	3.07
HAIS 3	500.0	6.03	34.5	11014	3516	3.13
HAIS 4	900.0	2.61	23.0	14816	4020	3.69

Conditions: Isotherms were conducted with 58-micron F400 carbon, I.S. = 0.10 M,  $C_0 = 23.3$ , 30-day equilibration time.

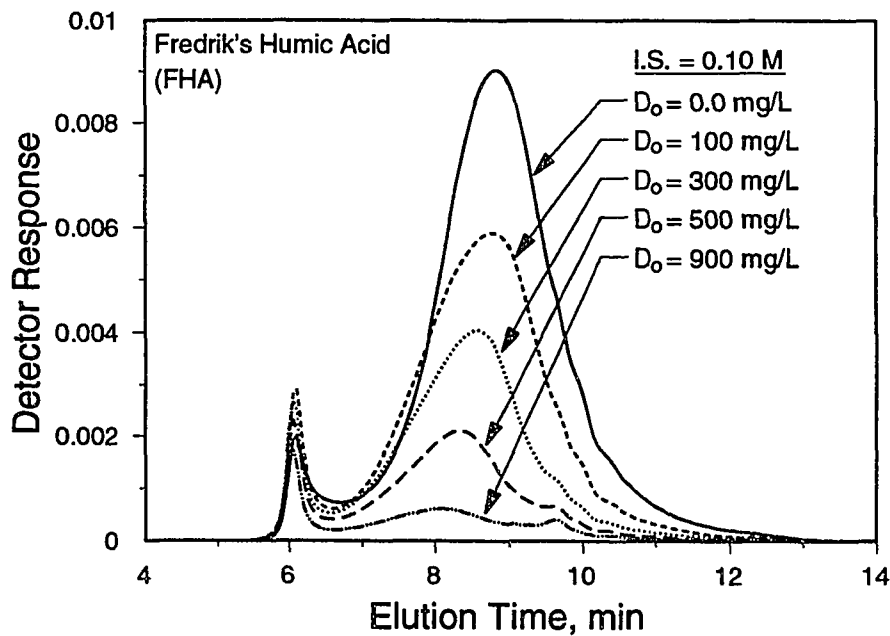


Figure 6-13. Effect of adsorbent dose on the molecular-weight distribution of Laurentian HA remaining in solution after adsorption on F400 activated carbon.  $C_0 = 23.3$  mg/L, I.S. = 0.10 M.

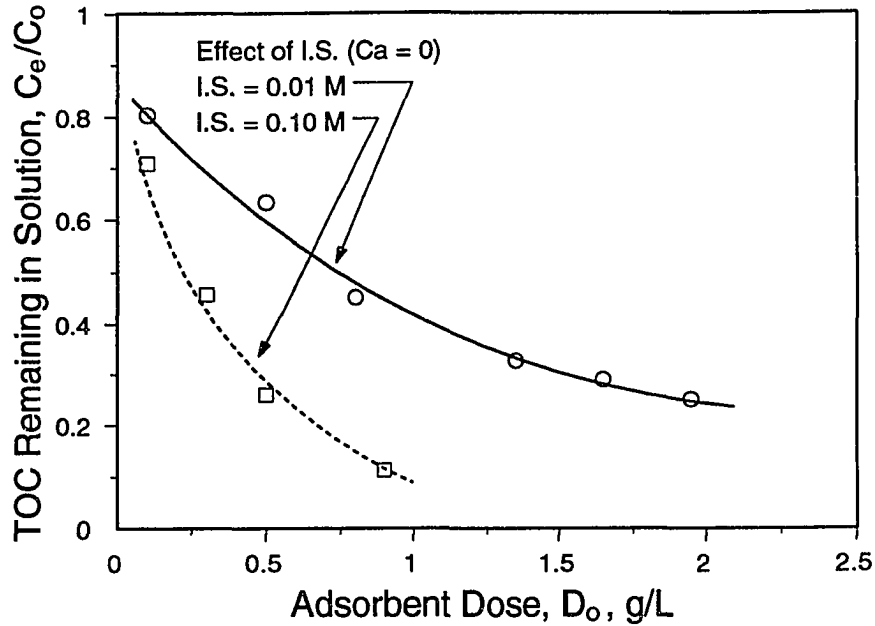


Figure 6-14. Effect of ionic strength on the fraction of TOC remaining in solution after adsorption on F400 carbon. Lines illustrate parametric trends.

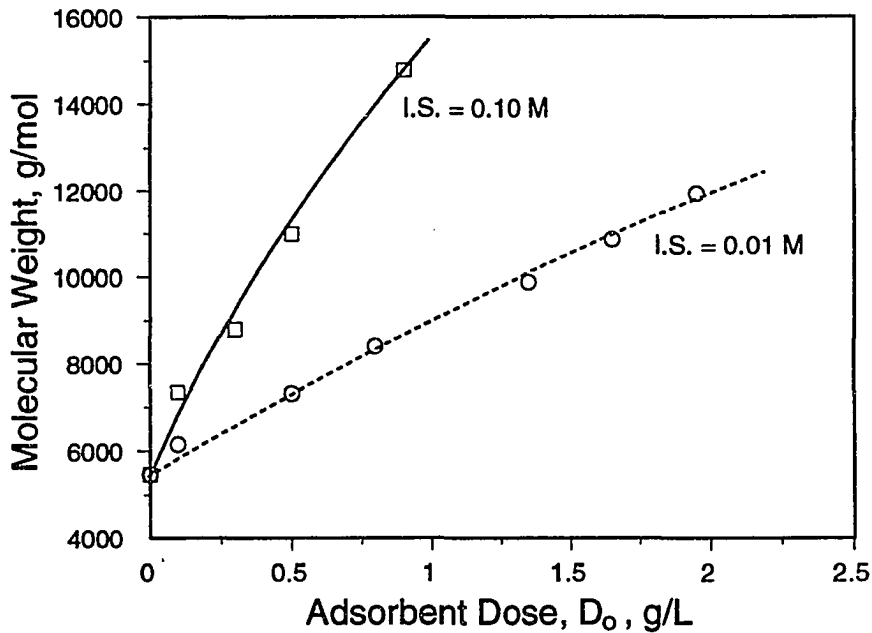


Figure 6-15. Effect of ionic strength on the average molecular weight of TOC remaining in solution after adsorption on F400 carbon. Lines illustrate parametric trends.



For microporous adsorbents such as activated carbon, the external surface area is negligible compared with the internal surface area; therefore, the greatest proportion of the organic matter is adsorbed within the adsorbent pores. The size of adsorbent pores poses a physical constraint on the adsorption of a macromolecular adsorbate. An increase in the extent of adsorption and a shift in the MWD of adsorbed molecules to higher molecular weights must be accompanied by one or more of the following: i) new adsorption sites must be formed; ii) the adsorption density, or surface concentration, must increase; or iii) additional surface area must be accessed. In this experiment, increases in ionic strength were accomplished by increasing the NaCl concentration. It is not likely that the sodium cation would be involved in the formation of additional adsorption sites. While it is plausible that increases in ionic strength could cause a tighter packing on the adsorbent surface, Summers and Roberts (1988a) have shown that a decrease in the adsorption density occurs, on the basis of available surface area, when the adsorbent has a net positive charge. It is most likely, therefore, that the increased ionic strength makes additional surface area available.

Additional surface area will only become accessible if the molecular size is decreased, allowing molecules to access smaller pores or to access surface area through constricted pore openings. Therefore, increases in the adsorbed molecular-weight distribution for a given adsorbent dose must be accompanied by a decrease in the adsorbed molecular size distribution. While the TOC in both isotherm experiments started with the same molecular-weight distribution, they did not start with the same molecular size distribution. This is because the size, or structural configuration, of a polyelectrolyte is itself a function of ionic strength.

It follows from this discussion that the mechanism of increased adsorption of polyelectrolytes in microporous adsorbents as a function of ionic strength results from a physical reduction in the macromolecule size. From measurements made of macromolecule diffusivity and membrane mass transfer, it has been shown that the increases in ionic strength cause a reduction of molecule size in solution; therefore, it is likely that a portion of the size reduction occurs prior to adsorption. This does not, in and of itself, rule out the possibility that additional changes in conformation may occur at the adsorbent surface due to screening of charge within the pore space.

If the dominant effect of ionic strength on the extent of adsorption is to change macromolecular configuration, then this phenomenon should explain the observed trends in the HA isotherms. The reduction in the Freundlich  $n$  value as a function of ionic strength (Table 6-6) indicates that the relative increase in the amount adsorbed is more pronounced at low values of  $C_e$ . Isotherm data in Table 6-7 and HPSEC chromatograms in Figure 6-13 show that in the low- $C_e$  region of the isotherm, the adsorbent concentration is high enough to remove larger molecules from solution. Therefore, the largest relative change in adsorbability occurs when the largest molecules are adsorbed.

If changes in adsorbability are due to changes in macromolecule size, then larger molecules would undergo larger relative changes in molecular size per unit change in ionic strength than smaller molecules. At the limit, this expectation seems reasonable. If a polyelectrolyte is comprised of a chain of monomer segments, then as the number of segments is reduced to a single monomer, no change in configuration with ionic strength would be expected. This explanation is consistent with the findings of Schlautman and Morgan (1994), who report that the low-molecular weight Suwanee humic and fulvic acids do not change their configuration as a function of ionic strength. The polystyrene sulfonate adsorption data shown in Figure 6-1 also corroborate this expectation. The 18K PSS exhibits a greater relative increase in the extent of adsorption in response to an increase in solution ionic strength from 0.01 M to 0.07 M than the 1.8K size fraction. Insofar as polyelectrolytes generally exhibit a minimum size at some ionic strength, this observation may depend on both the magnitude of the change in ionic strength, and the initial ionic strength.

Due to the preferential removal of low-molecular-weight components from solution, removing a given fraction of the initial TOC is equivalent to removing all molecules having molecular weights less than a certain value. Therefore, the molecular-weight distribution of the TOC remaining in solution is the same for the same fractional removal of TOC, regardless of ionic strength. This feature of HA adsorption is illustrated in Figure 6-16. However, since the average molecular size is smaller at higher ionic strength, a smaller dose of carbon is required to achieve the given reduction in TOC, as shown in Figure 6-14. This result suggests that an increase in ionic strength causes an increase in adsorption by shifting the molecular size distribution toward smaller sizes, but does not alter the

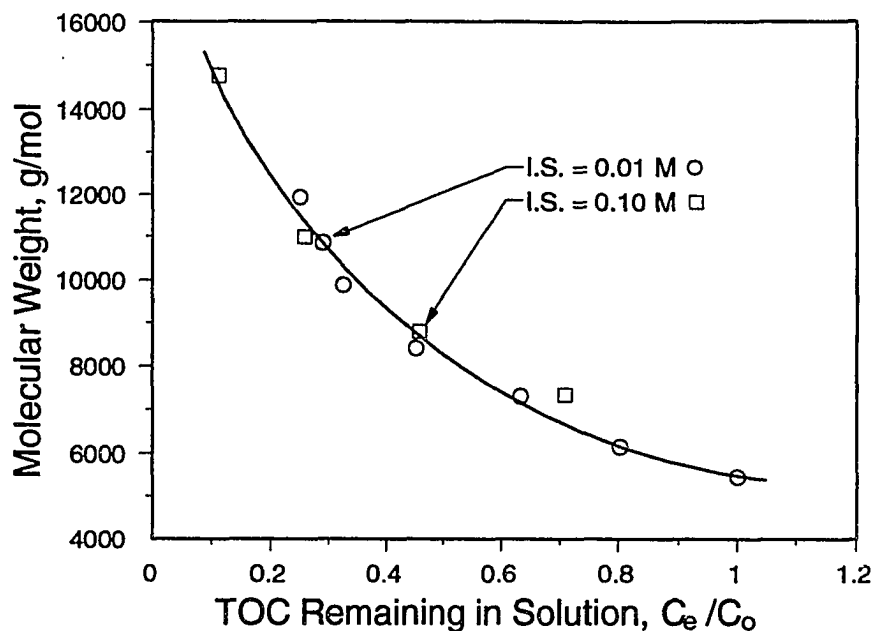


Figure 6-16. Effect of ionic strength on the average molecular weight of TOC remaining in solution after adsorption on F400 carbon, as a function of the fraction of TOC remaining in solution. Line illustrates parametric trends.

mechanism (or predominant surface reaction) involved in the adsorption. The effects of ionic strength on the adsorption of Laurentian HA are depicted schematically in Figure 6-17, and can be summarized as follows:

- 1) For a certain adsorbent dose (panel I. Equal  $D_0$ ), a higher removal of TOC will occur at a higher ionic strength (schematic A), and the average molecular weight of components remaining in solution will be shifted to higher values (schematics B and C). As a consequence, the adsorbed molecular-weight distribution will also be shifted to higher molecular weights. However, because a greater removal of TOC was achieved with the same adsorbent dose, the extent of adsorption is higher at higher ionic strength (schematic D).
- 2) For a certain TOC removal (panel II. Equal  $C_e$ ), the extent of adsorption is higher at higher ionic strength (schematic A), but the average molecular weight of components remaining in solution will be identical (schematic B), because the same fraction of the initial solution was removed. However, at the higher ionic strength, a smaller adsorbent mass is required to effect the reduction in TOC (schematics C and D).
- 3) Observations 2) and 3) lead to the following observation (not explicitly depicted in Figure 6-17): for a given amount adsorbed, the equilibrium concentration of TOC will be lower under higher ionic strength conditions, and a greater fraction of the initial TOC will have been adsorbed. Therefore, the molecular weight-distribution of components remaining in solution, and consequently the weight-distribution of adsorbed components, will be shifted to higher values.

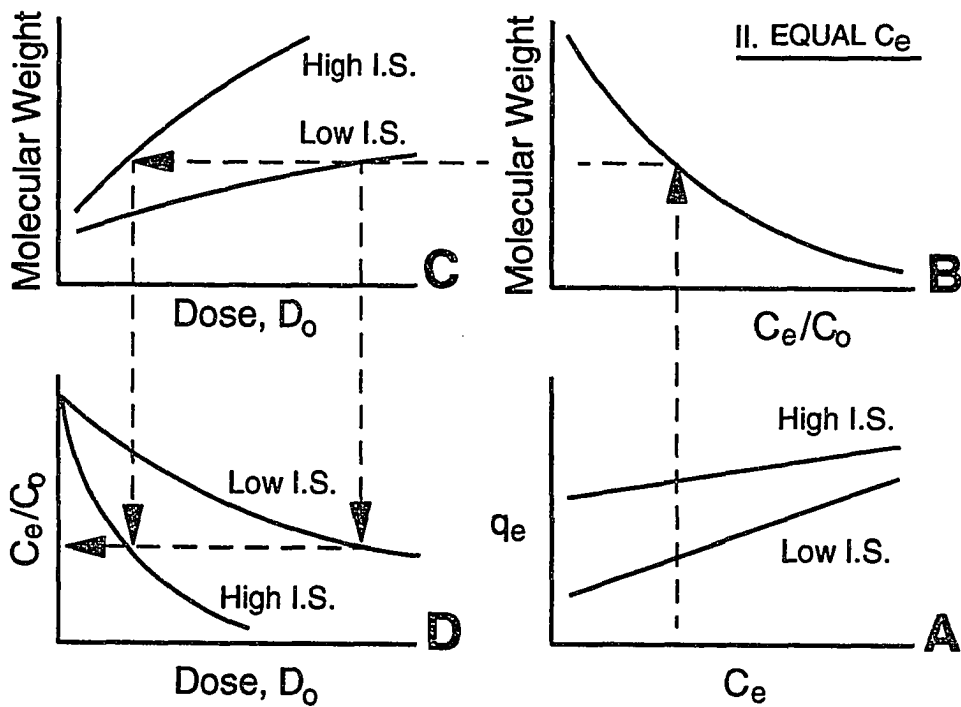
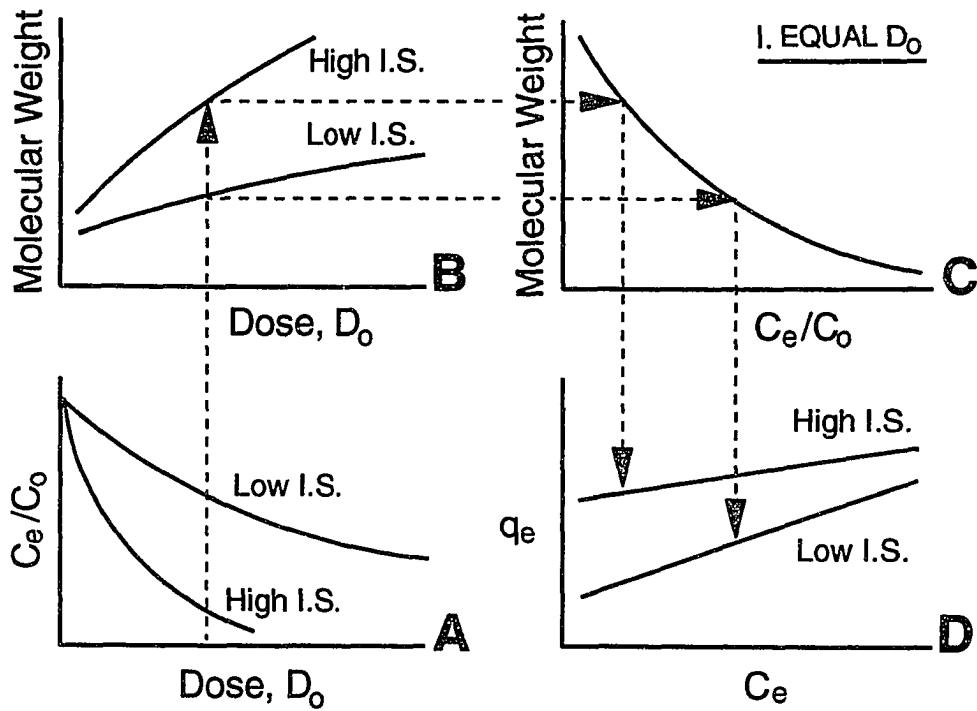


Figure 6-17. Schematic drawing showing the effect of ionic strength on the relationships among Laurentian humic acid molecular size, F400 adsorbent dose, the fraction of TOC removed from solution, and the TOC isotherm.

### Effect of Calcium on the Competitive Interactions among HA Components

Laurentian humic acid adsorption experiments were conducted at constant ionic strength (0.01 M) with varying calcium concentrations to investigate the effects of divalent cations on humic adsorption, and to compare the effects of calcium with the effects of sodium, an indifferent electrolyte. Isotherm data are tabulated in Table 6-8. A comparison between the data in Table 6-8 and the data plotted in Figure 6-14 shows that the effect of the presence of a divalent cation at constant ionic strength is qualitatively similar to the effect of the indifferent electrolyte concentration. For a given dose and ionic strength, the fraction of TOC remaining in solution is lower in the presence of calcium, and the reduction in TOC increases with an increase in calcium content. For example, by interpolation of the data in Figure 6-14 at a dose of 1.1 g/L, it is estimated that the fraction of TOC remaining at an ionic strength of 0.01 in the absence of calcium is about 0.39. All of the calcium adsorption experiments exhibited removals of 0.39 or higher, even one experiment which had an initial concentration of 39 mg TOC/L. Therefore, while several of the calcium experiments had  $C_0$  values less than the 23.4 mg TOC/L used in the adsorption experiments shown in Figure 6-14, the observed trends are not due to an initial TOC concentration effect. The findings of this study are consistent with those reported by Mazet et al. (1988), who found that the presence of calcium significantly enhanced the adsorption of sodium lauryl sulfate by activated carbon.

To gain insight into the mechanisms of increased adsorbability with increasing calcium concentration, samples obtained from the HA adsorption isotherm were analyzed using HPSEC, and isotherm results were interpreted in the context of changes in molecular-weight distributions. Detailed results of isotherm conditions, weight- and number-averaged molecular weights determined from HPSEC chromatograms, and chromatogram polydispersity are tabulated in Table 6-9. Size exclusion chromatograms of Laurentian HA remaining in solution after adsorption on F400 carbon in the presence of calcium at constant ionic strength are shown in Figure 6-18. The preferential adsorption of low-molecular weight molecules and a shift of the molecular-weight distribution to higher values is qualitatively similar in the presence of both an indifferent electrolyte and a divalent cation. Therefore, the shift in the molecular-weight distribution can be effected by

**Table 6-8. Adsorption of Laurentian HA on F400 Carbon: Effects of Calcium Concentration**

Calcium, mM	C <sub>0</sub> , mg TOC/L	C <sub>e</sub> , mg TOC/L	q <sub>e</sub> , mg/g	D <sub>0</sub> , g/L	C <sub>e</sub> /D <sub>0</sub> , mg/g	C <sub>e</sub> /C <sub>0</sub>
0.5	10.03	1.38	8.22	1.05	1.3	0.14
0.5	19.08	5.31	13.08	1.05	5.1	0.28
0.5	38.78	13.56	23.96	1.05	12.9	0.35
0.05	19.26	7.58	11.10	1.05	7.2	0.39
0.25	19.00	5.35	12.97	1.05	5.1	0.28
1.0	18.87	3.73	14.38*	1.05	3.6	0.20
2.0	18.86	0.82	17.14*	1.05	0.8	0.04

Conditions: Isotherm data collected with 165-micron F400 carbon, I.S. = 0.01 M, 30-day equilibration time.

**Table 6-9. HPSEC Analysis of Humic Acid Adsorption: Effect of Calcium Concentration**

Sample	Dose, mg/L	C <sub>e</sub> , mg/L	q <sub>e</sub> , mg/g	M <sub>w</sub>	M <sub>N</sub>	M <sub>w</sub> /M <sub>N</sub>
Whole HA	0.0	23.37	0.0	5465	1861	2.94
Ca=0.05 mM	1053.0	7.58	11.10	14161	4620	3.07
Ca=0.25 mM	1053.0	5.35	12.97	20786	6996	2.97
Ca=0.50 mM	1053.0	5.31	13.08	23575	9456	2.49
Ca=1.0 mM	1053.0	3.73	14.38	27229	4875	5.59

Conditions: Isotherm data collected with 165-micron F400 carbon, I.S. = 0.01 M, C<sub>0</sub> = 19 mg TOC/L, 30-day equilibration time.

i) increasing the adsorbent dose keeping the solution ionic composition constant; ii) increasing the ionic strength keeping the adsorbent dose constant; and, iii) increasing the divalent metal content keeping the ionic strength and adsorbent dose constant.

In contrast to the systems containing only NaCl, some aggregation of the humic substances was observed when calcium was present. Direct evidence for aggregation can be seen in the chromatograms shown in Figure 6-18. An increase in the high-molecular-weight (6-min elution time) peak was observed for all calcium experiments except the one

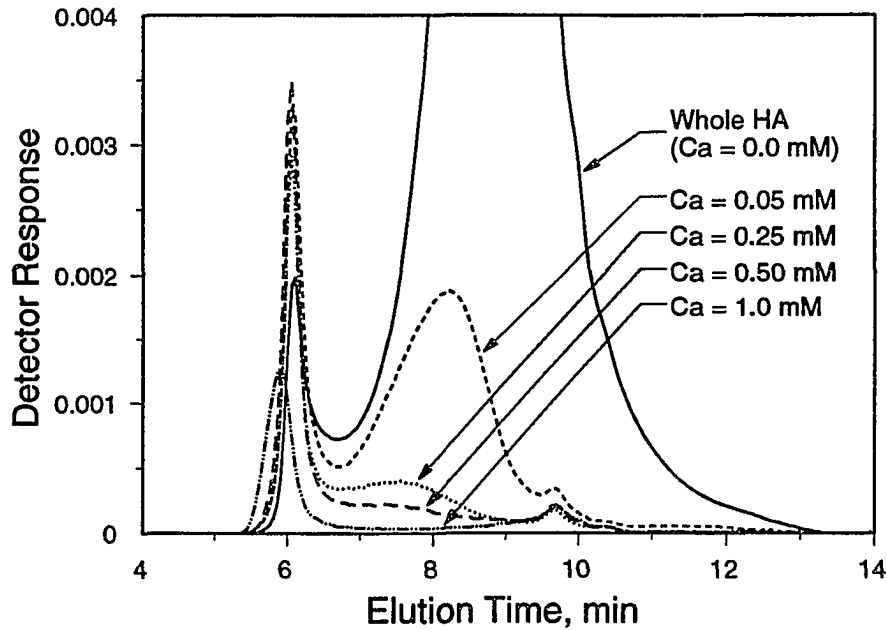


Figure 6-18. Effect of calcium content on the molecular-weight distribution of Laurentian HA remaining in solution after adsorption on F400 activated carbon.  $C_0 = 19 \text{ mg/L}$ ,  $I.S. = 0.01 \text{ M}$ .

conducted with a calcium concentration of 1 mM. For this experiment, the entire peak is shifted to higher molecular weights, but the peak height is reduced. This dramatic change in the chromatogram is likely due to the formation of a calcium/humic complex, as a brown precipitate was observed in the adsorption reactors. This is consistent with the findings of Weber et al. (1983), who reported finding a precipitate in adsorption experiments that contained calcium at a concentration of 1-mM.

The shift in the average molecular weight of the TOC remaining in solution after adsorption to higher values is augmented by aggregation. This effect is illustrated by comparing the average molecular weights reported in Tables 6-7 and 6-9. The highest value of  $M_w$  reported in the absence of calcium was less than 15,000 g/mol, corresponding to a  $C_e/C_0$  value of about 0.10. In contrast,  $M_w$  values reported in Table 6-9 range from 14,161 g/mol to 27,229 g/mol, corresponding to  $C_e/C_0$  values greater than 0.10. In the absence of calcium, the average molecular weight remaining in solution is uniquely related to the removal of a given fraction of the initial TOC, regardless of ionic strength over the range of 0.01 M to 0.10 M. When calcium is present, this relationship no longer holds

true, and for a certain TOC removal, the average molecular weight of components remaining in solution is shifted to higher values. This means that the molecular weights of TOC remaining in solution have been increased by a mechanism not related to adsorption, such as the aggregation of humic molecules. This explanation is consistent with the well-known ability of humic molecules to complex divalent cations (Hering and Morel 1988, Tipping et al. 1988, Alberts et al. 1992), and with the observations of humic substance removal from solution by coagulation (Randtke 1988).

However, aggregation is not the only mechanism causing the shift in molecular weights. If it were, the effect of calcium would be to lower the extent of adsorption, since the larger units formed would be less adsorbable. The fact that calcium instead increases the extent of adsorption suggests that either larger molecules are being adsorbed, or smaller molecules are being adsorbed more effectively. Both explanations are likely, because a divalent cation such as calcium has a greater ability to screen charge, and because new adsorption sites may be created on the surface via cation bridges.

Several experiments were performed to evaluate the extent of calcium adsorption in the absence of humic acid, and to determine whether complexation in solution was occurring. The experiments covered a wide range of F400 carbon doses (40.0 to 300.0 mg/L), initial calcium concentrations (20 to 80 mg/L) and initial calcium-to-adsorbent ratios (0.067 to 2 mg/mg). After one week of contact time, there was no measurable adsorption in any reactor. This likely resulted from like-charge exclusion of the divalent cation from the pore space, since the  $\text{pH}_{\text{pzc}}$  of the F400 is greater than the pH of the experiment. Nevertheless, a significant amount of calcium was removed from solution in the HA adsorption experiments. This is illustrated in Figure 6-19, which shows the amount of calcium removed from solution per unit mass of initial TOC present in the adsorption experiment.

There is substantial evidence for the binding of calcium to humic substances. The Laurentian humic acid supplier (Fredrik's Research) reports a bidentate complexing capacity of 2.5 mM Ca/g HA (Table 3-4). Tipping (1993) has summarized the results of several workers and reports calcium binding on soil humic materials ranging from  $2.5 \times 10^{-3}$  to 1.26 mM Ca/g HA. Mathuthu and Ephraim (1993) report calcium binding on a soil fulvic acid ranging from 0.35 to 0.61 mM Ca/g FA. The calcium removed from solution in



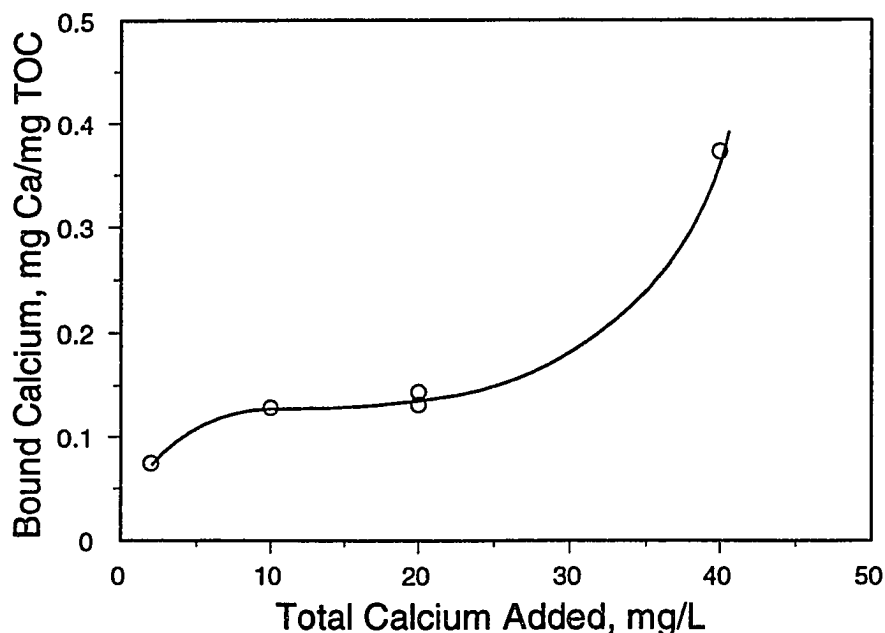


Figure 6-19. Calcium removed from solution by association with Laurentian HA. Line illustrates parametric trend.

the experiments conducted in this research was computed by the difference between the total calcium added, and the free calcium measured after adsorption using a specific ion electrode. Since the calcium was added to the humic solution prior to contacting the adsorbent, and since no adsorption of calcium by the GAC was measured in the absence of humic acid, the removal of calcium from solution was attributed to association with the HA. In these experiments, the calcium removed from solution ranged from 1.9 to 3.6 mM Ca/g TOC, which corresponds to a range from 0.95 to 1.80 mM Ca/g HA based on the reported carbon composition of 51.9% (Table 3-4). This is somewhat lower than the bidentate complexing capacity reported by the supplier of the Laurentian HA; however, the extent of binding depends on pH and the initial ratio of humic substance to metal ion, with the extent of binding per unit mass of HA increasing with decreasing HA/Ca ratios. Differences between the values obtained in this study and those reported in the literature can be accounted for by differences in experimental conditions; therefore, a complexation mechanism is considered consistent with observations of this study. In this system,

therefore, the interaction between calcium and the humic molecules precedes the adsorption step.

#### Effect of Adsorbent Characteristics on Interactions among HA Components

Humic acid isotherms were measured using several different activated carbons exhibiting a range of pore-size distributions and surface charge to investigate the effects of adsorbent characteristics on macromolecule adsorption. The effect of adsorbent characteristics on humic acid adsorption was investigated by choosing a series of carbons which were manufactured from different raw materials (coal versus wood), and activated to different degrees. A detailed discussion of adsorbent characteristics was provided in Chapter 3 (Section 3.1). The important features of the different carbons will be briefly reviewed. The coal-based carbons selected for this study, which was thermally activated, exhibit a range of microporosity (percentage of surface area in pores less than 10 Å radius) from 73.6 to 91.1 percent, and the range of surface area in pores of 10 to 50 Å radius is 8.5 to 25.6 percent. Table 3-2 contains results of adsorbent pore structure analysis.

In contrast to the coal adsorbents, the wood-based adsorbents were chemically activated. The wood-based carbons selected for this study exhibit a range of microporosity from 52.5 to 83.3 percent, and the range of surface area in pores of 10 to 50 Å radius is 16.6 to 43.8 percent.

The raw material and type of activation used to manufacture the carbon also has a significant impact on surface chemistry. The wood-based carbons have a more acidic character exemplified by a  $\text{pH}_{\text{pzc}}$  well below that of a neutral solution, while the coal-based carbons have a more basic character. At the pH of the adsorption experiments, the coal based carbons carry a net positive charge, while the surface of the wood-based carbons are negatively charged. Table 3-3 tabulates the results from experiments conducted to characterize adsorbent surface chemistry.

The impact of adsorbent characteristics on the adsorption of Laurentian humic acid is illustrated by the adsorption isotherms plotted in Figure 6-20. Adsorbent surface area, pore-size distribution and surface chemistry all play a role in determining the extent of humic acid adsorption. For the coal-based carbons, the extent of adsorption (on an adsorbent mass basis) increases with the extent of activation within a group of adsorbents

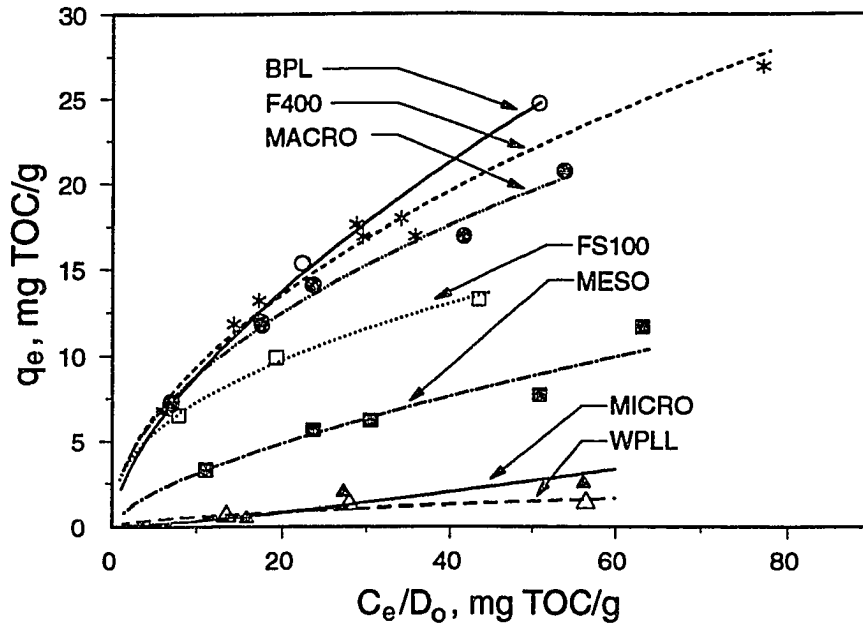


Figure 6-20. The effect of adsorbent type on the adsorption of Laurentian HA. I.S. = 0.01 M,  $D_0 = 1.05$  g/L,  $C_0$  range from 15 to 60 mg/L.

having the same source material and activation conditions (WPLL, FS100 and BPL). This can be explained, in part, on the basis of an increase in the percentage of surface area in pores in the mesopore size range (greater than 20 Å width), and an increase in total surface area. Comparing the extent of adsorption on a surface area basis, however, suggests that surface chemistry also plays a significant role in determining the extent of adsorption. The BPL carbon has the highest surface area, and its surface area should be more accessible, because a greater fraction of the total surface area is in larger pores. Nevertheless, on a surface area basis, both the F400 and FS100 carbons exhibit a greater extent of adsorption than the BPL carbon. This suggests that the surfaces of the F400 and FS100 carbons, as a result of their chemical properties, have a greater affinity for the Laurentian humic material.

The WPLL carbon exhibits a significantly lower extent of adsorption than the other coal-based carbons, on both a mass and surface area basis. While it is somewhat more microporous than the other carbons, differences in pore-size distribution and surface area determined from nitrogen adsorption do not seem sufficient to account for the differences in

humic adsorption. It is possible that characteristics of pore shape or structure not reflected in the nitrogen adsorption data may account for the trends in observed adsorption behavior.

For the wood-based carbons, the extent of adsorption (on an adsorbent mass basis) also increases with the extent of activation. This may be based, in part, on the increase in the percentage of surface area in pores in the mesopore size range (greater than 20 Å width), as these carbons have similar total surface areas. Surface area in pores having widths greater than 100 Å may contribute to the greater extent of adsorption exhibited by the MACRO carbon versus the MESO carbon. Surface charge does not account for the difference, because the MACRO carbon has a lower  $pH_{pzc}$ ; however, other differences in surface chemistry not characterized in this study may contribute to the observed trends.

Surface charge clearly plays a role when comparing the extent of adsorption on the basis of raw material type, however. Based on pore structure alone, both the MESO and MACRO would be expected to exhibit a greater extent of adsorption than all the coal-based carbons, and the MICRO carbon would be expected to exhibit a greater capacity than both the FS100 and WPLL carbons. The lower extent of adsorption observed can only be explained on the basis of surface chemistry. The adsorbent surface of the wood-based carbons is negatively charged at pH 7, the pH of the experiment. Therefore, both the surface and the adsorbate molecules are negatively charged; the repulsive forces developed as a result of like-charge repulsion may cause a reduction in the extent of adsorption. This explanation is consistent with the findings of Summers and Roberts (1988b).

Surface chemical properties also influence the adsorption capacity of the F400 carbon relative to other coal-based carbons. Based on pore structure alone, the capacity of the F400 carbon should be more similar to the FS100 than the BPL carbon. However, the F400 carbon is more basic, and therefore carries a greater net positive charge, increasing the extent of adsorption.

Size-exclusion chromatograms of TOC remaining in solution after adsorption by different carbons are shown in Figures 6-21 and 6-22. All solutions were prepared with an initial concentration of 15 mg TOC/L and used an adsorbent dose of 1.05 g/L. Despite significant differences in pore structure, total surface area, and surface charge, the data in these figures demonstrate the preferential adsorption of low-molecular weight molecules for both the coal and wood-based adsorbents. For a given source material and set of activation

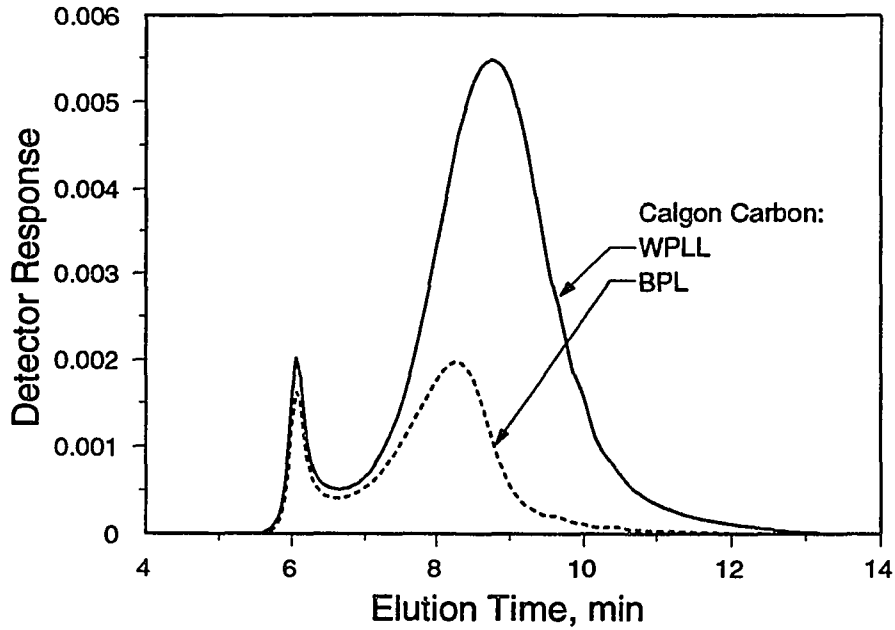


Figure 6-21. Effect of adsorbent type on the molecular-weight distribution of Laurentian HA remaining in solution after adsorption. Coal-based adsorbents.  $C_0 = 15 \text{ mg/L}$ , I.S. = 0.01 M.

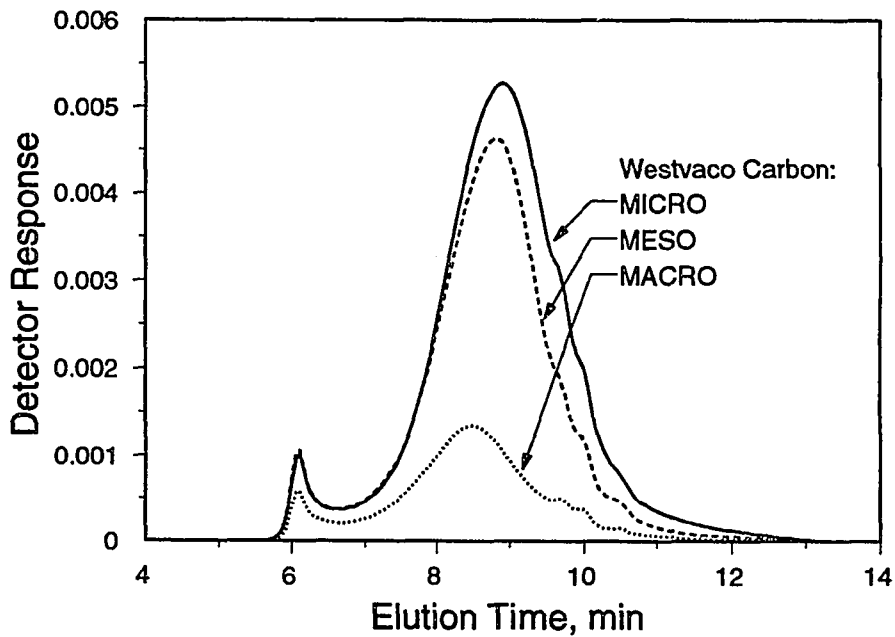


Figure 6-22. Effect of adsorbent type on the molecular-weight distribution of Laurentian HA remaining in solution after adsorption. Wood-based adsorbents.  $C_0 = 15 \text{ mg/L}$ , I.S. = 0.01 M.

conditions, increasing the degree of activation shifts the pore-size distribution to larger pore sizes, which results in the removal of a greater fraction of the lower molecular weight molecules. For adsorbents having widely different surface chemistry, such as the MESO and BPL carbons, the accessible area is more a function of surface charge than pore structure. The negatively-charged adsorbent removes a smaller fraction of the low-molecular weight molecules because of like-charge repulsion effects.

#### Effect of Organic Matter Type on Adsorption of Humic Substances

Adsorption isotherms for Laurentian humic and fulvic acid were measured and compared to determine if these different classes of natural organic matter exhibited significantly different adsorption behavior. Isotherm data were fit with the modified Freundlich isotherm model; model parameters and corresponding 95% confidence intervals are tabulated in Table 6-10. Figure 6-23 illustrates the isotherm data and modified Freundlich model fits. Isotherm data from both experiments were linearized on log-log coordinates when the amount adsorbed was plotted versus the non-adsorbed amount of TOC per unit adsorbent mass,  $C_e/D_0$ . The fulvic acid exhibits a significantly higher extent of adsorption than the humic material. One explanation for this might be based on the fact that the fulvic acid has a higher carboxylic acid content than the humic acid and therefore interacts specifically with the carbon surface, which has a net positive charge at pH 7. However, if this were the case, it would be expected that the Freundlich  $n$  value of the fulvic acid would be significantly lower than that of the humic, indicating a greater intensity of adsorption. Since this is not the case, a more likely explanation is that the greater capacity for fulvic acid is due to the smaller size of the fulvic molecules. For example, the whole FA had an ultrafiltration permeation factor of 0.652 ( $\pm 0.009$ ) as compared to a value of 0.618 ( $\pm 0.011$ ) obtained for the whole HA. While far from conclusive, this result suggests that macromolecule size may be a good predictor of the extent of adsorption for different types of organic matter.

**Table 6-10. Comparison of Laurentian HA and FA Adsorption**

Ionic Strength, M	$C_0$ , mg/L	N	$K_F$ (95% C.I.)	n (95% C.I.)
HA	36.7	13	6.32 (5.95, 6.70)	0.330 (0.313, 0.348)
FA	31.0	14	11.35 (11.03, 11.70)	0.293 (0.283, 0.302)

Conditions: Isotherms conducted with 58-micron F400 carbon, I.S. = 0.01 M, 30-day equilibration.

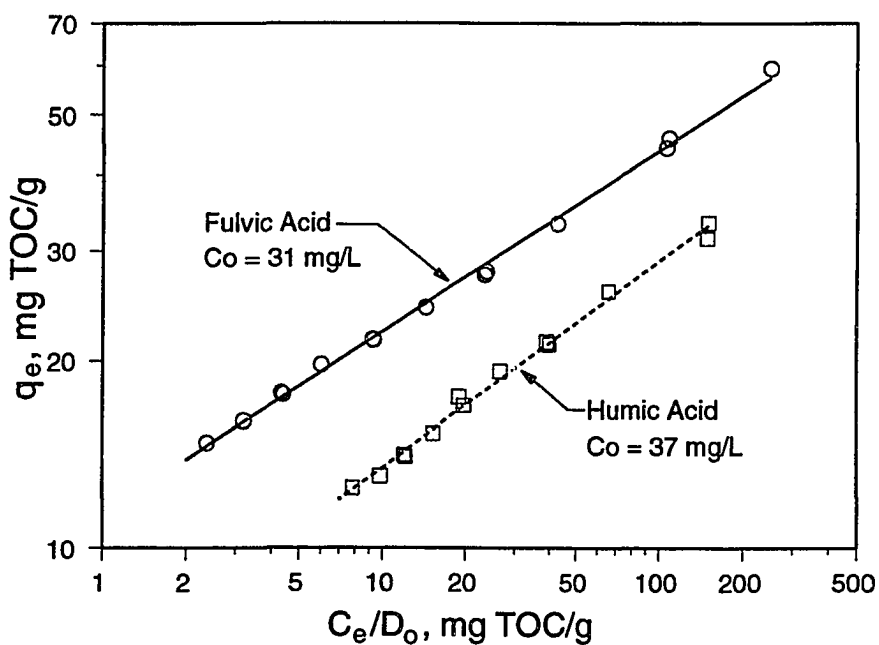


Figure 6-23. Adsorption of Laurentian HA and FA on 58-micron F400 carbon illustrating the effect of organic matter type on the DOM adsorption isotherm. FA:  $C_0 = 31$  mg TOC/L; HA:  $C_0 = 37$  mg TOC/L.

## 6.4 Conclusions

Experiments were conducted to characterize the adsorption of a synthetic polyelectrolyte, polystyrene sulfonate (PSS) and natural soil humic substances on activated carbon. PSS is commercially available in narrow molecular weight ranges and was therefore selected as a model compound to investigate the effects of molecular weight. PSS adsorption experiments showed that adsorption capacity increased with decreasing molecular weight, confirming that size-exclusion of molecules too large to access adsorbent surfaces does occur, and causes a reduction in their extent of adsorption relative to smaller molecules. The extent of adsorption also increased with increasing ionic strength, for a given molecular weight. Increases in ionic strength were shown, in Chapter 4 (Section 4.5), to reduce molecular size.

To investigate the multicomponent nature of humic adsorption, variable-dose isotherms were measured at different initial total organic carbon (TOC) concentrations, and a skimming experiment similar to that used by Jodellah and Weber (1985) was conducted. The isotherm relationship depended on the initial TOC concentration, and on whether there was prior adsorbent contact. These experiments clearly demonstrate that the humic material is a mixture of components having different adsorbabilities. A batch ultrafiltration system was used to fractionate humic solutions according to size, and adsorption isotherms measured for each fraction showed that the extent of natural organic matter adsorption increased with decreasing molecular size, which was consistent with results from the PSS adsorption studies. To determine how different size fractions competed when adsorbed from a mixture, ultrafiltration and size exclusion chromatography was used to determine changes in the molecular weight or size distribution of TOC remaining in solution changed after equilibration with activated carbon.

Size-exclusion chromatograms demonstrated that smaller molecular size fractions are adsorbed preferentially from whole humic solutions. Furthermore, regardless of the initial conditions of the adsorption experiment, as long as the same fraction of the initial TOC is removed from solution, the same molecular weight distribution will remain in solution. From mass-balance considerations, it follows that the molecular weight distribution of adsorbed TOC depends only on the fraction of TOC removed from solution.



As a result of preferential adsorption, isotherm data obtained from experiments having different combinations of initial TOC and adsorbent dose may be normalized by plotting the amount adsorbed as a function of either the fraction of initial TOC remaining in solution ( $C_e/C_0$ ) or the non-adsorbed TOC per unit mass of adsorbent ( $C_e/D$ ).

The preferential adsorption of low molecular weight components from humic substances, as determined by size-exclusion chromatography, was observed over a wide range of solution ionic strengths, divalent cation concentrations, adsorbent pore-size distributions and adsorbent surface charge. This phenomenon appears to be a general feature of humic adsorption on activated carbon.

The preferential adsorption of low molecular weight components of humic substances has particularly significant implications for water treatment practice. While a significant fraction of the TOC entering a treatment plant may be removed by coagulation processes, these processes selectively remove the larger molecular size components. Therefore, TOC removal by coagulation will not likely reduce the TOC uptake in subsequent adsorption processes.

The effects of ionic strength and calcium content on humic adsorption were investigated to determine potential effects of variations in source water chemistry, and changes in solution chemistry which may occur in water treatment processes. The extent of adsorption of humic substances increased with an increase in solution ionic strength over the 0.01 to 0.10 M range studied. Ultrafiltration measurements demonstrated that the size of humic molecules decreased with an increase in ionic strength, a phenomenon consistent with the conceptual model of humic structure proposed by Gosh and Schnitzer (1980). Size exclusion chromatography measurements demonstrated that the molecular weight of TOC remaining in solution after adsorption was a function only of the fraction of TOC adsorbed, and did not depend on the ionic strength. However, under high ionic strength conditions, a much lower adsorbent dose was required to effect the same TOC removal. This result, in concert with the ultrafiltration measurements, suggests that the mechanism of enhanced adsorption at high ionic strength is a decrease in molecular size, and that this decrease occurs in solution. The smaller molecular size allows access to a greater micropore surface area, increasing the extent of adsorption. This finding is consistent with

the findings of Summers and Roberts (1988), who showed that an increase in ionic strength does not result in a tighter packing on the adsorbent surface.

The extent of humic substance adsorption also increased with an increase in calcium content at constant ionic strength. In contrast to the findings of the ionic strength studies, the molecular weight of TOC remaining in solution after adsorption depended on both the fraction of TOC adsorbed and the calcium content. These results suggest an aggregation or coagulation phenomena facilitated by the divalent cation. The aggregation appeared to occur primarily among the larger molecular weight components; the aggregation of smaller molecules could not be assessed because they were readily adsorbed. The mechanism of enhanced adsorption in the presence of calcium was attributed to i) a decrease in the molecular size of smaller molecules for which the effects of aggregation are not significant, similar to the effect of ionic strength; and, ii) the possible formation of additional adsorption sites via cation bridges (Schlautman and Morgan 1994). The formation of cation bridges on the adsorbent surface may enhance the extent of adsorption of smaller molecules as well as larger molecules that may have undergone some degree of aggregation.

The effect of adsorbent characteristics on Fredrik's soil humic acid adsorption was investigated. Several different adsorbents were studied, including three acidic wood-based carbons and four basic coal-based carbons, having a range of pore size distributions. The impact of adsorbent characteristics on the adsorption of humic substances was observed to depend on pore structure, and the corresponding ability of the adsorbate to access internal surface area. Pore structure was governed, in large part, by the type of raw material, but also by activation conditions and the extent of activation. Surface charge also played an important role. Adsorbents with favorable pore structures but having negatively-charged surfaces exhibited a reduced extent of adsorption relative to carbons with positively charged surfaces. Surface functional groups other than those which can be characterized by acid or base neutralization may also play a role in the adsorption of humic substances, and may depend on both the raw material and the method of activation.

Regardless of whether changes in solution chemistry or adsorbent characteristics are responsible, any increase in the extent of adsorption is effected by removing a greater fraction of smaller molecular weight molecules from solution. Therefore, a qualitative

comparison of the molecular-weight distributions of adsorbed macromolecules for different adsorption conditions can be made. When comparing different adsorption conditions on the basis of a given amount adsorbed, the conditions exhibiting a greater extent of adsorption will have a molecular-weight distribution of adsorbed molecules shifted to greater values. This study further demonstrates the efficacy of High Performance Size Exclusion Chromatography (HPSEC) as a technique for quantitatively assessing changes in molecular-weight distributions of organic polyelectrolytes in adsorption systems.

**CHAPTER VII**  
**ADSORPTION OF TCE ON PRELOADED CARBON: MECHANISTIC**  
**INTERPRETATIONS**

**7.1 Introduction**

Several studies have been directed at quantifying the impact of DOM preloading on the subsequent adsorption of low-molecular-weight SOCs in both completely-mixed-batch and fixed-bed reactors (Carter et al. 1992). Based on trends in Freundlich isotherm parameters for TCE adsorption on carbon preloaded with Huron River water, Carter et al. (1992) proposed direct site competition and pore blockage as mechanisms by which preloaded organic matter reduced the extent of TCE adsorption. However, a systematic investigation into the mechanisms of preloading is lacking. Knowledge gained from such a systematic study will be used to further refine competitive modeling approaches and parameter estimation techniques, and will help identify optimal pretreatment strategies. The objective of this chapter is to study the effects of organic-matter preloading on the subsequent adsorption of trichloroethylene (TCE) by activated carbon. The focus is on the effect of preloading on the TCE isotherm relationship, which is investigated in a model system sufficiently well-characterized to provide mechanistic insight into the mechanisms of preloading.

TCE adsorption on virgin (non-preloaded) coal-based carbons was first characterized to provide a basis for evaluating preloading effects. Isotherm data were modeled using a three-parameter isotherm derived from the theory of heterogeneous surfaces developed in Chapter 2 (Section 2.4). Criteria for isotherm model selection is discussed. Each isotherm derived from this theory has a characteristic site-energy distribution, and isotherm parameters represent properties of the distribution. The

theoretical effects of hypothesized preloading mechanisms were investigated by performing sensitivity analysis on isotherm parameters.

A model bi-solute system consisting of two molecularly discrete compounds, TCE and trichlorobenzene (TCB), was chosen to study the effects of preloading. This system is sufficiently well characterized to allow thermodynamic predictions of preloading effects. Theoretical predictions of the impacts of preloaded TCB on subsequent TCE adsorption were made using the Ideal Adsorbed Solution Theory (IAST) (Radke and Prausnitz 1972, Sontheimer et al. 1989). Preliminary calculations showed that TCB is not displaced by TCE; therefore, the model system mimics an essential feature of preloading by natural humic substances. Adsorbent site-energy distributions were calculated from single-solute TCE isotherm data and from IAST predictions of TCE isotherms in the presence of TCB. The condensation approximation developed in Chapter 2 (Section 2.5) was used to compute distributions without having any *a priori* knowledge of their shape. Changes in site-energy distributions resulting from preloading were used to examine how the energetic character of the surface changed as a consequence of preloading. The theoretical analyses were verified experimentally by measuring TCE isotherms on TCB-preloaded carbon for a range of TCB loadings. Measured isotherms were compared to IAST predictions, and site-energy distributions were calculated from experimental data and compared to theoretical predictions. Physical changes which occurred in the adsorbent pore structure and surface area as a result of TCB preloading were measured using gas-phase N<sub>2</sub> adsorption at 77K.

## 7.2 Selection of an Equilibrium Modeling Approach

Different isotherm models were fit to representative experimental data to identify an appropriate isotherm model to describe the data collected in this research. A nonlinear least-squares regression analysis was used to estimate isotherm parameters, and the residual sum-of-squares (SSR) was used as a criterion for goodness-of-fit. A preliminary residuals analysis showed that the variance of the error was more constant (the homoscedascity assumption was better satisfied) when log-transformed data were regressed. This is equivalent to making the assumption of constant relative error, which is

appropriate for volatile compounds, because volatilization losses are related to concentration.

TCE adsorption data were described well by all of the three parameter isotherms discussed in Chapter 2 (Section 2.4). Preliminary analysis indicated that the addition of a fourth parameter was not statistically significant, and the four-parameter Generalized-Langmuir model was not considered further. A critical comparison of the three-parameter isotherm models was made, and the results are tabulated in Table 7-1 (LF = Langmuir-Freundlich, GF = General Freundlich, T = Toth, RP = Redlich-Peterson). Isotherm models were fitted to TCE adsorption data on F400 carbon. Parameter estimates determined by non-linear regression, estimated standard errors of the parameter estimates, residual sum-of-squares, and error in describing isotherm data at low concentration (2  $\mu\text{g/L}$ ) are reported in Table 7-1. The lowest SSR and low-concentration error was exhibited by the Toth isotherm. This isotherm had distinct disadvantages, however: i) the standard error of the maximum capacity parameter,  $Q^0$ , was greater than 100%; ii) the site-energy heterogeneity parameter exhibited was much lower than typically reported for TCE. The Redlich-Peterson model exhibited a low SSR value but did not fit the low concentration data as well as the Langmuir-Freundlich model. Because the TCE isotherm data exhibits linear behavior on log-log coordinates in the low concentration region, it was desirable to have a model which has a mathematical form able to replicate this behavior. Neither the Toth or Redlich-Peterson model have such a form. For all of the above reasons, neither the Toth or the Redlich-Peterson isotherm model were selected. Both the Generalized-Freundlich and the Langmuir-Freundlich isotherms exhibit Freundlich behavior at low solute concentrations, and were able to reproduce the linear behavior of the data (on log-log coordinates) at low solute concentrations. Of the two, the Langmuir-Freundlich model consistently fit the data with a lower SSR value, and more accurately described data in the low-concentration region. Therefore, the Langmuir-Freundlich model was chosen to describe the TCE isotherm data.

In many adsorption studies reported in the literature, the classical Freundlich isotherm equation is used to model adsorption data. While the Freundlich equation does not exhibit a Henry's region or a limiting capacity, it has been widely used to describe

**Table 7-1. TCE Single-Solute Adsorption Modeling: Comparison of Isotherm Models (N = 82 Data Points)**

Model	Param.	Param.Est.	Std. Error	SSR	%Error @ $C_e = 2 \mu\text{g/L}$
LF	$Q^0$	183.3	23.6	0.628	+2.75
	$b \times 10^4$	1.700	0.582		
	n	0.572	0.010		
GF	$Q^0$	109.8	9.99	0.688	+5.21
	$b \times 10^4$	3.046	0.721		
	n	0.546	0.009		
T	$Q^0$	5881	5983	0.579	-1.48
	$b \times 10^4$	87.42	0.001		
	m	0.119	0.021		
RP	$Q^0$	2.438	0.556	0.580	-4.41
	$b \times 10^4$	8372	3029		
	m	0.555	0.011		

adsorption data over ranges of concentration of interest in engineering applications. The Freundlich equation represents the low-concentration limit of the Langmuir-Freundlich isotherm equation: for  $bC_e \ll 1$ :

$$q_e = Q^0 b^n C_e^n = K_F C_e^n \quad (7-1)$$

It can be seen that the Freundlich unit capacity parameter,  $K_F$ , incorporates parameters representing maximum capacity, average site energy and site-energy heterogeneity. It is a capacity parameter because it reflects the extent of adsorption corresponding to a solution phase concentration equal to unity. To remain consistent with previous adsorption studies in the literature, isotherms measured in this research are also compared on the basis of the Freundlich unit capacity parameter,  $K_F$ , calculated from Langmuir-Freundlich parameters.

When isotherm data are linear on log-log coordinates, it is not possible to fit the data with three independent parameters, because the model is over-specified, and one

parameter may be chosen arbitrarily. In these cases, it is necessary to employ the two-parameter Freundlich model. In this research, even when the data exhibited some non-linearity on log-log coordinates, it was often still possible to fit the low concentration data (below 100  $\mu\text{g/L}$ ) with the Freundlich model. A particular advantage of the Freundlich model in this regard is that its two parameters can be estimated with greater statistical significance than the three parameters of the Langmuir-Freundlich model. This is particularly true for cases in which the impact of preloading manifests primarily in the low concentration region. Therefore, parameters for the conventional Freundlich model, fit to data in the low concentration region, were also reported.

### **7.3 TCE Isotherms on Non-Preloaded Carbon**

F400 carbon was selected for preloading studies using the model TCE/TCB system based on its adsorptive properties relative to the other carbons used in this research. The adsorptive properties of all carbons was evaluated by developing TCE adsorption isotherms to provide a basis for selecting one adsorbent to investigate further, and to provide baseline data to assess the effects of preloading. TCE adsorption data, and the corresponding Langmuir-Freundlich isotherm model fits, are shown in Figures 7-1 and 7-2. On a mass basis, the adsorption isotherms of the F400 and FS100 are quite similar and exhibit a greater extent of adsorption than the BPL and WPLL carbons over the entire range of concentration measured. On a surface area basis, the WPLL carbon has the greatest capacity, followed by the FS100, F400 and BPL. This is reflected in the average site-energy parameter for WPLL, which is significantly larger than for the other carbons. It is interesting to note that WPLL also has the greatest  $n$ -value, indicating a relatively narrow site-energy distribution. This may be related to the fact that the WPLL has been activated to a lesser degree, which may result in a lower diversity of functional groups formed on the surface.

A high capacity and a relatively high initial average site energy were criteria established for choosing a carbon for further investigation. The WPLL carbon fulfills this



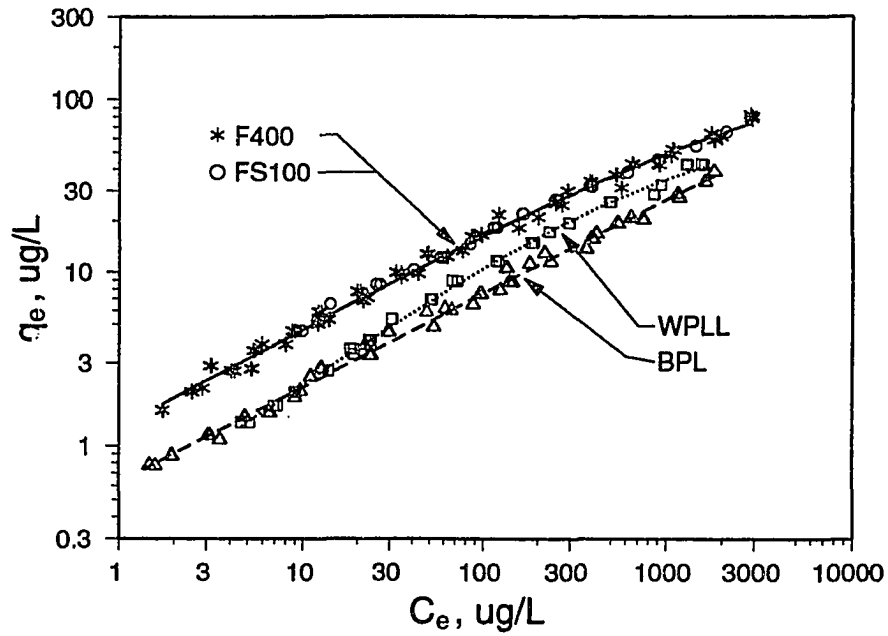


Figure 7-1. The adsorption of TCE on Calgon coal-based carbon, with capacity expressed on a mass basis. Isotherm data were fit with the Langmuir-Freundlich model.

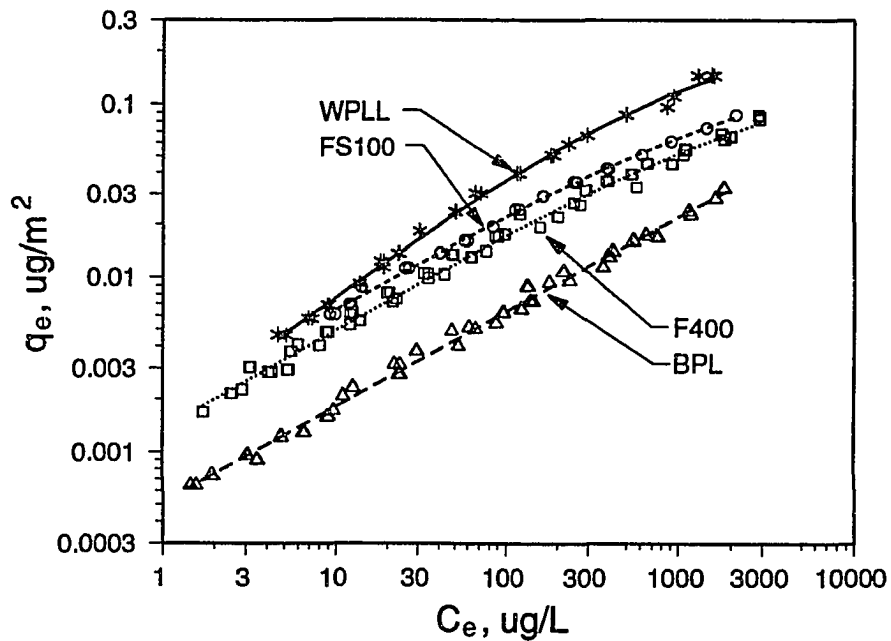


Figure 7-2. The adsorption of TCE on Calgon coal-based carbon, with capacity expressed on a surface area basis. Isotherm data were fit with the Langmuir-Freundlich model.

criteria on a surface area basis; however, on a mass-basis the WPLL exhibits a lower extent of adsorption resulting from its low surface area. The high capacity of the F400 carbon on a mass-basis reflects the fact that it is designed for water treatment applications, and confirms why it is often chosen in practice. While the FS100 carbon also has a high capacity, it is less commonly employed in practice. Based on these considerations, further analyses was conducted using the F400 carbon. A more complete comparative assessment of both the coal- and wood-based carbons is made in Chapter 8 (Section 8.6).

Isotherm parameters estimated from model fits to F400 adsorption data are tabulated in Table 7-2. The Langmuir-Freundlich parameters were obtained by fitting the entire data set and the Freundlich parameters were obtained by fitting only the low concentration data ( $< 100 \mu\text{g/L}$ ). For comparison, Freundlich unit capacity factor calculated from the three LF parameters ( $K_F = Q^0 b^n$ ) is also reported.

**Table 7-2. TCE Single-Solute Adsorption Data**

Exp.	Langmuir-Freundlich Isotherm					Freundlich Isotherm		
	Param.	Param. Est.	Std. Error	95% CI	$Q^0 b^n$	Param.	Param. Est.	95% CI
F400	$Q^0 \times 10^{-2}$	1.833	0.380	0.760	1.279	$K_F$	1.260	1.187, 1.337
N = 82	$b \times 10^4$	1.700	0.891	1.782		n	0.566	0.545, 0.586
	n	0.572	0.014	0.028		N = 48		

#### 7.4 Impacts of Preloading on TCE Adsorption: Theoretical Predictions

Three different approaches were taken to theoretically evaluate the impacts of adsorbent preloading on the subsequent adsorption of TCE. In the first approach, a sensitivity analysis was performed on the three-parameter Langmuir-Freundlich isotherm equation. Preloading mechanisms were hypothesized, and isotherm parameters were varied to reflect these hypotheses. In this way, trends in isotherm parameters were related to changes in the overall isotherm. In the second approach, designated a composite isotherm analysis, a Langmuir-Freundlich (composite) isotherm was constructed from four

individual Langmuir isotherms. The effects of hypothesized preloading mechanisms on the composite isotherm were investigated by varying the individual Langmuir isotherms. In the third approach, theoretical calculations predicting the impact of a strongly adsorbed, and non-displaceable species on the subsequent adsorption of TCE using the Ideal Adsorbed Solution Theory (IAST) were performed.

#### Langmuir-Freundlich Isotherm Sensitivity Analysis

Two primary mechanisms of competition between pre-adsorbed organic matter and subsequently adsorbed organic compounds have been proposed (Carter et al. 1992): i) direct competition for adsorption sites; and ii) blockage of pores, which restricts access to pore volume and surface area. From a thermodynamic point of view, high-energy sites play a dominant role in adsorption, especially at low sorbate concentrations (Jagiello et al. 1992). It is likely, therefore, that the preloading material will tend to occupy the highest energy sites first, subsequently changing the energetic nature of the adsorbent surface. In the following sensitivity analyses, it is assumed *a priori* that pre-adsorbed organic matter and TCE compete for the same adsorption sites.

Under the assumption that preloaded compounds compete for high energy sites, preloading may result in i) a reduction in the total number of sites; ii) a decrease in the average energy of the surface, and iii) a narrowing of the site-energy distribution. The depletion of high-energy sites may have little impact on the total number of sites or the average site energy when they comprise a relatively small fraction of the total; their depletion may be reflected primarily as a narrowing of the site-energy distribution. A reduction in the total number of sites may be the most significant effect of preloading when pore blockage occurs, with negligible changes in the energetic character of the surface. These various hypothetical scenarios were evaluated by performing a sensitivity analysis on the Langmuir-Freundlich isotherm parameters. Reductions in the average site energy were simulated by lowering the value of  $b$ , while a narrowing of the site-energy distribution was simulated by increasing the value of  $n$ . A reduction in the total number of sites was simulated by lowering the value of  $Q^0$ . The isotherm parameters for TCE adsorption on F400 carbon were taken as the reference condition for the sensitivity analysis.

Figure 7-3 shows the sensitivity analysis over a concentration range representative of adsorption systems designed to remove hydrophobic organic pollutants from solution; potable water treatment and groundwater restoration are two examples. It is clear that over a fairly large range of concentration, the behavior of the LF isotherm is linear on log-log coordinates, suggesting that data over this range could be adequately described by the Freundlich isotherm equation. For purposes of comparison, the effect of LF parameter variation will also be interpreted in terms of Freundlich parameters for the low-concentration data ( $< 100 \mu\text{g/L}$ ); these values are tabulated in Table 7-3.

An increase in the value of  $n$  may occur if the high-energy sites were selectively occupied by preloading compounds, and formed a small fraction of the total number of sites. An increase of 35% results in a dramatic decrease in the isotherm capacity at low solution phase concentrations, but does not have a significant influence at higher concentrations. In terms of the Freundlich parameters, the  $n$ -value increases nearly to the same extent as the LF  $n$ -value, while the  $K_F$  value is reduced by about 82%.

**Table 7-3. LF Isotherm Sensitivity Analysis: Effect on Freundlich Parameters Fit to Low Concentration Data ( $<100 \mu\text{g/L}$ )**

Scenario	Langmuir-Freundlich Equation			Freundlich Equation	
	$Q^o$	$b$	$n$	$K_F$	$n$
Non Preloaded	183	1.7E-4	0.570	1.28	0.563
n (+35%)	183	1.7E-4	0.770	0.229	0.767
b (-35%)	183	1.1E-4	0.570	1.00	0.564
$Q^o$ (-35%)	119	1.7E-4	0.570	0.829	0.562
Vary All	119	1.1E-4	0.770	0.107	0.767

A decrease in the average site-energy parameter,  $b$ , has a less dramatic effect on the isotherm. Reductions in this parameter displace the isotherm downward in the low concentration region, and result in a slower approach toward the ultimate capacity. The rate of curvature in the transition from the log-linear region to the plateau region is thus reduced, which extends the log-linear region of the isotherm. In terms of Freundlich

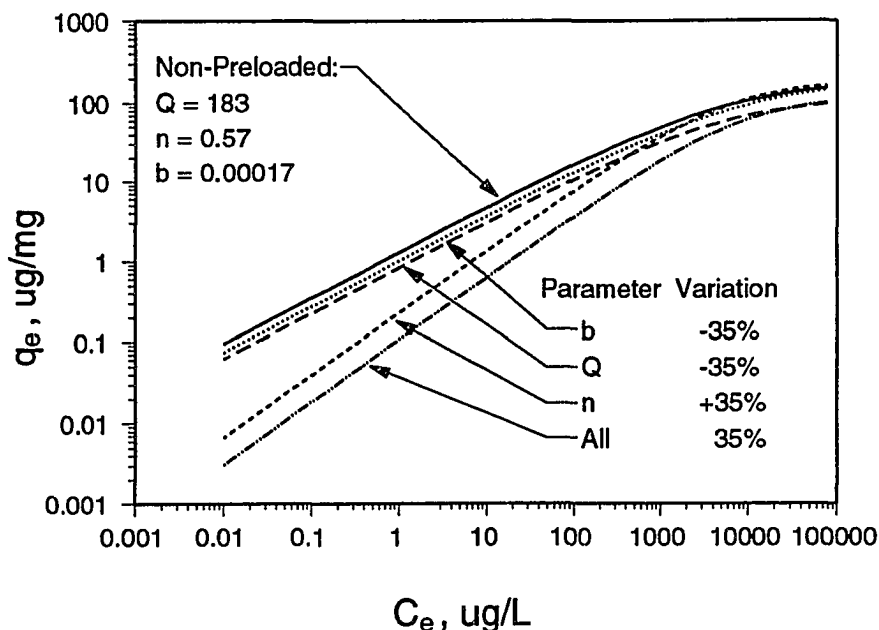


Figure 7-3. Sensitivity analysis of the Langmuir-Freundlich model.

parameters, the  $n$ -value is essentially the same as for the non-preloaded case, while the unit capacity parameter,  $K_F$ , shows a modest decrease of 22%.

A blockage of surface area would result in the reduction of the ultimate capacity of the adsorbent, lowering the value of  $Q^0$ . A given percentage reduction in the value of  $Q^0$  results in an equal percentage reduction in  $q_e$  over the entire isotherm. In terms of the Freundlich parameters, therefore, the value of  $n$  remains unchanged from the non-preloaded case, while the value of  $K_F$  decreases by the same percentage as  $Q^0$ , 35% in this analysis.

Under conditions of extensive preloading, it is possible that all parameters may vary simultaneously. Pre-adsorbed organic material may occupy high-energy sites and block pores, thereby reducing the total number of sites. This scenario is designated as the "All" in Figure 7-3. As expected, this scenario exhibits the greatest decrease in the extent of adsorption over the entire range of concentration, with the most significant decreases occurring at low solute concentrations. In terms of Freundlich parameters, the increase in  $n$  is the same as the increase in the LF  $n$ -value, while the decrease in  $K_F$  is about 92%. It should be noted that the "worst case" isotherm is essentially a parallel shift in the isotherm

obtained by varying the  $n$ -value only. This effect is consistent with the observations of Carter et al. (1992), who studied the effect of Huron River water on TCE adsorption. They measured changes in Freundlich isotherm parameters as a function of preloading time, and observed that at early times, preloading effects were reflected as changes in the  $n$ -value, whereas at longer preloading times, the  $n$ -value remained essentially constant, and the isotherm was shifted in a parallel manner.

#### Composite Isotherm Sensitivity Analysis

The concept of a composite isotherm, discussed by Weber et al. (1992), provides the basis for the second type of sensitivity analysis performed. The isotherm for TCE adsorption onto F400 carbon (Figure 7-1) was empirically fit by four different Langmuir isotherms. The Langmuir isotherm parameters were chosen such that at any value of  $C_e$ , the sum of the  $q_e$  values from each individual Langmuir isotherm equaled the  $q_e$  value represented by the TCE isotherm. This is consistent with the idea that the overall isotherm is comprised of local isotherms, each having a characteristic site energy, integrated (summed) over a site-energy distribution. The use of four different Langmuir isotherms is equivalent to constructing a discrete site-energy distribution comprised of four site energies. The site energies were distributed so that higher energy isotherms (larger  $b$ -values) had fewer sites (lower  $Q^0$  values); the highest energy isotherm represents only 1.2% of the total number of sites. Site energies were chosen over a wide range, with the objective of fitting the data with sufficient accuracy to allow a meaningful sensitivity analysis. The parameters chosen are tabulated in Table 7-4.

The composite isotherm is shown in Figure 7-4, panel A. The synthetic data, shown as open circles, were generated using the LF model with the best-fit parameters for TCE adsorption on F400 carbon. The individual Langmuir isotherms are shown as broken lines, and the composite of the four isotherms is shown as a solid line. It is remarkable that as few as four isotherms are able to fit data over a six order-of-magnitude range in solution concentration. Under the hypothesis that preloading by organic matter reduces high energy sites, the effects of preloading were simulated by subtracting the contribution of the highest energy isotherm from the composite isotherm.

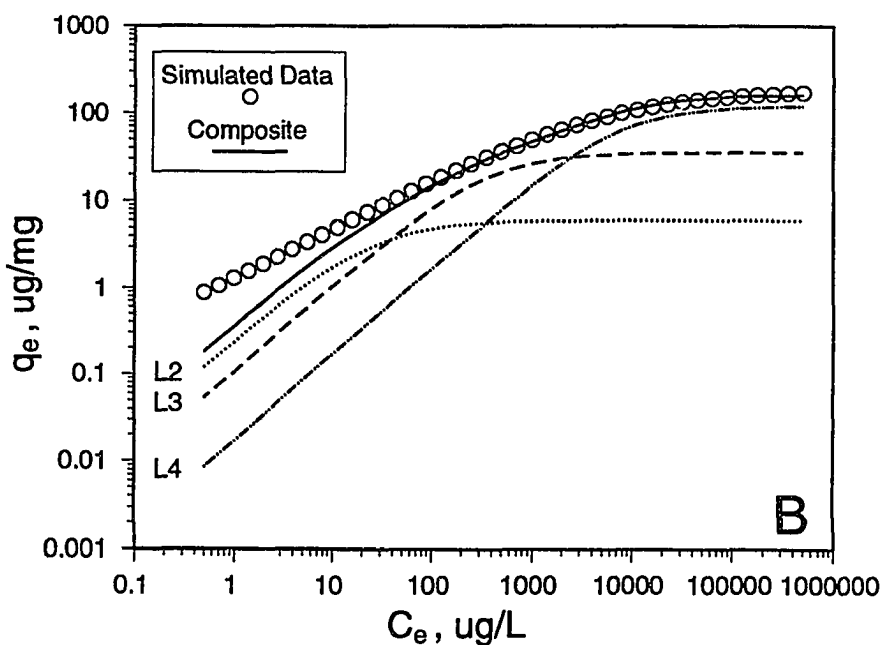
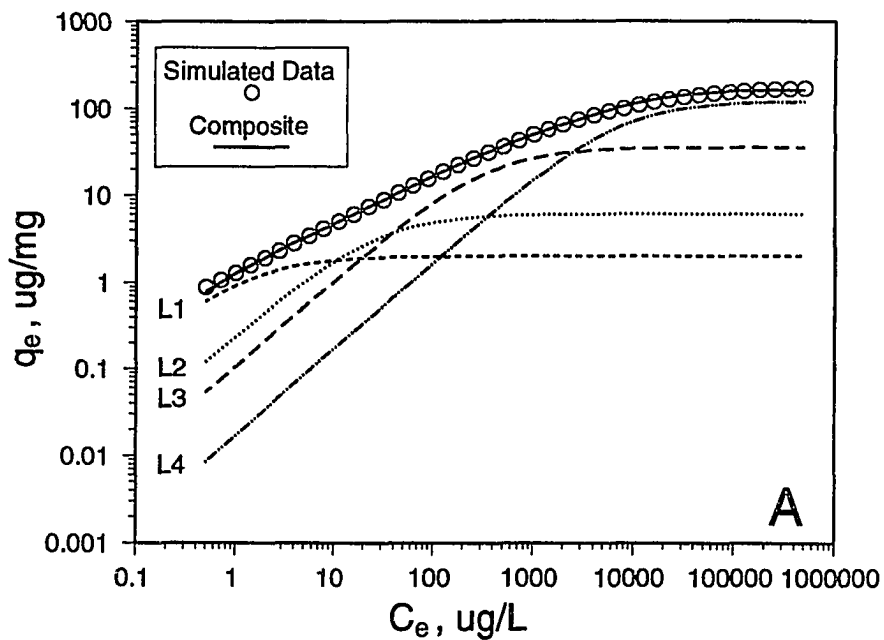


Figure 7-4. Synthetic "data" generated by the Langmuir-Freundlich model for TCE adsorption on F400 carbon is fit by a composite of four Langmuir isotherms (A). The individual Langmuir isotherms are shown as broken lines, and the composite of the four isotherms is shown as a solid line. Removing the contribution from the highest energy isotherm results in a significant decrease in capacity in the low concentration region (B).

**Table 7-4. LF Isotherm Sensitivity Analysis: Composite Isotherm**

Isotherm	$Q^0$	b	% Total Sites
L1	2	0.8500	1.2
L2	6	0.0400	3.7
L3	35	0.0030	22.0
L4	120	0.0014	73.0

The "preloading composite" isotherm comprised of the three remaining lower-energy Langmuir isotherms is shown in Figure 7-4, panel B. The preloading composite isotherm exhibits a significantly reduced extent of adsorption in the low-concentration region. Qualitatively, the effect on the isotherm is similar to the effect of increasing the Langmuir-Freundlich heterogeneity parameter,  $n$ , as described previously. Indeed, subtracting the highest energy isotherm causes a narrowing of the site-energy distribution from four discrete site energies to three, which is equivalent to increasing the  $n$ -value of the LF isotherm. There is no significant change in the maximum adsorption capacity ( $Q^0$ ) because the highest energy isotherm represents such a small fraction of the total number of sites. While the average site energy decreased, and this decrease may contribute to the reduction in adsorption capacity at low solute concentrations, it is evident that the change in the average site energy does not have a significant impact on the overall isotherm. In terms of Freundlich isotherm parameters, the effect of losing a small number of high energy sites is to lower the value of  $K_F$  significantly, and increase the value of  $n$ . This, in turn, may have a significant effect on the performance of adsorption systems and their ability to remove contaminants from water.

#### Preloading in a Model Bi-Solute System

Preloading of carbon by macromolecular DOM in fixed-bed reactors involves both thermodynamic and mass-transfer considerations. DOM is typically a mixture of molecules which adsorb more slowly than most SOCs. As a result, the wavefronts of DOM are more disperse and travel through FBRs more quickly than those typically exhibited by SOCs. This separation of mass-transfer zones results in the exposure of carbon to DOM prior to



the arrival of SOC molecules in the adsorber bed. Once inside the microporous structure of the carbon, humic molecules are not readily displaced. This lack of displacement may be due to a combination of factors, including steric hindrance and adsorption at multiple sites. While DOM has been shown to compete with SOCs during simultaneous adsorption, the effects of preloaded DOM are generally more severe. Thus, the impact of DOM in FBRs depends on the dynamics of both DOM and SOC adsorption, which is controlled, in large part, by mass-transfer controlled adsorption kinetics.

To investigate the mechanisms of preloading, a model system was sought for which mass-transfer effects could be eliminated as a significant factor. This requirement is met by choosing two molecularly discrete, low-molecular-weight compounds. However, it was necessary to retain an important feature of preloading by natural DOM, that is, the observed lack of displacement. This was accomplished by choosing one compound which adsorbed strongly enough that it could not be displaced significantly by TCE regardless of whether it was loaded simultaneously or whether it was preloaded. Indeed, from a purely thermodynamic point of view, the order of adsorption of two SOCs should have no bearing on their equilibrium distribution.

To identify a model bi-solute system which exhibits such characteristics, we performed (IAST) calculations for several candidate compounds to evaluate their tendency to be displaced by trichloroethylene (TCE). Our calculations showed that even at very low coverages, 1,2,4-trichlorobenzene (TCB), a strongly adsorbing aromatic compound, would exhibit no significant displacement in the presence of TCE over the concentration range of interest.

Ideal Adsorbed Solution Theory (IAST) calculations for the model bi-solute system were made to investigate whether thermodynamically-based model predictions of preloading effects were consistent with the preceding sensitivity analyses. It was not the primary objective of this work to characterize TCE/TCB bi-solute equilibria. Rather, the objective was to examine the effect of a non-displaceable species (TCB) on the subsequent adsorption of another compound (TCE). To replicate the physical system being modeled, the carbon was preloaded with TCB prior to adsorbing TCE. While not strictly necessary from a thermodynamic perspective, this approach accounts for any physical mechanisms of

competition which develop as a consequence of the structural characteristics of the adsorbent. Structural effects are not expected to be significant for the TCB/TCE system examined here, but they are likely to be quite important in systems containing macromolecular dissolved organic matter (Carter et al.1992).

Single solute isotherms of each component must be known to generate IAST predictions of bi-solute equilibria. Single-solute adsorption isotherms for TCE and TCB was measured on 165-micron F400 carbon, and are shown in Figure 7-5. Isotherm data was fitted with the Langmuir-Freundlich and Freundlich models; best-fit model parameters are reported in Table 7-5. It is evident that TCB is much more strongly adsorbed, which is reflected in significantly larger LF capacity and energy parameters, and a smaller n-value. The Freundlich isotherm parameters exhibit the same trends, and are also statistically significant.

For the purposes of IAST calculations, the low concentration regions of the TCE and TCB isotherms were fit with the Freundlich isotherm. For single solute data described by Freundlich isotherms, the IAST theory results in the following two equations which must be solved simultaneously:

$$C_{o1} - \frac{Mq_{e1}}{V} - \frac{q_{e1}}{q_{e1} + q_{e2}} \left[ \frac{q_{e1} + q_{e2}}{\frac{K_{F1}}{n_1}} \right]^{(1/n_1)} = 0 \quad (7-2)$$

$$C_{o2} - \frac{Mq_{e2}}{V} - \frac{q_{e2}}{q_{e1} + q_{e2}} \left[ \frac{q_{e1} + q_{e2}}{\frac{K_{F2}}{n_2}} \right]^{(1/n_2)} = 0 \quad (7-3)$$

Where  $M/V$  is the adsorbent dose,  $D_o$ , and the other terms have been previously defined.

Preliminary IAST calculations were performed to determine whether TCB exhibits significant displacement in the presence of TCE. The amount of TCB desorbed was calculated as the difference between the TCB concentration predicted in the presence of TCE and the TCB concentration estimated from the single-solute TCB isotherm. The percent TCB desorbed was calculated as the ratio of the amount desorbed to the total mass of TCB present in the system. A representative TCB loading of 22 mg/g was chosen for

Table 7-5. Single-solute Adsorption of TCE and TCB on F400 Carbon

Exp.	Langmuir-Freundlich Isotherm					Freundlich Isotherm		
	Param.	Param. Est.	Std. Error	95% CI	$Q^0 b^n$	Param.	Param. Est.	95% CI
TCB N = 35	$Q^0 \times 10^{-2}$	9.581	0.658	134.4	58.17	$K_F$	55.01	52.35, 57.80
	$b \times 10^4$	18.44	5.286	10.79		n	0.390	0.372, 0.408
	n	0.445	0.012	0.025		N = 48		
TCE N = 82	$Q^0 \times 10^{-2}$	1.833	0.380	0.760	1.279	$K_F$	1.260	1.187, 1.337
	$b \times 10^4$	1.700	0.891	1.782		n	0.566	0.545, 0.586
	n	0.572	0.014	0.028		N = 48		

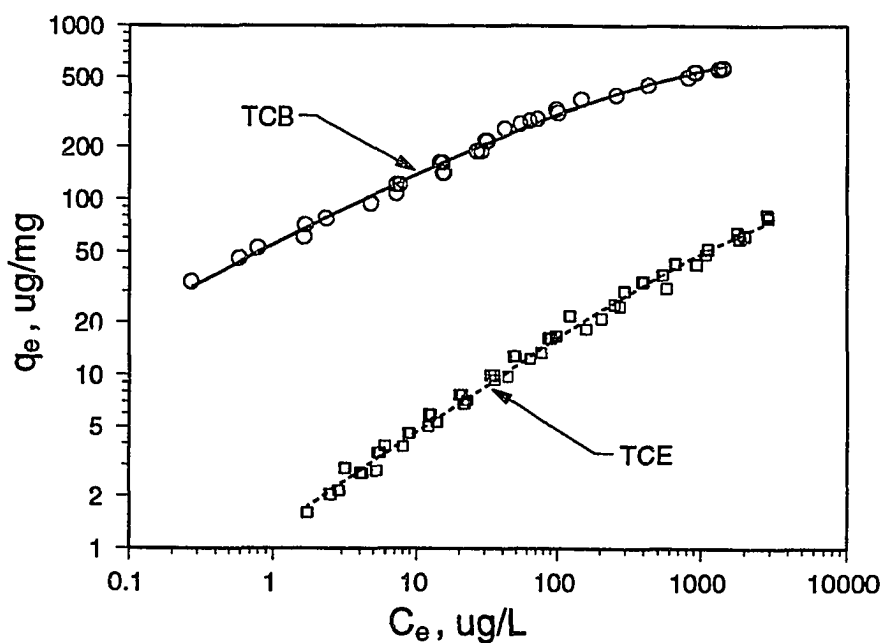


Figure 7-5. Adsorption of TCE and TCB on F400 carbon. Solid line represents the best fit with the Langmuir-Freundlich isotherm model.

the analysis; results are tabulated in Table 7-6. IAST calculations predict an insignificant amount of TCB displacement, although some displacement does occur as reflected in increases in TCB solution concentrations with increasing TCE concentrations. The maximum calculated displacement of TCB was less than 0.08% over a range of TCE concentrations from about 5 to 2400  $\mu\text{g/L}$ .

**Table 7-6. IAST Predictions of TCB Displacement in a Model Bi-Solute Preloading System**

Ce, TCE $\mu\text{g/L}$	Ce, TCB $\mu\text{g/L}$	qe, TCB $\mu\text{g/mg}$	Percent TCB Desorbed
5.4	0.094	21.798	0.000
10.8	0.097	21.798	0.001
21.8	0.101	21.797	0.001
56.2	0.115	21.797	0.003
93.0	0.130	21.797	0.004
261	0.194	21.795	0.012
601	0.309	21.792	0.025
1438	0.561	21.786	0.054
2409	0.826	21.779	0.084

TCE isotherms were predicted for several different loadings of TCB ranging from 0.01 to 275  $\text{mg/g}$  to examine effect of a non-displaceable sorbate on the subsequent adsorption of TCE. Humic substance loadings observed in this work were below 45  $\text{mg/g}$ , however, higher TCB loadings were chosen to define limiting behavior. Single-solute TCE data and IAST predictions of TCE adsorption on TCB-preloaded carbon are shown in Figure 7-6. The thermodynamic model predicts behavior quite similar to that suggested by the sensitivity analyses discussed in the previous section. At low loadings of TCB, the TCE isotherm slope is significantly increased, resulting in a reduction in capacity primarily in the low concentration region. As the loading of TCB is increased, the isotherm slope asymptotically approaches a limiting value of unity, and the entire isotherm is shifted downward relative to the  $q_e$ -axis in a parallel fashion.

Freundlich isotherm parameters were estimated by fitting the IAST-generated

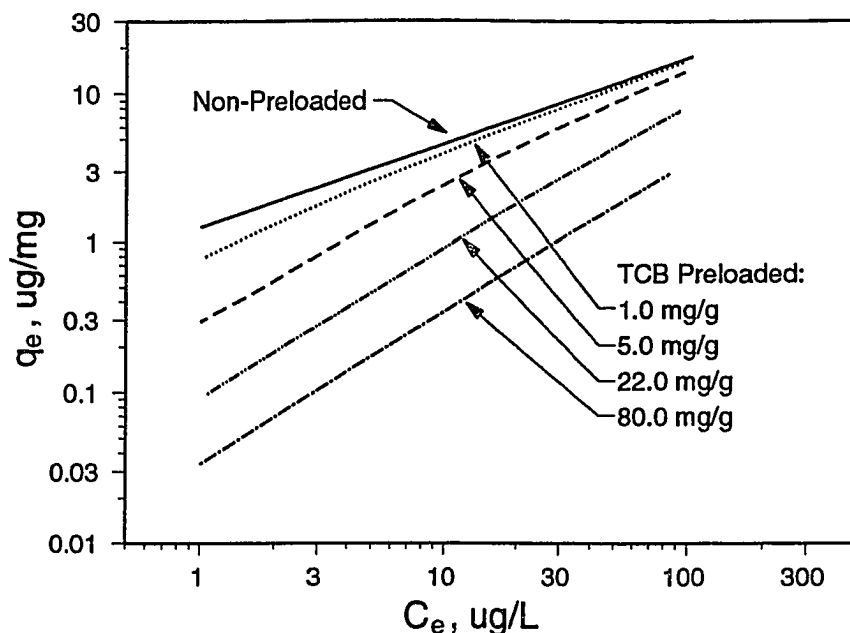


Figure 7-6. Adsorption of TCE on F400 carbon. Solid line represents Freundlich isotherm fit to single-solute data. Broken lines represent IAST predictions of TCE adsorption on TCB-preloaded carbon for different TCB loadings.

predictions of TCE adsorption to further quantify and interpret the IAST predictions. The effects of preloading on Freundlich isotherm parameters are illustrated in Figure 7-7. The presence of TCB significantly reduces the value of  $K_F$  and increases the value of  $n$ . As discussed previously, the unit capacity parameter,  $K_F$ , may be interpreted as a function of LF parameters,  $Q^0$ ,  $b$ , and  $n$ , representing the ultimate adsorption capacity, average site energy and site heterogeneity respectively (Equation 7-1). The reduction in  $K_F$ , therefore, is consistent with a reduction in the average site energy and ultimate capacity parameters, and an increase in the site heterogeneity parameter. The trends predicted by IAST are consistent with the preceding sensitivity analyses, and suggest that high energy sites, which dominate the adsorption at low solution phase concentration, are made unavailable as a result of preloading. As a consequence, the subsequent adsorption of more weakly adsorbing compounds, which cannot displace the preloaded compound, shows decreased capacity in the low concentration region. The narrower site-energy distribution is reflected by larger  $n$ -values.

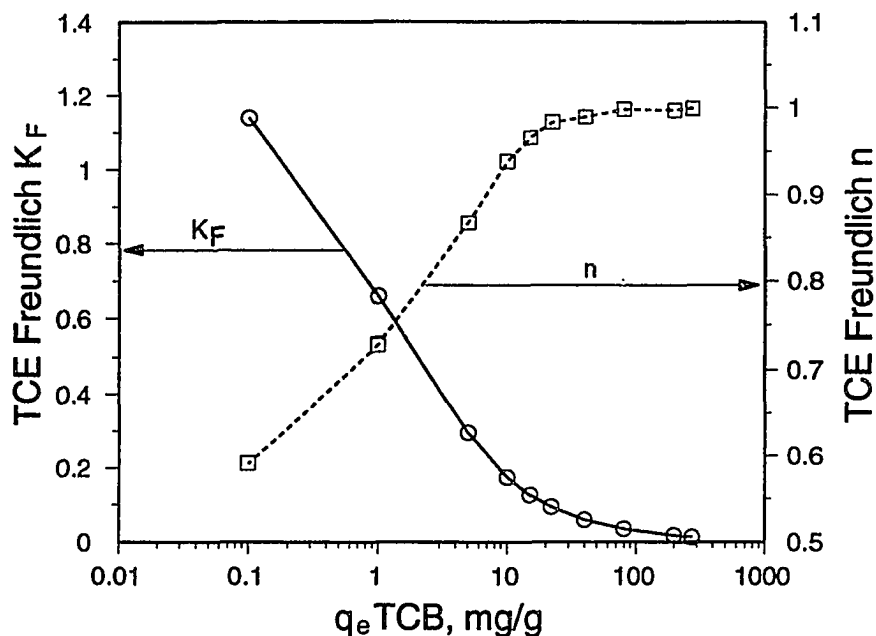


Figure 7-7. The effect of TCB preloading on Freundlich isotherm parameters for TCE . The Freundlich isotherm model was fit to IAST predictions of TCE adsorption in the presence of TCB.

### Site Energy Distributions

To gain further insight into the impacts of preloading, and how preloading changes the energetic character of an adsorbent, adsorbent site-energy distributions were calculated. Observed changes in experimentally measured isotherms resulting from preloading were related to changes in the energetic characteristics of sorbent surfaces by characterizing adsorbent site-energy distributions. In turn, observed changes in site-energy distributions determined from experimental data provided support for hypotheses regarding specific preloading mechanisms. Changes in site-energy distributions account for changes in the numbers, diversity and average energy of surface sites. The effects of changes in the adsorbent structure are included implicitly, because these effects are reflected phenomenologically in the adsorption isotherm. Pore blockage by preloaded solutes and restricted access to micropores are examples of potential structural changes. The theory of site-energy distributions was developed in Chapter 2 (Section 2.5). In this section, their application is demonstrated. Site energy distributions were computed for the isotherms

generated in the Langmuir-Freundlich isotherm parametric sensitivity analysis, and for the single-solute TCE isotherm on F400 carbon. To examine how changes in the energetic character of the adsorbent is reflected in Freundlich isotherm parameters, site-energy distributions are also computed for the low concentration region of the Langmuir-Freundlich isotherms. Finally, the IAST predictions of TCE adsorption in the presence of TCB were interpreted in the context of changes in calculated site-energy distributions.

The condensation approximation was used by Derylo-Marczewska et al (1984) to derive approximate site energy distributions from adsorption isotherm data. The approach involves taking the first derivative of the adsorption isotherm, and does not make any *a priori* assumptions about the underlying site energy distribution. To minimize artifacts resulting from variations in experimental data, a smoothing function is applied to the data collected in this research prior to computing the derivative. The three-parameter LF isotherm model was chosen as a smoothing function because it accurately describes the experimental data. The approximate site energy distribution function, therefore, is expressed in terms of LF isotherm parameters  $Q^0$ ,  $b$ , and  $n$ :

$$F(E) = - \frac{dq_e(E)}{d(E)} = \frac{Q^0 n (bC_s)^n}{RT} e^{(-nE/RT)} [1 + (bC_s)^n e^{(-nE/RT)}]^{-2} \quad (7-4)$$

If the experimental data (or range of data) is accurately described by the Freundlich isotherm model, it can be used as a smoothing function. The first derivative of the Freundlich isotherm yields an approximate site-energy distribution in terms of Langmuir-Freundlich adsorption parameters  $Q^0$ ,  $b$  and  $n$ , or in terms of Freundlich isotherm model parameters  $K_F$  and  $n$ :

$$F(E) = \frac{dq_e(E)}{dE} = \frac{Q^0 n (bC_s)^n}{RT} e^{(-nE/RT)} = \frac{K_F n C_s^n}{RT} e^{(-nE/RT)} \quad (7-5)$$

Site energy distributions were calculated using Equation 7-4 to determine how Langmuir-Freundlich isotherm parameters are related to the energetic character of the surface. Site energy distributions, shown in Figures 7-8 and 7-9, were calculated for the

Langmuir-Freundlich isotherms shown in Figure 7-3, using the parameters from Table 7-3. The distributions are illustrated for a range of energies from 0 to about 34 kJ/mol, corresponding to solution-phase TCE concentrations ranging from solubility (1100 mg/L) to a lower limit of about 1  $\mu\text{g/L}$ . Note that the upper limit of concentration measured experimentally in this research corresponds to a minimum site energy of about 14 kJ/mol.

Figure 7-8 shows that changes in the average site-energy parameter,  $b$ , shift the entire distribution on the energy axis, while changes in the value of  $n$  govern the spread of the distribution. From Figure 7-9, it is observed that a reduction in  $Q^0$  reduces the area under the curve but does not change the shape of the distribution or its position on the energy axis. This phenomenon demonstrates that the properties of both the approximate and theoretical distributions are reflected in the same way by these parameters. Therefore, while the calculated site-energy distributions are independent of any isotherm model, properties of the distributions can be interpreted in terms of experimentally-determined isotherm model parameters.

A reduction in the average site-energy parameter shifts the distribution to lower energies and reduces the number of high energy sites. An equal percentage increase in the  $n$ -value, however, results in greater reductions in the highest energy sites. Such trends are consistent with: i) the Langmuir-Freundlich isotherm sensitivity analysis, where an increase in the  $n$ -value caused a reduction in the extent of adsorption in the low-concentration region of the isotherm; and ii) the composite isotherm analysis, which exhibited an increase in the composite isotherm slope (and decrease in the extent of adsorption at low solution concentrations) after subtracting the contribution of the highest energy isotherm.

A reduction in the maximum adsorption parameter,  $Q^0$ , causes a constant relative reduction in the number of available sites across the energy spectrum, as shown in Figure 7-9; therefore, the average site energy or the shape of the distribution is not changed. A reduction of high-energy sites is observed; however, the highest energy sites are reduced to a greater extent when the  $n$ -value is increased an equal percentage. As expected, reducing both  $Q^0$  and  $b$  while increasing  $n$  results in a narrower distribution shifted to lower energies, and having a significantly smaller integrated area.

Site energy distributions were calculated using Equation 7-5 and parameters from



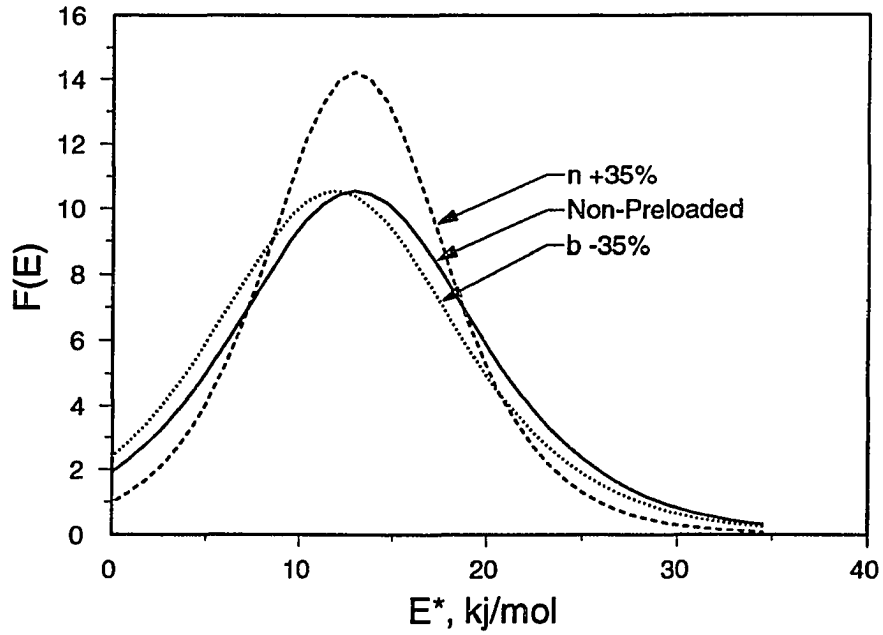


Figure 7-8. Sensitivity of the approximate site-energy distribution (Equation 7-4) to variations in Langmuir-Freundlich isotherm parameters: Effect of  $b$  and  $n$ .

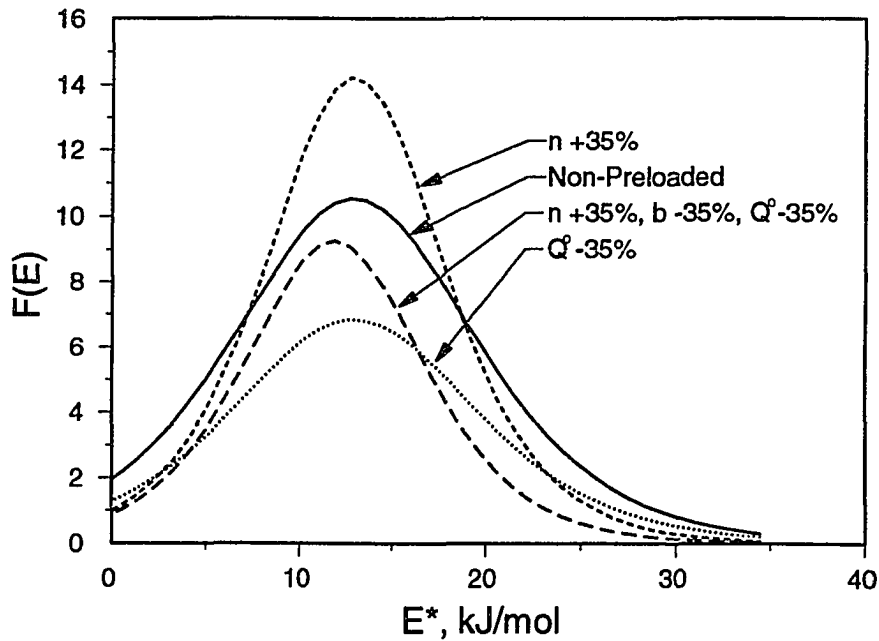


Figure 7-9. Sensitivity of the approximate site-energy distribution (Equation 7-4) to variations in Langmuir-Freundlich isotherm parameters: Effect of  $Q^0$  and  $n$ .

Table 7-3 to determine how changes in the energetic character of the surface are reflected in Freundlich isotherm parameters. Figure 7-10 shows site-energy distributions computed from low concentration data fit with the Freundlich isotherm model. The site distributions so derived are exponential, and are linearized in Figure 7-10 by plotting  $F(E)$  on a logarithmic scale. This representation facilitates comparison of distributions in the high energy region. Reductions in either  $b$  or  $Q^0$  result in a constant relative reduction in the number of sites over the entire range of energy values considered. On the semi-logarithmic coordinates of Figure 7-10, this results in a parallel displacement downward relative to the  $F(E)$  axis. As discussed in the context of the Langmuir-Freundlich isotherm sensitivity analysis, changes in these parameters also result in a parallel shift in the isotherm when plotted on log-log coordinates. Therefore, the Freundlich  $n$ -value remains constant while the  $K_F$  value decreases. In contrast, an increase in the  $n$ -value causes a greater relative reduction in the high energy sites, with a resultant increase in the isotherm slope when plotted on log-log coordinates, and a concomitant reduction in the  $K_F$  value.

To correlate the thermodynamic predictions with changes in adsorbent energetics, site-energy distributions corresponding to IAST model predictions of TCE isotherms in the presence of TCB were calculated. Figure 7-11 shows site-energy distributions which correspond to the IAST predictions plotted in Figure 7-6 and the Freundlich isotherm parameters plotted in Figure 7-7. Arithmetic coordinates were chosen for Figure 7-11 to illustrate the exponential nature of the distributions and because differences in the distributions can be clearly observed. A reduction in the high-energy sites is observed at all levels of TCB preloading. However, higher energy sites exhibit a greater relative depletion at low levels of preloading; indeed, most high-energy sites are depleted at TCB loadings less than 22 mg/g. This is reflected in a large increase in the Freundlich  $n$  value and decrease in the Freundlich  $K_F$  value at relatively low levels of TCB preloading, as Figure 7-7 shows. The value of  $n$  asymptotically approaches unity at higher levels of preloading, and the distribution shifts to lower energy values. The site-energy distribution becomes more narrow, and is comprised primarily of lower energy sites. The  $n$ -value (and therefore the isotherm slope) remains essentially constant at high levels of loading, and changes in the TCE isotherm are reflected as a downward displacement relative to the  $q_e$ -axis. This

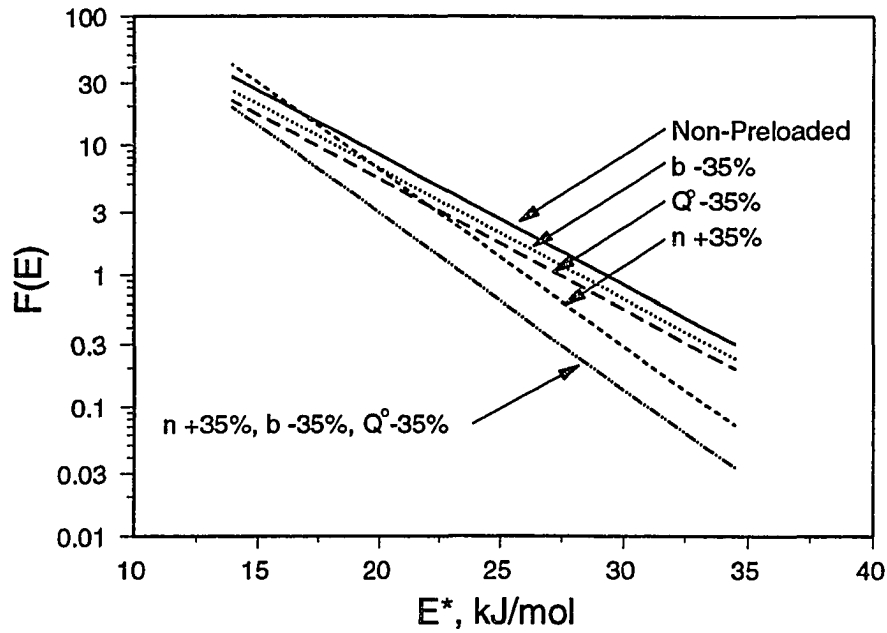


Figure 7-10. Sensitivity of the approximate site-energy distribution calculated for low concentration data (Freundlich region, Equation 7-5) to variations in Langmuir-Freundlich isotherm parameters.

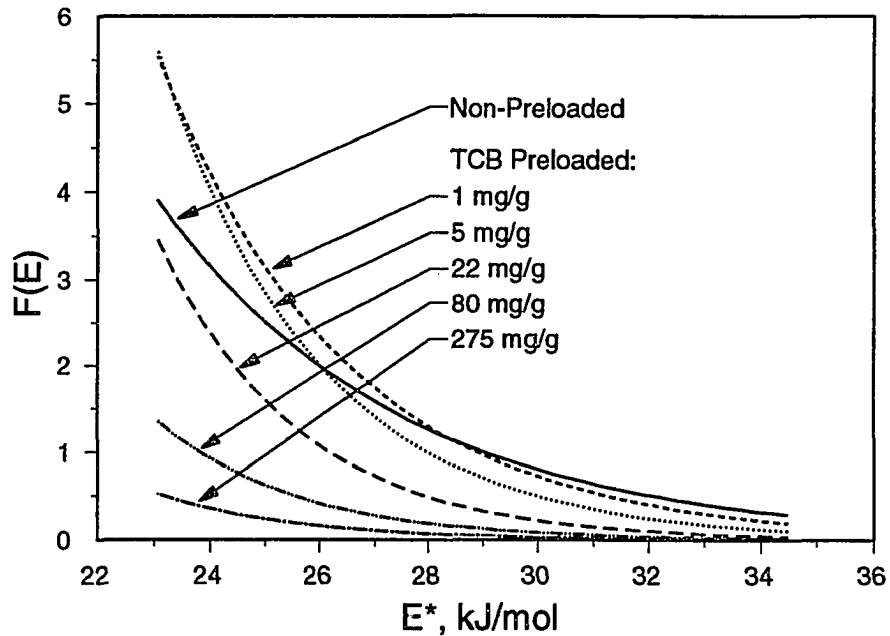


Figure 7-11. Site energy distributions computed using Freundlich isotherm parameters estimated for IAST predictions of TCE adsorption on carbon preloaded with different amounts of TCB.

downward displacement results from an equal relative reduction, across the energy spectrum, in the number of sites available to the TCE. While the average site energy and site-energy heterogeneity are still decreasing at high levels of preloading, changes in these sorbent characteristics are small, and do not contribute significantly to changes in the overall isotherm.

### **7.5 Impacts of Preloading on TCE Adsorption: Experimental Investigations**

In the previous section, the results of a theoretical investigation of the potential impacts of preloading in a model bi-solute system were presented. In this section, the same TCE/TCB bi-solute system is studied experimentally. The displacement of TCB by TCE was measured to validate IAST predictions. TCE adsorption isotherms on TCB preloaded carbon were measured for several different loadings of TCB, and are compared to theoretical predictions. The isotherms were fit by Langmuir-Freundlich and Freundlich isotherms where appropriate, and approximate site-energy distributions were calculated. The impacts of preloading observed experimentally are discussed in the context of the theoretical analysis discussed previously.

Experimental preloading conditions are shown in Table 7-7. F400 carbon was preloaded at five levels of TCB loading ranging from 22 to 275 mg/g. After equilibration with TCB, TCE was introduced into the adsorption reactors to yield final TCE equilibrium concentrations which ranged from about 1  $\mu\text{g/L}$  to 2500  $\mu\text{g/L}$ . The final equilibrium concentration of TCB in the aqueous phase varied somewhat as a function of the equilibrium TCE concentration, indicating that TCE does displace TCB to a small degree. The amount and percentage of TCB displaced was calculated as previously discussed, and is tabulated in Table 7-8. The measured displacement of TCB is greater than predicted by IAST calculations; however, the mass displaced is not significant, and did not have a significant impact on the amount of TCB adsorbed, at a TCB loading of 22 mg/g. The relative constancy of the amount of TCB adsorbed in all experiments is shown in Figure 7-12.

TCE isotherms on TCB-preloaded carbon and corresponding IAST predictions are shown in Figure 7-13 for three representative levels of TCB loading: 22, 80 and 275 mg/g.

**Table 7-7. TCB Preloading: Model Bi-Solute Preloading System**

Exp.	TCB Mass Added, mg	TCB $C_0$ , mg/L	TCB $C_e$ , $\mu\text{g/L}$	TCB $q_e$ , mg/g
E1V	0.00	0.000	0.00	0.00
EB22	0.22	0.872	0.28-10.6	21.7-21.9
EB40	0.40	1.580	0.6-6.6	39.8-39.9
EB80	0.80	3.160	2.2-17.1	78.3-79.8
EB200	2.00	7.930	21.7-49.2	196.5-199.0
EB275	2.75	11.07	42.5-99.4	276.9-279.3

**Table 7-8. Measured TCB Displacement in a Model Bi-Solute Preloading System for a TCB loading of 22 mg/g**

$C_e$ , TCE $\mu\text{g/L}$	$C_e$ , TCB $\mu\text{g/L}$	$q_e$ , TCB $\mu\text{g/mg}$	Percent TCB Desorbed
3.0	0.411	21.91	0.036
7.7	0.310	21.92	0.024
25.2	0.404	21.91	0.035
60.4	0.787	21.90	0.084
200	0.998	21.78	0.103
1146	7.44	21.89	0.842
1651	10.64	21.74	1.21

The best-fit isotherm model parameters for all experiments are tabulated in Table 7-9. The Langmuir-Freundlich model was fit to the data obtained from the isotherm measured on carbon preloaded with 22 mg TCB/g. The Freundlich isotherm was fit to the other isotherms because insufficient curvature was exhibited to allow independent determination of the three Langmuir-Freundlich parameters. The Freundlich isotherm was also fit to the low-concentration region of the data obtained from the carbon preloaded with 22 mg TCB/g.

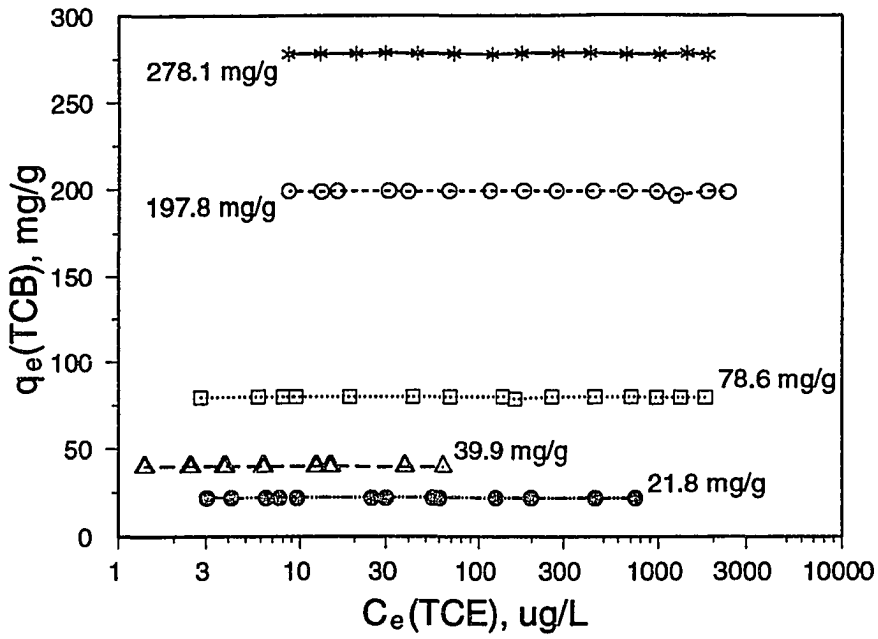


Figure 7-12. Adsorption of TCB on F400 carbon in the presence of TCE.

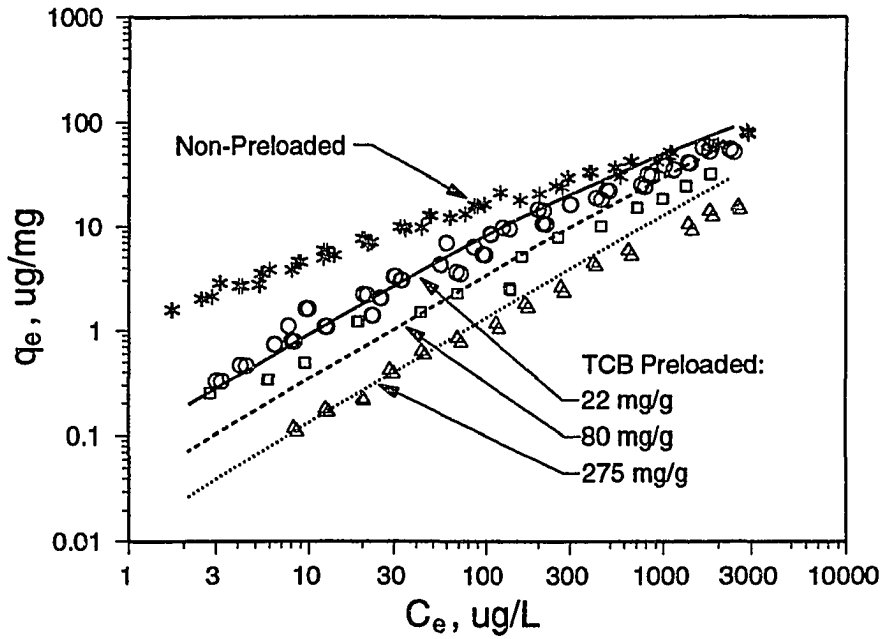


Figure 7-13. Experimental verification of IAST predictions of TCE adsorption on F400 carbon preloaded with TCB. Lines represent IAST predictions for different TCB loadings.

**Table 7-9. Adsorption of TCE on TCB-Preloaded F400 Carbon**

Exp.	Langmuir-Freundlich Isotherm					Freundlich Isotherm		
	Param.	Param. Est.	Std. Error	95% CI	$Q^0 b^n$	Param.	Param. Est.	95% CI
E1V N = 82	$Q^0 \times 10^{-2}$	1.833	0.380	0.760	1.279	$K_F$	1.260	1.187, 1.337
	$b \times 10^4$	1.700	0.891	1.782		n	0.566	0.545, 0.586
	n	0.572	0.014	0.028		N = 48		
EB22 N = 57	$Q^0 \times 10^{-2}$	1.182	0.263	0.532	0.152	$K_F$	0.157	0.119, 0.208
	$b \times 10^4$	3.644	1.389	2.807		n	0.819	0.728, 0.910
	n	0.841	0.024	0.049		N = 30		
EB40 N = 30	$Q^0 \times 10^{-2}$	ND	ND	ND	ND	$K_F$	0.236	0.214, 0.261
	$b \times 10^4$	ND	ND	ND		n	0.726	0.704, 0.747
	n	ND	ND	ND		N = 30		
EB80 N = 28	$Q^0 \times 10^{-2}$	ND	ND	ND	ND	$K_F$	0.096	0.080, 0.116
	$b \times 10^4$					n	0.766	0.729, 0.802
	n	ND	ND	ND		N = 28		
EB200 N = 30	$Q^0 \times 10^{-2}$	ND	ND	ND	ND	$K_F$	0.021	0.017, 0.027
	$b \times 10^4$					n	0.876	0.832, 0.920
	n	ND	ND	ND		N = 30		
EB275 N = 30	$Q^0 \times 10^{-2}$	ND	ND	ND	ND	$K_F$	0.019	0.016, 0.022
	$b \times 10^4$					n	0.872	0.846, 0.899
	n	ND	ND	ND		N = 30		

The data plotted in Figure 7-13 are clearly consistent with the theoretical predictions of the impact of TCB preloading on TCE adsorption. At low coverages, the most significant impact of preloading is to increase the TCE isotherm slope (on log-log coordinates) and therefore to reduce the capacity in the low concentration region. At higher TCB loadings, a smaller increase in the isotherm slope is observed, and the isotherm is displaced downward relative to the  $q_e$ -axis.

In all experiments, the slope of the IAST-predicted isotherm is greater than the measured isotherm slope. Indeed, over the range of TCB loadings considered, the IAST model predicts that the TCE isotherm slope asymptotically approaches a value of unity, while the measured values are slightly less than 0.90. In most cases, the IAST prediction

and the measured isotherm cross, indicating that the thermodynamic model over predicts the impact of preloading at low solute concentrations and under predicts the impact at higher solute concentrations. The differences between the measured TCE isotherms and the IAST predictions are likely due to a combination of factors including i) the effects of non-ideal competition; and ii) insufficient characterization of single solute equilibria at low concentrations (Henry's region). Effects of non-ideal competition have been observed in previous studies, and various modifications to the IAS theory have been proposed to account for these effects (Yonge and Keinath 1986, Smith 1991). However, most proposed modifications apply additional fitting parameters which provide no additional insight into the physical/chemical phenomena involved. Therefore, no attempt is made to account for the effects of non-ideality in this research.

Approximate site energy distributions were calculated using to interpret changes in the TCE isotherm in the context of i) changes in isotherm parameters, and ii) corresponding changes in the site-energy distributions. These distributions are shown in Figure 7-14, panel A (on arithmetic coordinates) and in panel B (on logarithmic coordinates). As noted above, the Langmuir-Freundlich isotherm model could only be fit to the isotherm measured on the sample preloaded with 22 mg TCB/g. Therefore, the distributions for this sample and for the non-preloaded carbon were calculated using the Langmuir-Freundlich isotherm equation as the smoothing function, while the other distributions were calculated using the Freundlich isotherm equation as the smoothing function.

The distributions shown in Figure 7-14(A) follow the trends predicted by the site-energy distributions shown in Figure 7-11, computed from isotherms predicted by IAST. Site energies shown in Figure 7-11 correspond to a concentration range of 1 to 100  $\mu\text{g/L}$ , the range of data over which the Freundlich isotherms were fit, while in Figure 7-14, the range of energies corresponds to the full range of experimental data. It is apparent from the reduction in area under the distributions in Figure 7-14 that the effect of preloading is to lower the available number of adsorption sites. High energy sites are reduced preferentially, causing a narrowing of the site-energy distribution and a reduction in the average site energy. These changes in the energetic character of the adsorbent are reflected



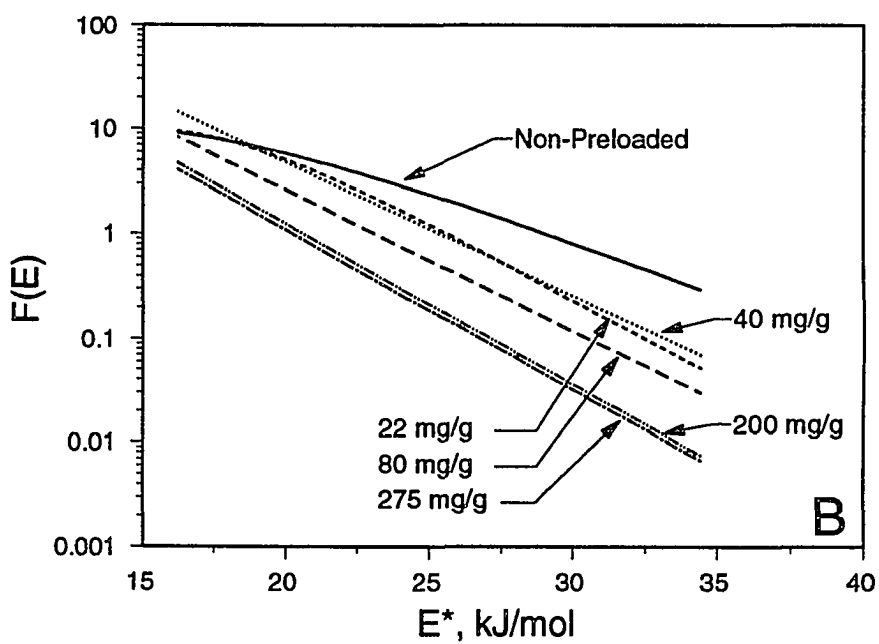
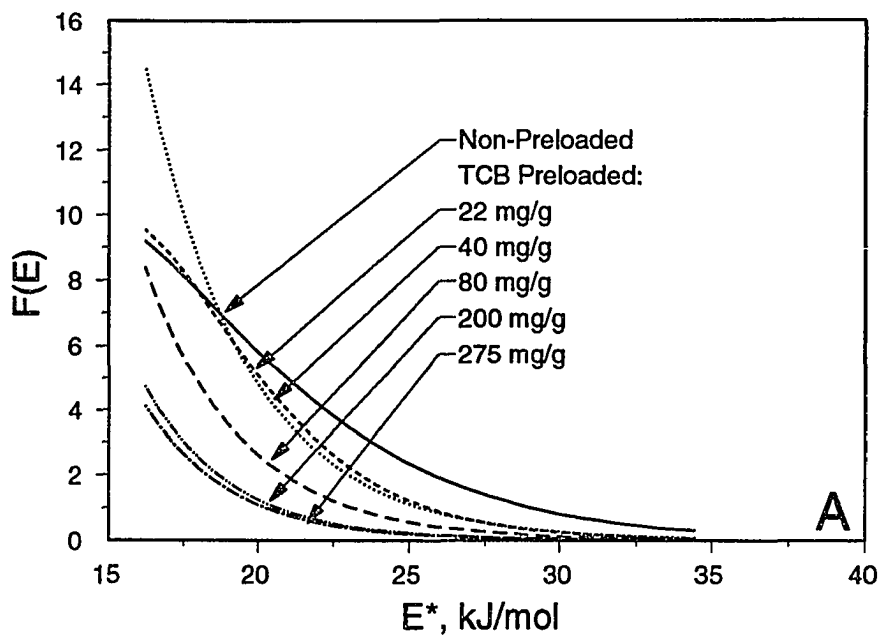


Figure 7-14. Site energy distributions computed from TCE adsorption isotherms on TCB-preloaded F400 carbon.

in statistically significant decreases in the Freundlich  $K_F$  value, and increases in the  $n$ -value.

In general, as Table 7-8 shows, the value of  $K_F$  decreases and the value of  $n$  increases with increasing TCB loading, and each parameter appears to reach a limiting or asymptotic value. This trend is consistent with the theoretically predicted trends plotted in Figure 7-7. While the Freundlich parameters for the two highest levels of loading are not significantly different from each other, they are significantly different from the parameters obtained from the lower loadings. An exception to this trend is the sample loaded with 22 mg TCB/g, which exhibits lower  $K_F$  values and higher  $n$ -values than is commensurate with the level of loading. In fact, these data are quite similar to the sample loaded with 40 mg TCB/g, with the exception of several of the lowest concentration data points; the anomalous behavior may be attributed to experimental error at low concentrations. An alternative explanation is that the mechanism of competition undergoes a change at a loading level between about 20 and 40 mg TCB/g. It is conceivable that at low concentrations, the adsorbed TCB occupies surface sites, while at higher loadings, it forms a more condensed phase in micropores. This condensed phase may serve as a partitioning medium for the TCE. While purely speculative, this phenomenon could explain why i) the IAST prediction over-estimated the impact of preloading at low concentrations, and ii) the  $n$ -values reach asymptotic values lower than those predicted by IAST.

An evaluation of the changes in Langmuir-Freundlich parameters obtained from the 22 mg TCB/g preloaded sample illustrates both the potential and the possible limitations of this type of analysis. The average site-energy parameter,  $b$ , of the Langmuir-Freundlich model, is lower for the preloaded carbon than for the non-preloaded adsorbent, which is consistent with a reduction in higher-energy sites, and with an increase in the site-energy heterogeneity parameter,  $n$ . However, an examination of the confidence intervals reveals that the difference is not statistically significant. One explanation for the lack of statistical significance is that the data does not span a sufficiently wide range of concentration to permit a reliable estimate of the  $b$  parameter. The preceding sensitivity analysis show that in the low concentration range, the isotherm is relatively insensitive to changes in the average site-energy parameter, while the isotherm is quite sensitive to changes in the

heterogeneity parameter. Therefore, the value of  $n$  can be estimated more reliably than the value of  $b$ .

Another explanation for the lack of statistical significance is that the *average* energy of the surface under study is not impacted greatly at low levels of preloading. A small change in the average surface energy is consistent with the likelihood that the fraction of high-energy sites on the surface is small. As the composite isotherm analysis illustrated, the removal of relatively few high energy sites can have a significant impact on the isotherm slope and capacity in the low-concentration region, but the impact on the average energy of the surface may be rather small. Therefore, it is likely that while low loadings of TCB have a significant impact on the site-energy heterogeneity as a result of depleting high-energy sites, the impact on the average site energy is not significant.

The Langmuir Freundlich maximum capacity parameter,  $Q^0$ , decreased from 183 to 118  $\mu\text{g}/\text{mg}$  with preloading; however, the result is not statistically significant.  $Q^0$  is a quantity representative of high surface coverages associated with high solute concentrations. In this study, the maximum aqueous phase concentration is less than 1% of solubility, typical of many environmental systems. Large changes in  $Q^0$ , therefore, may not occur at low levels of preloading. Further, unless the isotherm exhibits a significant degree of curvature on log-log coordinates, the value of  $Q^0$  is difficult to estimate with statistical confidence. Despite the relatively small changes in the average site-energy and the maximum capacity parameters, the surface heterogeneity parameter was nonetheless greatly affected by preloading. This result suggests that low loadings of TCB significantly change the site-energy distribution, and the mechanism is a depletion of the highest energy sites. The data further suggest that the high-energy sites preferentially occupied by the TCB do not comprise a large fraction of the total number of sites.

These results point out an important distinction between the value of  $Q^0$ , the Langmuir-Freundlich maximum capacity parameter, and the Freundlich  $K_F$  parameter. The  $K_F$  parameter is rigorously a *unit capacity* parameter, and represents the adsorption capacity at unit concentration, but is commonly interpreted as a "capacity" parameter. While the value of  $Q^0$  does not exhibit a statistically significant change, the  $K_F$  value decreases nearly ten-fold, from 1.26 to 0.157. The value of  $K_F$  shows a significant decrease because the

loss of high-energy sites causes a concomitant reduction in adsorption capacity in the low concentration range. If  $K_F$  is interpreted mathematically as a function of Langmuir-Freundlich isotherm parameters (Equation 7-1), then the reduction in the value of  $K_F$  is due primarily to a significant decrease in the site-energy heterogeneity as reflected by an increase in the heterogeneity parameter,  $n$ .

Some site-energy distributions, primarily those calculated from isotherms on carbon loaded at low to moderate levels, actually show an increase in the number of low-energy sites as a result of preloading. This effect may be an artifact of not characterizing the high-concentration region of the isotherm with enough detail. An alternative explanation is that some higher energy sites are not completely eliminated, but have somehow had their net adsorption energies reduced. It may also be possible that new, low energy adsorption sites are created as a result of molecular association with the adsorbed TCB, as discussed previously.

## **7.6 Effects of Preloading on Adsorbent Pore Structure**

The mechanistic effects of preloading analyzed thus far have focused on changes in TCE isotherms, which were interpreted in the context of changes in isotherm parameters and in adsorbent site-energy distributions. In this section, changes in the physical characteristics of the adsorbent due to TCB preloading are assessed, and used to further interpret TCE adsorption on preloaded carbon. Our approach was to characterize the pore structure and surface area of virgin F400 carbon and carbon preloaded with TCB, using gas-phase  $N_2$  adsorption at 77 K. The results of this analysis are tabulated in Table 7-10. Total pore volume was determined from the volume of nitrogen adsorbed at a relative pressure ( $p/p_0$ ) of 0.995; average pore radius was calculated as the ratio of total pore volume to total surface area; and the surface area distribution was calculated from the  $N_2$  adsorption isotherm.

From the data in Table 7-10, it is evident that TCB preloading has a significant impact on the adsorbent surface area and pore structure. The total pore volume and surface area decrease significantly, as Figures 7-15 and 7-16 show. A comparison of the two curves in Figure 7-15, one showing total surface area and the other showing micropore

**Table 7-10. Effect of TCB Adsorption on Adsorbent Characteristics**

Exp.	TCB $q_e$ , mg/g	Pore Volume, $\text{cm}^3/\text{g}$	Avg. Pore Radius, cm	Surface Area, $\text{m}^2/\text{g}$	Percentage of Area in Pores Having Widths ( $\text{\AA}$ ) in the Stated Range		
					$<20 \text{ \AA}$	20 to 200	$>200 \text{ \AA}$
E1V	0.0	0.536	11.41	955	85.60	13.90	0.50
EB22	21.8	0.484	11.28	857	86.49	12.95	0.56
EB40	39.9	0.450	11.35	793	85.58	13.86	0.56
EB80	79.1	0.416	11.83	703	83.27	16.11	0.62
EB200	198.0	0.277	13.58	408	72.82	26.22	0.96
EB275	278.0	0.246	15.60	316	64.85	33.74	1.41

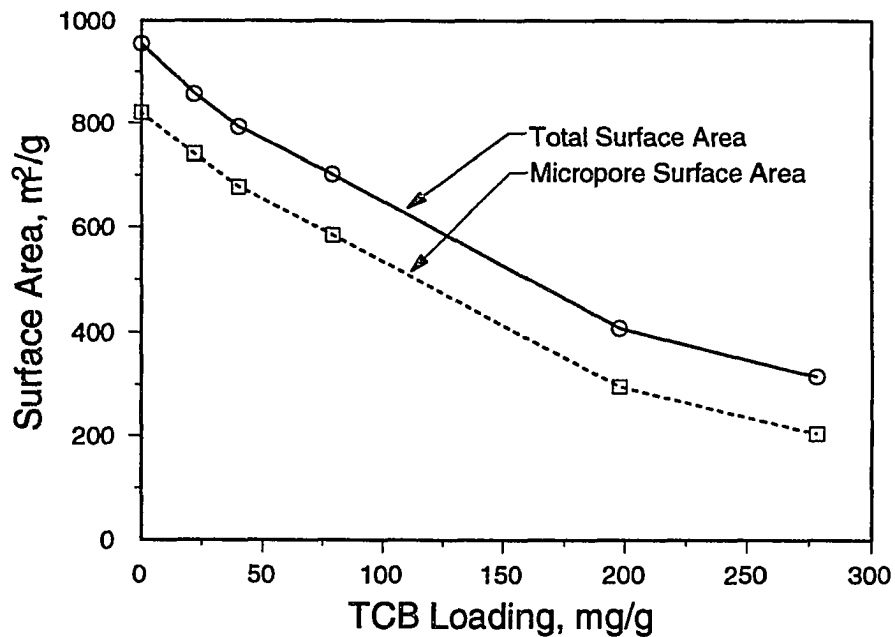


Figure 7-15. Effect of TCB preloading on total F400 carbon surface area and surface area in pores having widths less than 20  $\text{\AA}$ .

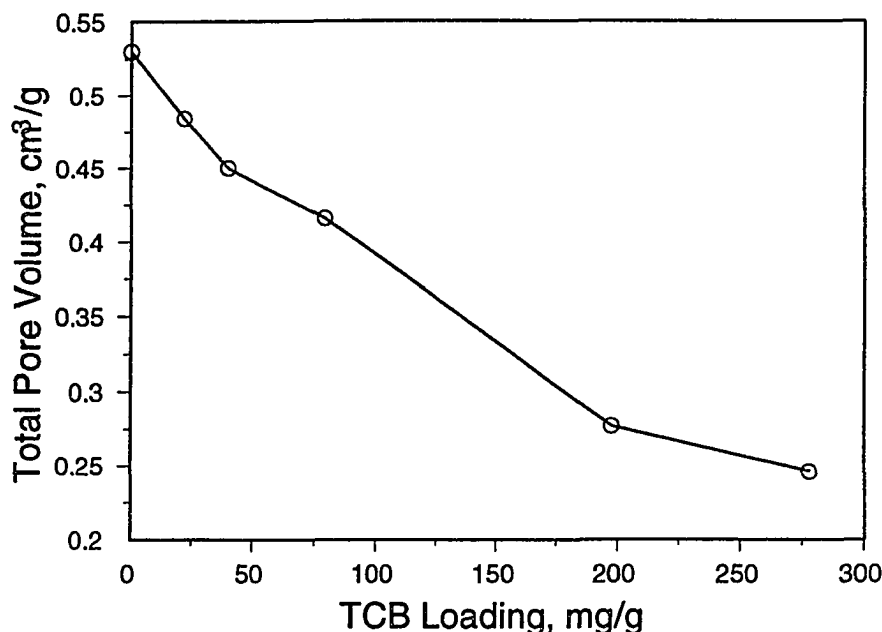


Figure 7-16. Effect of TCB preloading on total F400 carbon pore volume.

surface area, suggests that nearly all of the reduction in total surface area is due to a reduction in micropore surface area. Therefore, a reduction in the total surface area is accompanied by a shift in the surface-area distribution to larger pore sizes. Figure 7-17 shows an excellent correlation between total pore volume and micropore surface area for different levels of TCB loading. These results suggest that the adsorption of TCB occurs primarily in micropores. As increased amounts of adsorbed TCB occupy micropore volume, the total pore volume accessible to  $N_2$ , and presumably to other adsorbates including TCE, decreases. Further analysis suggests, however, that the reduction in the extent of TCE adsorption is not well correlated to reductions in surface area or pore volume. Figure 7-18 shows the TCE Freundlich unit capacity parameter,  $K_F$ , plotted as a function of the micropore surface area. The figure shows that the value of  $K_F$  for TCE falls off much more sharply than the surface area, particularly at lower TCB loadings. This result suggests that decreases in isotherm capacity at low levels of preloading are not due primarily to reductions in surface area or pore volume. As suggested by the site-energy distribution analyses presented previously, the capacity reductions which occur at low levels of preloading are likely due to the loss of high energy sites, causing a narrowing of

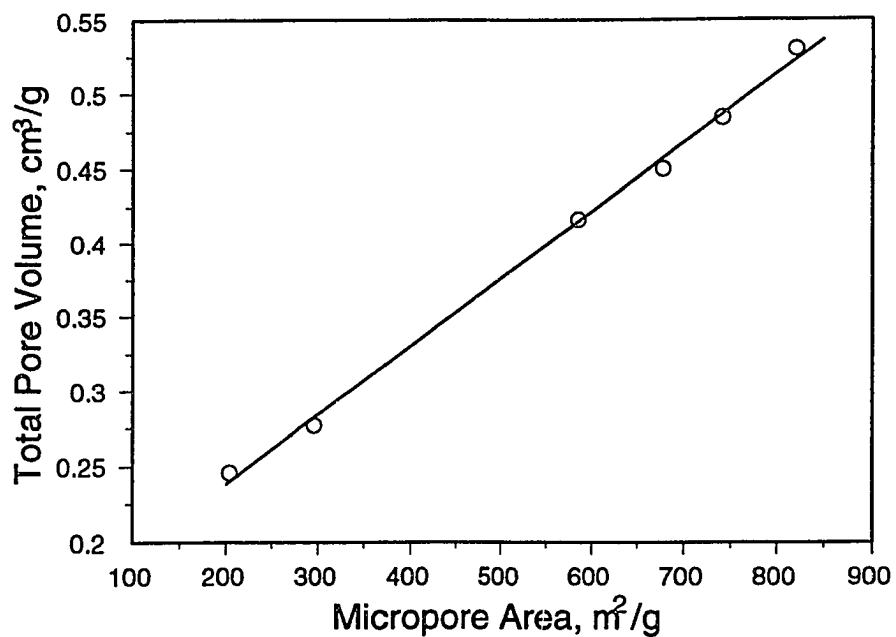


Figure 7-17. Linear correlation between micropore surface area and total pore volume for TC3 preloaded F400 carbon.

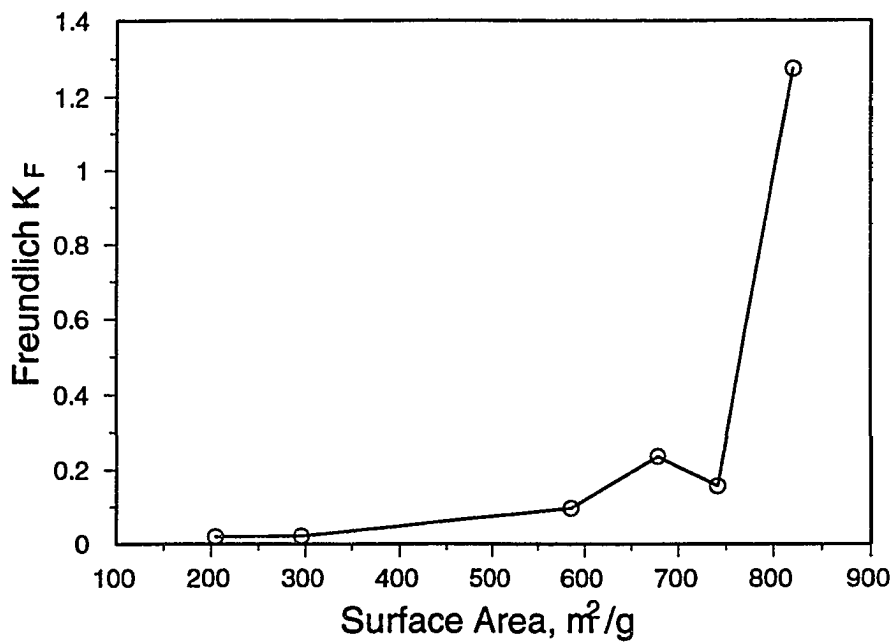


Figure 7-18. Effect of reduction in F400 carbon micropore surface area as a result of preloading on the Freundlich unit capacity parameter.

the site-energy distribution and an increase in the isotherm site heterogeneity parameter,  $n$ . At higher levels of preloading, the reductions in  $K_F$  are better correlated with reductions in surface area and pore volume. When this is the primary mechanism of capacity reduction, the site-energy heterogeneity is relatively constant with increased levels of preloading, and the TCE isotherm is displaced in a parallel fashion downward relative to the  $q_e$ -axis.

## 7.7 Summary and Conclusions

The Langmuir-Freundlich isotherm model, a three-parameter model derived from the theory of adsorption on heterogeneous surfaces, successfully described the adsorption of single solute TCE and TCB on F400 carbon, and TCE on F400 carbon preloaded with TCB. However, in some cases, isotherm model parameters could not be determined with statistical confidence. In contrast, the two Freundlich isotherm parameters were estimated with statistical confidence, although accurate description of the adsorption data was usually limited to the low concentration range.

It was demonstrated that changes in the isotherm parameters could be interpreted in terms of changes in the site-energy distribution. The Langmuir Freundlich parameters  $Q^0$ ,  $b$ , and  $n$  represent the area under the distribution, the position of the distribution on the energy axis, and the width or variance of the distribution respectively. By expressing the Freundlich isotherm as a simplification of the more general three-parameter Langmuir-Freundlich isotherm, and by relating changes in site-energy distributions to Freundlich isotherm parameters, it was demonstrated that Freundlich isotherm parameters have physical significance. The Freundlich  $n$  parameter represents site energy heterogeneity, while the  $K_F$  parameter incorporates isotherm capacity, energy and site energy heterogeneity. A reduction in  $K_F$ , therefore, is due to some combination of a reduction in the average site energy and ultimate capacity parameters, and an increase in the site heterogeneity parameter. It was demonstrated that changes in the isotherm parameters could be interpreted in terms of changes in the site-energy distribution.

Isotherm sensitivity analysis, IAST model predictions and experimental measurements give a clear, consistent mechanistic interpretation of the impacts of adsorbent preloading. At low loadings of the preloading compound, the most significant effect of



preloading is to reduce the number of high energy sites available to the subsequently adsorbed compound. The loss of high energy sites causes a significant reduction in the site-energy heterogeneity, and reduces the extent of adsorption in the low concentration region. These changes are reflected in a significant increase in the Langmuir-Freundlich and Freundlich  $n$ -values, and a significant decrease in the Freundlich  $K_F$  value. At low levels of preloading, changes in the Langmuir-Freundlich  $Q^0$  and  $b$  parameters were not statistically significant.

At higher levels of preloading, the site-energy distribution is further shifted to lower energies, resulting in a reduction in the average site energy, and maximum adsorption capacity. Changes in the site-energy heterogeneity are small, and both the Langmuir-Freundlich and Freundlich  $n$ -values are relatively constant. This reflects in a shift in the TCE isotherm downward relative to the  $q_e$ -axis, in a parallel fashion. A sensitivity analysis suggests that reductions in Langmuir-Freundlich maximum capacity and average energy parameters are significant; however, this could not be verified experimentally because the isotherms were linear on log-log coordinates and three isotherm parameters could not be independently estimated.

Measurements of adsorbent surface area and pore volume indicate that observed changes in TCE adsorption resulting from TCB preloading are associated with changes in the physical characteristics of the adsorbent. TCB adsorbs primarily in micropores, and increased levels of preloading reduced the micropore surface area, total surface area and pore volume. However, reductions in the Freundlich  $K_F$  parameter correlated with surface area reductions only at higher levels of preloading. This finding further supports the hypothesis that low levels of preloading are associated with a loss of high-energy sites, and provides a further mechanistic explanation of the parallel shifts in the TCE isotherm at higher levels of preloading.

## CHAPTER VIII

### EFFECTS OF HUMIC SUBSTANCE PRELOADING ON TCE ADSORPTION

#### 8.1 Introduction

In previous chapters, the factors which influence humic acid adsorption were investigated, and preloading mechanisms were identified by performing theoretical analyses and by studying a well-characterized, model bi-solute system. In this chapter, the effects of preloading by less well-characterized, heterogeneous natural humic substances are described. The effects of humic and fulvic acid adsorption on subsequent TCE adsorption was studied for a range of conditions in batch systems. The effects of macromolecule size and size distribution, solution ionic strength, the presence of divalent cations, and adsorbent characteristics including pore-size distribution and surface chemistry were investigated.

TCE isotherms were measured on virgin carbon, and on carbon preloaded under different conditions. TCE isotherm data were fit with the Langmuir-Freundlich and Freundlich isotherm models, and differences in the adsorption isotherms are interpreted in terms of changes in isotherm model parameters. Changes in measured isotherms, isotherm model parameters, and adsorbent site-energy distributions are related to different preloading conditions. The effects of preloaded HA on adsorbent surface area and pore structure were measured, and the impacts of preloading by natural humic material are compared to the effects observed the model, bi-solute system discussed in Chapter 7 (Sections 7.4 and 7.5).

It was necessary to characterize adsorbed molecular-size distributions to investigate the effects of macromolecule size on subsequent TCE adsorption. Two different fractionation techniques were used for this purpose. As demonstrated in Chapter 4

(Section 4.5) and Chapter 6 (Section 6.3), humic substances occur naturally as mixtures of compounds with various molecular sizes. Ultrafiltration was used to fractionate the mixture into distinct size fractions, as described in Chapter 4 (Section 4.5). Each fraction exhibited a polydispersity much lower than the original solution. Adsorbents were preloaded with relatively narrow molecular-size fractions, and with mixtures of size fractions to examine the effects of size and initial size distribution. The second approach was based on the adsorptive fractionation phenomenon in which the preferential adsorption of low-molecular-weight fractions from solution fractionates HA mixtures according to size. The molecular-size distribution of adsorbed macromolecules was controlled, therefore, by preloading the carbon under different combinations of initial HA concentration and adsorbent dose.

The effects of solution chemistry were investigated by preloading humic acid at different ionic strengths and divalent metal (calcium) concentrations. Additional experiments are conducted to test whether the effects of calcium depended on the order of mixing. Carbons having different pore-size distributions and surface chemistry were preloaded with different amounts of HA to investigate the effects of adsorbent characteristics. The impacts of preadsorbed humic substances on the subsequent adsorption of TCE were interpreted in the context of the TCE isotherm.

## **8.2 Single-Solute TCE Adsorption by Non-Preloaded Carbon**

The adsorption of TCE on several virgin (non-preloaded) coal- and wood-based carbons was characterized to provide a basis for assessing changes in TCE isotherms resulting from preloading. Isotherm data were modeled using the three-parameter Langmuir-Freundlich and the two-parameter Freundlich isotherms discussed in Chapter 2 (Section 2.4) and Chapter 7 (Section 7.2). Isotherm model fits to TCE adsorption data on a variety of adsorbents are tabulated in Table 8-1. Langmuir-Freundlich parameters were estimated by fitting the entire data set, and Freundlich parameters were estimated by fitting the low concentration data ( $< 100 \mu\text{g/L}$ ). For comparison, the Freundlich unit capacity factors calculated from the three Langmuir-Freundlich parameters ( $K_F = Q^0 b^0$ ) are also reported. TCE adsorption isotherms (symbols) and isotherm model fits (lines) for coal-based carbons were shown in Chapter 7 as Figures 7-1 and 7-2, and are repeated here for

**Table 8-1. Single-Solute TCE Adsorption Data**

Exp.	Langmuir-Freundlich Model					Freundlich Model		
	Param.	Param. Est.	Std. Error	95% CI	Q <sub>0</sub> b <sup>n</sup>	Param.	Param. Est.	95% CI
WPLL N = 37	Q <sup>o</sup> x10 <sup>-2</sup>	0.755	0.071	0.145	0.436	K <sub>F</sub>	0.422	0.389, 0.457
	b x10 <sup>4</sup>	8.007	1.749	3.571		n	0.718	0.692, 0.745
	n	0.723	0.015	0.031		N = 20		
FS100 N = 23	Q <sup>o</sup> x10 <sup>-2</sup>	1.625	0.293	0.611	1.354	K <sub>F</sub>	1.451	1.245, 1.692
	b x10 <sup>4</sup>	2.152	1.007	2.101		n	0.527	0.480, 0.574
	n	0.567	0.015	0.031		N = 11		
F400 N = 82	Q <sup>o</sup> x10 <sup>-2</sup>	1.833	0.380	0.760	1.279	K <sub>F</sub>	1.260	1.187, 1.337
	b x10 <sup>4</sup>	1.700	0.891	1.782		n	0.566	0.545, 0.586
	n	0.572	0.014	0.028		N = 48		
BPL N = 68	Q <sup>o</sup> x10 <sup>-2</sup>	3.384	ND	ND	0.607	K <sub>F</sub>	0.600	0.561, 0.642
	b x10 <sup>4</sup>	0.115	ND	ND		n	0.557	0.533, 0.580
	n	0.556	ND	ND		N = 36		
WI N = 26	Q <sup>o</sup> x10 <sup>-2</sup>	0.695	0.344	0.712	0.149	K <sub>F</sub>	0.138	0.127, 0.149
	b x10 <sup>4</sup>	0.548	0.540	1.117		n	0.648	0.622, 0.674
	n	0.626	0.019	0.039		N = 12		
WE N = 45	Q <sup>o</sup> x10 <sup>-2</sup>	0.240	0.051	0.103	0.077	K <sub>F</sub>	0.072	0.057, 0.091
	b x10 <sup>4</sup>	2.305	1.049	2.12		n	0.710	0.620, 0.799
	n	0.686	0.017	0.034		N = 14		
WA N = 25	Q <sup>o</sup> x10 <sup>-2</sup>	0.242	0.112	0.232	0.025	K <sub>F</sub>	0.020	0.015, 0.026
	b x10 <sup>4</sup>	1.894	1.486	3.082		n	0.875	0.793, 0.957
	n	0.802	0.035	0.073		N = 14		

convenience as Figures 8-1 and 8-2. The slight curvature of the isotherms on log-log coordinates is described well by the Langmuir-Freundlich model. On a mass basis, the adsorption isotherms of the F400 and FS100 carbons are quite similar and exhibit a greater extent of adsorption than the BPL and WPLL carbons over the entire range of concentrations examined. The WPLL carbon has the lowest degree of activation and surface area, while the BPL represents the highest degree of activation and surface area of the coal-based carbons studied. Therefore, the BPL has a low capacity on a mass-basis despite having a high surface area. These trends are reflected to varying degrees by the Langmuir Freundlich and Freundlich isotherms parameters.

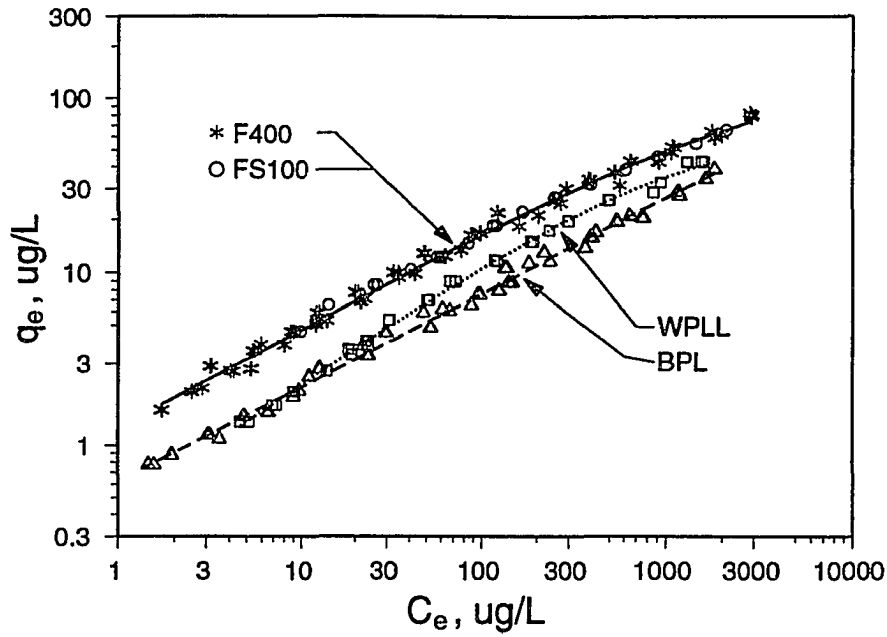


Figure 8-1. The adsorption of TCE on Calgon coal-based carbon, with capacity expressed on a mass basis. Isotherm data were fit with the Langmuir-Freundlich model.

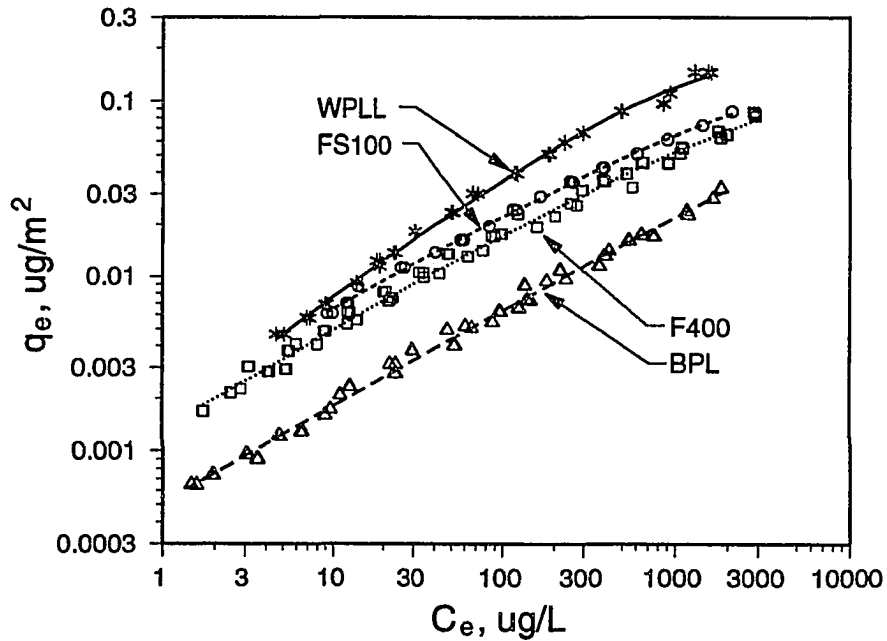


Figure 8-2. The adsorption of TCE on Calgon coal-based carbon, with capacity expressed on a surface area basis. Isotherm data were fit with the Langmuir-Freundlich model.

The Langmuir-Freundlich capacity parameter,  $Q^0$ , for the WPLL carbon is the lowest among the coal-based carbons, and due to the greater degree of curvature exhibited by the WPLL isotherm, also has the narrowest 95% CI. The WPLL capacity parameter is lower than that of both the FS100 and F400 carbons, and the difference is statistically significant, i.e., the confidence intervals do not overlap. In contrast, the BPL capacity parameter is higher, which may result from its higher surface area. However, standard errors for the Langmuir-Freundlich parameters could not be estimated for the BPL carbon, because the data exhibited almost no curvature on log-log coordinates. These results illustrate the difficulty of estimating the Langmuir-Freundlich capacity parameter in some cases. The Freundlich unit capacity parameter,  $K_F$ , can be estimated with greater statistical significance because only two model parameters,  $K_F$  and  $n$ , are estimated. The  $K_F$  values for the FS100 and F400 are statistically similar and are statistically greater than the WPLL and BPL values.

On a surface area basis, the WPLL carbon emerges as having the greatest capacity, followed by the FS100, F400 and BPL. This is reflected in an average site-energy parameter which is significantly larger than that measured for the other carbons. It is interesting to note that WPLL also has the greatest  $n$ -value, indicating a relatively narrow site-energy distribution. This may be related to the fact that the WPLL has been activated to a lesser degree, which may result in a lower diversity of functional groups formed on the surface. More detailed surface characterization would be needed to verify this hypothesis.

It does not appear that differences in the extent of TCE adsorption are due to the ability of TCE to access adsorbent surfaces. The extent of TCE adsorption per unit surface area is greatest on WPLL, the most microporous carbon, and is the least on BPL, which has the largest pore sizes. Furthermore, a correlation developed to predict isotherm capacity based on adsorbent pore structure (Urano et al. 1982) fails to account for the low capacity of the BPL carbon. Since TCE is a relatively small molecule, it is not too surprising that pore structure does not play a significant role in determining differences in adsorption capacity. The available data suggest that the observed differences in adsorption behavior may be related to differences in surface chemical properties. This explanation is consistent with the observation that the WPLL carbon exhibited a greater site-energy parameter.

Jagiello et al. (1992) showed that increases in surface acidity as measured by the Boehm technique were correlated with i) carboxylic acidity and ii) the specific electron acceptor capacity of the surface, as measured by an inverse gas chromatography technique. The data presented in Table 3-5 show that the WPLL carbon has the highest total acidity and carboxyl content as measured by NaOH and NaHCO<sub>3</sub> neutralization, respectively. The extent of adsorption for all coal-based adsorbents on a surface area basis is correlated with surface acidity; however, surface acidity does not explain the difference in extent of adsorption between the F400 and BPL carbons. Further, the extent of adsorption for the different carbons also correlates with the HCl consumption. It is apparent that measurements of surface acidity are indirect measures of surface functional groups and do not provide specific information about reactivity with organic compounds such as TCE.

TCE adsorption isotherms on wood-based carbons are shown in Figure 8-3. The surface areas of these three adsorbents are similar, and the trends observed on a mass basis would not be changed by expressing the isotherms on a surface area basis. The trends in capacity are similar to those observed for the coal-based carbons: on a mass basis, the carbons activated to a lesser extent exhibit a greater extent of adsorption over the entire range of concentration measured. These trends are reflected in the Langmuir-Freundlich maximum capacity parameter,  $Q^0$ , but the differences are not statistically significant. The average site-energy parameters for the three carbons are also similar. There appears to be a trend in the  $n$ -value, which increases with the degree of activation. The  $n$ -value for the MACRO carbon is higher than the other carbons, and the difference is statistically significant. The Freundlich  $K_F$  values decrease in the order MICRO>MESO>MACRO, and the differences are all statistically significant.

The data presented in Table 3-5 shows that the surface acidity of the MICRO carbon is the highest of the three, but the extent of adsorption exhibited by the MESO and MACRO carbons is different even though they have similar total acidities. Further, the carboxyl content is essentially the same for all three carbons. Therefore, surface acidity does not appear to be as good a predictor of capacity for the wood-based carbons. Moreover, it is not a good basis for comparing the coal-based with the wood-based adsorbents. It is possible that the L-type wood carbons may have a more hydrophilic surface for reasons which are not reflected in the surface acidity measurement. While the HCl consumption

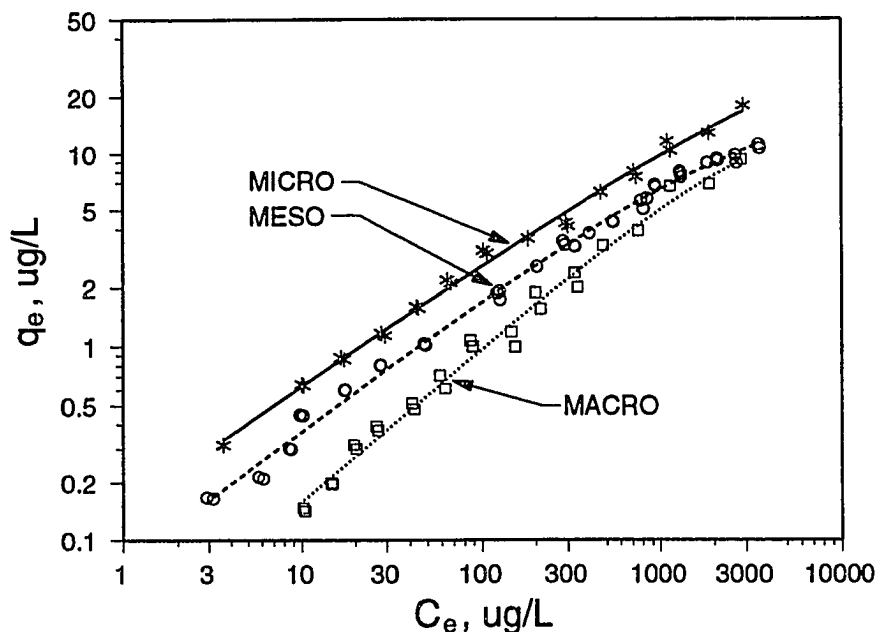


Figure 8-3. The adsorption of TCE on Westvaco wood-based carbon, with capacity expressed on a mass basis. Isotherm data were fit with the Langmuir-Freundlich model.

correlates rather well with the extent of adsorption for both the wood- and coal-based carbons, little is known about the nature of these basic groups. More sophisticated surface characterization than the methods used in this research would be required to show definitively which functionalities on the adsorbent surface contribute to differences in capacity between adsorbents manufactured from different sources.

### 8.3 TCE Adsorption by Carbon Preloaded with Discrete Size Fractions

#### Preloading with UF Size Fractions: Effects of Molecular Size

The effects of macromolecule size on adsorbent preloading and the subsequent adsorption of TCE were investigated by preloading F400 carbon with different ultrafiltration size fractions. These fractions are designated according to the nominal membrane molecular-weight cutoff values: <3K, 3-10K, 10-30K, 30-100K and >100K. The preparation of these fractions and their size characterization were discussed in Chapter 4 (Section 4.5). The preloading experiments were designed to compare the effects of different, relatively narrow molecular-size ranges at similar TOC loadings. The



experimental conditions for each preloading experiment are shown in Table 8-2. An adsorbent dose of 0.556 g/L was used for all experiments, and the initial humic acid concentration was adjusted to yield similar adsorbed amounts. The initial concentrations for all but the lowest size fraction are higher than typically found in natural systems.

TCE isotherms are shown in Figures 8-4 and 8-5. The isotherms shown in Figure 8-4 suggest that carbon preloaded with size fractions larger than the <3K fraction exhibits the same extent of adsorption as non-preloaded carbon. This conclusion, reached by visual inspection of Figure 8-4, is confirmed by the statistics for both the Langmuir-Freundlich and Freundlich isotherm model parameters given in Table 8-3. The carbon preloaded with the <3K fraction, however, exhibits a decrease in the extent of adsorption, as shown in Figure 8-5. The decrease in the extent of adsorption, as expressed in terms of the Freundlich unit capacity factor,  $K_F$ , is statistically significant, as depicted graphically in Figure 8-6. The carbon preloaded with 12.1 mg/g of the <3 K fraction exhibited a statistically significant reduction in TCE capacity while carbon preloaded with larger size fractions (14.6 to 18.1 mg/g) had no effect on TCE adsorption. This suggests that the ability to access micropore surface area is required for a macromolecule to exert any significant effect, and while physical blockage of micropores may be an important preloading mechanism, blockage of meso- and macropore openings by large molecular-weight material may not be important in many systems.

**Table 8-2. HA Preloading of F400 Carbon with UF Size Fractions-- Experimental Conditions**

Fraction	$C_0$ , mg TOC/L	$C_0/D_0$	$C_e$ , mg TOC/L	$q_e$ , mg/g	$C_e/D_0$	$C_e/C_0$
<3K	8.0	14.4	1.3	12.1	2.3	0.162
3-10 K	16.9	30.4	7.6	16.7	13.7	0.451
10-30 K	35.4	63.7	26.8	16.4	48.3	0.758
30-100 K	40.9	73.6	30.8	18.1	55.5	0.754
>100 K	18.9	34.0	9.6	16.6	17.3	0.510
>3 K	36.9	66.4	28.8	14.6	51.8	0.780

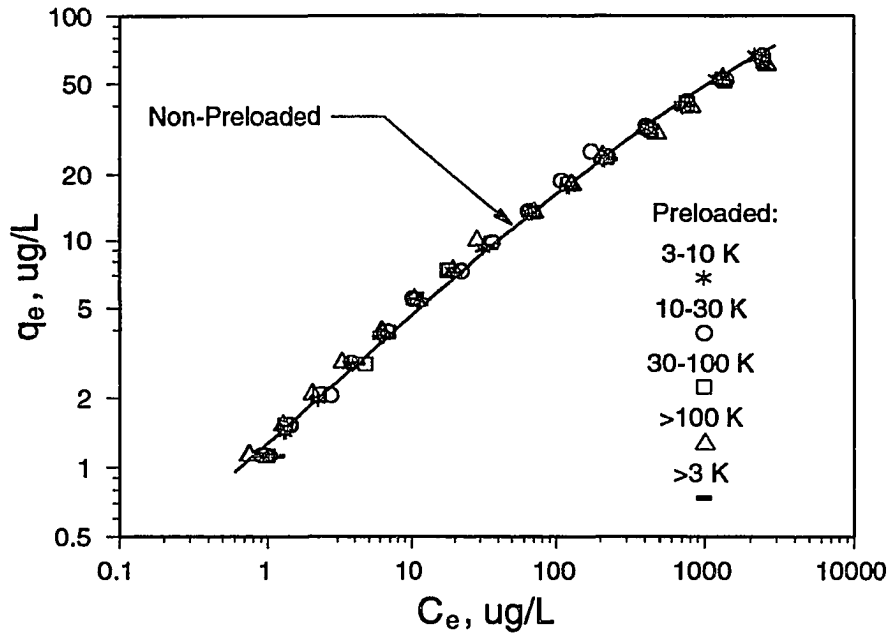


Figure 8-4. The adsorption of TCE on F400 carbon preloaded with various size fractions of Laurentian HA. Solid line represents Langmuir-Freundlich best-fit isotherm model for TCE adsorption on non-preloaded carbon.

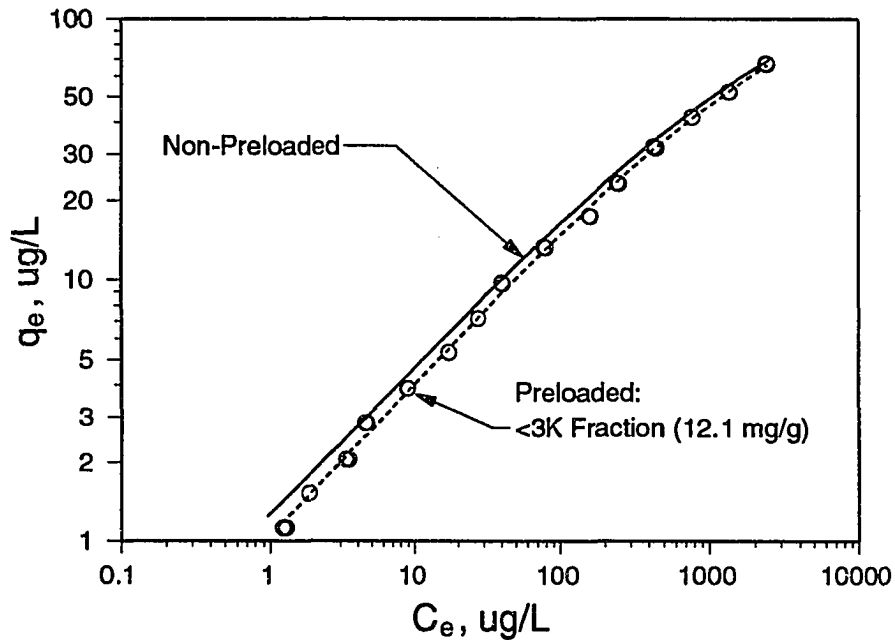


Figure 8-5. The adsorption of TCE on F400 carbon preloaded with the <3K size fraction of Laurentian HA. Lines represents Langmuir-Freundlich isotherm model fits.

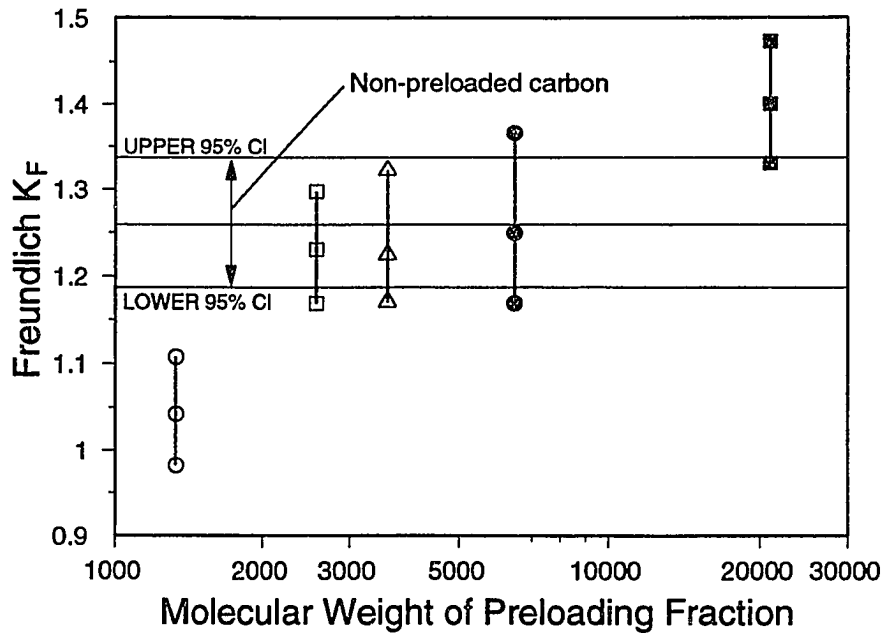


Figure 8-6. The effect of preloaded Laurentian HA size fractions on Freundlich  $K_F$  value for TCE. Solid horizontal lines represent best-fit  $K_F$  values and 95% confidence limits for TCE adsorption on non-preloaded carbon. Symbols with vertical lines represent best-fit  $K_F$  values and 95% confidence limits for TCE adsorption on carbon preloaded with UF fractions.

The data suggest that the >100 K fraction behaves somewhat differently from the lower size fractions. A loading of about 16.6 mg TOC/g was obtained with a relatively low  $C_e/D_0$  ratio, suggesting that the adsorption mechanism for this fraction is different than that of smaller fractions. It is possible that this large molecular-size fraction is removed from solution, in part, by a colloid destabilization or precipitation mechanism. While not statistically significant, the carbon preloaded with the >100 K fraction appears to have a slightly higher Freundlich  $K_F$  value and a lower  $n$ -value. The increase in sorption may result from the adsorbed humic substances acting as partitioning medium as suggested by Carter et al. (1992).

A slight increase in the Freundlich  $n$ -value was observed for all fractions except the >100 K fraction, although the increase was not statistically significant. This result suggests that some competition for high-energy adsorption sites may occur, but that the surface area on which competition occurs is small relative to the total surface area, and

**Table 8-3. HA Preloading of F400 Carbon with UF Fractions -- Isotherm Analysis**

Exp.	Langmuir-Freundlich Model					Freundlich Model		
	Param.	Param. Est.	Std. Error	95% CI	$Q_0 b^n$	Param.	Param. Est.	95% CI
3K12 12 mg/g N = 29	$Q_0 \times 10^{-2}$	1.757	0.172	0.354	1.056	$K_F$	1.042	0.982, 1.107
	$b \times 10^4$	1.746	0.402	0.827		n	0.588	0.566, 0.611
	n	0.591	0.007	0.014		N = 17		
3-10 N = 30	$Q_0 \times 10^{-2}$	1.339	0.163	0.334	1.253	$K_F$	1.231	1.168, 1.297
	$b \times 10^4$	3.641	1.131	2.321		n	0.587	0.565, 0.609
	n	0.590	0.010	0.021		N = 18		
10-30 N = 30	$Q_0 \times 10^{-2}$	1.125	0.117	0.240	1.244	$K_F$	1.244	1.170, 1.322
	$b \times 10^4$	6.057	1.628	3.341		n	0.582	0.556, 0.607
	n	0.608	0.011	0.023		N = 18		
30-100 N = 30	$Q_0 \times 10^{-2}$	1.166	0.124	0.254	1.266	$K_F$	1.249	1.168, 1.366
	$b \times 10^4$	4.935	1.395	2.863		n	0.581	0.553, 0.609
	n	0.594	0.011	0.023		N = 18		
>100 N = 29	$Q_0 \times 10^{-2}$	1.160	0.133	0.273	1.413	$K_F$	1.400	1.330, 1.473
	$b \times 10^4$	4.322	1.359	2.794		n	0.555	0.532, 0.577
	n	0.569	0.011	0.023		N = 17		
>3 N = 30	$Q_0 \times 10^{-2}$	1.394	0.194	0.398	1.225	$K_F$	1.198	1.123, 1.278
	$b \times 10^4$	3.230	1.139	2.337		n	0.587	0.560, 0.614
	n	0.589	0.011	0.023		N = 18		

therefore has little effect on the overall site heterogeneity.

The reactivity of the various size fractions can be quantified using the size characterization results presented in Chapter 4 (Sections 4.5 and 4.6). The <3K fraction had a weight-averaged molecular weight of 1383 g/mol, determined by the HPSEC molecular-weight measurement technique described in Chapter 4 (Section 4.6, Table 4-2). This compares with a value of 2696 for the 3-10K fraction, and about 4,000 to 22,000 for the larger fractions. The <3K fraction had a membrane permeation factor equal to 0.90, compared to 0.82 for the 3-10K fraction; larger size fractions had lower values (Table 4-1). These measurements suggest that the impacts of preloaded natural organic matter on TCE adsorption can be assessed by measurements of molecular weight or molecular size. To test this hypothesis, the membrane permeation factor and average molecular weight of

Huron river water were measured to determine whether the size of the river organic matter was consistent with the significant preloading effects observed by Carter et al. (1992). An average molecular weight of 1047 g/mol and a permeation factor equal to 0.90 were measured, supporting the relationship between molecular size and the impacts of preloading.

Based on the demonstrated reactivity of small molecular-size molecules in adsorption systems, additional preloading experiments were performed with the <3K fraction to evaluate further the effects of preloaded organic matter on TCE adsorption.

#### Preloading with UF Size Fractions: <3K Fraction

Four preloading experiments were conducted using the <3K fraction, including the experiment discussed in the previous section, to investigate the effects of TOC loading and equilibration time. Experimental conditions are shown in Table 8-4. In two experiments (designated 3K12 and 30-day), the <3K fraction was preloaded for the full 30-day equilibration time. It is assumed that the carbon preloaded in these experiments reached an operational equilibrium condition ( $C_{\text{final}} = C_e$ ). In one experiment, designated 0-day, the adsorbent was simultaneously contacted with TCE and humic acid, and equilibrated for a two week period. A final experiment was conducted in which the carbon was preloaded for two weeks.

To investigate the effect of TOC loading, two different types of preloading techniques were used with the <3K fraction because i) the maximum concentration attainable in the UF system was limited by the fact that it passed the smallest available membrane and could not be concentrated further; and, ii) this fraction represented a small percentage of the whole humic mixture and therefore only a limited amount could be produced. In the experiment designated 3K12, preloading was conducted as discussed in Chapter 3 (Section 3.2), using an initial concentration of 8.0 mg TOC/L and an adsorbent dose of 0.556 g/L ( $C_0/D_0 = 14.4$ ). Carbon was separated from the preloading solution and vacuum-dried before use in subsequent TCE isotherm experiments. The advantage of this method was that a large amount of adsorbent could be preloaded for further analysis and characterization. In the other experiments listed in Table 8-4, the preloading and the TCE isotherm were conducted in the same 250-ml batch reactor. First, the adsorbent (40 mg)

was equilibrated with a humic acid solution of 4.1 mg/L ( $C_0/D_0 = 102.5$ ) for one of the times indicated. After the preloading period, TCE was spiked into the reactor, and allowed to equilibrate for an additional two weeks. The advantage of this method was that high HA concentration to adsorbent dose ratios could be maintained, even when HA concentrations were low, because the adsorbent dose used in the TCE isotherm experiment was small. Speth (1991) measured preloading isotherms for dichloroethene, and found that these two different techniques for preparing preloaded carbon yielded similar results.

**Table 8-4. HA Preloading of F400 Carbon with the <3K Fraction -- Experimental Conditions**

Exp.	$C_0$ , mg TOC/L	$C_0/D_0$	$C_e$ , mg TOC/L	$q_e$ , mg/g	$C_e/D_0$	$C_e/C_0$
3K12	8.0	14.4	1.29	12.07	2.32	0.161
0 days	4.08	102.0	ND	ND	ND	ND
14 days	4.08	102.0	3.07	25.3	76.8	0.753
30 days	4.08	102.0	2.60	39.2	65.0	0.637

Note: Equilibrium was not achieved in the samples preloaded less than 30 days, therefore, the concentrations and adsorbed amounts do not represent equilibrium values.

TCE isotherms measured on carbon preloaded with the <3K fraction are shown in Figure 8-7, on both log-log (panel A) and arithmetic (panel B) coordinates. The simultaneous adsorption isotherm is not shown, because it is similar to the isotherm measured on carbon preloaded for 14 days. A significant reduction in TCE capacity as a result of HA preloading is observed. The effect of HA loading on the TCE isotherm is consistent with the theoretical expectations discussed in Chapter 7 (Section 7.4): preloaded HA causes a significant decrease in TCE capacity in the low concentration region, and an increase in the isotherm slope when plotted on log-log coordinates. Panel B of Figure 8-7 illustrates that a significant decrease in capacity occurs throughout the concentration range examined, although the relative reduction is greater at lower concentrations.

Langmuir-Freundlich and Freundlich isotherm model fits to the data are tabulated in Table 8-5. As discussed previously, the Freundlich isotherm model was only fit to the

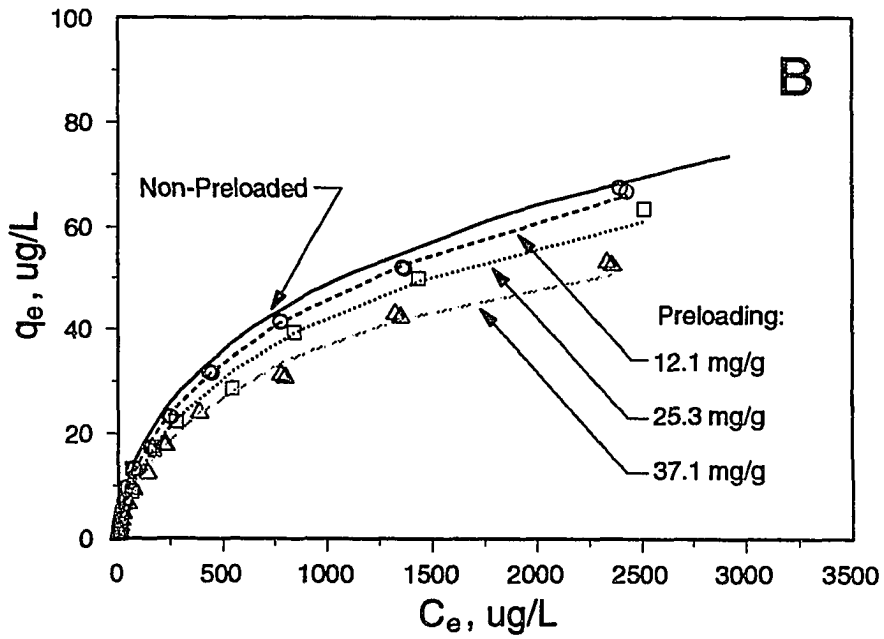
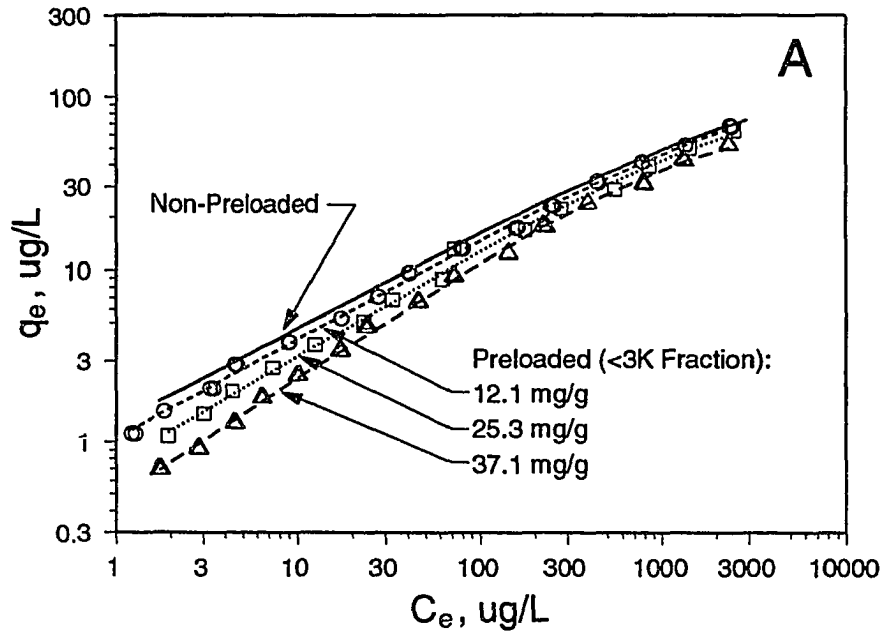


Figure 8-7. The effect of preloaded Laurentian HA (<3K fraction) on the adsorption of TCE on F400 carbon. Lines represent Langmuir-Freundlich isotherm model fits to the data. Panels A & B represent the isotherms plotted on log-log and linear coordinates, respectively.

**Table 8-5. HA Preloading of F400 Carbon with the <3K Fraction -- Isotherm Analysis**

Exp.	Langmuir-Freundlich Isotherm					Freundlich Isotherm		
	Param.	Param Est.	Std. Error	95% CI	$Q^0 b^n$	Param.	Param Est.	95% CI
F400 N = 82	$Q^0 \times 10^{-2}$	1.833	0.380	0.760	1.279	$K_F$	1.260	1.187, 1.337
	$b \times 10^4$	1.700	0.891	1.782		n	0.566	0.545, 0.586
	n	0.572	0.014	0.028		N = 48		
3K12 12 mg/g N = 29	$Q^0 \times 10^{-2}$	1.757	0.172	0.354	1.056	$K_F$	1.042	0.982, 1.107
	$b \times 10^4$	1.746	0.402	0.827		n	0.588	0.566, 0.611
	n	0.591	0.007	0.014		N = 17		
0 day $q_e = ND$ N = 30	$Q^0 \times 10^{-2}$	1.426	0.131	0.269	0.753	$K_F$	0.746	0.706, 0.788
	$b \times 10^4$	3.295	0.683	1.402		n	0.647	0.627, 0.667
	n	0.654	0.008	0.016		N = 18		
14 day 25 mg/g N = 15	$Q^0 \times 10^{-2}$	1.367	0.398	0.867	0.754	$K_F$	0.731	0.623, 0.858
	$b \times 10^4$	2.847	1.760	3.833		n	0.641	0.584, 0.698
	n	0.637	0.021	0.046		N = 9		
30 day 39 mg/g N = 30	$Q^0 \times 10^{-2}$	0.881	0.095	0.195	0.470	$K_F$	0.461	0.436, 0.488
	$b \times 10^4$	6.484	1.513	3.105		n	0.710	0.689, 0.731
	n	0.713	0.011	0.023		N = 18		

low-concentration data (<100  $\mu\text{g/L}$ ). In contrast to the TCE isotherms on TCB-preloaded carbon, the isotherms exhibited significant curvature on log-log coordinates, and were therefore modeled with the Langmuir-Freundlich isotherm. The Langmuir-Freundlich maximum capacity parameter,  $Q^0$ , decreases with increasing TOC loading, and the 30-day preloaded sample shows a statistically significant decrease. All isotherms exhibit an increase in the heterogeneity parameter, n, for both the Freundlich and Langmuir Freundlich isotherms, and the increase is statistically significant for all but the lowest level of preloading. The average site-energy parameter appears to increase somewhat at high levels of preloading, but the increase is not statistically significant, and no strong trend is evident. There is good agreement between the Freundlich unit-capacity parameter computed from Langmuir-Freundlich parameters, and that estimated by fitting the Freundlich isotherm to the low-concentration data. The Freundlich  $K_F$ -value shows a



statistically significant decrease for all preloading conditions. A plot of Freundlich isotherm parameters  $K_F$  and  $n$  as a function of HA preloading is shown in Figure 8-8. These results are consistent with the theoretical analysis discussed in Chapter 7, and with the experimental results reported by Carter et al. (1992) for TCE adsorption on carbon preloaded with Huron river water and synthetic polymaleic acid.

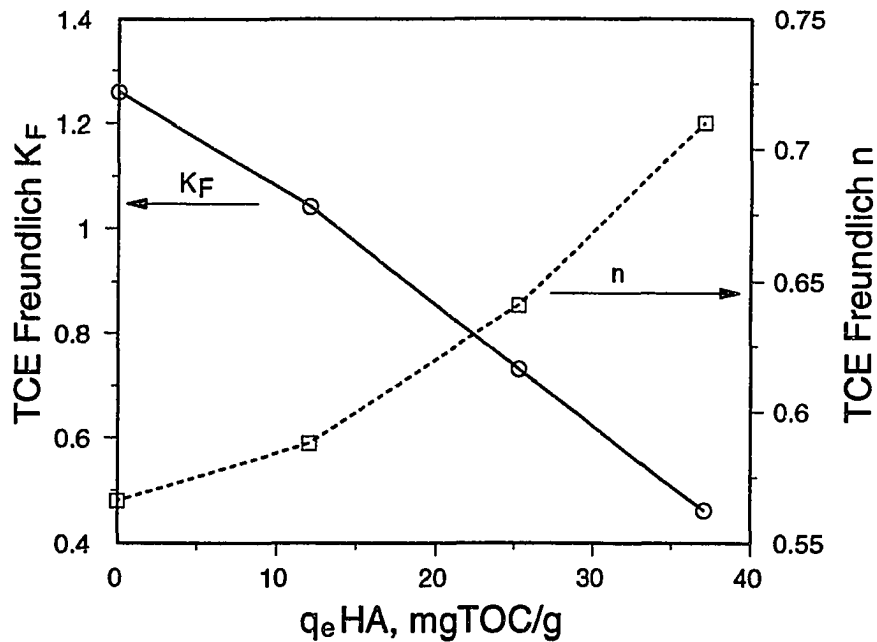


Figure 8-8. The effect of preloaded Laurentian HA (<3K fraction) on Freundlich isotherm parameters for TCE. The Freundlich model was fit to low concentration data (<100  $\mu\text{g/l}$ ).

To evaluate how changes in isotherm parameters reflect changes in the energetic character of the adsorbent surface, site-energy distributions were computed using the methods developed in Chapter 2 (Section 2.5) and applied in Chapter 7 (Section 7.4). These distributions are shown in Figure 8-9, and are plotted on both arithmetic and logarithmic coordinates to illustrate all features of the distributions. The distributions are similar to those presented in Chapter 7 (Section 7.5) for TCE adsorption on TCB-preloaded carbon. It is clear, however, that the impact of natural humic materials on TCE adsorption is less significant for similar TOC loadings. This can be explained by recognizing that the

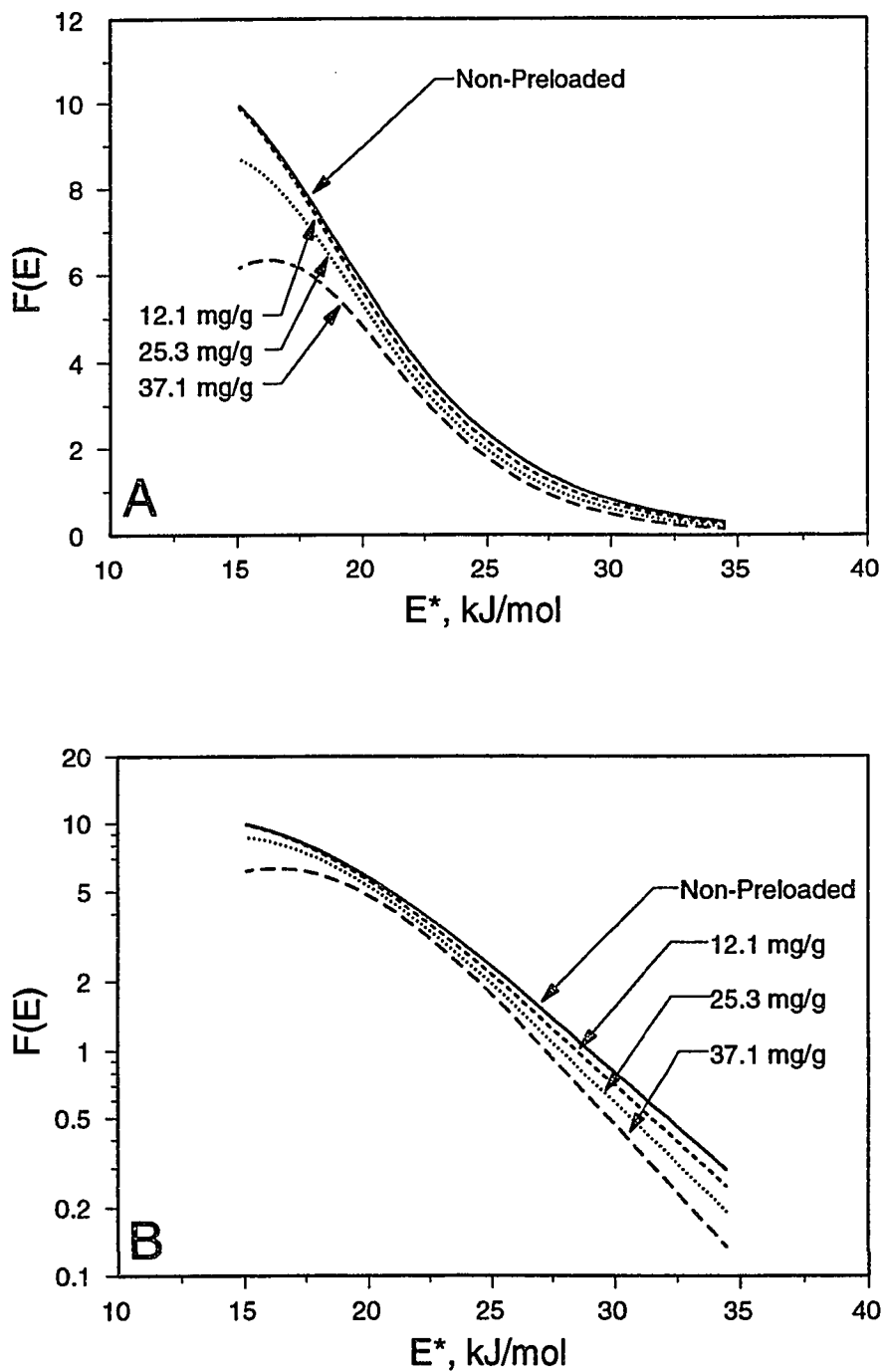


Figure 8-9. Site energy distributions calculated using the condensation approximation showing the effect of preloaded Laurentian HA (<3K fraction) on the adsorption of TCE on F400 carbon. Panels A & B represent the same distributions plotted on different coordinates.

smaller TCB molecule can access a much greater fraction of the adsorbent surface area. Nevertheless, preferential depletion of high-energy sites resulting from HA preloading is observed. In general, TCE isotherms on HA preloaded carbon exhibit a greater degree of curvature at higher concentrations than isotherms on TCB preloaded carbon. This characteristic is reflected in a slightly concave downward site-energy distribution in the low-energy region, in contrast to the distributions for TCB preloaded carbon.

Neither the isotherms nor the site-energy distributions for the isotherms on HA preloaded exhibit the same degree of parallel displacement as the isotherms measured on TCB preloaded carbon. As a result, the  $n$ -values plotted in Figure 8-8 do not exhibit a plateau region. Similar observations can be made for several of the systems studied by Carter et al. (1992). It is possible that the TOC loading range for the HA is too low to exhibit these effects, and that a leveling of both the  $K_F$  and  $n$ -value would be observed at higher TOC loadings. It is also possible that due to its larger molecular size, the HA is restricted to larger pore regions, and therefore competes with TCE differently. Despite these differences, however, these results confirm that the effects of preloading by humic substances conforms to the trends predicted by theoretical analyses.

Data from the experiment in which preloading was investigated as a function of time, reported in Table 8-4, was compared with the findings of Carter et al. (1992). In their study, as in many studies, preloading effects were studied as a function of preloading time. This information was used to develop empirical relationships to describe how adsorption model parameters varied with time, which were then incorporated into a dynamic model. The effects of preloading relate fundamentally to the mass (or molar) loading of the preloaded compound, as demonstrated by the theoretical and experimental results presented in Chapter 7. The effects of mass (TOC) loading and contact time are reconciled by recognizing that the rate of macromolecule adsorption can be slow. As demonstrated in Chapter 5 (Sections 5.3 and 5.4), months may be required for macromolecules to attain true equilibrium, particularly for particle sizes used in full-scale adsorbers. Therefore, the TOC loading of macromolecules, and the subsequent impacts due to preloading, may vary over extended periods of time.

The data for the <3K HA fraction illustrate the relationship between preloading time, TOC loading, and the impact on subsequent TCE adsorption. The 14-day and 30-

day experiments each have the same initial TOC concentration and adsorbent dose (Table 8-4), but exhibit significantly different TCE isotherms (Table 8-5). The additional two weeks of preloading allowed a closer approach to equilibrium, and resulted in a greater HA mass adsorbed. Thus, the impact of preloading on TCE adsorption can be expressed alternatively in terms of TOC loading or time. Knowledge of the macromolecule adsorption rate can be used to convert from one basis to another. In practice, the polydispersity of humic substances and the different adsorptive properties of different fractions make this difficult.

It is interesting to note that the effect of 0-day and 14-day preloading is quite similar. It is difficult to interpret this result because the TOC loading of the 0-day sample could not be determined accurately. It is documented that the presence of HA can reduce the extent of adsorption of a simultaneously adsorbing low-molecular-weight synthetic organic contaminant (Carter et al. 1992). It is possible that the <3K fraction contains relatively low-molecular-weight components which exhibit rapid adsorption kinetics and which can compete effectively with TCE without having been preloaded.

#### **8.4 TCE Adsorption by Carbon Preloaded with Macromolecule Mixtures**

##### Preloading by Adsorptive Fractionation

Adsorptive fractionation occurs because low-molecular-weight components are adsorbed preferentially from a mixture, as demonstrated in Chapter 6 (Section 6.3). The results of ultrafiltration fraction preloading showed that smaller molecular-size components cause greater reductions in TCE adsorption. Based on these results, we hypothesized that greater reductions in TCE adsorption capacity would be observed when the adsorbed molecular-weight distribution was shifted to smaller molecular weights. This hypothesis was tested by equilibrating carbon samples to achieve a range of  $C_e/D_0$  ratios, thereby creating different adsorbed molecular-size distributions. Large values of  $C_e/D_0$  ratios shift the adsorbed molecular-size distribution to smaller sizes, while small values of this ratio shift the adsorbed distribution toward that of the original solution. A significant advantage of preloading by adsorptive fractionation is that preloaded molecules are adsorbed from a mixture. Competitive effects among mixture components, if any, will therefore be

reflected. Preloading by adsorptive fractionation has one significant limitation, however. Shifts in the adsorbed molecular-weight distribution are accompanied by changes in the TOC loading; therefore, it is difficult to investigate these two effects independently.

To fractionate solutions by adsorption, different amounts of F400 activated carbon were equilibrated with Laurentian humic and fulvic acids in large 1L reactors, as described in Chapter 3 (Section 3.2). Five adsorbent doses, 0.26, 0.53, 1.05, 2.04, and 4.17 g/L and three nominal initial TOC concentrations of 15, 30 and 60 mg/L were used for the humic acid, while only the three smaller doses were used for the fulvic acid. The design of preloading conditions was based on the humic adsorption isotherms shown in Figure 6-4. A summary of preloading conditions for both the humic and fulvic acids is tabulated in Appendix B.

TCE isotherms were measured on preloaded carbon and the data were fit with the Langmuir-Freundlich and Freundlich isotherms. Representative isotherms were chosen to illustrate the observed trends. Isotherms measured on carbon preloaded with similar amounts of humic material as the <3K fraction preloading experiments were selected to provide a basis for comparing the two sets of experiments. Isotherm data and Langmuir-Freundlich model fits are shown in Figure 8-10, and best-fit model parameters for the representative data are tabulated in Table 8-6. Isotherm model parameters for all adsorptive fractionation preloading experiments are tabulated in Appendix C.

The isotherms measured on carbon preloaded by adsorptive fractionation exhibit trends similar to those observed on carbon preloaded with the <3K fraction, and are consistent with the theoretical analyses presented in Chapter 7. The greatest relative reduction in TCE capacity occurs in the low concentration region, with a concomitant increase in the isotherm slope when plotted on log-log coordinates. A significant decrease in capacity occurs throughout the concentration range examined, as observed with the <3K fraction. The isotherms exhibit significant curvature on log-log coordinates, and are well-described by the Langmuir-Freundlich isotherm. The Langmuir-Freundlich maximum capacity parameter,  $Q^0$ , decreases with increasing TOC loading, and at a loading of 45.3 mg TOC/g, the decrease is statistically significant. All isotherms exhibit an increase in the heterogeneity parameter,  $n$ , for both the Freundlich and Langmuir Freundlich isotherm models, and the increase is statistically significant for all but the lowest (11.8 mg TOC/g)

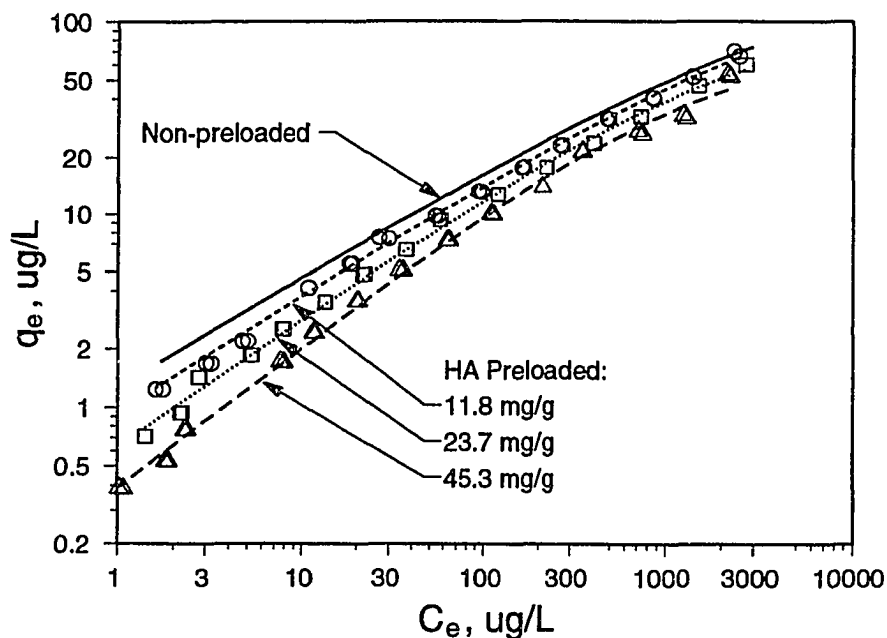


Figure 8-10. The adsorption of TCE on F400 preloaded with Laurentian HA by adsorptive fractionation. Lines represent Langmuir-Freundlich isotherm model fits to the data.

**Table 8-6. HA Preloading of F400 Carbon by Adsorptive Fractionation: Isotherm Analysis**

Loading	Langmuir-Freundlich Isotherm					Freundlich Isotherm		
	Param.	Param. Est.	Std. Error	95% CI	$Q_0 b^n$	Param.	Param. Est.	95% CI
0.0 mg/g N = 82	$Q_0 \times 10^{-2}$	1.833	0.380	0.760	1.279	$K_F$	1.260	1.187, 1.337
	$b \times 10^4$	1.700	0.891	1.782		$n$	0.566	0.545, 0.586
	$n$	0.572	0.014	0.028		N = 48		
11.8 mg/g N = 29	$Q_0 \times 10^{-2}$	1.701	0.473	0.971	0.954	$K_F$	0.947	0.823, 1.089
	$b \times 10^4$	1.823	1.188	2.438		$n$	0.597	0.547, 0.647
	$n$	0.602	0.019	0.039		N = 17		
23.7 mg/g N = 30	$Q_0 \times 10^{-2}$	1.095	0.078	0.160	0.630	$K_F$	0.604	0.558, 0.653
	$b \times 10^4$	4.086	0.706	1.446		$n$	0.674	0.642, 0.705
	$n$	0.661	0.009	0.018		N = 18		
45.3 mg/g N = 28	$Q_0 \times 10^{-2}$	0.785	0.059	0.121	0.387	$K_F$	0.376	0.352, 0.402
	$b \times 10^4$	6.680	1.127	2.317		$n$	0.731	0.705, 0.758
	$n$	0.726	0.012	0.025		N = 16		

TOC loading. The Freundlich unit capacity parameter exhibits a statistically significant decreases for all TOC loadings.

The effects of preloading over a wide range of initial concentrations and adsorbent doses were expressed in terms of the relative Freundlich capacity parameter,  $K_F/K_{F0}$ , defined as the ratio of the  $K_F$  parameter obtained on preloaded carbon to that obtained on virgin carbon. This parameter can be interpreted as the fraction of the original adsorbent capacity remaining after preloading. If greater reductions in TCE adsorption occur when the adsorbed molecular-size distribution is shifted to smaller molecules, the relative Freundlich capacity parameter should decrease with increasing values of  $C_e/D_0$ , the dose-normalized equilibrium concentration of the preloaded humic acid. This hypothesis is supported by the data depicted in Figures 8-11 and 8-12, which show relative Freundlich capacity parameters for TCE on carbon preloaded with humic and fulvic acids, respectively.

These results are consistent with the results of the ultrafiltration fraction preloading experiments, and demonstrate that macromolecule size (or size distribution) is an important factor in determining both the extent of humic substance adsorption and the subsequent impact on low molecular-weight synthetic organic contaminants.

The shift in the adsorbed molecular-size distribution to larger values at low  $C_e/D_0$  ratios means that a large fraction of the initial solution has been adsorbed, including nearly all of the low molecular-weight fraction. The low molecular-weight fraction is therefore present on the adsorbent surface at nearly all values of  $C_e/D_0$ , yet significant decreases in TCE capacity are only observed at high values of this parameter.

Two different hypotheses can explain this behavior. It is possible that at the low  $C_e/D_0$  ratios necessary to adsorb a significant fraction of the high molecular-weight components, the surface loading or adsorption density is simply too low to exert a significant effect on subsequently adsorbed TCE. A second explanation is that the presence of larger molecular-weight components reduces the ability of low molecular-weight fractions to compete with TCE. TCE isotherms on carbon preloaded with the <3K fraction were compared to isotherms on carbon preloaded in adsorptive fractionation experiments to test this hypothesis. Under this hypothesis, the extent of TCE adsorption on carbon preloaded with the <3K fraction should be less than that on carbon preloaded with

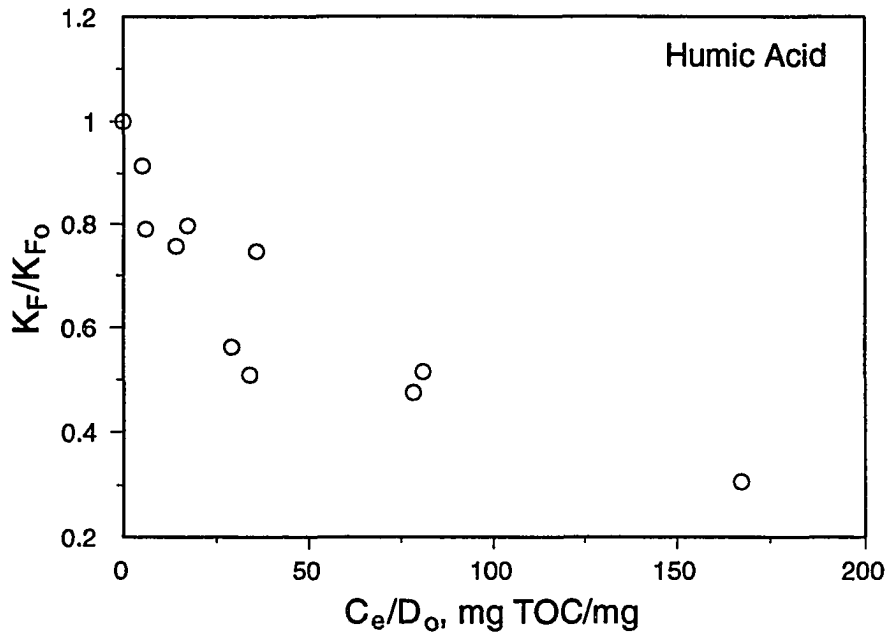


Figure 8-11. The effect of HA preloading by adsorptive fractionation on the fraction of F400 virgin carbon capacity remaining ( $K_F/K_{F_0}$ ) for the subsequent adsorption of TCE.

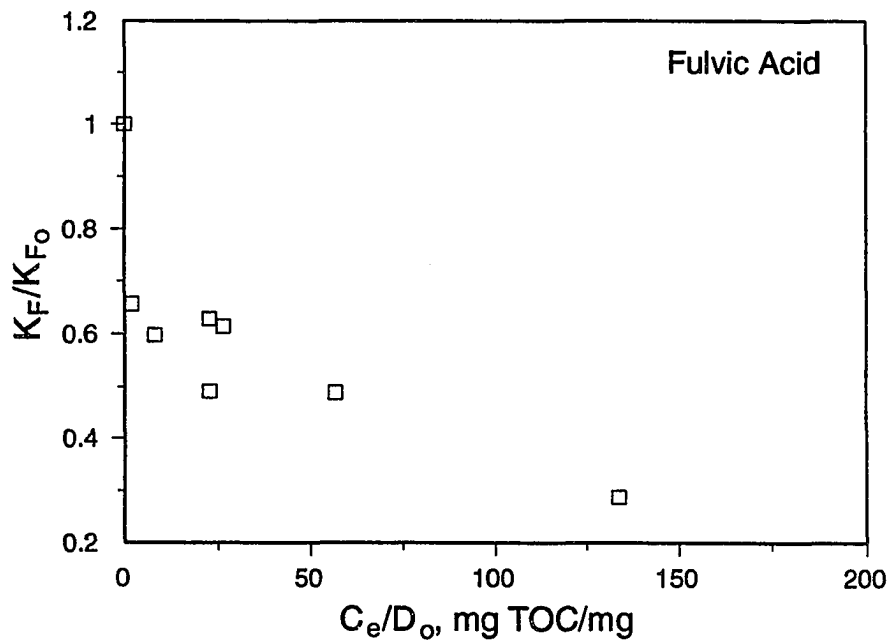


Figure 8-12. The effect of FA preloading by adsorptive fractionation on the fraction of F400 virgin carbon capacity remaining ( $K_F/K_{F_0}$ ) for the subsequent adsorption of TCE.



similar amounts of humic acid by adsorptive fractionation. Isotherm model parameters for these two sets of experiments were presented in Tables 8-5 and 8-6, and a comparison of the isotherm model fits is shown in Figure 8-13. The hypothesis is not supported by the data. The isotherms are similar for similar amounts of preloaded HA. Further, the Langmuir-Freundlich isotherm parameters show no statistically significant difference between the two different preloading experiments for similar HA loadings. Indeed, the carbon preloaded by adsorptive fractionation exhibits a slightly greater reduction in TCE capacity than that preloaded with the <3K fraction, as reflected in the consistently lower values of the Langmuir-Freundlich maximum capacity parameter,  $Q^0$ , and higher values of the heterogeneity parameter,  $n$ . The similarity of the TCE isotherms is reflected in the site-energy distributions, shown in Figure 8-14. As suggested by the lower Langmuir-Freundlich  $Q^0$  values, the distributions determined from isotherms on carbon preloaded by adsorptive fractionation show a slight displacement to lower  $F(E)$  values. The distributions are otherwise similar, however.

These results suggest that the smaller molecular-size components represent the most reactive components of the whole mixture. Further, the presence of larger molecules in the adsorbent pore space does not appear to impact the adsorption capacity of TCE greatly. The smaller effects of preloading (relatively high values of  $K_F/K_{F0}$ ) which occur when the adsorbed molecular-size distribution is shifted to larger sizes (low values of  $C_e/D_0$ ) appear to be related to the smaller amount of humic material adsorbed. This conclusion is further supported by the dependence of the relative Freundlich capacity parameter,  $K_F/K_{F0}$ , and the amount of humic acid adsorbed, shown in Figure 8-15. All the data are well-correlated, and the data from the <3K fraction fall within the general trend observed for the data from both the humic and fulvic acids preloaded by adsorptive fractionation. The greatest reductions in TCE capacity occur when the molecular-size distribution of preloaded humic substances is shifted to smaller sizes, which is caused by high  $C_e/D_0$  ratios, and which results in increased amounts of smaller molecular-size components adsorbed.

While not statistically significant, the effects of preloading by adsorptive fractionation appear to be somewhat greater than the effects generated by preloading the <3K fraction. The presence of wider adsorbed molecular-size distribution appears to

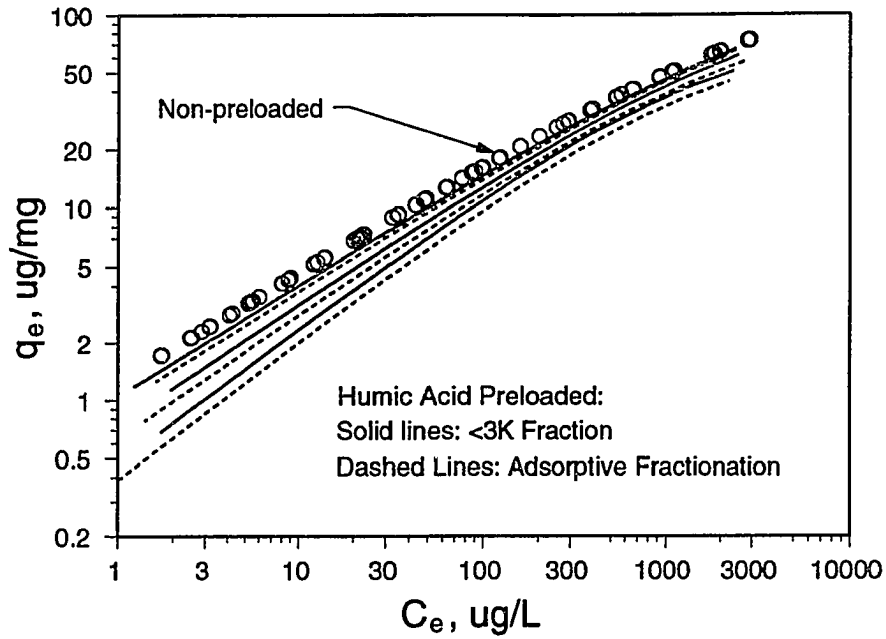


Figure 8-13. Langmuir-Freundlich model fits for TCE adsorption by preloaded carbon comparing the effects of carbon preloaded with the <3K fraction and with the whole solution by adsorptive fractionation.

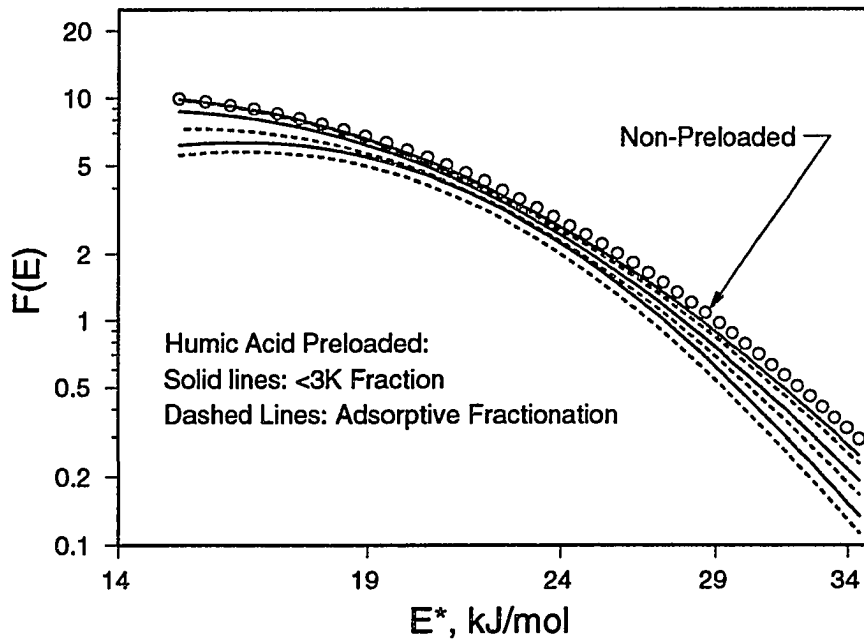


Figure 8-14. Site energy distributions computed from TCE isotherms on preloaded carbon using the condensation approximation. The effects of carbon preloaded with the <3K fraction and with the whole solution by adsorptive fractionation are compared.

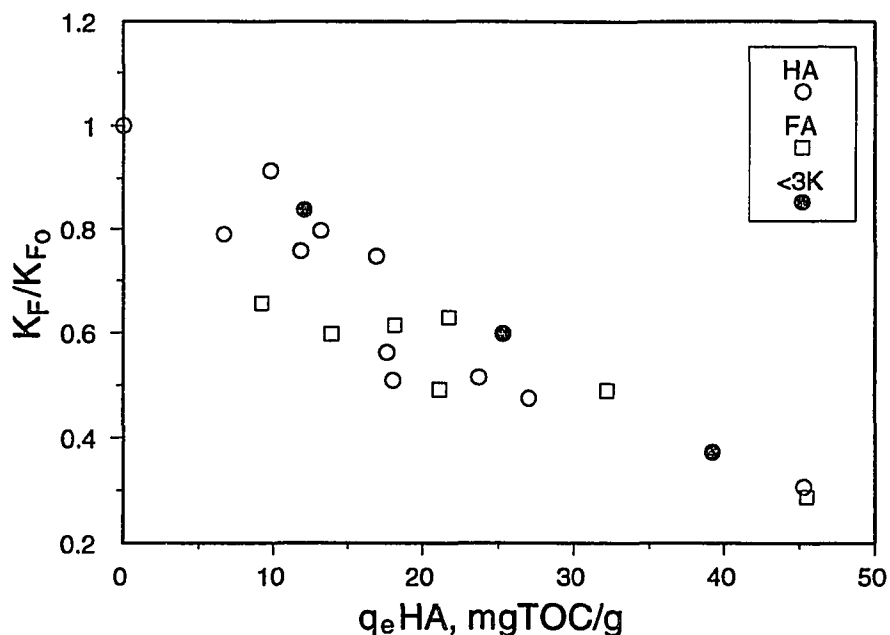


Figure 8-15. The effect of humic substance preloading on the fraction of F400 virgin carbon capacity remaining ( $K_F/K_{F0}$ ) for the subsequent adsorption of TCE.

augment the preloading effects. The effect of preloading on TCE adsorption was the same at a TOC loading of approximately 12 mg/g regardless of whether the carbon was preloaded with the <3K fraction or by adsorptive fractionation. At this level of preloading, about 44% of the initial TOC was removed from solution. Assuming that the <3K fraction comprises no more than about 20% of the whole humic acid, about half of the preadsorbed components were larger than the <3K fraction. It is possible that a fairly low molecular-weight component is retained on the 3K membrane, and is therefore absent from the <3K fraction. The wider molecular-size distribution in the adsorptive fractionation experiments may result in a greater packing density of adsorbed molecules, enhancing their ability to block adsorbent pores.

#### TCE Adsorption by Carbon Preloaded with Mixtures of UF Fractions

Potential interactions between different size components of a humic acid mixture were investigated by preloading F400 carbon with different combinations of UF size fractions. Carbon was preloaded with the <3K and 10-30K fractions in various

proportions to determine if larger molecular-size components could interact with smaller, more reactive components. Experimental conditions are tabulated in Table 8-7. In this experiment, the mass of the <3K fraction per unit mass of adsorbent was held approximately constant, and the initial concentration of the preloading solution was increased by increasing the concentration of the 10-30K fraction. Increases in the amount adsorbed resulting from higher  $C_e/D_0$  ratios could only be due to the 10-30K fraction, and the adsorbed molecular-size distribution increased as the  $C_e/D_0$  ratio *increased*. While the percentage of the <3K fraction in the initial mixture was reduced, the initial concentration of the <3K fraction was constant. Therefore, if no interactions occurred between the different size fractions, and the smaller molecules are adsorbed preferentially, the amount of the <3K fraction adsorbed should remain constant even as the adsorbed molecular-size distribution was shifted to larger sizes. This situation stands in contrast to the adsorptive fractionation experiments, in which i) the initial size distribution remained constant; ii) the mass of the <3K fraction initially present and subsequently adsorbed per unit mass of adsorbent decreased as the  $C_e/D_0$  ratio decreased and the adsorbed molecular-size distribution shifted to larger sizes.

**Table 8-7. Effect of Initial Molecular Size Distribution: Experimental Conditions**

Exp.	Initial 10-30K Mass Fraction	$C_0$ , mg TOC/L	$C_e$ , mg TOC/L	$q_e$ , mg/g	$C_e/D_0$ , mg/g	$1-C_e/C_0$ , percent
3K12	0.000	8.0	1.3	12.1	2.3	83.8
MWD1	0.539	16.2	8.3	16.3	17.3	48.8
MWD2	0.735	25.2	16.7	19.3	38.4	33.7
10-30K	1.000	35.4	26.8	16.4	51.4	24.3

Based on the results previously presented, it was hypothesized that the effect of adsorbed humic acid on subsequent TCE adsorption results from the adsorption of smaller size components. Further, because smaller components adsorb preferentially, increases in the adsorption of the larger-size fraction should not influence the TCE isotherm measured on the preloaded carbon in this experiment. The effects of preloading should be

independent of the initial molecular-size distribution or the initial mass fraction of the 10-30K fraction, as long as the quantity of the <3K fraction per mass of adsorbent is constant. This hypothesis was supported by the TCE isotherm data, reflected in the Langmuir-Freundlich and Freundlich isotherm model parameters tabulated in Table 8-8, and depicted graphically in Figure 8-16. TCE isotherms on carbon preloaded with the <3K fraction and mixtures containing the <3K fraction exhibit reductions in the Langmuir-Freundlich maximum capacity parameter and increases in the heterogeneity parameter relative to non-preloaded carbon; however, the differences are not statistically significant. Statistically significant reductions in the Freundlich  $K_F$ -value were observed, however. Further, there are no statistically significant differences between the effects of preloading on TCE adsorption for initial solutions comprised of up to 74% of the 10-30K fraction by mass. When no <3K fraction is present, however, no significant reduction in the Freundlich  $K_F$  value was observed. These results further illustrate that the smaller molecular-size fraction is preferentially adsorbed, and the effects of preloading are due primarily to this fraction. Larger molecular-size components present in the 10-30K fraction do not significantly displace or otherwise interact with the smaller components. Therefore, there is no effect of the initial size distribution as long as the amount of the <3K fraction available per adsorbent mass is held constant.

A sequential adsorption experiment was conducted to further investigate potential displacement or other interaction mechanisms. In this experiment, the <3K and 10-30K fractions were loaded in two sequential stages ("primary" and "secondary") to determine whether the order of adding different size fractions influenced the effect of preadsorbed humic acid on subsequent TCE adsorption. In one experiment, the carbon was first equilibrated with the <3K fraction, after which time the supernatant was decanted, and the carbon was subsequently equilibrated with the 10-30K fraction. In the second experiment, the order of equilibration was reversed. Experimental conditions for the sequential loading experiment are shown in Table 8-9, and Langmuir-Freundlich and Freundlich isotherm model fits to the data are tabulated in Table 8-10.

The carbon first preloaded with the <3K fraction exhibited a lower Langmuir-Freundlich maximum capacity parameter,  $Q^0$ , and a higher  $n$ -value relative to non-

**Table 8-8. Effect of Initial Molecular Size Distribution: Isotherm Analysis**

Exp.	Langmuir-Freundlich Model					Freundlich Model		
	Param.	Param. Est.	Std. Error	95% CI	$Q_{ob}^n$	Param.	Param. Est.	95% CI
MWD1 N = 30	$Q^o \times 10^{-2}$	1.455	0.187	0.384	1.129	$K_F$	1.097	1.050, 1.147
	$b \times 10^4$	2.724	0.847	1.738		n	0.596	0.578, 0.613
	n	0.592	0.009	0.018		N = 18		
MWD2 N = 30	$Q^o \times 10^{-2}$	1.377	0.651	1.336	1.110	$K_F$	1.085	1.029, 1.144
	$b \times 10^4$	3.030	3.906	8.015		n	0.595	0.574, 0.616
	n	0.595	0.043	0.088		N = 18		

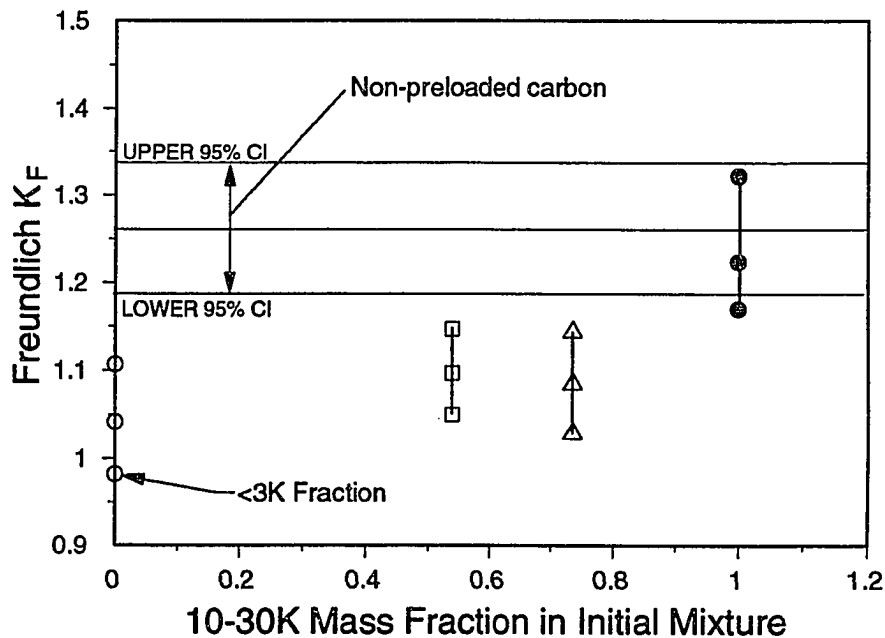


Figure 8-16. Freundlich  $K_F$ -values for TCE adsorption on carbon preloaded with mixtures of <3K and 10-30K UF size fractions. Solid horizontal lines represent best-fit  $K_F$  values and 95% confidence limits for TCE adsorption on non-preloaded carbon. Symbols with vertical lines represent best-fit  $K_F$  values and 95% confidence limits for TCE adsorption on carbon preloaded with UF fractions. kfmwd.drw

**Table 8-9. Sequential Loading Experiment: Experimental Conditions**

Fraction	Primary Loading			Secondary Loading			Final		
	C <sub>0</sub> , mg TOC/L	C <sub>e</sub> , mg TOC/L	q <sub>e</sub> , mg/g	Fraction	C <sub>0</sub> , mg TOC/L	C <sub>e</sub> , mg TOC/L	q <sub>e</sub> , mg/g	D <sub>0</sub> , g/L	q <sub>e</sub> , mg/g
<3K	8.0	3.4	7.8	10-30K	19.7	15.2	8.1	0.556	15.9
10-30K	35.4	28.3	13.1	<3K	8.9	3.3	10.3	0.543	23.4

**Table 8-10. Sequential Loading Experiment: Isotherm Analysis**

Exp.	Langmuir-Freundlich Isotherm					Freundlich Isotherm		
	Param.	Param. Est.	Std. Error	95% CI	Q <sup>0</sup> <sub>b</sub> n	Param.	Param. Est.	95% CI
SEQ1	Q <sup>0</sup> x10 <sup>-2</sup>	1.137	0.124	0.254	1.006	K <sub>F</sub>	0.983	0.923, 1.046
N = 30	b x10 <sup>4</sup>	4.758	1.320	2.709		n	0.613	0.589, 0.638
	n	0.618	0.011	0.023		N = 18		
SEQ2	Q <sup>0</sup> x10 <sup>-2</sup>	1.537	0.125	0.257	1.162	K <sub>F</sub>	1.144	1.096, 1.195
N = 30	b x10 <sup>4</sup>	2.431	0.495	1.016		n	0.583	0.565, 0.601
	n	0.587	0.007	0.014		N = 18		

preloaded carbon; however, the differences were not significant. As in the case of the previous experiment, the Freundlich K<sub>F</sub> values did show statistically significant differences. When the <3K fraction was loaded before the 10-30K fraction, a significant reduction in the K<sub>F</sub> value for TCE was observed, while no significant effect was observed when the order was reversed, even at a fairly high composite loading of 23.4 mg TOC/g. Adsorption of the larger fraction effectively prevented subsequent adsorption of the <3K fraction from competing with TCE. This implies that the <3K fraction was restricted from the smaller pores and probably occupied larger meso- and macropores.

Neither fraction appeared to significantly displace the other. Consistent with the findings of Summers and Roberts (1988), the lower molecular-weight <3K fraction may have a lower intrinsic affinity for the surface than the 10-30K fraction, and therefore could not displace this component. Although the 10-30K fraction may have a higher intrinsic

affinity for the surface, it probably could not access surfaces on which the <3K fraction was adsorbed, thereby making displacement impossible. The lack of displacement may also relate to steric hindrances of both the potential displacer and the adsorbed species.

These findings have significant implications for the operation of fixed-bed adsorbers. Modifying the adsorbent surface by preloading the carbon with a large molecular-size component prior to placing the bed in service may be a way to reduce the impacts of preloading. This process may occur naturally in some systems. If the natural organic matter is fractionated by size along the GAC bed, smaller, more adsorbable components would be removed earlier in the bed. Larger components would penetrate deeper into the bed, loading the carbon ahead of the smaller components. This process would effectively limit the impacts of preloading from the smaller size components. Organic matter with a polydisperse size distribution would be required for size fractionation to occur along a GAC bed, however. Many natural waters may not meet this criterion; organic matter from the Huron river is an example.

## **8.5 Effects of Solution Chemistry on TCE Adsorption by Preloaded Carbon**

### Effects of Ionic Strength on TCE Adsorption by Preloaded Carbon

Several adsorptive fractionation experiments were conducted to investigate the impact of ionic strength on reductions in TCE adsorption by preloaded carbon. The experiments were conducted at 0.05-M and 0.10-M ionic strength adjusted with NaCl; other conditions for these experiments are shown in Table 8-11. It was shown in Chapter 6 (Section 6.3) that increasing ionic strength increases the extent of humic acid adsorption by reducing the initial size distribution. A smaller adsorbent dose was therefore required to effect a given fractional removal of TOC, resulting in an increased amount adsorbed,  $q_e$ . It was also shown that the average molecular weight remaining in solution correlated with the fraction of the initial TOC removed, consequently, the amount adsorbed under high ionic strength conditions was greater for a given molecular weight remaining in solution. Based on these considerations and the results of previous experiments, which showed that the



**Table 8-11. Effect of Ionic Strength on HA Preloading: Experimental Conditions**

Exp	I.S., M	C <sub>0</sub> , mg TOC/L	C <sub>e</sub> , mg TOC/L	q <sub>e</sub> , mg/g	C <sub>e</sub> /D <sub>0</sub> , mg/g	1-C <sub>e</sub> /C <sub>0</sub> , percent
U515	0.05	15.2	1.86	12.67	1.8	87.76
U530	0.05	30.6	9.05	20.47	8.6	70.42
U560	0.05	60.9	34.19	25.37	32.6	43.86
U115	0.10	15.3	1.28	13.32	1.2	91.63
U130	0.10	30.7	7.63	21.92	7.3	75.15
U160	0.10	62.2	30.68	29.94	29.2	50.68

effect of preloaded humic acid was related to the amount of the smaller size fraction adsorbed, it was hypothesized that for a given percentage of TOC removal (or average molecular weight remaining in solution), greater reductions in TCE adsorption would occur with increasing ionic strength.

This hypothesis was supported by the TCE isotherm data measured on preloaded carbon. Langmuir-Freundlich and Freundlich isotherm parameters are shown in Table 8-12, and the reduction in the relative Freundlich unit capacity parameter as a function of the TOC removal percentage is shown in Figure 8-17. A single, relatively high adsorbent dose of 1.05 g/L was used in all the ionic strength experiments, resulting in TOC removal percentages that did not cover as wide a range as those in the adsorptive fractionation experiments, which used a range of adsorbent doses. Nevertheless, clearly different trends are observed for each ionic strength, ranging from 0.01 M (used in the adsorptive fractionation experiments) to 0.10 M. For a given TOC removal, higher ionic strengths result in greater amounts of humic acid adsorbed, and greater reductions in TCE adsorption. Similar results were obtained when the data were plotted as a function of  $C_e/D_0$ , as in Figure 8-11. However, the data from the ionic strength experiments did not cover as wide a range of  $C_e/D_0$  values, and the trends in the data can be seen more clearly as plotted in Figure 8-17.

In most cases, the Langmuir-Freundlich maximum capacity parameters obtained from TCE isotherms on carbon preloaded at high ionic strength were lower than those for non-preloaded carbon; however, the differences were not statistically significant. In

**Table 8-12. Effect of Ionic Strength on HA Preloading: Isotherm Analysis**

Exp.	Langmuir-Freundlich Model					Freundlich Model		
	Param.	Param. Est.	Std. Error	95% CI	$Q^o b^n$	Param.	Param. Est.	95% CI
U115 N = 30	$Q^o \times 10^{-2}$	1.701	0.504	1.032	0.870	$K_F$	0.868	0.742, 1.017
	$b \times 10^4$	1.680	1.159	2.374		n	0.596	0.541, 0.650
	n	0.607	0.021	0.043		N = 18		
U130 N = 30	$Q^o \times 10^{-2}$	1.166	0.286	0.586	0.734	$K_F$	0.616	0.523, 0.725
	$b \times 10^4$	4.844	2.843	5.822		n	0.740	0.675, 0.805
	n	0.664	0.029	0.059		N = 16		
U160 N = 30	$Q^o \times 10^{-2}$	1.100	0.149	0.305	0.568	$K_F$	0.587	0.518, 0.665
	$b \times 10^4$	5.014	1.558	3.191		n	0.663	0.619, 0.707
	n	0.693	0.017	0.035		N = 16		
U515 N = 30	$Q^o \times 10^{-2}$	1.794	0.480	0.983	1.080	$K_F$	1.102	0.981, 1.239
	$b \times 10^4$	1.829	1.190	2.437		n	0.570	0.526, 0.613
	n	0.594	0.019	0.039		N = 18		
U530 N = 30	$Q^o \times 10^{-2}$	1.999	0.539	1.214	0.888	$K_F$	0.862	0.764, 0.973
	$b \times 10^4$	1.218	0.741	1.518		n	0.604	0.562, 0.646
	n	0.601	0.016	0.033		N = 18		
U560 N = 30	$Q^o \times 10^{-2}$	1.426	0.325	0.666	0.688	$K_F$	0.650	0.548, 0.771
	$b \times 10^4$	2.663	1.380	2.826		n	0.666	0.603, 0.729
	n	0.648	0.019	0.039		N = 16		

general, the heterogeneity parameter, n, was higher, and the differences were statistically significant for the three experiments in which the carbon was loaded with 22 mg/g or more. Significant decreases in the Freundlich  $K_F$ -value were observed in all cases except the experiment which resulted in the lowest level of TOC loading (I.S. = 0.05 M,  $C_0$  = 15 mg/L). Statistically significant increases in the Freundlich n-value were also observed for the three highest level of preloading.

Several preloading data from the three different ionic strength experiments had similar TOC removal percentages, and the effects of TCE adsorption were compared on that basis. For a given TOC removal percentage, an increase in ionic strength resulted in statistically significant decreases in the Freundlich  $K_F$ -value. Increases in the Freundlich n-value were also observed, and were statistically significant in several, but not all, cases.

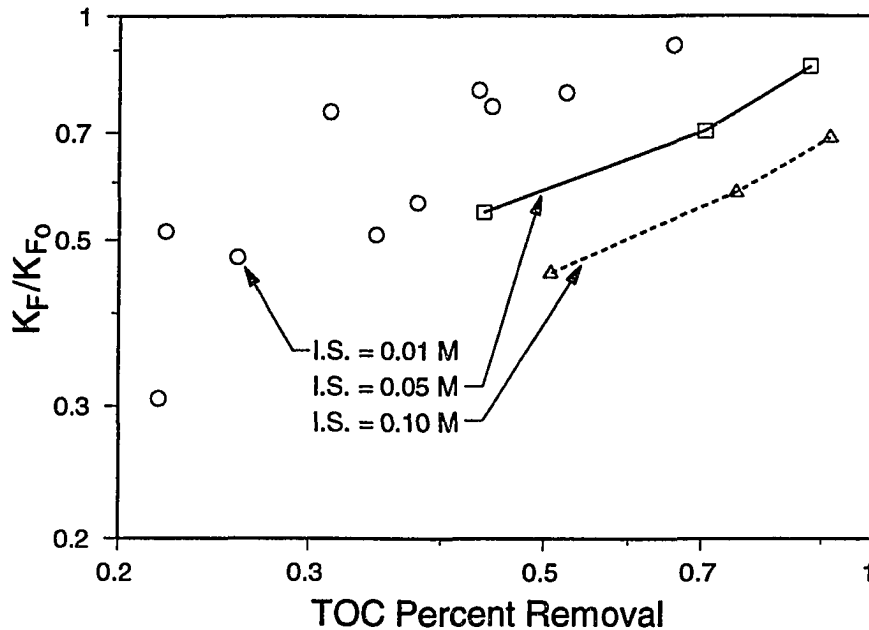


Figure 8-17. The effect of HA preloading by adsorptive fractionation on the fraction of F400 virgin carbon capacity remaining ( $K_F/K_{F_0}$ ) for the subsequent adsorption of TCE, illustrating the effect of ionic strength conditions during preloading.

If the  $K_F/K_{F_0}$  trends observed for the high ionic strength conditions are extrapolated to lower TOC percentage removals, the data for all ionic strengths appear to converge. This observation is consistent with the idea that at low TOC removals (high  $C_0/D_0$  ratios), only the smallest molecular-size components are adsorbed regardless of the ionic strength. While molecular sizes can be made smaller by increasing the ionic strength and causing larger components to adopt more compact configurations, there are limits to the potential magnitude of this effect. As the permeation factor measurements in Chapter 4 (Section 4.5) demonstrate, an asymptotic limit to conformational changes which can occur as a result of increases in ionic strength exists. Further, depending on the fundamental molecular-weight distribution, there is a limit to the amount of material which can become sufficiently small to access adsorbent pores small enough to compete with TCE.

It has been demonstrated that for a given reduction in TOC, carbon preloaded under high ionic strength conditions adsorbs a greater amount of humic acid and results in greater reductions in subsequent TCE adsorption. The relative Freundlich capacity factor for TCE was plotted in terms of the amount of humic acid adsorbed under all ionic strength

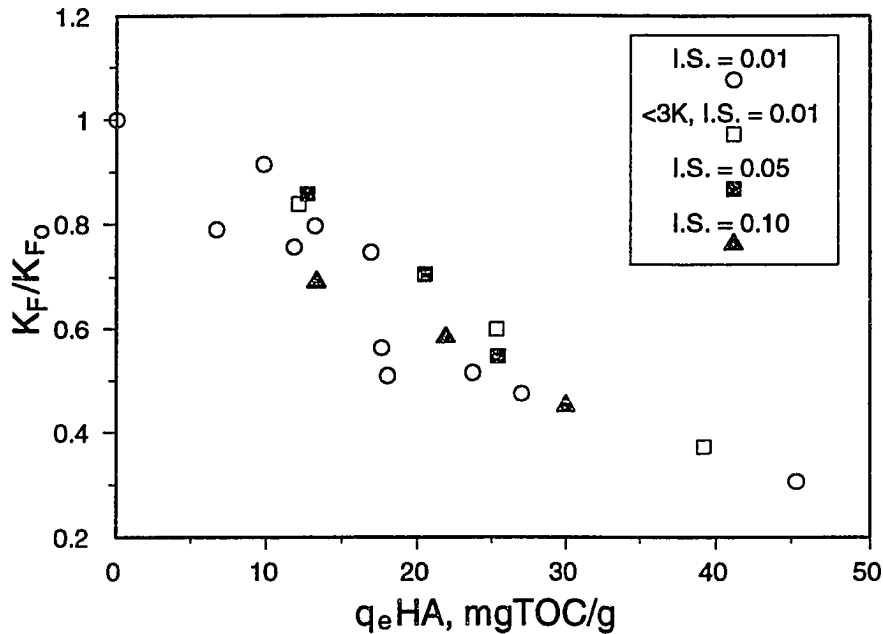


Figure 8-18. The effect of HA preloading by adsorptive fractionation on the fraction of F400 virgin carbon capacity remaining ( $K_F/K_{F0}$ ) for the subsequent adsorption of TCE, illustrating the effect of ionic strength conditions during preloading.

conditions, as shown in Figure 8-18. Consistent with the data presented in Figure 8-15, the reduction in TCE adsorption is fundamentally related to the amount of humic material adsorbed, regardless of the ionic strength conditions during preloading. When the amount of adsorbed humic acid is similar, the Freundlich  $K_F$  and  $n$  values are statistically similar for all ionic strength conditions. These results demonstrate that decreases in the initial molecular-size distribution resulting from increases in ionic strength increase the extent of humic adsorption, but do not appear to change the way in which humic acids compete with TCE.

#### Effects of Calcium on TCE Adsorption by Preloaded Carbon

Calcium is the principal cation in most natural fresh waters, both surface and groundwater, (Hem 1970) deriving from the dissolution of igneous silicates and feldspars (anorthite), sedimentary carbonates (calcite and aragonite, dolomite) and sulfates (gypsum and anhydrite), and some metamorphic rocks. Given the predominance of this constituent of natural waters, and its demonstrated ability to increase the extent of humic substance

adsorption, the effect of calcium on the preloading of humic acid and the subsequent adsorption of TCE was investigated.

In the first set of experiments, F400 carbon (1.05 g/L) was preloaded with humic acid solutions having an ionic strength of 0.01 M, an initial calcium concentration of 0.50 mM, and several different nominal initial TOC concentrations ranging from 10 to 40 mg/L. In a second set of experiments, the initial TOC concentration was held constant at a nominal value of 20 mg/L and the calcium content was varied from 0.05 to 2.0 mM. In all cases, calcium was added as the chloride salt, and ionic strength was adjusted to 0.01 M with NaCl. The experimental conditions for both sets of experiments are shown in Table 8-13.

**Table 8-13. Effect of Calcium Content on HA Preloading: Experimental Conditions**

Exp.	Calcium, mM	C <sub>0</sub> , mg TOC/L	C <sub>e</sub> , mg TOC/L	q <sub>e</sub> , mg/g	C <sub>e</sub> /D <sub>0</sub> , mg/g	1-C <sub>e</sub> /C <sub>0</sub> , percent
C5010	0.50	10.0	1.4	8.2	1.3	86.2
C5020	0.50	19.1	5.3	13.1	5.1	72.2
C5040	0.50	38.8	13.6	24.0	12.9	65.0
C520	0.05	19.3	7.6	11.1	7.2	60.6
C2520	0.25	19.0	5.4	13.0	5.1	71.8
C10020	1.0	18.9	3.7	14.4*	3.6	80.2
C20020	2.0	18.9	0.8	17.1*	0.8	95.7

Note: Values of q<sub>e</sub> indicated by an asterisk represent the sum of adsorbed and precipitated humic material.

At environmental temperatures and pressures, the solubility of calcium is often controlled by aragonite, and the theoretical solubility of calcium in a system open to the atmosphere is about 0.5 mM, which is equivalent to 20 mg/L and 50 mg/L as CaCO<sub>3</sub>. Evidence for association of the calcium with humic acid was observed and described in Chapter 6 (Section 6.3), and based on these results, an initial calcium concentration of 0.5 mM was expected to result in free calcium concentrations well below solubility. The experiments were conducted in the absence of phosphate to avoid confounding effects from the potential precipitation of hydroxyapatite.

The two experiments conducted with initial calcium concentrations greater than 0.5 mM were designed to exceed calcium solubility to investigate the impact of precipitate formation. The formation of this precipitate at calcium concentrations greater than 0.5 mM is consistent with the observations of Weber et al. (1983), but depends on the pH and the type and concentration of organic ligands present. To increase the likelihood of precipitation in the experiment conducted with a calcium concentration of 2 mM, the pH was adjusted to 8.0. After equilibration, a brown precipitate was visible in both reactors, suggesting the presence of a humic/calcium solid. The high calcium concentrations may have destabilized the larger molecular-weight humic components causing aggregation and subsequent removal from solution. It is also possible that a calcium carbonate precipitate formed, and humic molecules may have associated with the precipitate by an adsorption or enmeshment mechanism.

It was shown in Chapter 6 (Section 6.3) that increasing the calcium content increases the extent of humic acid adsorption. It is expected that these increases are due, in part, to the mechanisms responsible for increases in adsorption that occur with increasing ionic strength. However, calcium may form cation bridges between humic molecules and negatively charged functional groups on the adsorbent surface, creating new adsorption sites. Further, evidence of aggregation in the presence of calcium was observed in the size-exclusion chromatograms discussed in Chapter 6 (Section 6.3). If aggregation occurred among small molecular-size components, access to micropore surfaces would be more difficult, and the impacts of preloading may be reduced. Despite the complexity of various factors which may influence the effects of preloading in the presence of calcium, as a result of its ability to enhance the adsorption of humic substances, it was hypothesized that the effects of calcium would be similar in nature to the effects of ionic strength. Therefore, for a given percentage reduction in TOC (or average molecular weight remaining in solution) after preloading, greater reductions in TCE adsorption should occur with increasing calcium content.

Langmuir-Freundlich and Freundlich isotherm parameters are given in Table 8-14, and reductions in the relative Freundlich unit capacity parameters as a function of the percentage of TOC removal are shown in Figure 8-19. Reductions in the extent of TCE

**Table 8-14. Effect of Calcium Content on HA Preloading: Isotherm Analysis**

Exp.	Langmuir-Freundlich Model					Freundlich Model		
	Param.	Param. Est.	Std. Error	95% CI	$Q_0 b^n$	Param.	Param. Est.	95% CI
C520 N = 30	$Q_0 \times 10^{-2}$	1.559	0.369	0.756	0.766	$K_F$	0.772	0.707, 0.842
	$b \times 10^4$	2.671	1.301	2.664		n	0.631	0.598, 0.665
	n	0.646	0.013	0.027		N = 20		
C2520 N = 30	$Q_0 \times 10^{-2}$	1.447	0.207	0.424	0.815	$K_F$	0.818	0.773, 0.867
	$b \times 10^4$	3.255	1.010	2.068		n	0.628	0.606, 0.650
	n	0.645	0.010	0.020		N = 20		
C5020 N = 58	$Q_0 \times 10^{-2}$	1.093	0.141	0.285	0.806	$K_F$	0.804	0.743, 0.870
	$b \times 10^4$	7.466	2.221	4.489		n	0.667	0.631, 0.702
	n	0.682	0.015	0.030		N = 36		
C10020 N = 38	$Q_0 \times 10^{-2}$	1.347	0.214	0.437	0.695	$K_F$	0.717	0.672, 0.765
	$b \times 10^4$	3.509	1.202	2.454		n	0.630	0.607, 0.653
	n	0.662	0.012	0.025		N = 23		
C20020 N = 30	$Q_0 \times 10^{-2}$	2.018	0.790	1.618	1.148	$K_F$	1.147	1.038, 1.267
	$b \times 10^4$	1.687	1.456	2.982		n	0.585	0.543, 0.627
	n	0.595	0.018	0.037		N = 20		
C5010 N = 59	$Q_0 \times 10^{-2}$	1.832	0.410	0.829	1.004	$K_F$	1.023	0.947, 1.105
	$b \times 10^4$	2.019	0.983	1.987		n	0.587	0.556, 0.619
	n	0.612	0.012	0.024		N = 39		
C5040 N = 56	$Q_0 \times 10^{-2}$	1.119	0.256	0.517	0.630	$K_F$	0.613	0.542, 0.693
	$b \times 10^4$	5.436	2.702	5.461		n	0.690	0.644, 0.737
	n	0.689	0.022	0.044		N = 34		

adsorption were attributed to adsorption of humic acid or a humic/calcium complex because no effect of calcium alone on TCE adsorption was observed in control experiments.

As shown in Figure 8-19, carbon preloaded in the presence of calcium at 0.01-M ionic strength exhibits reductions in TCE capacity comparable to carbon preloaded at higher ionic strengths. In comparison to carbon preloaded in the absence of calcium, greater amounts of humic acid are adsorbed, and greater reductions in TCE adsorption are exhibited. Similar results were obtained when the data were plotted as a function of  $C_e/D_0$ , as was done in Figure 8-11.

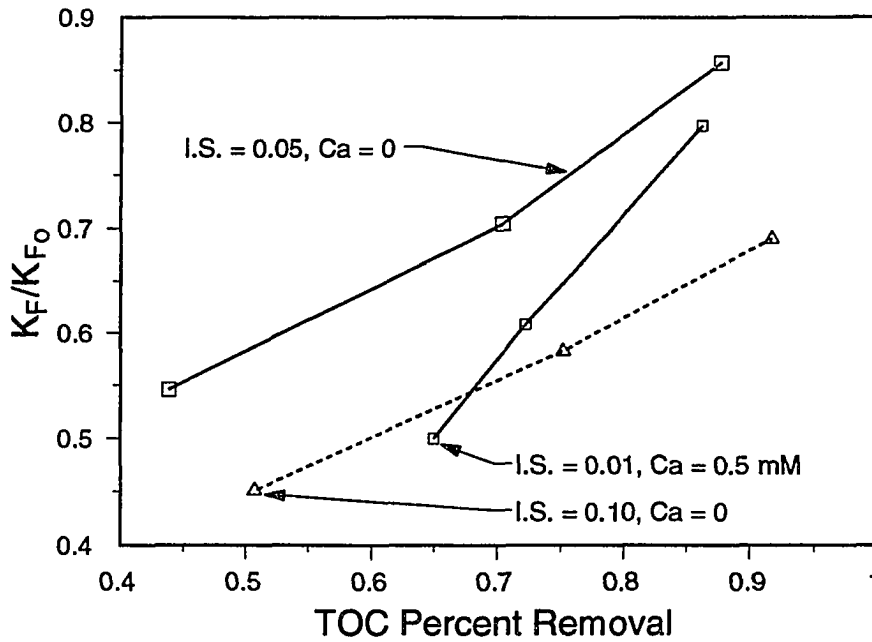


Figure 8-19. The effect of HA preloading by adsorptive fractionation on the fraction of F400 virgin carbon capacity remaining ( $K_F/K_{F_0}$ ) for the subsequent adsorption of TCE, illustrating the effect of ionic strength conditions and the presence of calcium during preloading.

In most cases, the Langmuir-Freundlich maximum capacity parameters for TCE isotherms on carbon preloaded in the presence of calcium were lower than those on non-preloaded carbon; however, the differences were not statistically significant. In general, the heterogeneity parameter,  $n$ , was also higher, and the differences were statistically significant in all but two experiments -- the experiment which had the lowest HA loading, and the experiment containing the highest amount of calcium. The implications of this latter result will be discussed in more detail below. Significant decreases in the Freundlich  $K_F$ -value were observed in all cases except the experiment containing the highest amount of calcium. Statistically significant increases in the Freundlich  $n$ -value were also observed for all but two experiments -- the one having the lowest HA loading, and the experiment with the highest calcium concentration.

The carbon preloaded in the presence of 2 mM calcium did not exhibit any statistically significant reduction in TCE adsorption capacity. A brown precipitate was observed in this reactor and the TOC concentration after equilibration was only 0.8 mg/L.



Therefore, removal of TOC from solution was apparently due to both adsorption and precipitation, and it is possible that a significant fraction of the reactive molecular sizes were removed from solution but were not adsorbed. Based on the evidence for aggregation observed in the molecular-weight distributions presented in Chapter 6 (Section 6.3), another explanation is that reactive molecules were aggregated to form larger species which did not access adsorbent surfaces. Furthermore, larger molecular aggregates could have been adsorbed, subsequently preventing the access of smaller molecular-size components.

As the data in Figure 8-19 shows, TCE isotherms on carbon preloaded in the presence of calcium at 0.01-M ionic strength exhibited lower Freundlich  $K_F$ -values and higher  $n$ -values than carbon preloaded at 0.05 M in the absence of calcium, for similar TOC percentage removals; however, the differences were not statistically significant.

It was shown previously that the extent of TCE adsorption was related fundamentally to the amount of humic acid (TOC) adsorbed. This finding was further supported by the Freundlich parameters for TCE adsorption on carbon preloaded with about 24 mg TOC/g in the presence of calcium. At this level of TOC loading, isotherm parameters for TCE adsorption on carbon preloaded both in the presence and absence of calcium were statistically similar. At lower levels of TOC loading, however, the presence of calcium appears to cause additional decreases in TCE capacity relative to carbon preloaded in the absence of calcium.

Freundlich unit capacity parameters,  $K_F$ , for TCE adsorption on carbon preloaded with 11.1 to 13.1 mg TOC/g in the presence of calcium are shown in Figure 8-20. For comparison, the relative unit capacity parameter obtained from carbon preloaded to 11.8 mg/g in the absence of calcium is also depicted. In all cases, the presence of calcium results in lower Freundlich unit capacity factors and higher  $n$ -values. The differences are only statistically significant (i.e., no confidence interval overlap) for the carbon preloaded in the presence of 1 mM calcium; however, among all carbons preloaded in the presence of calcium, the Freundlich unit capacity parameters are statistically similar. This suggests that the effects of calcium can result from relatively low calcium concentrations.

In the experiments conducted thus far, increases in calcium concentration were associated with increases in the amount of TOC adsorbed. An experiment was designed to investigate the effect of calcium for a constant adsorbed amount of humic material. Carbon

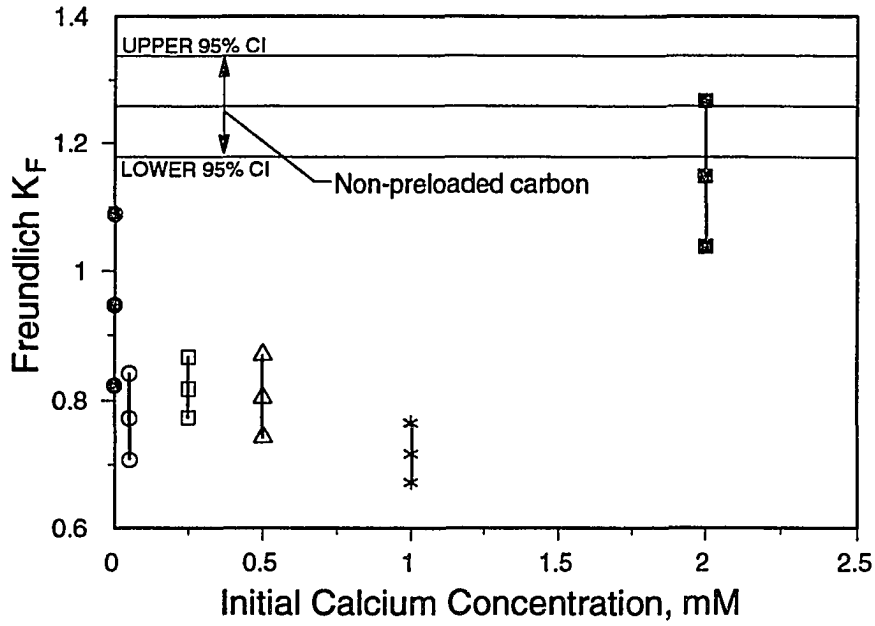


Figure 8-20. Freundlich  $K_F$ -values for TCE adsorption on carbon preloaded with humic acid in the presence of calcium. Solid horizontal lines represent best-fit  $K_F$  values and 95% confidence limits for non-preloaded carbon. Symbols with vertical lines represent best-fit  $K_F$  values and 95% confidence limits for TCE adsorption on preloaded carbon.

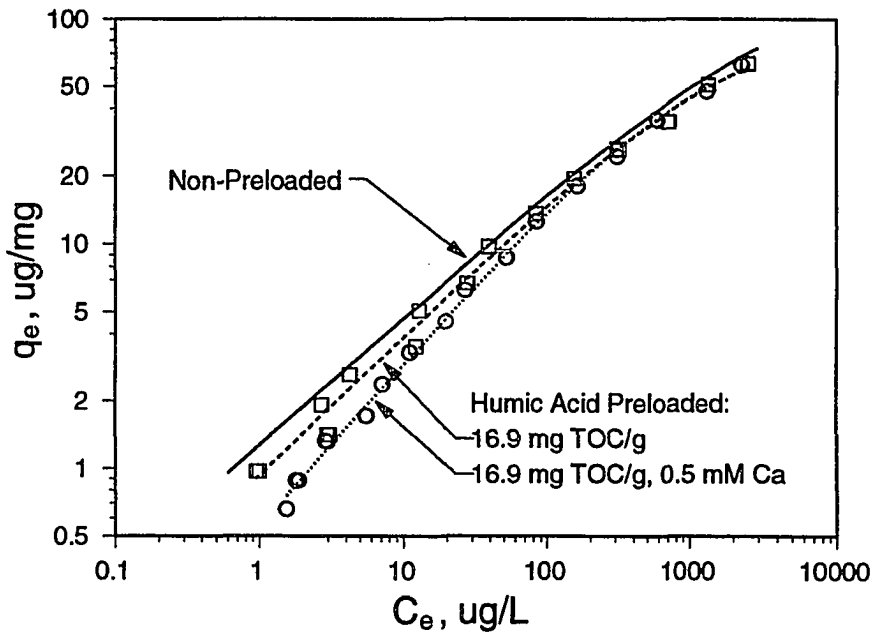


Figure 8-21. The adsorption of TCE on F400 carbon preloaded with Laurentian HA, demonstrating the effects of calcium. Lines represents Langmuir-Freundlich isotherm model fits.

**Table 8-15. Effect of Calcium Content at Constant HA Preloading: Isotherm Analysis**

Exp.	Langmuir-Freundlich Model					Freundlich Model		
	Param.	Param. Est.	Std. Error	95% CI	$Q^0 b^n$	Param.	Param. Est.	95% CI
EH17 N = 28	$Q^0 \times 10^{-2}$	1.191	0.275	0.565	0.941	$K_F$	0.941	0.815, 1.086
	$b \times 10^4$	4.272	2.455	5.047		n	0.606	0.551, 0.661
	n	0.624	0.023	0.047		N = 18		
EH17C N = 30	$Q^0 \times 10^{-2}$	0.932	0.137	0.281	0.557	$K_F$	0.556	0.515, 0.600
	$b \times 10^4$	8.907	1.960	4.014		n	0.711	0.682, 0.740
	n	0.729	0.006	0.012		N = 18		

was preloaded in the absence of calcium with 17.6 mg TOC/g and recovered from the preloading reactor. This preloaded carbon was then used in a TCE adsorption experiment using a background solution which contained calcium. In this experiment, the presence of calcium could have no effect on the amount of humic material or the fraction of the initial solution adsorbed. The isotherms developed in this experiment are shown in Figure 8-21, and the isotherm parameters are shown in Table 8-15. The presence of calcium in the buffer during TCE adsorption results in a reduction in the Langmuir-Freundlich maximum capacity parameter,  $Q^0$ , and a statistically significant increase in the heterogeneity parameter, n. The Freundlich unit capacity factor was reduced and the n-value was increased; in both cases the change was statistically significant. This result suggest that the presence of calcium increases the ability of preloaded humic material to compete with TCE.

The increase in the heterogeneity parameter suggests further depletion of high-energy sites which does not occur in the absence of calcium. The association of calcium with humic material can occur after the humic has been adsorbed; therefore, the formation of a humic-calcium association in solution, as suggested by the findings reported in Chapter 6 (Section 6.3), is not required. It is possible that the presence of calcium promotes cation bridging with the formation of new binding sites for the humic acid which subsequently block TCE access. The formation of new adsorption sites would represent a mechanism fundamentally different than that which occurs in the absence of calcium, and could explain the differences in the trends shown in Figure 8-19.

## **8.6 Effects of Adsorbent Characteristics on TCE Adsorption by Preloaded Carbon**

Four coal-based adsorbents and three wood-based adsorbents having different pore-size distributions, surface chemical characteristics and affinities for TCE were preloaded with Laurentian humic acid. TCE adsorption isotherms were measured on the preloaded carbon to determine how adsorbent properties affected the competitive interactions between TCE and preloaded humic material. An objective was to identify adsorbent properties which minimized the impact of preloading and which could potentially be further tailored to mitigate preloading effects. Various scenarios relating to the effects of adsorbent characteristics were hypothesized.

The effects of preloaded humic material on TCE adsorption may be mitigated if the adsorbent pore sizes were small enough to prevent access of even the smallest humic components. Based on this hypothesis, adsorbents which were activated to a lesser degree would exhibit i) lower amounts of humic material adsorbed; and ii) a reduced impact of preloading. The results for the adsorption of humic acid on Calgon WPLL and Westvaco MICRO carbons confirm that more microporous carbons exhibit a lower extent of humic substance adsorption.

At the other extreme, adsorbents with large pore sizes adsorb a greater amount of the larger components. For F400 carbon, it was found that the adsorption of larger components reduced the impact of preloading. The ability to adsorb larger molecular sizes may therefore reduce the impacts of preloading. It is possible, however, that the larger pore-size distribution simply increases the effective size of the reactive fraction. This would tend to exacerbate the effects of preloading. In practice, it is difficult to change the pore-size distribution of GAC without also changing the surface chemistry to some extent.

It was found that the extent of TCE adsorption on an adsorbent surface area basis increased with decreasing extent of activation. Thus, the more microporous carbons exhibited a higher affinity for TCE. If all other factors remain constant, adsorbents exhibiting lower affinities for TCE should exhibit greater percentage reductions in the extent of TCE adsorption after preloading, because adsorbed TCE is less able to effectively compete with the preloaded material. However, it is possible that the factors which reduce

the affinity for TCE also reduce the affinity for the humic acid, thereby lessening this effect.

The coal-based and wood-based adsorbents have different surface charges, which was shown to have a significant effect on the adsorption of humic substances. The negatively-charged wood-based adsorbents exhibit a lower extent of humic adsorption, especially in relation to their relative pore sizes. As a result of differences in surface charge, it is likely the structure of adsorbed humics is different, even when the surface loading is similar.

The detailed experimental conditions and isotherm analyses for the coal- and wood-based carbons are tabulated in Tables 8-16 and 8-17, respectively, and the corresponding isotherm data for these experiments are shown in Tables 8-18 and 8-19. Parameters reported in these tables may be compared to parameters obtained on non-preloaded carbon, reported in Table 8-1. For all seven adsorbents, 1.05 g/L doses were equilibrated with whole Laurentian humic acid solutions having nominal initial concentrations of 15, 30 and 60 mg TOC/L. In addition, the BPL and MACRO carbons were preloaded with several size fractions to investigate whether larger humic acid components cause reductions in TCE adsorption when preloaded on adsorbents having larger pores.

**Table 8-16. Effect of Coal-Based Adsorbent Characteristics on HA Preloading: Experimental Conditions**

Carbon Type	$C_0$ , mg TOC/L	$C_e$ , mg TOC/L	$q_e$ , mg/g	$D_0$ , g/L	$C_e/D_0$ , mg/g	$1-C_e/C_0$ , percent
WPLL	14.8	14.2	0.59	1.05	13.5	4.22
WPLL	30.8	29.5	1.3	1.05	28.0	4.40
WPLL	60.9	59.5	1.4	1.05	56.6	2.37
FS100	15.1	8.3	6.5	1.05	7.9	45.27
FS100	30.7	20.3	9.9	1.05	19.3	33.95
FS100	59.8	45.8	13.3	1.05	43.6	23.36
BPL	14.9	7.3	7.2	1.05	7.0	50.74
BPL	30.9	18.3	11.9	1.05	17.5	40.67
BPL	61.6	42.9	17.8	1.05	40.9	30.34

**Table 8-17. Effect of Wood-Based Adsorbent Characteristics on HA Preloading: Experimental Conditions**

Carbon Type	C <sub>0</sub> , mg TOC/L	C <sub>e</sub> , mg TOC/L	q <sub>e</sub> , mg/g	D <sub>0</sub> , g/L	C <sub>e</sub> /D <sub>0</sub> , mg/g	1-C <sub>e</sub> /C <sub>0</sub> , percent
MICRO	15.1	14.63	0.45	1.05	13.9	3.13
MICRO	30.8	28.74	1.96	1.05	27.4	6.70
MICRO	61.8	59.19	2.48	1.05	56.4	4.23
MESO	15.1	11.63	3.30	1.05	11.1	22.98
MESO	30.8	24.87	5.64	1.05	23.7	19.27
MESO	61.5	53.38	7.72	1.05	50.8	13.21
MACRO	15.1	7.36	7.35	1.05	7.0	51.26
MACRO	30.8	18.40	11.78	1.05	17.5	40.25
MACRO	61.6	43.76	16.94	1.05	41.7	28.95

#### TCE Adsorption on Preloaded Coal-Based Adsorbents

The impact of preloading on TCE adsorption isotherm parameters for each adsorbent type was assessed, and the effects of preloading for different adsorbent types were compared and related to adsorbent characteristics. The effects of preloading on adsorbents manufactured from coal will be discussed first, because the majority of preloading data were obtained with these adsorbents.

WPLL. This carbon exhibits low HA adsorption capacity, a maximum of only 1.4 mg/g was preloaded even at high solution TOC concentrations. Langmuir-Freundlich isotherm parameters were not significantly affected by preloading, although an increase in the n-value was observed at the two highest TOC loadings. Likewise, there is an increase in the Freundlich n-value at the higher TOC loadings, but the increase is not statistically significant. There is, however, a statistically significant decrease in the Freundlich K<sub>F</sub>-value for the two highest TOC loadings. No preloading experiment conducted with the F400 carbon resulted in TOC loadings low enough to allow a direct comparison with the WPLL results; however, the finding that significant reductions in TCE adsorption may occur at low levels of preloading has important practical implications..

**Table 8-18. Effect of Coal-Based Adsorbent Characteristics on HA Preloading: Isotherm Analysis**

Exp.	Langmuir-Freundlich Model					Freundlich Model		
	Param.	Param. Est.	Std. Error	95% CI	$Q_{ob}^n$	Param.	Param. Est.	95% CI
<b>BPL</b>								
EH7 N = 28	$Q^{\circ} \times 10^{-2}$	5.118	RE	RE	0.577	$K_F$	0.552	0.504, 0.605
	$b \times 10^4$	0.0399	RE	RE		n	0.576	0.536, 0.615
	n	0.546	RE	RE		N = 16		
EH12 N = 28	$Q^{\circ} \times 10^{-2}$	0.761	0.169	0.347	0.527	$K_F$	0.528	0.485, 0.575
	$b \times 10^4$	3.080	1.575	3.238		n	0.599	0.565, 0.633
	n	0.615	0.015	0.031		N = 20		
EH18 N = 30	$Q^{\circ} \times 10^{-2}$	0.899	0.270	0.553	0.400	$K_F$	0.402	0.350, 0.461
	$b \times 10^4$	1.656	1.093	2.232		n	0.608	0.552, 0.665
	n	0.622	0.018	0.037		N = 18		
<b>FS100</b>								
EH7 N = 30	$Q^{\circ} \times 10^{-2}$	1.333	0.254	.519	1.125	$K_F$	1.093	0.989, 1.207
	$b \times 10^4$	3.453	1.775	3.625		n	0.600	0.560, 0.640
	n	0.599	0.020	0.041		N = 18		
EH10 N = 30	$Q^{\circ} \times 10^{-2}$	1.745	0.404	0.825	1.237	$K_F$	1.177	1.079, 1.284
	$b \times 10^4$	2.088	1.209	2.469		n	0.606	0.569, 0.643
	n	0.584	0.017	0.035		N = 18		
EH13 N = 23	$Q^{\circ} \times 10^{-2}$	1.331	0.210	.429	1.005	$K_F$	0.984	0.922, 1.051
	$b \times 10^4$	4.127	1.584	3.235		n	0.606	0.581, 0.632
	n	0.627	0.017	0.035		N = 20		
<b>WPLL</b>								
EH6 N = 30	$Q^{\circ} \times 10^{-2}$	0.755	0.066	0.135	0.410	$K_F$	0.410	0.384, 0.437
	$b \times 10^4$	6.942	1.337	2.730		n	.700	0.675, 0.726
	n	0.717	0.010	0.020		N = 20		
EH13 N = 30	$Q^{\circ} \times 10^{-2}$	0.789	0.123	0.252	0.305	$K_F$	0.296	0.269, 0.326
	$b \times 10^4$	5.429	1.772	3.629		n	0.741	0.706, 0.775
	n	0.739	0.018	0.037		N = 20		
EH14 N = 30	$Q^{\circ} \times 10^{-2}$	0.807	0.129	0.264	0.322	$K_F$	0.314	0.286, 0.345
	$b \times 10^4$	5.667	1.905	3.901		n	0.740	0.706, 0.775
	n	0.739	0.018	0.037		N = 20		

**Table 8-19. Effect of Wood-Based Adsorbent Characteristics on HA Preloading: Isotherm Analysis**

Exp.	Langmuir-Freundlich Isotherm					Freundlich Isotherm		
	Param.	Param. Est.	Std. Error	95% CI	$Q_{ob}^0/n$	Param.	Param. Est.	95% CI
<b>MICRO</b>								
EH0 N = 30	$Q^0 \times 10^{-2}$	0.379	0.065	0.133	0.081	$K_F$	0.079	0.069, 0.090
	$b \times 10^4$	1.702	0.564	1.155		n	0.711	0.670, 0.753
	n	0.709	0.013	0.027		N = 16		
EH1 N = 30	$Q^0 \times 10^{-2}$	0.541	0.168	0.344	0.106	$K_F$	0.100	0.091, 0.100
	$b \times 10^4$	0.748	0.446	0.913		n	0.675	0.644, 0.707
	n	0.656	0.012	0.025		N = 16		
EH2 N = 30	$Q^0 \times 10^{-2}$	1.12	RE	RE	0.061	$K_F$	0.064	0.050, 0.083
	$b \times 10^4$	0.258	RE	RE		n	0.692	0.610, 0.773
	n	0.711	RE	RE		N = 14		
<b>MESO</b>								
EH3 N = 30	$Q^0 \times 10^{-2}$	0.205	0.046	0.094	0.052	$K_F$	0.046	0.038, 0.056
	$b \times 10^4$	2.827	1.251	2.562		n	0.766	0.706, 0.826
	n	0.732	0.021	0.043		N = 16		
EH6 N = 30	$Q^0 \times 10^{-2}$	0.286	0.033	0.068	0.073	$K_F$	0.075	0.066, 0.085
	$b \times 10^4$	1.338	0.308	0.631		n	0.652	0.612, 0.693
	n	0.670	0.009	0.018		N = 16		
EH8 N = 30	$Q^0 \times 10^{-2}$	0.403	0.322	0.659	0.071	$K_F$	0.058	0.048, 0.071
	$b \times 10^4$	0.682	1.027	2.103		n	0.732	0.672, 0.791
	n	0.661	0.030	0.061		N = 16		
<b>MACRO</b>								
EH7 N = 28	$Q^0 \times 10^{-2}$	0.226	0.075	0.154	0.040	$K_F$	0.031	0.020, 0.047
	$b \times 10^4$	2.796	1.768	3.635		n	0.860	0.725, 0.996
	n	0.775	0.035	0.072		N = 14		
EH12 N = 27	$Q^0 \times 10^{-2}$	0.201	0.029	0.060	0.074	$K_F$	0.071	0.063, 0.079
	$b \times 10^4$	3.533	1.110	2.287		n	0.714	0.679, 0.748
	n	0.705	0.017	0.035		N = 16		
EH17 N = 30	$Q^0 \times 10^{-2}$	0.161	0.029	0.059	0.061	$K_F$	0.058	0.047, 0.072
	$b \times 10^4$	5.045	1.977	4.049		n	0.744	0.673, 0.814
	n	0.734	0.024	0.049		N = 14		



FS100. This carbon was preloaded with 6.5 to 13.3 mg TOC/g, which represents fairly low TOC loadings in comparison to the loadings achieved in the adsorptive fractionation experiments conducted with the F400 carbon. There is no clear trend in the Langmuir-Freundlich maximum capacity parameter, and the heterogeneity parameter increases with increased TOC loading, but not by a statistically significant amount. However, the Freundlich unit capacity parameter,  $K_F$ , was reduced a statistically significant amount at all TOC loadings. The  $n$ -value increased for all TOC loadings, and the increase was statistically significant when the carbon was loaded with 13.3 mg/g. Reductions in the extent of TCE adsorption on preloaded FS100 carbon are comparable to those found with the F400 carbon, although no statistically significant increase in the

Freundlich  $n$ -value was found on F400 carbon preloaded with less than 17 mg/g. This suggests that some sites on the FS100 carbon have a higher affinity for TCE, which is consistent with the somewhat greater extent of single-solute adsorption observed.

BPL. The BPL carbon was preloaded with 7.2 to 17.8 mg TOC/g, which represents moderate TOC loadings in comparison with the experiments conducted with the F400 carbon. The isotherms on virgin carbon and carbon preloaded with 7.2 mg/g did not exhibit significant curvature on log-log coordinates and the standard errors for the Langmuir-Freundlich parameters could not be estimated due to round-off error. While a decrease in the maximum capacity parameter and an increase in the heterogeneity parameter were observed, the statistical significance of the differences could not be assessed. The Freundlich unit capacity parameter decreased and the  $n$ -value increased with increased TOC loading, although the only change which was statistically significant was the decrease in the unit capacity parameter at a loading of 17.8 mg TOC/g. This is in contrast to the other coal-based adsorbents which showed statistically significant decreases in the Freundlich  $K_F$  value at lower humic loadings.

Comparison of TCE adsorption isotherm parameters for different carbon types reveals subtle differences in the effects of preloading. Based on the statistical significance of changes in the Freundlich parameters for comparable amounts of preloaded humic acid, it is concluded that the effect of preloading on TCE adsorption increases with decreasing extent of raw material activation. The WPLL carbon exhibited statistically significant reductions in the Freundlich unit capacity parameter when preloaded with less than 2 mg/g,

while a loading of over 17 mg TOC/g was required to cause a significant reduction in TCE adsorption on preloaded BPL carbon. TCE isotherms and Langmuir-Freundlich model fits for these preloading conditions are shown in Figure 8-22.

The small amount of humic acid adsorbed by the WPLL carbon after equilibrating with nearly 60 mg/L humic acid suggests that only the most adsorbable fraction was adsorbed, and that small amounts of this fraction were able to restrict TCE access to adsorbent surfaces. The relatively small changes in the Freundlich  $n$ -value which accompanied the statistically significant reduction in  $K_F$  suggest significant pore blockage occurred. This explanation is consistent with the fact that the WPLL carbon is relatively microporous compared to the other coal-based carbons. The differences in pore structure between the WPLL carbon and the FS100 and F400 carbons are not so great as to suggest that pore structure alone is responsible for the effects of preloading, however. The WPLL carbon has the most reactive surface in terms of affinity for TCE, and has the highest functional group density as measured by acid/base titration. These characteristics may also result in a strong affinity for the small amounts of humic acid that do adsorb.

The relatively small reduction of TCE capacity on preloaded BPL carbon may relate to the low reactivity of the surface. The BPL carbon had the lowest single-solute TCE capacity on a surface-area basis; therefore, the factors which reduce the affinity for TCE may also reduce the affinity for the humic acid, thereby lessening the effect of preloading. This explanation is supported by the observation that the BPL carbon adsorbed less humic acid on a surface area basis than the F400 and FS100 (discussed in Chapter 6, Section 6.3). Thus, the surface density of adsorbed humic molecules is likely lower, which may mitigate preloading effects. The effects of preloading may also be related to pore structure. The greater percentage of surface area in mesopores may result in a smaller fraction of molecules present in micropores, where TCE is more likely to adsorb. Larger molecules present in the meso and macropores may restrict access of the smaller components to micropore surfaces, mitigating the effects of preloading to some degree. While TCE adsorption on preloaded BPL carbon is reduced to a lesser extent than on F400 carbon, at a loading of about 18 mg TOC/g, the F400 carbon still exhibits a greater extent of TCE adsorption. Therefore, the BPL carbon would not be selected in preference to F400 carbon on the basis of equilibrium TCE adsorption capacity .

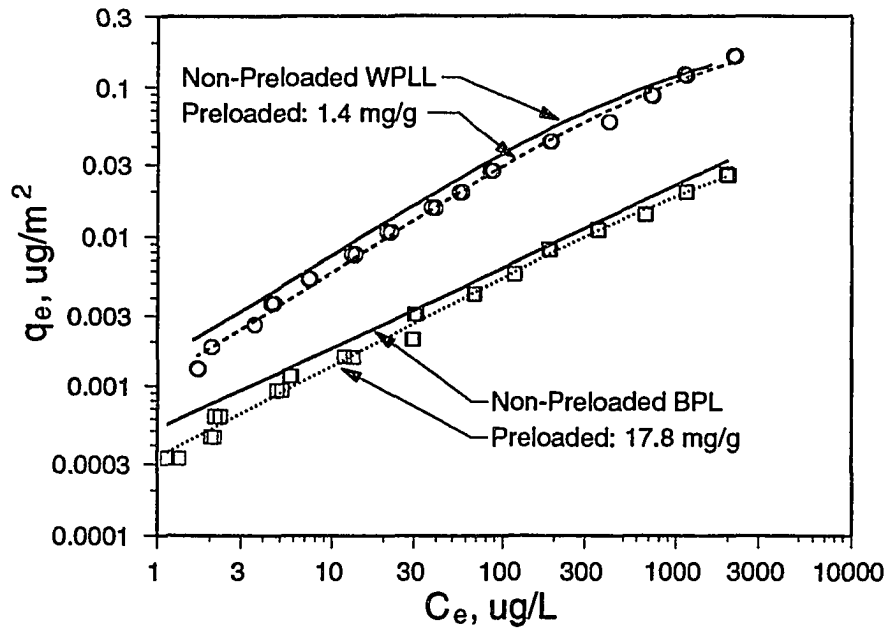


Figure 8-22. Comparison of TCE adsorption by WPLL and BPL carbons preloaded with Laurentian HA. Lines represent Langmuir-Freundlich isotherm model fits.

### TCE Adsorption on Preloaded Wood-Based Adsorbents

The trends observed for the coal-based carbons were also observed for the wood-based MICRO and MESO carbons: the effect of preloading on TCE adsorption increases with decreasing extent of raw material activation, increasing extent of microporosity, and increasing affinity for TCE adsorption. Further, both the WPLL and MICRO carbons exhibited the lowest extent of humic acid adsorption. TCE adsorption on MICRO carbon preloaded with 2.5 mg/g was significantly reduced while the MESO carbon showed only slight effects at loadings up to 7.7 mg TOC/g. TCE isotherms on MICRO carbon preloaded with 2.0 and 2.5 mg TOC/g are shown in Figure 8-23.

The adsorption of TCE on preloaded MACRO carbon did not follow the trends exhibited by any of the adsorbents under any of the preloading conditions investigated thus far. TCE adsorption on preloaded MACRO carbon was actually enhanced in comparison to non-preloaded carbon, and the extent of TCE adsorption increased with increasing TOC loading. Langmuir-Freundlich isotherm parameters do not exhibit any statistically

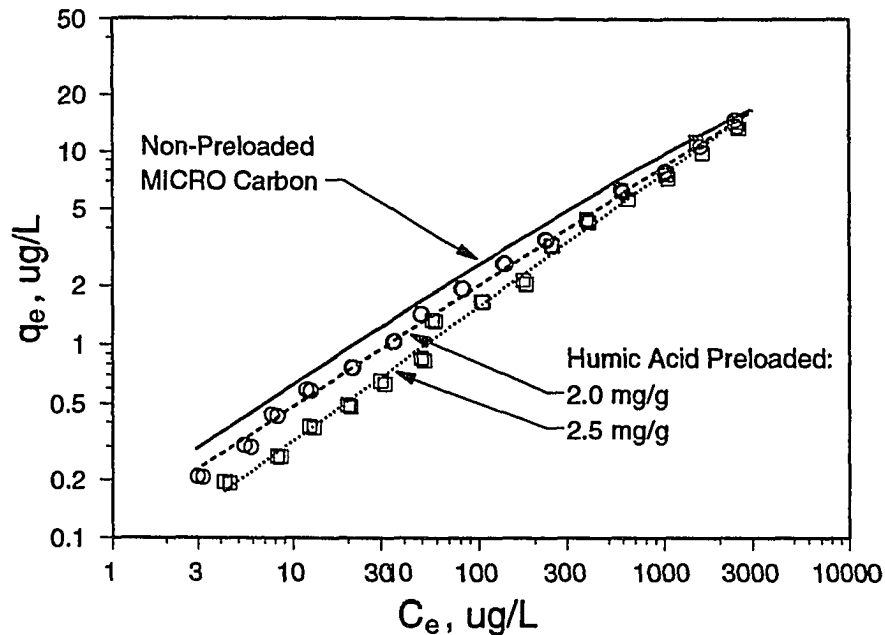


Figure 8-23. The adsorption of TCE on MICRO carbon preloaded with Laurentian HA. Lines represents Langmuir-Freundlich or Freundlich isotherm model fits.

significant trends; however, the Freundlich  $K_F$ -value is higher in every case, and the increase is statistically significant at TOC loadings of 11.8 mg TOC/g or more. The Freundlich  $n$ -values are generally lower, although no significant trend is evident. The TCE isotherms on preloaded MACRO carbon are shown in Figure 8-24.

The MACRO carbon has several characteristics which distinguish it from the other adsorbents used in this study: i) it has the lowest affinity for TCE among all adsorbents; ii) it has the lowest  $pH_{pzc}$ ; iii) it adsorbs the least amount of acid; iv) it has the greatest percentage of surface area in the meso- and macro-pore size ranges. It is possible that these characteristics promote an adsorbed humic configuration that enables it to act as a partitioning medium for TCE. The negative surface charge and large pore sizes may cause the adsorbed humic to adopt a compact configuration containing hydrophobic micro-environments into which TCE can partition or onto which TCE could adsorb. While the energy of this mechanism is not expected to be high, it may be high enough to enhance the initially low surface energy. The non-preloaded MACRO carbon had a high value of  $n$  ( $>0.8$ ) which suggests a relatively uniform surface energy distribution. The presence of humic material on the surface acting as a partitioning medium may widen the energy

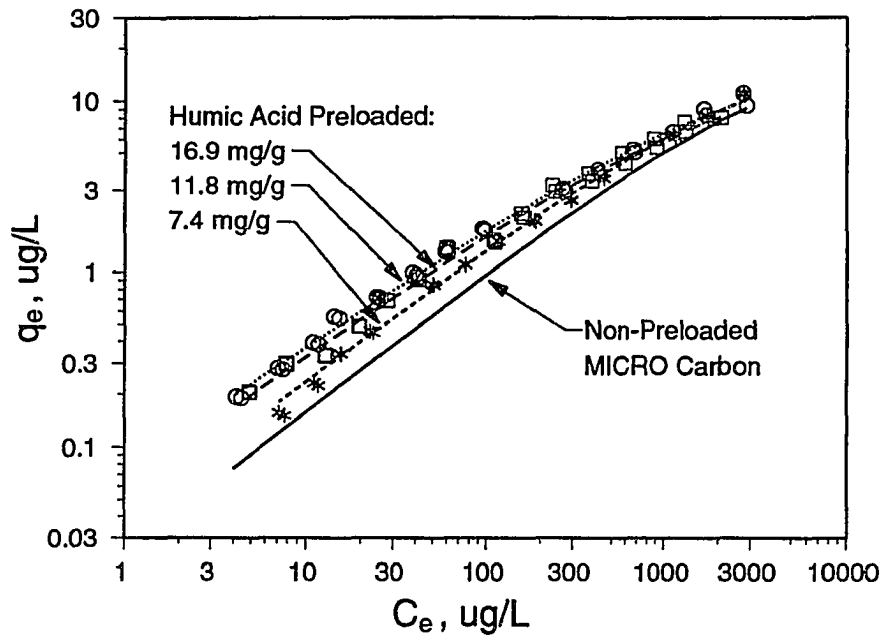


Figure 8-24. The adsorption of TCE on MACRO carbon preloaded with Laurentian HA. Lines represents Langmuir-Freundlich or Freundlich isotherm model fits.

distribution in the direction of lower energies, reflected in lower Langmuir-Freundlich and Freundlich  $n$ -values. While the mechanism of partitioning to preloaded organics has been discussed in the literature (Carter et al. 1992), this result was not anticipated.

#### TCE Adsorption on BPL and MACRO Adsorbents Preloaded with UF Fractions

The two adsorbents having the largest pore sizes, BPL and MACRO, were preloaded with UF fractions to determine if the conclusions drawn about the effects of molecular size based on experiments conducted with F400 carbon applied to these adsorbents. Each carbon was preloaded with both the largest and smallest size fractions (<3K and >100K). In addition, the BPL carbon was preloaded with the 30-100K fraction. The experimental preloading conditions are shown in Table 8-20, and the Langmuir-Freundlich and Freundlich isotherm model fits to TCE adsorption data are shown in Table 8-21.

The adsorption of TCE on BPL carbon preloaded with UF size fractions showed the same general trends as TCE adsorption on F400 carbon preloaded with size fractions.

Table 8-20. Effect of Molecular Size on HA Preloading: Experimental Conditions

Carbon Type	C <sub>0</sub> , mg TOC/L	C <sub>e</sub> , mg TOC/L	q <sub>e</sub> , mg/g	D <sub>0</sub> , g/L	C <sub>e</sub> /D <sub>0</sub> , mg/g	1-C <sub>e</sub> /C <sub>0</sub> , percent
<b>BPL</b>						
<3K	8.0	1.33	12.00	0.556	2.4	83.38
30-100K	37.56	32.03	9.95	0.556	57.6	14.7
>100K	36.09	28.70	13.29	0.556	51.6	20.48
<b>MACRO</b>						
<3K	8.0	3.28	8.49	0.556	5.9	59.00
>100K	37.53	26.81	19.28	0.556	48.2	28.6

Table 8-21. Effect of Molecular Size on HA Preloading: Isotherm Analysis

Exp.	Langmuir-Freundlich Isotherm					Freundlich Isotherm		
	Param.	Param. Est.	Std. Error	95% CI	Q <sup>o</sup> b <sup>n</sup>	Param.	Param. Est.	95% CI
<b>MACRO</b>								
<3K N = 24	Q <sup>o</sup> x 10 <sup>-2</sup>	0.342	0.059	0.122	0.111	K <sub>F</sub>	0.106	0.099, 0.115
	b x 10 <sup>4</sup>	1.210	0.444	0.921		n	0.653	0.624, 0.681
	n	0.635	0.010	0.021		N = 12		
>100K N = 24	Q <sup>o</sup> x 10 <sup>-2</sup>	0.356	0.114	0.236	0.131	K <sub>F</sub>	0.128	0.177, 0.139
	b x 10 <sup>4</sup>	1.148	0.782	1.622		n	0.623	0.589, 0.656
	n	0.618	0.015	0.031		N = 14		
<b>BPL</b>								
<3K N = 26	Q <sup>o</sup> x 10 <sup>-2</sup>	0.626	0.162	0.334	0.420	K <sub>F</sub>	0.427	0.368, 0.495
	b x 10 <sup>4</sup>	4.169	2.476	5.110		n	0.622	0.568, 0.675
	n	0.643	0.023	0.047		N = 15		
30100 N = 30	Q <sup>o</sup> x 10 <sup>-2</sup>	0.724	0.066	0.135	0.609	K <sub>F</sub>	0.606	0.566, 0.650
	b x 10 <sup>4</sup>	3.622	0.829	1.698		n	0.590	0.564, 0.616
	n	0.603	0.009	0.018		N = 18		
>100K N = 30	Q <sup>o</sup> x 10 <sup>-2</sup>	0.625	0.098	0.201	0.619	K <sub>F</sub>	0.608	0.548, 0.673
	b x 10 <sup>4</sup>	5.054	2.055	4.209		n	0.598	0.559, 0.637
	n	0.608	0.017	0.035		N = 18		

Freundlich isotherm parameters determined from carbon preloaded with 12.0 mg TOC/g of the <3K fraction showed a statistically significant decrease in the unit capacity parameter,  $K_F$ , and an increase in the n-value. In contrast to TCE adsorption on the F400 carbon, however, the effect of the <3K fraction was greater than the effect of carbon preloaded by adsorptive fractionation. This provides additional evidence that the reactive fraction of the humic mixture is comprised of the low molecular-size components, supporting the findings of the F400 carbon preloading experiments, and extending the result to adsorbents having significantly different properties.

Also consistent with the previous results on F400 carbon, TCE adsorption on BPL carbon preloaded with the 30-100K and >100K fractions, at loadings of 10.0 and 13.3 mg TOC/g respectively, was not statistically different from adsorption by non-preloaded carbon. Indeed, the Freundlich  $K_F$ -values were slightly higher on the carbon preloaded with the larger size fractions. Larger size components do not appear to be reactive, even when preloaded on adsorbents having pore-size distributions shifted to larger sizes.

Both the <3K and the >100K fractions increased the extent of TCE adsorption on MACRO carbon, and both fractions exhibited increases greater than that observed on carbon preloaded with similar amounts of humic material by adsorptive fractionation. Statistically significant increases in the Freundlich  $K_F$  parameter and statistically significant decreases in the n-value were observed. The Freundlich  $K_F$  value for carbon preloaded with 19.3 mg/g of the >100K fraction was greater than the value obtained for carbon preloaded with 8.5 mg/g of the <3K fraction; however, the difference may be related to the difference in the amount preloaded.

## 8.7 Conclusions

TCE adsorption isotherms were measured on F400 carbon preloaded with Laurentian humic and fulvic acids under a wide variety of conditions. Effects of preloading were expressed in terms of Langmuir-Freundlich and Freundlich isotherm parameters. There was consistently good agreement between the Freundlich unit-capacity parameter computed from Langmuir-Freundlich parameters, and that estimated by fitting the Freundlich isotherm to the low-concentration data. In general, the effects of preloading

were consistent with the theoretical analyses presented in chapter 7, although the impact of natural humic materials on TCE adsorption is less significant for similar mass loadings.

The effects of molecular size were investigated by preloading carbon with ultrafiltration size fractions, mixtures of size fractions, and whole humic and fulvic solutions. TCE adsorption on carbon preloaded with the <3K fraction (MW = 1380 g/mol as PSS) was significantly reduced in comparison to adsorption on non-preloaded carbon. Adsorption by carbon preloaded with larger size fractions (MW > 3000 g/mol as PSS) was statistically similar to adsorption by non-preloaded carbon. These results are particularly significant in the context of the performance of pretreatment systems designed to remove dissolved organic matter. It is known that chemical processes such as coagulation and membrane processes such as ultrafiltration preferentially remove the larger molecular-weight fraction of the organic matter, leaving smaller molecules in solution. To mitigate the effects of preloading, these processes must be designed to specifically target the more reactive low-molecular-weight fraction.

Adsorptive fractionation experiments were conducted to investigate the effects of the adsorbed molecular-size distribution. The greatest reductions in TCE capacity occurred when the molecular-size distribution of preloaded humic substances was shifted to smaller sizes, which is caused by high  $C_e/D_0$  ratios, and which results in increases in the amount of smaller molecular-size components adsorbed. Isotherm parameters from carbon preloaded with the <3K fraction fall within the general trend observed for the data from both the humic and fulvic acids preloaded by adsorptive fractionation. These results suggest that the smaller molecular-size components represent the most reactive components of the whole mixture, and the presence of larger molecular-weight components does not reduce the ability of low molecular-weight fractions to compete with TCE.

Carbon was preloaded with synthetic mixtures of ultrafiltration fractions to determine if different size components interact. The effects of preloading were independent of the initial molecular-size distribution or the initial mass fraction of the 10-30K fraction, as long as the amount of the <3K fraction per mass of adsorbent was constant. These results further illustrate that the smaller molecular-size fraction is preferentially adsorbed, and the effects of preloading are due primarily to this fraction. Larger molecular-size



components present in the 10-30K fraction do not significantly displace or otherwise interact with the smaller components.

A sequential adsorption experiment was conducted to further investigate potential displacement or other interaction mechanisms. In this experiment, the <3K and 10-30K fractions were loaded in two sequential stages. Adsorption of the larger fraction effectively prevented subsequent adsorption of the <3K fraction from competing with TCE, and neither fraction appeared to significantly displace the other.

We demonstrated that for a given percentage of TOC removal (or average molecular weight remaining in solution), greater reductions in TCE adsorption occurred with increasing ionic strength. However, the reduction in TCE adsorption was fundamentally related to the amount of humic material adsorbed, regardless of the ionic strength conditions during preloading. When the amount of adsorbed humic acid is similar, the Freundlich  $K_F$  and  $n$  values are statistically similar for all ionic strength conditions.

At lower levels of preloading the presence of calcium appears to decrease the adsorption of TCE to a greater extent than carbon preloaded in the absence of calcium, and this effect was observed at relatively low (0.05 mM) calcium concentrations. These results suggest that the presence of calcium increases the ability of preloaded humic material to compete with TCE. This result was confirmed by exposing a carbon preloaded in the absence of calcium to a buffer solution containing calcium. TCE adsorption from the calcium-containing buffer exhibited a significant decrease as compared to adsorption from a calcium-free buffer. An increase in the heterogeneity parameter was observed, suggesting further depletion of high-energy sites which did not occur in the absence of calcium. The association of calcium with the humic material can occur after the humic has been adsorbed, therefore, the formation of a humic calcium association in solution, as suggested by the findings reported in Chapter 6 (Section 6.3), is not required.

TCE adsorption was measured on several different adsorbents preloaded with humic acid to evaluate the effects of adsorbent properties. Reductions in TCE adsorption due to preloading increased with decreasing extent of raw material activation, increasing extent of microporosity, and increasing affinity for TCE adsorption. Microporous adsorbents exhibited significant reductions in TCE adsorption for relatively low levels of TOC loading. For similar levels of preloading, TCE adsorption by preloaded macroporous

carbons exhibited smaller reductions. This result suggests that when comparing adsorbents, effects of preloading do not necessarily correlate with extent of humic adsorption, and designing microporous carbons to exclude humic materials does not appear to be a feasible approach to mitigate preloading effects.

Reductions in TCE adsorption were negligible on wood-based carbons having larger pore sizes than the predominantly microporous carbon. In fact, TCE adsorption by the wood-based carbon having the largest pore sizes was increased after preloading. However, these carbons exhibited low capacities for TCE whether they were preloaded or not. Nevertheless, these results suggest that surface charge may be an adsorbent property which can be further tailored to mitigate preloading effects.

## CHAPTER IV CONCLUSIONS AND RECOMMENDATIONS

### 9.1 Conclusions

The overall objectives of the research were to investigate the adsorption of DOM and the effect of preloaded DOM on the subsequent adsorption of target contaminants. The goal was to provide information that could be incorporated into design protocols, mathematical models, and model parameter estimation methods. This research focused on the effects of DOM molecular size, the chemical and physical heterogeneity of adsorbent materials, solution ionic strength, and calcium composition.

Pursuant to the hypothesis that molecular size and size distribution are critical factors governing the adsorption of DOM and hence the subsequent adsorption of SOCs on preloaded carbon, the first phase of this research was devoted to molecular size characterization and size fractionation. A single-parameter ultrafiltration permeation model was developed and validated for describing the permeation of organic, random-coil macromolecules in ultrafiltration systems. It was demonstrated that under the conditions of this study, solute uptake by membrane surfaces was negligible. Under certain experimental conditions, however, it was found that the permeation factor decreased with increasing volume throughput, presumably due to the onset of concentration polarization phenomena.

Permeation behavior in ultrafiltration systems depends strongly on macromolecular structure, which is governed by solution ionic strength. Membranes should be calibrated with random-coil polymers of known molecular weight, in inorganic background matrices similar to the water sample to be fractionated. Polystyrene sulfonate was found to have coiling characteristics similar to that found for natural humic and fulvic acids, and may be useful for membrane calibration.

The permeation model proved useful for designing fractionation protocols, and ultrafiltration was demonstrated to be a useful technique for fractionating mixtures of macromolecules according to size. High-Performance Size-Exclusion chromatography was used to measure molecular weight distributions of whole humic solutions and humic size fractions, and average molecular weights were determined from the first moment of the HPSEC distribution. The molecular size characterizations of the ultrafiltration and size-exclusion techniques were found to be consistent, and the average molecular weights of the ultrafiltration size fractions were found to correlate linearly with the membrane permeation factors.

The adsorption of several polyelectrolytes, including a synthetic polymer, polystyrene sulfonate (PSS), and Laurentian humic and fulvic acids extracted from soil, was characterized on activated carbon. The heterogeneous nature of humic substances was observed to manifest in an adsorption isotherm which showed a dependence on adsorbent dose and initial concentration. Several techniques were used to demonstrate that the sorptive heterodispersity of humic substances can be attributed, at least in part, to molecular size, or molecular-size distribution. These techniques included i) comparison to model polyelectrolyte adsorption; ii) sorptive fractionation; and iii) ultrafiltration membrane permeation and size exclusion chromatography measurements made on TOC remaining in solution after equilibration with activated carbon.

Adsorption isotherms of size fractions prepared by ultrafiltration demonstrated that the Laurentian humic acid is a polydisperse mixture of molecular sizes, and that the smaller molecular size components adsorb to a greater degree on an adsorbent mass basis. Nearly an order-of-magnitude increase in the amount of TOC adsorbed occurred with a decrease in molecular weight over a range of about 20,000 to 2,000 (g/mol as PSS); however, most of the increases in capacity were observed for molecules having molecular weights below about 4,000 g/mol as PSS. This finding, in conjunction with the results which showed that ultrafiltration permeation factors were linearly related to average molecular weights determined by HPSEC, suggest that permeation factor measurements may provide a useful screening technique for rapid assessment of the adsorbability of natural humic substances.

A unique adsorption isotherm for humic and fulvic acids was obtained when the equilibrium humic acid concentration was normalized by the adsorbent dose, providing evidence for near-complete preference for more adsorbable components. Measured ultrafiltration permeation factors and size exclusion chromatography analysis confirm that smaller molecules are adsorbed preferentially from solution. As the adsorbent dose approached zero, the size distribution of components remaining in solution, and therefore the permeation factor, asymptotically approached that of the original solution. As the adsorbent dose was increased, a greater mass of humic acid was removed from solution, and the HPSEC molecular weight distribution was shifted to larger sizes. These results demonstrate conclusively that small molecular size components are adsorbed preferentially from an humic mixture, and that adsorptive fractionation occurs on the basis of molecular size.

It was demonstrated that increasing solution ionic strength can change the configuration of polyelectrolytes and shift the size distribution to smaller sizes, resulting in a significant increase in the extent of humic acid adsorption. An analysis of humic components remaining in solution after equilibration with activated carbon demonstrated that for a given adsorbent dose, the extent of adsorption was greater at higher ionic strength, and the adsorbed molecular weight distribution was shifted to higher molecular weights. The adsorbed molecular size distribution was identical for a given percentage reduction in the initial humic concentration, but a smaller adsorbent mass was required to effect a given reduction with increasing ionic strength. For a given amount adsorbed, the equilibrium concentration of humic acid was lower under higher ionic strength conditions, and a greater fraction of the initial humic acid was adsorbed. Therefore, the adsorbed molecular size distribution was shifted to higher molecular weights.

The presence of calcium was shown to increase the adsorption of humic acids from solution at constant ionic strength. The removal of free calcium from solution was attributed to complexation mechanism with the HA. Evidence for aggregation of humic acids in solution in the presence of calcium was also found. On the basis of size, the formation of aggregates would be expected to decrease the extent of adsorption. The fact that calcium increases the extent of adsorption in opposition to the aggregation effect

suggests that either larger molecules are being adsorbed, or smaller molecules are being adsorbed more effectively. Both explanations are likely, because the divalent cation has a greater ability to screen charge, and because new adsorption sites may be created on the surface via cation bridges.

Adsorbent surface area, pore-size distribution and surface chemistry all play a role in determining the extent of humic acid adsorption. For both the coal- and wood-based carbons, the extent of adsorption (on an adsorbent mass basis) increases with the extent of activation within a group of adsorbents having the same source material and activation conditions (e.g., WPLL, FS100 and BPL). This can be explained, in part, on the basis of an increased percentage of surface area in pores in the mesopore size range (greater than 20 Å width), and an increase in total surface area. Surface charge clearly plays an important role when comparing the extent of adsorption of different adsorbents. A lower extent of adsorption was observed on adsorbents having negatively charged surfaces. Despite significant differences in pore structure and surface chemistry, however, the preferential adsorption of low-molecular weight molecules is demonstrated for both coal and wood-based carbons.

The effects of preloading on the TCE adsorption isotherm were investigated using isotherm model sensitivity analysis, IAST predictions and an experimental program using a well-characterized bi-solute system. The impacts of preloading were interpreted in the context of i) changes in isotherm parameters; and ii) changes in adsorbent site-energy distributions. The Langmuir-Freundlich isotherm model, a three-parameter model derived from the theory of adsorption on heterogeneous surfaces, successfully described the adsorption data. It was demonstrated that changes in the isotherm parameters could be interpreted in terms of changes in the site-energy distribution. However, in many cases, the parameters could not be determined with statistical confidence. In contrast, the two Freundlich isotherm parameters were estimated with statistical confidence, although accurate description of the adsorption data was usually limited to the low concentration range. Nevertheless, by expressing the Freundlich isotherm as a simplification of the more general three-parameter Langmuir-Freundlich isotherm, and by relating changes in site

energy distributions to Freundlich isotherm parameters, it was demonstrated that Freundlich isotherm parameters have physical significance.

Isotherm sensitivity analysis, IAST model predictions and experimental measurements give a consistent mechanistic interpretation of the impacts of adsorbent preloading. At low mass loadings of the preloading compound, the most significant effect of preloading is to reduce the number of high energy sites available to the subsequently adsorbed compound. The loss of high energy sites causes a significant reduction in the site energy heterogeneity, and reduces the extent of adsorption in the low concentration region. This is reflected in a significant increase in the Langmuir-Freundlich and Freundlich  $n$ -values, and a significant decrease in the Freundlich  $K_F$  value. At low levels of preloading, changes in the Langmuir-Freundlich  $Q^0$  and  $b$  parameters were not statistically significant.

At higher levels of preloading, the site energy distribution is further shifted to lower energies, resulting in a reduction in the average site energy, and maximum adsorption capacity. Further increases in the site energy heterogeneity were typically small, and after an initial increase, both the Langmuir-Freundlich and Freundlich  $n$ -values remained relatively constant. This reflects in a shift in the TCE isotherm downward relative to the  $q_e$ -axis, in a parallel fashion.

Measurements of adsorbent surface area and pore volume indicated that observed changes in TCE adsorption resulting from TCB preloading were associated with changes in the physical characteristics of the adsorbent. TCB adsorbed primarily in micropores, and increased levels of preloading reduced micropore surface area, total surface area and pore volume. However, reductions in the Freundlich  $K_F$  parameter correlated with surface area only at higher levels of preloading. This finding further supports the hypothesis that low levels of preloading are primarily associated with a loss of high energy sites, and provides a further mechanistic explanation of the parallel shifts in the TCE isotherm at higher levels of preloading.

TCE adsorption isotherms were measured on F400 carbon preloaded with Laurentian humic and fulvic acids under a wide variety of conditions. Effects of preloading were expressed in terms of changes in Langmuir-Freundlich and Freundlich isotherm parameters. There was consistently good agreement between the Freundlich unit-capacity

parameter computed from Langmuir-Freundlich parameters, and that estimated by fitting the Freundlich isotherm to the low-concentration data. In general, the effects of preloading were consistent with the theoretical predictions, although the impact of natural humic materials on TCE adsorption was less significant for similar mass loadings.

The effects of molecular size were investigated by preloading carbon with ultrafiltration size fractions, mixtures of size fractions and whole humic and fulvic solutions. TCE adsorption on carbon preloaded with the <3K fraction (MW = 1380 g/mol as PSS) was significantly reduced in comparison to adsorption on non-preloaded carbon. Adsorption by carbon preloaded with larger size fractions (MW > 3000 g/mol as PSS) was statistically similar to adsorption by non-preloaded carbon.

Adsorptive fractionation experiments were conducted to investigate the effects of the adsorbed molecular-size distribution. The greatest reductions in TCE capacity occurred when the molecular size distribution of preloaded humic substances was shifted to smaller sizes, caused by high  $C_e/D_0$  ratios, and resulting in an increased amount of smaller molecular size components adsorbed. Isotherm parameters from carbon preloaded with the <3K fraction fall within the general trend observed for the data from both the humic and fulvic acids preloaded by adsorptive fractionation. These results suggest that the smaller molecular size components represent the most reactive components of the whole mixture, and the presence of larger molecular weight components does not reduce the ability of low molecular weight fractions to compete with TCE.

The effects of preloading were independent of the initial molecular size distribution or the initial mass fraction of the 10-30K fraction, as long as the amount of the <3K fraction per mass of adsorbent was constant. These results further confirm that i) smaller molecular size components are preferentially adsorbed, and the effects of preloading are due primarily to this fraction; and ii) larger molecular size components present in the 10-30K fraction do not significantly displace or otherwise interact with the smaller components.

A sequential adsorption experiment was conducted to further investigate potential displacement or other interaction mechanisms. In this experiment, the <3K and 10-30K fractions were loaded in two sequential stages. Adsorption of the larger fraction effectively



prevented subsequent adsorption of the <math>\lt;3\text{K}</math> fraction from competing with TCE, and neither fraction appeared to displace the other.

For a given percentage of TOC removal (or average molecular weight remaining in solution), greater reductions in TCE adsorption occurred with increasing ionic strength. However, the reduction in TCE adsorption was fundamentally related to the amount of humic material adsorbed, regardless of the ionic strength conditions during preloading. When the amount of adsorbed humic acid was similar, the Freundlich  $K_F$  and  $n$  values were statistically similar for all ionic strength conditions.

In systems with lower TOC loadings, the presence of calcium appears to decrease the adsorption of TCE to a greater extent than in systems where the carbon was preloaded in the absence of calcium, and this effect was observed at relatively low (0.05 mM) calcium concentrations. These results suggest that the presence of calcium increases the ability of preloaded humic material to compete with TCE. This hypothesis was confirmed by exposing a carbon preloaded in the absence of calcium to a buffer solution containing calcium. TCE adsorption from the calcium-containing buffer was considerably less than adsorption from a calcium-free buffer. An increase in the isotherm heterogeneity parameter was observed, suggesting further depletion of high-energy sites which did not occur in the absence of calcium. The association of calcium with the humic material can occur after the humic has been adsorbed, therefore, the formation of a humic calcium association in solution is not required.

TCE adsorption was measured on several different adsorbents preloaded with humic acid to evaluate the effects of adsorbent properties. Reductions in TCE adsorption due to preloading increased with decreasing extent of raw material activation, increasing extent of microporosity, and increasing affinity for TCE adsorption. Microporous adsorbents exhibited significant reductions in TCE adsorption for relatively low levels of preloading. For similar levels of preloading, TCE adsorption by preloaded macroporous carbons exhibited smaller reductions. This result suggests that when comparing adsorbents, effects of preloading do not necessarily correlate with extent of humic adsorption, and that designing microporous carbons to exclude humic materials does not appear to be a feasible approach to mitigate preloading effects.

Reductions in TCE adsorption were negligible on wood-based carbons having larger pore sizes than the predominantly microporous carbon. In fact, TCE adsorption by the macroporous wood-based carbon was increased after preloading. However, these carbons exhibited low capacities for TCE whether they were preloaded or not. Nevertheless, these results suggest that surface charge may be an adsorbent property which can be further tailored to mitigate preloading effects.

## 9.2 Recommendations for Further Research

The work summarized in this thesis represents a significant advance in the implementation of macromolecule size characterization techniques and our understanding of the interactions between macromolecular dissolved organic matter and low molecular weight synthetic organic contaminants in activated carbon adsorption systems. Several areas of future work are suggested by the results found in this study. These areas will be briefly outlined below.

---

Solute transport was modeled in this research using a simple single-parameter model. Research should be conducted to develop of membrane transport models which explicitly account for changes in the membrane transport properties as a result of i) changes in the molecular size distribution of molecules in the retentate, and ii) changes in the conditions at the membrane surface caused by concentration polarization phenomena. Studies should be conducted to identify the transport properties of mixtures, to identify whether membrane selectivity is related to mixture composition, and whether specific components of mixtures contribute primarily to membrane fouling.

Incorporation of humic adsorption into a thermodynamic framework would allow the development of equilibrium models which could be incorporated into dynamic fixed-bed reactor models to explicitly account for the effects of preloading in adsorption systems. Research should be conducted to explore the possibility of apply IAST modeling approaches to the adsorption of humic substances taking into account molecular size as a characteristic which governs adsorbability. The IAS model has been used to model HA adsorption by assuming the HA is comprised of several "fictive components"; this research

suggests that real components, based on molecular size, could be used in the IAST analysis.

While this research conclusively identified molecular size as an important consideration, DOM from different sources having the same size but much different chemical characteristics may exhibit different adsorption characteristics and preloading impacts. The effects of factors other than macromolecule size on the adsorption of humic substances and the subsequent impacts on SOC adsorption should be investigated. Macromolecule charge, aromaticity, structure, and functionality are all factors which may contribute to the adsorption behavior of humic substances and DOM.

The results obtained in this study apply directly to batch systems, but only indirectly to other reactor configurations. Research should be directed at identifying the interactions of DOM components in fixed-bed systems to evaluate the propagation of wavefronts of different size components, and the competitive interactions between DOM components and between DOM and SOC.

The humic adsorption experiments conducted in this study always had sufficient headspace to maintain oxic conditions in the adsorption reactors. The adsorption of humic substances may depend on the presence of molecular oxygen. The interactions among humic components in batch and fixed-bed systems under different redox conditions could be evaluated to simulate conditions which may develop in full-scale adsorbers.

This research showed that adsorbent properties had an affect on the adsorption of humic substances and the impact of preloading. Research into the effects of different adsorbent properties and different types of adsorbents on the adsorption of humics and the subsequent adsorption of SOC should be conducted. One area of focus would be the development of new adsorbents to mitigate preloading effects. Another area of focus would be to investigate the feasibility of process integration, such as combining ion-exchange and adsorption processes.

Research into the effects of preloaded compounds on the diffusion-controlled mass-transfer rates of SOC in batch and fixed-bed adsorption systems should be conducted. The effects carbon preloaded with humic substances on rates of TCE adsorption should be

evaluated, and the results synthesized with the equilibrium data compiled in this work to fully assess the impacts of preloading on fixed bed adsorber performance.

Research should be conducted to evaluate whether the findings of this study apply to other environmental pollutants of interest, which may exhibit physical and chemical characteristics significantly different than the TCE studied in this research. This research would include assessing whether the primary impact of preloading is on equilibrium capacity or adsorption rate, which may depend on SOC size, hydrophobicity and affinity for humic materials.

## **APPENDICES**

---

## APPENDIX A

## NOMENCLATURE

**Symbols**


---

a	absorptivity, UV/TOC, ( $L M^{-1} L^{-1}$ )
$b_l$	Langmuir adsorption energy parameter ( $L mol^{-1}$ )
b	Generalized-Lanmuir adsorption energy parameter ( $L mol^{-1}$ )
$A_m$	membrane surface area ( $L^2$ )
C	concentration ( $M L^{-3}$ )
$C_D$	drag coefficient (-)
$C_e$	equilibrium concentration ( $M L^{-3}$ )
$C_f$	feed concentration ( $M L^{-3}$ )
$C_{f0}$	initial feed concentration ( $M L^{-3}$ )
$C_0$	initial concentration or influent concentration ( $M L^{-3}$ )
$C_{surf}$	concentration at the particle surface ( $M L^{-3}$ )
$C_s$	solubility of solute ( $M L^{-3}$ )
$C_p$	permeate or pore concentration ( $M L^{-3}$ )
D	effective diffusion coefficient ( $L^2 T^{-1}$ )
$D_l$	free-liquid diffusivity ( $L^2 T^{-1}$ )
$D_h$	hydrodynamic dispersion coefficient ( $L^2 T^{-1}$ )
$D_0$	adsorbent dose or solids concentration ( $M L^{-3}$ )
$D_p$	pore-diffusion coefficient ( $L^2 T^{-1}$ )
$d_p$	particle diameter (L)
$D_s$	surface diffusion coefficient ( $L^2 T^{-1}$ )
E	site energy, ( $kJ mol^{-1}$ )
$E_0$	characteristic site energy ( $kJ mol^{-1}$ )
$E_s$	site energy corresponding to solute solubility, $C_s$ ( $kJ mol^{-1}$ )
$E^*$	site energy in excess of $E_s$ ( $E-E_s$ ) ( $kJ mol^{-1}$ )
F	Faraday constant, coulombs/mol
$h_i$	UV detector response (-)
$J_s$	solute flux ( $M L^{-2} T^{-1}$ )
$J_w$	solvent (water) flux ( $M L^{-2} T^{-1}$ )
$K_c$	advective membrane hindrance factor (-)

$K_d$	diffusional membrane hindrance factor (-)
$K_F$	Freundlich unit capacity parameter ( $M_{(\text{solute})} M_{(\text{sorbent})}^{-1} (M_{(\text{solute})} L^{-3})^n$ )
$k_f$	film mass-transfer coefficient ( $L T^{-1}$ )
$K_H$	Henry's constant ( $\text{atm m}^3 \text{mol}^{-1}$ )
$K_{oc}$	Octanol-water partition coefficient (-)
LF	Langmuir Freundlich isotherm model,
$L_p$	coefficient of hydraulic conductivity ( $L T^{-1}$ )
$M$	molarity ( $\text{mol L}^{-1}$ )
$M_i$	mass of component i (M)
$M_N$	number-averaged molecular weight ( $M \text{mol}^{-1}$ )
$M_T$	total mass of sample (M)
$M_w$	weight-averaged molecular weight ( $M \text{mol}^{-1}$ )
$MW_i$	molecular weight of component i ( $M \text{mol}^{-1}$ )
$N$	normality ( $\text{eq mol}^{-1}$ )
$n$	Freundlich or Langmuir-Freundlich exponent (-)
$p_a$	applied pressure
$P_F$	membrane permeation factor (-)
$P_v$	vapor pressure
$Q$	volumetric flowrate ( $L^3 T^{-1}$ )
$Q^0$	Langmuir-Freundlich maximum capacity parameter ( $M_{(\text{solute})} M_{(\text{sorbent})}^{-1}$ )
$q_e$	amount adsorbed, ( $M_{(\text{solute})} M_{(\text{sorbent})}^{-1}$ )
$R$	solute rejection (-)
$r$	membrane pore radius (L)
$R_p$	adsorbent particle radius (L)
$S$	specific surface area, ( $L^2 M^{-1}$ )
$t$	time (T)
$V$	volume ( $L^3$ )
$v$	velocity, subscripted to indicate direction ( $L T^{-1}$ )
$V_b$	bed void volume ( $L^3$ )
$V_i$	intraparticle void volume ( $L^3$ )
$V_o$	initial volume ( $L^3$ )
$V_p$	volume throughput ( $L^3$ )
$V_r$	final retentate volume ( $L^3$ )
$V_s$	system volume ( $L^3$ )
$v_s$	settling velocity ( $L T^{-1}$ )

**Geek Symbols**

---

$\Gamma_i$	adsorption density, (mol L <sup>-2</sup> )
$\beta_i$	regression coefficient (-)
$\sigma$	surface charge, (C L <sup>-2</sup> ) (Chapter 2)
$\sigma$	membrane reflection coefficient (-) (Chapter 4)
$\Pi$	osmotic pressure (M L <sup>-1</sup> T <sup>-2</sup> )
$\epsilon_m$	membrane porosity (-)
$\epsilon_r$	reactor void fraction (-)
$\epsilon_p$	particle void fraction (-)
$\tau$	membrane tortuosity (-)
$\mu$	absolute viscosity (M L <sup>-1</sup> T <sup>-1</sup> )
$\nu$	kinematic viscosity (L <sup>2</sup> T <sup>-1</sup> )
$\delta$	membrane thickness (L)
$\rho_l$	liquid density (M L <sup>-3</sup> )
$\rho_s$	solid density (M L <sup>-3</sup> )
$\phi$	particle sphericity (-)
$\rho_p$	particle density (M L <sup>-3</sup> )
$\omega$	diffusive membrane transport coefficient (-)

**Dimensionless Groups**

---

$N_{Pe}$	Peclet number
$N_{Sc}$	Schmidt number
$N_{Sh}$	Sherwood number
$N_{Bi}$	Biot number
$N_{Dg}$	solute distribution parameter

**Acronyms**

---

BET	Brunauer, Emmet and Teller (adsorption isotherm)
CI	Confidence Interval
CMBR	completely mixed batch reactor
DOM	dissolved organic matter
FA	fulvic acid
FBR	fixed bed reactor
GAC	granular activated carbon
GC	gas chromatograph



GF	General Freundlich (isotherm model)
GL	Generalized-Langmuir isotherm model
HA	humic acid
HPSEC	high-performance size-exclusion chromatography
HSDM	homogeneous surface diffusion model
IAST	ideal adsorbed solution theory
IHSS	International Humic Substance Society
IS	ionic strength
L	Langmuir (isotherm model)
LF	Langmuir-Freundlich (isotherm model)
MQ	Milli-Q (a water purification system and processed water)
MTZ	mass transfer zone
MW	molecular weight
MWC	molecular weight cutoff
MWD	molecular weight distribution
PSDM	pore-surface diffusion model
PSIG	pounds per square inch gauge
PSS	polystyrene sulfonate
PSDM	pore-surface diffusion model
PZC	point of zero charge (equivalent to the zero proton condition)
RP	Redlich-Peterson (isotherm model)
RSSCT	rapid small-scale column test
SOC	synthetic organic chemical or contaminant
T	Toth (isotherm model)
TCB	trichlorobenzene
TCE	trichloroethylene
TOC	total organic carbon
UF	ultrafiltration
USEPA	United States Environmental Protection Agency
UV	ultraviolet
ZPC	zero proton condition (equivalent to the point of zero charge)

## APPENDIX B

## PRELOADING DATA

Note: This Appendix represents a complete listing of all preloading experiments; however, TCE isotherms were not conducted on all preloaded carbons listed in these Tables.

**Table B1. Adsorption of Laurentian Humic Acid by F400 Carbon: Effect of  $C_0/D_0$  Ratio and Loading**

$C_0$ , mg TOC/L	$C_e$ , mg TOC/L	$q_e$ , mg/g	$D_0$ , g/L	$C_e/D_0$ , mg/g	$1-C_e/C_0$ , percent	Isotherm
62.11	21.11	9.84	4.17	5.1	66.01	EH10
62.11	35.18	13.19	2.04	17.3	43.36	EH13
55.42	37.60	16.93	1.05	35.8	31.35	EH17
55.42	42.95	23.69	0.53	81.0	22.10	EH24
55.42	43.51	45.26	0.26	167.4	21.83	EH45
27.41	14.96	11.83	1.05	14.3	44.59	EH12
27.41	17.96	17.95	0.53	33.9	34.70	EH18
27.41	20.32	26.94	0.26	78.2	25.81	EH27
13.43	6.35	6.73	1.05	6.1	52.41	EH6
13.43	8.39	9.60	0.53	15.8	37.70	EH9
12.20	7.57	17.61	0.26	29.1	37.98	EH176

**Table B2. Adsorption of Laurentian Humic Acid by F400 Carbon: Effect of Ionic Strength**

I.S., M	C <sub>0</sub> , mg TOC/L	C <sub>e</sub> , mg TOC/L	q <sub>e</sub> , mg/g	D <sub>0</sub> , g/L	C <sub>e</sub> /D <sub>0</sub> , mg/g	1-C <sub>e</sub> /C <sub>0</sub> , percent
0.05	15.2	1.86	12.67	1.05	1.8	87.76
0.05	30.6	9.05	20.47	1.05	8.6	70.42
0.05	60.9	34.19	25.37	1.05	32.6	43.86
0.10	15.3	1.28	13.32	1.05	1.2	91.63
0.10	30.7	7.63	21.92	1.05	7.3	75.15
0.10	62.2	30.68	29.94	1.05	29.2	50.68

**Table B3. Adsorption of Laurentian Humic Acid by F400 Carbon: Effect of Calcium Content**

Calcium, mM	C <sub>0</sub> , mg TOC/L	C <sub>e</sub> , mg TOC/L	q <sub>e</sub> , mg/g	D <sub>0</sub> , g/L	C <sub>e</sub> /D <sub>0</sub> , mg/g	1-C <sub>e</sub> /C <sub>0</sub> , percent
0.5	10.03	1.38	8.22	1.05	1.3	86.2
0.5	19.08	5.31	13.08	1.05	5.1	72.2
0.5	38.78	13.56	23.96	1.05	12.9	65.0
0.05	19.26	7.58	11.10	1.05	7.2	60.6
0.25	19.00	5.35	12.97	1.05	5.1	71.8
1.0	18.87	3.73	14.38*	1.05	3.6	80.2
2.0	18.86	0.82	17.14*	1.05	0.8	95.7

**Table B4. Adsorption of Laurentian Fulvic Acid by F400 Carbon: Effect of  $C_0/D_0$  Ratio and Loading**

$C_0$ , mg TOC/L	$C_e$ , mg TOC/L	$q_e$ , mg/g	$D_0$ , g/L	$C_e/D_0$ , mg/g	$1-C_e/C_0$ , percent	Isotherm
46.79	23.92	21.73	1.05	22.8	48.36	EF22
46.79	31.29	29.45	0.53	59.0	32.77	EF30
46.79	34.82	45.49	0.26	133.9	25.79	EF45
23.22	7.79	14.66	1.05	7.4	65.23	EF15
23.22	12.15	21.05	0.53	22.9	46.43	EF21
23.22	14.75	32.22	0.26	56.7	37.20	EF32
11.65	1.97	9.20	1.05	1.9	83.79	EF9
11.65	4.34	13.91	0.53	8.2	63.22	EF14
11.65	6.90	18.08	0.26	26.5	40.62	EF18

**Table B5. Adsorption of Laurentian Humic Acid by F400 Carbon: Effect of Time**

Time, days	$C_0$ , mg TOC/L	$C_e$ , mg TOC/L	$q_e$ , mg/g	$D_0$ , g/L	$C_e/D_0$ , mg/g	$1-C_e/C_0$ , percent
$\mu = 0.01$ M, Ca = 0.0 M						
5	29.77	21.61	7.75	1.05	20.6	27.41
9	30.53	19.19	10.77	1.05	18.3	37.14
19	30.52	17.86	12.03	1.05	17.0	41.48
30	30.51	16.02	13.77	1.05	15.3	47.49
40	30.76	15.68	14.33	1.05	14.9	49.02
$\mu = 0.05$ M, Ca = 0.0 M						
5	29.90	14.88	14.27	1.05	14.2	50.23
9	31.90	12.69	18.25	1.05	12.1	60.22
19	31.71	11.09	19.59	1.05	10.6	65.03
30	31.14	9.24	20.81	1.05	8.8	70.32
40	31.59	8.82	21.63	1.05	8.4	72.08
$\mu = 0.01$ M, Ca = 0.5 mM						
5	29.64	14.27	14.60	1.05	13.6	57.86
9	31.20	13.00	17.29	1.05	12.4	58.33
19	31.84	11.91	18.93	1.05	11.3	62.59
30	31.93	10.97	19.91	1.05	10.4	65.64
40	32.01	10.57	20.37	1.05	10.1	66.98

**Table B6. Adsorption of Laurentian Humic Acid by Coal-Based Carbon: Effect of Molecular Size**

Carbon Type	C <sub>0</sub> , mg TOC/L	C <sub>e</sub> , mg TOC/L	q <sub>e</sub> , mg/g	D <sub>0</sub> , g/L	C <sub>e</sub> /D <sub>0</sub> , mg/g	1-C <sub>e</sub> /C <sub>0</sub> , percent
<u>F400</u>						
<3K	8.0	1.29	12.07	0.556	2.3	83.88
<3K(2W)	4.08	3.07	25.3	0.040	76.8	24.75
<3K(4W)	4.08	2.60	39.2	0.040	65.0	36.27
3-10K	16.90	7.63	16.67	0.556	13.7	54.9
30-100K	19.04	13.91	9.23	0.556	25.0	26.9
30-100K	40.90	30.85	18.08	0.556	55.5	24.57
>100K	18.88	9.63	16.64	0.556	17.3	49.0
>100K	35.54	22.17	24.05	0.556	39.9	37.6
>3K	19.12	12.16	12.52	0.556	21.9	36.4
>3K	36.92	28.83	14.55	0.556	51.9	21.91
<u>BPL</u>						
<3K	8.0	1.33	12.00	0.556	2.4	83.38
30-100K	37.56	32.03	9.95	0.556	57.6	14.7
>100K	36.09	28.70	13.29	0.556	51.6	20.48
>3K	37.43	29.39	14.46	0.556	52.9	21.5
<u>WPLL</u>						
<3K	8.0	7.82	0.324	0.556	14.1	2.25

**Table B7. Adsorption of Laurentian Humic Acid by Wood-Based Carbon: Effect of Molecular Size**

Carbon Type	C <sub>0</sub> , mg TOC/L	C <sub>e</sub> , mg TOC/L	q <sub>e</sub> , mg/g	D <sub>0</sub> , g/L	C <sub>e</sub> /D <sub>0</sub> , mg/g	1-C <sub>e</sub> /C <sub>0</sub> , percent
<u>MICRO</u>						
<3K	8.0	7.30	1.26	0.556	13.1	8.75
>100K	35.78	33.86	3.45	0.556	60.9	5.4
>3K	38.71	36.12	4.66	0.556	65.0	6.7
<u>MESO</u>						
<3K	8.0	5.28	4.89	0.556	9.5	34.00
30-100K	38.58	35.71	5.16	0.556	64.2	7.44
>100K	37.78	29.97	14.05	0.556	53.9	20.7
>3K	38.65	35.70	5.31	0.556	64.2	7.6
<u>MACRO</u>						
<3K	8.0	3.28	8.49	0.556	5.9	59.00
>100K	37.53	26.81	19.28	0.556	48.2	28.6
>3K	39.18	31.08	14.57	0.556	55.9	20.7

**Table B8. Adsorption of Laurentian Humic Acid by F400 Carbon: Effect of Original MWD, Experimental Conditions**

Exp.	Volume <3K Fraction, ml	Volume 10-30K Fraction, ml	Initial mass of <3K Fraction	Initial mass of 10-30K Fraction	Initial <3K Mass Fraction
3K12	450	0	3.60	0.00	1.000
MWD1	500	40	3.85	4.51	0.461
MWD2	500	95	3.87	10.76	0.265
10-30K	0	120	0.00	13.50	0.000

**Table B9. Adsorption of Laurentian Humic Acid by F400 Carbon: Effect of Original MWD, Preloading Data**

Exp.	C <sub>o</sub> , mg TOC/L	C <sub>e</sub> , mg TOC/L	q <sub>e</sub> , mg/g	D <sub>o</sub> , g/L	C <sub>e</sub> /D <sub>o</sub> , mg/g	1-C <sub>e</sub> /C <sub>o</sub> , percent
3K12	8.0	1.3	12.1	0.556	2.3	83.8
MWD1	16.2	8.3	16.3	0.481	17.3	48.8
MWD2	25.2	16.7	19.3	0.435	38.4	33.7
10-30K	35.4	26.8	16.4	0.521	51.4	24.3

**Table B10. Adsorption of Laurentian Humic Acid by F400 Carbon: Effect of Sequential Loading**

Fraction	First Loading			Fraction	Second Loading			Final	
	C <sub>o</sub> , mg TOC/L	C <sub>e</sub> , mg TOC/L	q <sub>e</sub> , mg/g		C <sub>o</sub> , mg TOC/L	C <sub>e</sub> , mg TOC/L	q <sub>e</sub> , mg/g	D <sub>o</sub> , g/L	q <sub>e</sub> , mg/g
<3K	8.0	3.4	7.8	10-30K	19.7	15.2	8.1	0.556	15.9
10-30K	35.4	28.3	13.1	<3K	8.9	3.3	10.3	0.543	23.4



**Table B11. Adsorption of Laurentian Humic Acid: Effect of Carbon Type (Coal-Based)**

Carbon Type	C <sub>0</sub> , mg TOC/L	C <sub>e</sub> , mg TOC/L	q <sub>e</sub> , mg/g	D <sub>0</sub> , g/L	C <sub>e</sub> /D <sub>0</sub> , mg/g	1-C <sub>e</sub> /C <sub>0</sub> , percent
WPLL	14.8	14.18	0.59	1.05	13.5	4.22
WPLL	30.8	29.45	1.29	1.05	28.0	4.40
WPLL	60.9	59.46	1.37	1.05	56.6	2.37
FS100	15.11	8.27	6.50	1.05	7.9	45.27
FS100	30.72	20.29	9.91	1.05	19.3	33.95
FS100	59.76	45.80	13.26	1.05	43.6	23.36
BPL	14.9	7.34	7.18	1.05	7.0	50.74
BPL	30.9	18.33	11.94	1.05	17.5	40.67
BPL	61.6	42.91	17.76	1.05	40.9	30.34
BPL	19.83	11.75	15.36	0.53	22.2	40.7
BPL	39.68	26.69	24.70	0.53	50.4	32.7

**Table B12. Adsorption of Laurentian Humic Acid: Effect of Carbon Type (Wood-Based)**

Carbon Type	C <sub>0</sub> , mg TOC/L	C <sub>e</sub> , mg TOC/L	q <sub>e</sub> , mg/g	D <sub>0</sub> , g/L	C <sub>e</sub> /D <sub>0</sub> , mg/g	1-C <sub>e</sub> /C <sub>0</sub> , percent
MICRO	15.1	14.63	0.45	1.05	13.9	3.13
MICRO	30.8	28.74	1.96	1.05	27.4	6.70
MICRO	61.8	59.19	2.48	1.05	56.4	4.23
MESO	15.1	11.63	3.30	1.05	11.1	22.98
MESO	30.8	24.87	5.64	1.05	23.7	19.27
MESO	61.5	53.38	7.72	1.05	50.8	13.21
MESO	19.27	16.02	6.18	0.53	30.2	16.9
MESO	39.36	33.22	11.67	0.53	62.7	15.6
MACRO	15.1	7.36	7.35	1.05	7.0	51.26
MACRO	30.8	18.40	11.78	1.05	17.5	40.25
MACRO	61.6	43.76	16.94	1.05	41.7	28.95
MACRO	19.83	12.41	14.11	0.53	23.4	37.4
MACRO	39.23	28.32	20.74	0.53	53.4	27.8

## APPENDIX C

## ISOTHERM REGRESSION ANALYSIS

Table C1. TCE Single-Solute Isotherms

Exp.	Param.	Langmuir-Freundlich Isotherm				Freundlich Isotherm			
		Param. Est.	Std. Error	95% CI	$Q_0 b^n$	Param. Est.	95% CI		
WPLL N=37	$Q_0 \times 10^{-2}$	0.755	0.071	0.145	0.436	K <sub>F</sub>	0.422	0.389, 0.457	
	$b \times 10^4$	8.007	1.749	3.571		n	0.718		
	n	0.723	0.015	0.031		N=20			
FS100 N=23	$Q_0 \times 10^{-2}$	1.625	0.293	0.611	1.354	K <sub>F</sub>	1.451	1.245, 1.692	
	$b \times 10^4$	2.152	1.007	2.101		n	0.527		0.480, 0.574
	n	0.567	0.015	0.031		N=11			
F400 N=82	$Q_0 \times 10^{-2}$	1.833	0.380	0.760	1.279	K <sub>F</sub>	1.260	1.187, 1.337	
	$b \times 10^4$	1.700	0.891	1.782		n	0.566		0.545, 0.586
	n	0.572	0.014	0.028		N=48			
BPL N=68	$Q_0 \times 10^{-2}$	3.384	ND	ND	0.607	K <sub>F</sub>	0.600	0.561, 0.642	
	$b \times 10^4$	0.115	ND	ND		n	0.557		0.533, 0.580
	n	0.556	ND	ND		N=36			
MICRO N=26	$Q_0 \times 10^{-2}$	0.695	0.344	0.712	0.149	K <sub>F</sub>	0.138	0.127, 0.149	
	$b \times 10^4$	0.548	0.540	1.117		n	0.648		0.622, 0.674
	n	0.626	0.019	0.039		N=12			
MESO N=45	$Q_0 \times 10^{-2}$	0.240	0.051	0.103	0.077	K <sub>F</sub>	0.072	0.057, 0.091	
	$b \times 10^4$	2.305	1.049	2.12		n	0.710		0.620, 0.799
	n	0.686	0.017	0.034		N=14			
MACRO N=25	$Q_0 \times 10^{-2}$	0.242	0.112	0.232	0.025	K <sub>F</sub>	0.020	0.015, 0.026	
	$b \times 10^4$	1.894	1.486	3.082		n	0.875		0.793, 0.957
	n	0.802	0.035	0.073		N=14			

**Table C2. Adsorption of TCE by F400 Carbon Preloaded with Lauerntian Humic Acid: Effect of Macromolecule Size**

Exp.	Param.	Langmuir-Freundlich Isotherm				Freundlich Isotherm		
		Param. Est.	Std. Error	95% CI	$Q^0 b^n$	Param.	Param. Est.	95% CI
3K5M N = 30	$Q^0 \times 10^{-2}$	1.426	0.131	0.269	0.753	$K_F$	0.746	0.706, 0.788
	$b \times 10^4$	3.295	0.683	1.402		n	0.647	0.627, 0.667
	n	0.654	0.008	0.016		N = 18		
3K12 N = 29	$Q^0 \times 10^{-2}$	1.757	0.172	0.354	1.056	$K_F$	1.042	0.982, 1.107
	$b \times 10^4$	1.746	0.402	0.827		n	0.588	0.566, 0.611
	n	0.591	0.007	0.014		N = 17		
3K2W N = 15	$Q^0 \times 10^{-2}$	1.367	0.398	0.867	0.754	$K_F$	0.731	0.623, 0.858
	$b \times 10^4$	2.847	1.760	3.833		n	0.641	0.584, 0.698
	n	0.637	0.021	0.046		N = 9		
3K4W N = 30	$Q^0 \times 10^{-2}$	0.881	0.095	0.195	0.470	$K_F$	0.461	0.436, 0.488
	$b \times 10^4$	6.484	1.513	3.105		n	0.710	0.689, 0.731
	n	0.713	0.011	0.023		N = 18		
MWD1 N = 30	$Q^0 \times 10^{-2}$	1.455	0.187	0.384	1.129	$K_F$	1.097	1.050, 1.147
	$b \times 10^4$	2.724	0.847	1.738		n	0.596	0.578, 0.613
	n	0.592	0.009	0.018		N = 18		
MWD2 N = 30	$Q^0 \times 10^{-2}$	1.377	0.651	1.336	1.110	$K_F$	1.085	1.029, 1.144
	$b \times 10^4$	3.030	3.906	8.015		n	0.595	0.574, 0.616
	n	0.595	0.043	0.088		N = 18		
MWD3 N = 30	$Q^0 \times 10^{-2}$	1.125	0.117	0.240	1.244	$K_F$	1.224	1.170, 1.322
	$b \times 10^4$	6.057	1.628	3.341		n	0.582	0.556, 0.607
	n	0.608	0.011	0.023		N = 18		
10-30K	n	0.608	0.011	0.023				N = 18

**Table C3. Adsorption of TCE by F400 Carbon Preloaded with Lauerntian Humic Acid: Effect of Macromolecule Size (cont'd)**

Exp.	Param.	Langmuir-Freundlich Isotherm				Freundlich Isotherm		
		Param. Est.	Std. Error	95% CI	$Q_0 b^n$	Param. Est.	95% CI	
SEQ1 N=30	$Q_0 \times 10^{-2}$	1.137	0.124	0.254	1.006	$K_F$	0.983	0.923, 1.046
	$b \times 10^4$	4.758	1.320	2.709		n	0.613	0.589, 0.638
	n	0.618	0.011	0.023		N=18		
SEQ2 N=30	$Q_0 \times 10^{-2}$	1.537	0.125	0.257	1.162	$K_F$	1.144	1.096, 1.195
	$b \times 10^4$	2.431	0.495	1.016		n	0.583	0.565, 0.601
	n	0.587	0.007	0.014		N=18		
3-10 N=30	$Q_0 \times 10^{-2}$	1.339	0.163	0.334	1.253	$K_F$	1.231	1.168, 1.297
	$b \times 10^4$	3.641	1.131	2.321		n	0.587	0.565, 0.609
	n	0.590	0.010	0.021		N=18		
10-30 N=30	$Q_0 \times 10^{-2}$	1.125	0.117	0.240	1.244	$K_F$	1.244	1.170, 1.322
	$b \times 10^4$	6.057	1.628	3.341		n	0.582	0.556, 0.607
	n	0.608	0.011	0.023		N=18		
30-100 N=30	$Q_0 \times 10^{-2}$	1.166	0.124	0.254	1.266	$K_F$	1.249	1.168, 1.366
	$b \times 10^4$	4.935	1.395	2.863		n	0.581	0.553, 0.609
	n	0.594	0.011	0.023		N=18		
>3K N=30	$Q_0 \times 10^{-2}$	1.394	0.194	0.398	1.225	$K_F$	1.198	1.123, 1.278
	$b \times 10^4$	3.230	1.139	2.337		n	0.587	0.560, 0.614
	n	0.589	0.011	0.023		N=18		
>100K N=29	$Q_0 \times 10^{-2}$	1.160	0.133	0.273	1.413	$K_F$	1.400	1.330, 1.473
	$b \times 10^4$	4.322	1.359	2.794		n	0.555	0.532, 0.577
	n	0.569	0.011	0.023		N=17		

**Table C4. Adsorption of TCE by F400 Carbon Preloaded with TCB**

Exp.	Param.	Langmuir-Freundlich Isotherm				Freundlich Isotherm		
		Param. Est.	Std. Error	95% CI	$Q_0 b^n$	Param.	Param. Est.	95% CI
TCB/ F400 N=35	$Q_0 \times 10^{-2}$	9.581	0.565	1.154	58.17	$K_F$	55.01	52.35, 57.80
	$b \times 10^4$	18.44	4.610	9.414		n	0.390	0.372, 0.408
	n	0.445	0.010	0.020		N=48		
TCE/ F400 N=82	$Q_0 \times 10^{-2}$	1.833	0.380	0.760	1.279	$K_F$	1.260	1.187, 1.337
	$b \times 10^4$	1.700	0.891	1.782		n	0.566	0.545, 0.586
	n	0.572	0.014	0.028		N=48		
EB22 N=57	$Q_0 \times 10^{-2}$	1.182	0.263	0.532	0.152	$K_F$	0.157	0.119, 0.208
	$b \times 10^4$	3.644	1.389	2.807		n	0.819	0.728, 0.910
	n	0.841	0.024	0.049		N=30		
EB40 N=30	$Q_0 \times 10^{-2}$	ND	ND	ND	ND	$K_F$	0.236	0.214, 0.261
	$b \times 10^4$	ND	ND	ND		n	0.726	0.704, 0.747
	n	ND	ND	ND		N=30		
EB80 N=28	$Q_0 \times 10^{-2}$	ND	ND	ND	ND	$K_F$	0.096	0.080, 0.116
	$b \times 10^4$	ND	ND	ND		n	0.766	0.729, 0.802
	n	ND	ND	ND		N=28		
EB200 N=30	$Q_0 \times 10^{-2}$	ND	ND	ND	ND	$K_F$	0.021	0.017, 0.027
	$b \times 10^4$	ND	ND	ND		n	0.876	0.832, 0.920
	n	ND	ND	ND		N=30		
EB275 N=30	$Q_0 \times 10^{-2}$	ND	ND	ND	ND	$K_F$	0.019	0.016, 0.022
	$b \times 10^4$	ND	ND	ND		n	0.872	0.846, 0.899
	n	ND	ND	ND		N=30		

**Table C5. Adsorption of TCE by F400 Carbon Preloaded with Laurentian Humic Acid: Effect of  $C_0/D_0$  Ratio and Loading**

Exp.	Param.	Langmuir-Freundlich Isotherm				Freundlich Isotherm		
		Param. Est.	Std. Error	95% CI	$Q_{ob}^n$	Param.	Param. Est.	95% CI
F400	$Q^o \times 10^{-2}$	1.833	0.380	0.760	1.279	$K_F$	1.260	1.187, 1.337
N = 82	$b \times 10^4$	1.700	0.891	1.782		n	0.566	0.545, 0.586
	n	0.572	0.014	0.028		N = 48		
EH6	$Q^o \times 10^{-2}$	1.510	0.295	0.596	0.996	$K_F$	0.962	0.877, 1.055
N = 58	$b \times 10^4$	2.697	1.272	2.571		n	0.614	0.582, 0.645
	n	0.611	0.016	0.032		N = 33		
EH9	$Q^o \times 10^{-2}$	0.962	0.112	0.229	0.750	$K_F$	0.741	0.689, 0.798
N = 30	$b \times 10^4$	6.758	1.906	3.903		n	0.653	0.624, 0.681
	n	0.665	0.014	0.029		N = 20		
EH10	$Q^o \times 10^{-2}$	1.101	0.106	0.218	1.152	$K_F$	1.179	1.064, 1.306
N = 29	$b \times 10^4$	6.945	1.836	3.767		n	0.594	0.557, 0.631
	n	0.627	0.014	0.029		N = 17		
EH12	$Q^o \times 10^{-2}$	1.701	0.473	0.971	0.954	$K_F$	0.947	0.823, 1.089
N = 29	$b \times 10^4$	1.823	1.188	2.438		n	0.597	0.547, 0.647
	n	0.602	0.019	0.039		N = 17		
EH13	$Q^o \times 10^{-2}$	1.330	0.238	0.487	1.004	$K_F$	1.026	0.895, 1.176
N = 30	$b \times 10^4$	4.127	1.850	3.789		n	0.601	0.557, 0.646
	n	0.627	0.020	0.041		N = 18		
EH17	$Q^o \times 10^{-2}$	1.191	0.275	0.565	0.941	$K_F$	0.941	0.815, 1.086
N = 28	$b \times 10^4$	4.272	2.455	5.047		n	0.606	0.551, 0.661
	n	0.624	0.023	0.047		N = 18		
EH17C	$Q^o \times 10^{-2}$	0.932	0.137	0.281	0.557	$K_F$	0.556	0.515, 0.600
N = 30	$b \times 10^4$	8.907	1.960	4.014		n	0.711	0.682, 0.740
Calcium	n	0.729	0.006	0.012		N = 18		

**Table C6. Adsorption of TCE by F400 Carbon Preloaded with Laurentian Humic Acid: Effect of  $C_0/D_0$  Ratio and Loading**

Exp.	Param.	Langmuir-Freundlich Isotherm			$Q_{ob}^n$	Freundlich Isotherm		
		Param. Est.	Std. Error	95% CI		Param.	Param. Est.	95% CI
EH176 N = 30	$Q^o \times 10^{-2}$	1.139	0.086	0.176	0.709	$K_F$	0.685	0.649, 0.724
	$b \times 10^4$	4.601	0.811	1.661		n	0.671	0.647, 0.695
	n	0.661	0.008	0.016		N = 18		
EH18 N = 30	$Q^o \times 10^{-2}$	0.875	0.120	0.246	0.641	$K_F$	0.610	0.562, 0.662
	$b \times 10^4$	7.482	2.509	5.138		n	0.697	0.662, 0.732
	n	0.683	0.017	0.035		N = 18		
EH24 N = 30	$Q^o \times 10^{-2}$	1.095	0.078	0.160	0.630	$K_F$	0.604	0.558, 0.653
	$b \times 10^4$	4.086	0.706	1.446		n	0.674	0.642, 0.705
	n	0.661	0.009	0.018		N = 18		
EH27 N = 30	$Q^o \times 10^{-2}$	1.057	0.073	0.150	0.782	$K_F$	0.770	0.734, 0.807
	$b \times 10^4$	4.856	0.789	1.618		n	0.641	0.620, 0.661
	n	0.643	0.007	0.014		N = 18		
EH45 N = 28	$Q^o \times 10^{-2}$	0.785	0.059	0.121	0.387	$K_F$	0.376	0.352, 0.402
	$b \times 10^4$	6.680	1.127	2.317		n	0.731	0.705, 0.758
	n	0.726	0.012	0.025		N = 16		

**Table C7. Adsorption of TCE by F400 Carbon Preloaded with Laurentian Humic Acid: Effect of Ionic Strength**

Exp.	Param.	Langmuir-Freundlich Isotherm				Freundlich Isotherm		
		Param. Est.	Std. Error	95% CI	$Q^{obn}$	Param.	Param. Est.	95% CI
U115 N = 30	$Q^o \times 10^{-2}$	1.701	0.504	1.032	0.870	$K_F$	0.868	0.742, 1.017
	$b \times 10^4$	1.680	1.159	2.374		n	0.596	0.541, 0.650
	n	0.607	0.021	0.043		N = 18		
U130 N = 30	$Q^o \times 10^{-2}$	1.166	0.286	0.586	0.734	$K_F$	0.616	0.523, 0.725
	$b \times 10^4$	4.844	2.843	5.822		n	0.740	0.675, 0.805
	n	0.664	0.029	0.059		N = 16		
U160 N = 30	$Q^o \times 10^{-2}$	1.100	0.149	0.305	0.568	$K_F$	0.587	0.518, 0.665
	$b \times 10^4$	5.014	1.558	3.191		n	0.663	0.619, 0.707
	n	0.693	0.017	0.035		N = 16		
U515 N = 30	$Q^o \times 10^{-2}$	1.794	0.480	0.983	1.080	$K_F$	1.102	0.981, 1.239
	$b \times 10^4$	1.829	1.190	2.437		n	0.570	0.526, 0.613
	n	0.594	0.019	0.039		N = 18		
U530 N = 30	$Q^o \times 10^{-2}$	1.999	0.539	1.214	0.888	$K_F$	0.862	0.764, 0.973
	$b \times 10^4$	1.218	0.741	1.518		n	0.604	0.562, 0.646
	n	0.601	0.016	0.033		N = 18		
U560 N = 30	$Q^o \times 10^{-2}$	1.426	0.325	0.666	0.688	$K_F$	0.650	0.548, 0.771
	$b \times 10^4$	2.663	1.380	2.826		n	0.666	0.603, 0.729
	n	0.648	0.019	0.039		N = 16		



**Table C8. Adsorption of TCE by F400 Carbon Preloaded with Laurentian Humic Acid: Effect of Calcium Concentration**

Exp.	Param.	Langmuir-Freundlich Isotherm				Freundlich Isotherm		
		Param. Est.	Std. Error	95% CI	$Q^0/bn$	Param. Est.	95% CI	
C520	$Q^0 \times 10^{-2}$	1.559	0.369	0.756	0.766	$K_F$	0.772	0.707, 0.842
N = 30	$b \times 10^4$	2.671	1.301	2.664		n	0.631	0.598, 0.665
	n	0.646	0.013	0.027		N = 20		
C2520	$Q^0 \times 10^{-2}$	1.447	0.207	0.424	0.815	$K_F$	0.818	0.773, 0.867
N = 30	$b \times 10^4$	3.255	1.010	2.068		n	0.628	0.606, 0.650
	n	0.645	0.010	0.020		N = 20		
C5020	$Q^0 \times 10^{-2}$	1.093	0.141	0.285	0.806	$K_F$	0.804	0.743, 0.870
N = 58	$b \times 10^4$	7.466	2.221	4.489		n	0.667	0.631, 0.702
	n	0.682	0.015	0.030		N = 36		
C10020	$Q^0 \times 10^{-2}$	1.347	0.214	0.437	0.695	$K_F$	0.717	0.672, 0.765
N = 38	$b \times 10^4$	3.509	1.202	2.454		n	0.630	0.607, 0.653
	n	0.662	0.012	0.025		N = 23		
C20020	$Q^0 \times 10^{-2}$	2.018	0.790	1.618	1.148	$K_F$	1.147	1.038, 1.267
N = 30	$b \times 10^4$	1.687	1.456	2.982		n	0.585	0.543, 0.627
	n	0.595	0.018	0.037		N = 20		
C5010	$Q^0 \times 10^{-2}$	1.832	0.410	0.829	1.004	$K_F$	1.023	0.947, 1.105
N = 59	$b \times 10^4$	2.019	0.983	1.987		n	0.587	0.556, 0.619
	n	0.612	0.012	0.024		N = 39		
C5040	$Q^0 \times 10^{-2}$	1.119	0.256	0.517	0.630	$K_F$	0.613	0.542, 0.693
N = 56	$b \times 10^4$	5.436	2.702	5.461		n	0.690	0.644, 0.737
	n	0.689	0.022	0.044		N = 34		

**Table C9. Adsorption of TCE by F400 Carbon Preloaded with Laurentian Fulvic Acid: Effect of  $C_0/D_0$  Ratio and Loading**

Exp.	Param.	Langmuir-Freundlich Isotherm				Freundlich Isotherm		
		Param. Est.	Std. Error	95% CI	$Q_0/b^n$	Param. Est.	95% CI	
EF9	$Q^0 \times 10^{-2}$	1.659	0.235	0.483	0.827	$K_F$	0.842	0.777, 0.912
N = 28	$b \times 10^4$	2.696	0.866	1.780		n	0.624	0.595, 0.653
	n	0.645	0.012	0.025		N = 18		
EF14	$Q^0 \times 10^{-2}$	1.956	0.663	1.358	0.753	$K_F$	0.774	0.669, 0.895
N = 30	$b \times 10^4$	0.834	0.634	1.298		n	0.575	0.524, 0.626
	n	0.592	0.017	0.035		N = 16		
EF15	$Q^0 \times 10^{-2}$	1.312	0.402	0.827	0.544	$K_F$	0.475	0.277, 0.813
N = 28	$b \times 10^4$	3.907	2.674	5.498		n	0.744	0.557, 0.931
	n	0.699	0.038	0.078		N = 12		
EF18	$Q^0 \times 10^{-2}$	0.909	0.127	0.260	0.774	$K_F$	0.780	0.679, 0.897
N = 30	$b \times 10^4$	7.388	2.603	5.331		n	0.639	0.586, 0.693
	n	0.661	0.020	0.041		N = 16		
EF21	$Q^0 \times 10^{-2}$	1.638	0.403	0.825	0.619	$K_F$	0.688	0.595, 0.795
N = 30	$b \times 10^4$	1.849	0.989	2.025		n	0.592	0.541, 0.642
	n	0.649	0.018	0.037		N = 16		
EF22	$Q^0 \times 10^{-2}$	1.768	0.436	0.893	0.792	$K_F$	0.750	0.628, 0.896
N = 30	$b \times 10^4$	1.496	0.829	1.698		n	0.635	0.566, 0.704
	n	0.614	0.016	0.033		N = 16		
EF30	$Q^0 \times 10^{-2}$	1.034	0.119	0.244	0.341	$K_F$	0.322	0.272, 0.380
N = 30	$b \times 10^4$	4.337	1.103	2.259		n	0.748	0.694, 0.801
	n	0.738	0.018	0.037		N = 16		
EF32	$Q^0 \times 10^{-2}$	1.341	0.211	0.432	0.616	$K_F$	0.549	0.487, 0.618
N = 30	$b \times 10^4$	3.243	1.102	2.257		n	0.713	0.669, 0.757
	n	0.670	0.014	0.029		N = 16		
EF45	$Q^0 \times 10^{-2}$	0.849	0.085	0.174	0.362	$K_F$	0.350	0.334, 0.366
N = 30	$b \times 10^4$	5.729	1.200	2.458		n	0.743	0.724, 0.762
	n	0.731	0.011	0.023		N = 18		

**Table C10. Adsorption of TCE by F400 Carbon Preloaded with Laurentian Humic Acid: Effect of Preloading Time**

Exp.	Param.	Langmuir-Freundlich Isotherm				Freundlich Isotherm		
		Param. Est.	Std. Error	95% CI	Q <sub>0</sub> b <sup>n</sup>	Param. Est.	95% CI	
ET5 N=30	Q <sup>o</sup> x10 <sup>-2</sup>	1.438	0.088	0.180	1.247	K <sub>F</sub>	1.238	1.165, 1.316
	b x10 <sup>4</sup>	3.379	0.537	1.100		n	0.579	0.555, 0.602
	n	0.594	0.007	0.014		N=18		
ET9 N=27	Q <sup>o</sup> x10 <sup>-2</sup>	1.320	0.115	0.237	0.881	K <sub>F</sub>	0.914	0.836, 1.001
	b x10 <sup>4</sup>	3.961	0.904	1.862		n	0.627	0.595, 0.659
	n	0.632	0.012	0.025		N=17		
ET19 N=28	Q <sup>o</sup> x10 <sup>-2</sup>	1.286	0.278	0.572	0.682	K <sub>F</sub>	0.644	0.514, 0.805
	b x10 <sup>4</sup>	4.062	2.023	4.159		n	0.688	0.600, 0.776
	n	0.671	0.024	0.049		N=14		
ET30 N=30	Q <sup>o</sup> x10 <sup>-2</sup>	0.573	0.189	0.387	1.008	K <sub>F</sub>	1.028	0.933, 1.133
	b x10 <sup>4</sup>	20.56	15.17	31.07		n	0.603	0.567, 0.639
	n	0.653	0.032	0.066		N=24		
ET40 N=29	Q <sup>o</sup> x10 <sup>-2</sup>	1.441	0.164	0.337	1.188	K <sub>F</sub>	1.151	1.073, 1.234
	b x10 <sup>4</sup>	3.457	0.997	2.046		n	0.606	0.577, 0.635
	n	0.602	0.011	0.023		N=16		
ET40C N=30	Q <sup>o</sup> x10 <sup>-2</sup>	1.261	0.125	0.256	0.802	K <sub>F</sub>	0.761	0.723, 0.801
	b x10 <sup>4</sup>	4.029	0.943	1.931		n	0.660	0.640, 0.680
	n	0.647	0.010	0.020		N=16		

**Table C11. Adsorption of TCE by BPL Carbon Preloaded with Laurentian Humic Acid**

Exp.	Param.	Langmuir-Freundlich Isotherm				Freundlich Isotherm		
		Param. Est.	Std. Error	95% CI	$Q_0 b^n$	Param.	Param. Est.	95% CI
BPL	$Q^o \times 10^{-2}$	3.384	RE	RE	0.607	$K_F$	0.600	0.561, 0.642
	$b \times 10^4$	0.115	RE	RE		n	0.557	0.533, 0.580
N=68	n	0.556	RE	RE		N=36		
EH7	$Q^o \times 10^{-2}$	5.118	RE	RE	0.577	$K_F$	0.552	0.504, 0.605
	$b \times 10^4$	0.0399	RE	RE		n	0.576	0.536, 0.615
N=28	n	0.546	RE	RE		N=16		
EH12	$Q^o \times 10^{-2}$	0.761	0.169	0.347	0.527	$K_F$	0.528	0.485, 0.575
	$b \times 10^4$	3.080	1.575	3.238		n	0.599	0.565, 0.633
	n	0.615	0.015	0.031		N=20		
EH18	$Q^o \times 10^{-2}$	0.899	0.270	0.553	0.400	$K_F$	0.402	0.350, 0.461
	$b \times 10^4$	1.656	1.093	2.232		n	0.608	0.552, 0.665
N=30	n	0.622	0.018	0.037		N=18		
<3K	$Q^o \times 10^{-2}$	0.626	0.162	0.334	0.420	$K_F$	0.427	0.368, 0.495
	$b \times 10^4$	4.169	2.476	5.110		n	0.622	0.568, 0.675
N=26	n	0.643	0.023	0.047		N=15		
30100	$Q^o \times 10^{-2}$	0.724	0.066	0.135	0.609	$K_F$	0.606	0.566, 0.650
	$b \times 10^4$	3.622	0.829	1.698		n	0.590	0.564, 0.616
N=30	n	0.603	0.009	0.018		N=18		
>100K	$Q^o \times 10^{-2}$	0.625	0.098	0.201	0.619	$K_F$	0.608	0.548, 0.673
	$b \times 10^4$	5.054	2.055	4.209		n	0.598	0.559, 0.637
N=30	n	0.608	0.017	0.035		N=18		

**Table C12. Adsorption of TCE by FS100 Carbon Preloaded with Laurentian Humic Acid**

Exp.	Param.	Langmuir-Freundlich Isotherm				Freundlich Isotherm		
		Param. Est.	Std. Error	95% CI	Q <sub>0</sub> b <sup>n</sup>	Param. Est.	95% CI	
FS100 N = 23	Q <sup>o</sup> x10 <sup>-2</sup>	1.625	0.293	0.611	1.354	K <sub>F</sub>	1.451	1.245, 1.692
	b x10 <sup>4</sup>	2.152	1.007	2.101		n	0.527	0.480, 0.574
	n	0.567	0.015	0.031		N = 11		
EH7 N = 30	Q <sup>o</sup> x10 <sup>-2</sup>	1.333	0.254	.519	1.125	K <sub>F</sub>	1.093	0.989, 1.207
	b x10 <sup>4</sup>	3.453	1.775	3.625		n	0.600	0.560, 0.640
	n	0.599	0.020	0.041		N = 18		
EH10 N = 30	Q <sup>o</sup> x10 <sup>-2</sup>	1.745	0.404	0.825	1.237	K <sub>F</sub>	1.177	1.079, 1.284
	b x10 <sup>4</sup>	2.088	1.209	2.469		n	0.606	0.569, 0.643
	n	0.584	0.017	0.035		N = 18		
EH13 N = 23	Q <sup>o</sup> x10 <sup>-2</sup>	1.331	0.210	.429	1.005	K <sub>F</sub>	0.984	0.922, 1.051
	b x10 <sup>4</sup>	4.127	1.584	3.235		n	0.606	0.581, 0.632
	n	0.627	0.017	0.035		N = 20		

**Table C13. Adsorption of TCE by WPLL Carbon Preloaded with Laurentian Humic Acid**

Exp.	Param.	Langmuir-Freundlich Isotherm				Freundlich Isotherm		
		Param. Est.	Std. Error	95% CI	Q <sub>0</sub> b <sup>n</sup>	Param. Est.	95% CI	
WPLL N = 37	Q <sup>o</sup> x10 <sup>-2</sup>	0.755	0.071	0.145	0.436	K <sub>F</sub>	0.422	0.389, 0.457
	b x10 <sup>4</sup>	8.007	1.749	3.571		n	0.718	0.692, 0.745
	n	0.723	0.015	0.031		N = 20		
EH6 N = 30	Q <sup>o</sup> x10 <sup>-2</sup>	0.755	0.066	0.135	0.410	K <sub>F</sub>	0.410	0.384, 0.437
	b x10 <sup>4</sup>	6.942	1.337	2.730		n	.700	0.675, 0.726
	n	0.717	0.010	0.020		N = 20		
EH13 N = 30	Q <sup>o</sup> x10 <sup>-2</sup>	0.789	0.123	0.252	0.305	K <sub>F</sub>	0.296	0.269, 0.326
	b x10 <sup>4</sup>	5.429	1.772	3.629		n	0.741	0.706, 0.775
	n	0.739	0.018	0.037		N = 20		
EH14 N = 30	Q <sup>o</sup> x10 <sup>-2</sup>	0.807	0.129	0.264	0.322	K <sub>F</sub>	0.314	0.286, 0.345
	b x10 <sup>4</sup>	5.667	1.905	3.901		n	0.740	0.706, 0.775
	n	0.739	0.018	0.037		N = 20		

**Table C14. Adsorption of TCE by MICRO Carbon Preloaded with Laurentian Humic Acid**

Exp.	Param.	Langmuir-Freundlich Isotherm				Freundlich Isotherm		
		Param. Est.	Std. Error	95% CI	$Q^0 b^n$	Param. Est.	95% CI	
MICRO N = 26	$Q^0 \times 10^{-2}$	0.695	0.344	0.712	0.149	$K_F$	0.138	0.127, 0.149
	$b \times 10^4$	0.548	0.540	1.117		n	0.648	0.622, 0.674
	n	0.626	0.019	0.039		N = 12		
EH0 N = 30	$Q^0 \times 10^{-2}$	0.379	0.065	0.133	0.081	$K_F$	0.079	0.069, 0.090
	$b \times 10^4$	1.702	0.564	1.155		n	0.711	0.670, 0.753
	n	0.709	0.013	0.027		N = 16		
EH1 N = 30	$Q^0 \times 10^{-2}$	0.541	0.168	0.344	0.106	$K_F$	0.100	0.091, 0.100
	$b \times 10^4$	0.748	0.446	0.913		n	0.675	0.644, 0.707
	n	0.656	0.012	0.025		N = 16		
EH2 N = 30	$Q^0 \times 10^{-2}$	1.12	RE	RE	0.061	$K_F$	0.064	0.050, 0.083
	$b \times 10^4$	0.258	RE	RE		n	0.692	0.610, 0.773
	n	0.711	RE	RE		N = 14		

**Table C15. Adsorption of TCE by MESO Carbon Preloaded with Laurentian Humic Acid**

Exp.	Param.	Langmuir-Freundlich Isotherm				Freundlich Isotherm		
		Param. Est.	Std. Error	95% CI	$Q^0 b^n$	Param. Est.	95% CI	
MESO N = 45	$Q^0 \times 10^{-2}$	0.240	0.051	0.103	0.077	$K_F$	0.072	0.057, 0.091
	$b \times 10^4$	2.305	1.049	2.12		n	0.710	0.620, 0.799
	n	0.686	0.017	0.034		N = 14		
EH3 N = 30	$Q^0 \times 10^{-2}$	0.205	0.046	0.094	0.052	$K_F$	0.046	0.038, 0.056
	$b \times 10^4$	2.827	1.251	2.562		n	0.766	0.706, 0.826
	n	0.732	0.021	0.043		N = 16		
EH6 N = 30	$Q^0 \times 10^{-2}$	0.286	0.033	0.068	0.073	$K_F$	0.075	0.066, 0.085
	$b \times 10^4$	1.338	0.308	0.631		n	0.652	0.612, 0.693
	n	0.670	0.009	0.018		N = 16		
EH8 N = 30	$Q^0 \times 10^{-2}$	0.403	0.322	0.659	0.071	$K_F$	0.058	0.048, 0.071
	$b \times 10^4$	0.682	1.027	2.103		n	0.732	0.672, 0.791
	n	0.661	0.030	0.061		N = 16		

**Table C16. Adsorption of TCE by MACRO Carbon Preloaded with Laurentian Humic Acid**

Exp.	Param.	Langmuir-Freundlich Isotherm				Freundlich Isotherm		
		Param. Est.	Std. Error	95% CI	$Q^0/b^n$	Param. Est.	95% CI	
MACRO N=25	$Q^0 \times 10^{-2}$	0.242	0.112	0.232	0.025	$K_F$	0.020	0.015, 0.026
	$b \times 10^4$	1.894	1.486	3.082		n	0.875	0.793, 0.957
	n	0.802	0.035	0.073		N=14		
<3K N=24	$Q^0 \times 10^{-2}$	0.342	0.059	0.122	0.111	$K_F$	0.106	0.099, 0.115
	$b \times 10^4$	1.210	0.444	0.921		n	0.653	0.624, 0.681
	n	0.635	0.010	0.021		N=12		
EH7 N=28	$Q^0 \times 10^{-2}$	0.226	0.075	0.154	0.040	$K_F$	0.031	0.020, 0.047
	$b \times 10^4$	2.796	1.768	3.635		n	0.860	0.725, 0.996
	n	0.775	0.035	0.072		N=14		
EH12 N=27	$Q^0 \times 10^{-2}$	0.201	0.029	0.060	0.074	$K_F$	0.071	0.063, 0.079
	$b \times 10^4$	3.533	1.110	2.287		n	0.714	0.679, 0.748
	n	0.705	0.017	0.035		N=16		
EH17 N=30	$Q^0 \times 10^{-2}$	0.161	0.029	0.059	0.061	$K_F$	0.058	0.047, 0.072
	$b \times 10^4$	5.045	1.977	4.049		n	0.744	0.673, 0.814
	n	0.734	0.024	0.049		N=14		
>100K N=24	$Q^0 \times 10^{-2}$	0.356	0.114	0.236	0.131	$K_F$	0.128	0.177, 0.139
	$b \times 10^4$	1.148	0.782	1.622		n	0.623	0.589, 0.656
	n	0.618	0.015	0.031		N=14		

## APPENDIX D

## SIZE EXCLUSION CHROMATOGRAPHY ANALYSIS

Table D1. HPSEC Analysis of Natural Organic Matter Adsorption

Sample	D <sub>0</sub> , mg/L	C <sub>e</sub> , mg/L	q <sub>e</sub> , mg/g	M <sub>w</sub>	M <sub>N</sub>	M <sub>w</sub> /M <sub>N</sub>
LHA C <sub>0</sub>	0.0	23.37	0.0	5465	1861	2.94
LHA1	100.0	18.77	46.0	6143	2065	2.98
LHA2	500.0	14.78	16.9	7312	2444	2.99
LHA3	800.0	10.55	16.1	8414	2656	3.17
LHA4	1350.0	7.62	11.7	9896	3084	3.21
LHA5	1650.0	6.78	10.1	10878	2970	3.66
LHA6	1950.0	5.86	9.0	11955	3028	3.95
PHA C <sub>0</sub>	0.0	10.11	0.0	7246	2606	2.78
PHA1	67.0	9.32	11.9	6640	2672	2.48
PHA2	183.0	8.69	9.2	7117	3137	2.27
PHA3	619.0	7.23	4.7	8432	3797	2.22
PHA4	1095.0	6.21	3.8	9574	4909	1.95
PMA C <sub>0</sub>	0.0	10.00	0.0	2612	2006	1.30
PMA1	149.0	11.13	19.2	2502	2019	1.24
PMA2	1071.0	1.37	8.1	3694	2941	1.26
HRW C <sub>0</sub>	0.0	5.93	0.0	1047	774	1.35
HRW1	101.0	2.86	30.4	1314	1053	1.25
HRW2	500.0	1.77	8.3	1330	1143	1.16
HRW3	1500.0	1.35	3.1	1305	1004	1.30

LHA = Laurentian Humic Acid, PHA = IHSS Peat Humic Acid, PMA = Polymaleic Acid, HRW = Huron River Water. PHA, PMA and HRW data from Tanju Karanfil.



**Table D2. HPSEC Analyses of Laurentian Humic Acid Adsorption: Effect of Solution Chemistry**

Sample	Dose, mg/L	C <sub>e</sub> , mg/L	q <sub>e</sub> , mg/g	M <sub>w</sub>	M <sub>n</sub>	M <sub>w</sub> /M <sub>n</sub>	
<u>LHA C<sub>0</sub></u>	0.0	23.37	0.0	5465	1861	2.94	
<u>I.S. = 0.01 M</u>	100.0	18.77	46.0	6143	2065	2.98	
	500.0	14.78	16.9	7312	2444	2.99	
	800.0	10.55	16.1	8414	2656	3.17	
	1350.0	7.62	11.7	9896	3084	3.21	
	1650.0	6.78	10.1	10878	2970	3.66	
	1950.0	5.86	9.0	11955	3028	3.95	
<u>I.S. = 0.10 M</u>	100.0	16.50	68.0	7337	2403	3.05	
	300.0	10.65	42.2	8803	2863	3.07	
	500.0	6.03	34.5	11014	3516	3.13	
	900.0	2.61	23.0	14816	4020	3.69	
<u>I.S. = 0.01 M</u>	Ca=0.05 mM	1053.0	7.58	11.10	14161	4620	3.07
	Ca=0.25 mM	1053.0	5.35	12.97	20786	6996	2.97
	Ca=0.50 mM	1053.0	5.31	13.08	23575	9456	2.49
	Ca=0.50 mM	1053.0	13.56	17.14	18550	5624	3.30
	Ca=1.0 mM	1053.0	3.73	14.38	27229	4875	5.59

**Table D3. Adsorption Isotherm Conditions**

Solute	Adsorbent Size, $\mu\text{m}$	C <sub>0</sub> , mg TOC/L	Adsorbent Conc. mg/L	Ionic Strength, M	pH
FHA	165	23.37	100-2000	0.01	7.0
PHA	165	10.11	67-1095	0.002	7.0
PMA	165	10.00	149-1071	0.002	7.0
HRW	165	5.93	101-1500	0.005	7.0

## **REFERENCES**

## REFERENCES

- Abbt-Braun, G., et al. (1989) Structural Investigations of Aquatic Humic Substances by Pyrolysis-Field Ionization Mass Spectrometry and Pyrolysis-Gas Chromatography/Mass Spectrometry. *Water Research*, 23: 1579-1591.
- Adam, U.S. and Robb, I.D. (1983) Adsorption and Exchange of Polyelectrolytes on Crystal Surfaces, *J. Chem. Soc. Faraday Trans. 1*, 79: 2745.
- Adham, S.S., Snoeyink, V.L., Clark, M.M., Bersillon, J-L. (1991) *Journal AWWA*, 83: 81-91.
- Arico, A.S., Antonucci, V., Minutoli, M. and Giordano, N. (1989) The Influence of Functional Groups on the Surface Acid-Base Characteristics of Carbon Blacks. *Carbon*, 27: 337-347.
- Alberts, J.J., Schindler, J.E., Nutter, D.E., and Davis, E. (1976) Elemental, Infra-red Spectrophotometric and Electron Spin Resonance Investigations of Non-chemically Isolated Humic Material. *Geochimica et Cosmochimica Acta*, 40: 369-372.
- Alberts, J.J., Filip, Z., and Hertkorn, N. (1992) Fulvic and Humic Acids Isolated From Groundwater: Compositional Characteristics and Cation Binding. *Journal of Contaminant Hydrology*, 11: 317-330.
- Amy, G.L., Narbaitz, R.M., and Cooper, W.J. (1987) Removing VOCs From Groundwater Containing Humic Substances by Means of Coupled Air Stripping and Adsorption. *Journal AWWA*, 79(8): 49-54.
- Amy, G.L., Collins, M.R., Kuo, C.J., and King, P.H. (1987) Comparing Gel Permeation Chromatography and Ultrafiltration for the Molecular Weight Characterization of Aquatic Organic Matter. *Journal AWWA*, 79(1): 43-49.
- Bain, D.R., Cafe, M.C., Robb, I.D., and Williams, P.A. (1982) The Fractionation of Polyelectrolytes by Adsorption onto Ionic Crystals. *Journal of Colloid and Interface Science*, 88: 467-470.
- Baldauf, G. (1986) Einfluss natürlicher organischer Wasserinhaltsstoffe auf die Adsorption von Spurenstoffen in Aktivkohlenfiltern. *Vom Wasser*, 66, 21-31.
- Beckett, R., Jue, Z., and Giddings, C. (1987) Determination of Molecular Weight Distributions of Fulvic and Humic Acids Using Flow Field-Flow Fractionation. *Environmental Science and Technology*, 21: 289-295.
- Berthouex, P.M. and Hunter, W.G. (1971) Problems Associated with Planning BOD Experiments, *Journal of the Sanitary Engineering Division, ASCE*, 97, 333.
- Bird, R.B., Stewart, W. E. and Lightfoot (1960) *Transport Phenomena*, John Wiley, New York.

- Blatt, W.F. (1976) Principles and Practice of Ultrafiltration, in *Membrane Separation Processes*, Patrick Meares, Editor, Elsevier Scientific Publishing Company, New York, pp. 81-120.
- Boehm, H.P. (1966) Chemical Identification of Surface Groups. *Advances in Catalysis*, 16: 179-271.
- Brown, M. (1975) High Molecular Weight Material in Baltic Seawater. *Marine Chemistry*, 3: 253-258.
- Buffle, J., Deladoey, P., and Haerdi, W. (1978) The Use of Ultrafiltration for the Separation and Fractionation of Organic Ligands in Fresh Waters. *Analytica Chimica Acta*, 101, 339-357.
- Buffle, J. (1990) The Analytical Challenge Posed by Fulvic and Humic Acids. *Analytica Chimica Acta*, 232: 1-2.
- Buros, O.K. (1989) Desalting Practices in the United States. *Journal AWWA*, 81(11): 38-42.
- Butler, J.H.A., and Ladd, J.N. (1969) Effect of Extractant and Molecular Size on the Optical and Chemical Properties of Soil Humic Acids. *Australian Journal of Soil Research*, 7: 229-239.
- Butt, J.B. (1980) *Reaction Kinetics and Reactor Design*. Prentice-Hall, Inc., Englewood Cliffs, NJ.
- Callaway, J.Y., Gabbita, K.V. and Vilker, V.L. (1984) Reduction of Low Molecular Weight Halocarbons in the Vapor Phase Above Concentrated Humic Acid Solutions. *Environmental Science and Technology*, 18: 890.
- Cameron, R.S., Thornton, B.K., Swift, R.S., and Posner, A.M. (1972) Molecular Weight and Shape of Humic Acid from Sedimentation and Diffusion Measurements on Fractionated Extracts. *Journal of Soil Science*, 23: 394-408.
- Cannon, F.S. and Roberts, P.V. (1982) Activated Carbon: Sorption of DOC from Wastewater. *Journal of the Environmental Engineering Division, Proceedings of the ASCE*, 108(EE4):766-783.
- Carter, M.C., Weber, W.J., Jr. and Olmstead, K.P. (1991) Effects of Background Dissolved Organic Matter on TCE Adsorption by GAC. *Journal AWWA*, 73(8): 81-91.
- Cerofolini, G.F. (1974) Localized Adsorption on Heterogeneous Surfaces. *Thin Solid Films*, 23: 129-152.
- Chadik, P.A., and Amy, G.L. (1987) Molecular Weight Effects on THM Control by Coagulation and Adsorption. *Journal of Environmental Engineering*, 113: 1234.
- Chin, Y.P., and Gschwend, P.M. (1991) The Abundance, Distribution, and Configuration of Porewater Organic Colloids in Recent Sediments. *Geochimica et Cosmochimica Acta*, 55: 1309-1317.

- Chin, Y.P., and Weber, W.J., Jr. (1989) Estimating the Effects of Dispersed Organic Polymers on the Sorption of Contaminants by Natural Solids. I. A Predictive Thermodynamic Humic Substance-Organic Solute Interaction Model. *Environmental Science and Technology*, 23: 978.
- Chin, Y.P., Weber, W.J. Jr., and Eadie, B.J. (1990) Estimating the Effects of Dispersed Organic Polymers on the Sorption of Contaminants by Natural Solids. II. Sorption in the Presence of Humic and Other Natural Macromolecules. *Environmental Science and Technology*, 24: 837-842, and personal communication.
- Chin, Y.P., Aiken, G., and O'Laughlin, E. (1994) Molecular Weight, Polydispersity, and Spectroscopic Properties of Aquatic Humic Substances. *Environmental Science and Technology*, 28: 1853-1858.
- Chiou, C.T., Kile, D.T., Brinton, T.I., Malcolm, R.L., Leenheer, J.A., and MacCarthy, P. (1987) A Comparison of Water Solubility Enhancements of Organic Solutes by Aquatic Humic Materials and Commercial Humic Acids. *Environmental Science and Technology*, 21: 1231-1234.
- Conlon, W. J. and McClellan, S. A. (1989) Membrane Softening: A Treatment Process Comes of Age. *Journal AWWA*, 81: 47.
- Cornel, P.K., Summers, R.S., and Roberts, P. V. (1986) Diffusion of Humic Acid in Aqueous Solution. *Journal of Colloid and Interface Science*, 110: 149-164.
- Cosgrove, T., Obey, T.M., and Vincent, B. (1986) The Configuration of Sodium Poly(Styrene Sulfonate) at Polystyrene/Solution Interface. *Journal of Colloid and Interface Science*, 111: 409-418.
- Crittenden, J.C., and Weber, W.J., Jr. (1978a) Predictive Model for Design of Fixed-Bed Adsorbers: Parameter Estimation and Model Development. *Journal of the Environmental Engineering Division, Proceedings of the ASCE*, 104: 185.
- Crittenden, J.C., and Weber, W.J., Jr. (1978b) Predictive Model for Design of Fixed-Bed Adsorbers: Single Component Model Verification. *Journal of the Environmental Engineering Division, Proceedings of the ASCE*, 104: 433-443.
- Crittenden, J.C., and Weber, W.J., Jr. (1978c) A Model for Design of Multicomponent Adsorption Systems. *Journal of the Environmental Engineering Division, Proceedings of the ASCE*, 104(EE6): 1175-1195.
- Crittenden, J.C., Berrigan, J.K., Hand, D.W., and Lykins, B. (1987) Design of Rapid Fixed-Bed Adsorption Tests for Nonconstant Diffusivities. *Journal of Environmental Engineering*, 113: 243.
- Crittenden, J.C., Hutzler, N.J., Geyer, D.G., Oravitz, J.L., Friedman, G. (1986) Transport of Organic Compounds with Saturated Groundwater Flow: Model Development and Parameter Sensitivity. *Water Resources Research*, 22: 271-284.
- Crittenden, J.C., Reddy, P.S., Arora, H., Trynoski, J., Hand, D.W., Perram, D.L., and Summers, R.S. (1991) Predicting GAC Performance with Rapid Small-Scale Column Tests. *Journal AWWA*, 83(1): 77.

- Curtis, G.P. (1984) *Sorption of Halogenated Organic Solutes on to Aquifer Materials: Comparisons Between Laboratory Results and Field Observations*. Eng. Thesis, Department of Civil Engineering, Stanford University, Stanford, CA.
- Cussler, E.L., *Diffusion, Mass Transfer in Fluid Systems*, Cambridge University Press, New York, 1984.
- deBoer, J.H., et al. (1958) The Shapes of Capillaries, in *The Structure and Properties of Porous Materials, Proceedings of the Tenth Symposium of the Colston Research Society*, Everett, D.H. and Stone, F.S., Editors, Butterworths Scientific Publications, London, 68-94.
- deBoer, J.H., et al. (1965a) Studies on Pore Systems in Catalysts, VI. The Universal t-Curve. *Journal of Catalysis*, 4: 643-648.
- deBoer, J.H., et al. (1965b) Studies on Pore Systems in Catalysts, VII. Description of the Dimensions of Carbon Blacks by the t-Method. *Journal of Catalysis*, 4: 649-653.
- deBoer, J.H., et al. (1966) The t-Curve of Multimolecular N<sub>2</sub> Adsorption. *Journal of Colloid and Interface Science*, 21: 405-414.
- DeHaan, H., Jones, R.I., and Salonen, K. (1987) Does Ionic Strength Affect the Configuration of Aquatic Humic Substances, as Indicated by Gel Filtration? *Freshwater Biology*, 17: 453-459.
- Derylo-Marczewska, A., Jaroniec, M., Gelbin, D., and Seidel, A. (1984) Heterogeneity Effects in Single-Solute Adsorption from Dilute Aqueous Solutions on Solids. *Chemica Scripta*, 24: 239-246.
- Dobbs, R.A., and Cohen, J.M. (1980) *Carbon Isotherms for Toxic Organics*, Municipal Environmental Research Laboratory, Office of Research and Development, U.S. Environmental Protection Agency, Cincinnati, OH, EPA-600/8-80-023.
- Draper, N.R., and Smith, H. (1980) *Applied Regression Analysis*, John Wiley and Sons, New York, NY.
- Duranceau, S.J., Taylor, J.S., and Mulford, L.A. (1992) SOC Removal in a Membrane Softening Process. *Journal AWWA*, 84: 68-78.
- Edzwald, J.K., Becker, W.C., and Wattier, K.L. (1985) Surrogate Parameters for Monitoring Organic Matter and THM Precursors. *Journal AWWA*, 77: 122-132.
- El-Rehaili, A.M., and Weber, W.J., Jr. (1987) Correlation of Humic Substance Trihalomethane Formation Potential and Adsorption Behavior to Molecular Weight Distribution in Raw and Chemically Treated Waters. *Water Research*, 21: 573-582.
- El-Rehaili, A.M., and Weber, W.J., Jr. (1986) The Effects of Humic Acid Speciation on Adsorption and Trihalomethane Formation Potential. *Proceedings of the American Water Works Association Annual Conference*, Denver CO.
- Endicott, D.D. and Weber, W.J., Jr. (1985) Lumped-Parameter Modeling of Multicomponent Adsorption in the Treatment of Coal-Conversion Wastewater by GAC. *Environmental Progress*, 4: 105-111.

- Fettig, J., and Sontheimer, H. (1987a) Kinetics of Adsorption on Activated Carbon: I. Single Solute Systems. *Journal of Environmental Engineering*, 113: 764-779
- Fettig, J., and Sontheimer, H. (1987b) Kinetics of Adsorption on Activated Carbon: II. Multisolute Systems. *Journal of Environmental Engineering*, 113: 780-794
- Fettig, J., and Sontheimer, H. (1987c) Kinetics of Adsorption on Activated Carbon: III. Natural Organic Matter. *Journal of Environmental Engineering*, 113: 795-810
- Fu, P.L.K. and Symons, J.M. (1990) Removing Aquatic Organic Substances by Anion Exchange Resins. *Journal AWWA*, 82: 70-77.
- Ghosh, K., and Schnitzer, M. (1979), UV and Visible Adsorption Spectroscopic Investigation in Relation to Macromolecular Characteristics of Humic Substances. *Journal of Soil Science*, 30: 735.
- Ghosh, K., and Schnitzer, M. (1980) Macromolecular Structures of Humic Substances. *Soil Science*, 129: 266-276
- Glaze, W.H., and Wallace, J.L. (1984) Control of Trihalomethane Precursors in Drinking Water: Granular Activated Carbon With and Without Preozonation. *Journal AWWA*, 76: 68-75
- Gloor, R., Leidner, K., Wuhrmann, K., and Fleishmann, T. (1981) Exclusion Chromatography with Carbon Detection. A Tool for Further Characterization of Dissolved Organic Carbon. *Water Research*, 15: 457-462.
- Graham, D. (1955) Characterization of Physical Adsorption Systems. III. The Separate Effects of Pore Size and Surface Acidity Upon the Adsorbent Capacities of Activated Carbons. *Journal of Physical Chemistry*, 59: 896-900.
- Gregg, S.J., and Sing, K.S.W. (1982) *Adsorption, Surface Area and Porosity*, Academic Press, New York.
- Hallstedt, P.A., et al. (1986) Application of the Hazard Ranking System to the Prioritization of Organic Compounds Identified at Hazardous Waste Remedial Action Sites, *Hazardous Waste and Hazardous Materials*, 3: 221-231.
- Halsey, G. and Taylor, H.S. (1947) The Adsorption of Hydrogen on Tungsten Powders. *The Journal of Chemical Physics*, 15: 624-630.
- Hand, D.W., Crittenden, J.C., Arora, H., Miller, J.M., and Lykins, B.W., Jr. (1989) Designing Fixed-Bed Adsorbers to Remove Mixtures of Organics. *Journal AWWA*, 81: (1), 67-77.
- Hand, D.W., Crittenden, J.C., and Thacker, W.E. (1983) User-Oriented Batch Reactor Solutions to the Homogeneous Surface Diffusion Model. *Journal of Environmental Engineering*, 109: 82-101.
- Hand, D.W., Crittenden, J.C., and Thacker, W.E. (1984) Simplified Models for Design of Fixed-Bed Adsorption Systems. *Journal of Environmental Engineering*, 110: 440-456.

- Harrington G.W., and DiGiano, F.A. (1989) Adsorption Equilibria of Natural Organic Matter After Ozonation. *Journal AWWA*, 81(6): 93-101.
- Harvey, G.R., Boran, D.A., Chesal, L.A., and Tokar, J.M. (1983) The Structure of Marine Fulvic and Humic Acids. *Marine Chemistry*, 12, 119-132
- Hashimoto, K., Miura, K., Yoshikawa, F., and Imai, I. (1979) Change in Pore Structure of Carbonaceous Materials During Activation and Adsorption Performance of Activated Carbon. *Industrial and Engineering Chemistry Process Design and Development*, 18: 72-80.
- Hatcher, P.G., and Spiker, E.C. (1988) Selective Degradation of Plant Biomolecules, in *Humic Substances and Their Role in the Environment*, E.H. Frimmel and R.F. Christman, Eds., John Wiley and Sons Limited, New York, pp. 59-74.
- Hayase, K., and Tsubota, H. (1983) Sedimentary Humic Acid and Fulvic Acid as Surface Active Substances. *Geochimica et Cosmochimica Acta*, 47, 947-952.
- Hedges, J.I. (1988) Polymerization of Humic Substances in Natural Environments, in *Humic Substances and Their Role in the Environment*, E.H. Frimmel and R.F. Christman, Eds., John Wiley and Sons Limited, New York, pp. 45-58.
- Heimenz, P.C. (1986) *Principles of Colloid and Surface Chemistry*, Marcel Dekker, Inc., New York.
- Hem, J.D. (1970) *Study and Interpretation of the Chemical Characteristics of Natural Water. Second Edition*. Geological Survey Water Supply Paper 1473, U.S. Government Printing Office, Washington, D.C.
- Hennig, G.R. (1962) Catalytic Oxidation of Graphite. *Journal of Inorganic Nuclear Chemistry*, 24: 1129-1137.
- Hering, J.G., and Morel, F.M.M. (1988) Humic Acid Complexation of Calcium and Copper. *Environmental Science and Technology*, 22: 1234-1237.
- Hine, P.T., and Bursill, D.B. (1984) Gel Permeation Chromatography of Humic Acid: Problems Associated with Sephadex Gel. *Water Research*, 11: 1461-1465.
- Hlady, V., Lyklema, J., and Fleer, G. J. (1982) Effect of Polydispersity on the Adsorption of Dextran on Silver Iodide. *Journal of Colloid and Interface Science*, 87: 395-406.
- Howard, P.H. (1989) *Handbook of Environmental Fate and Exposure Data, Volume 1*, Lewis Publishers, Chelsea, MI.
- Howard, P.H. (1990) *Handbook of Environmental Fate and Exposure Data, Volume 2* Lewis Publishers, Chelsea, MI.
- Huang, C.P. (1980) Chemical Interactions Between Inorganics and Activated Carbon. In *Carbon Adsorption Handbook*, Cheremisinoff, P.N. and Ellerbusch, F., Editors, Ann Arbor Science, Ann Arbor MI.
- Huang, C.P., and Wu, M.H. (1977) The Removal of Chromium (VI) from Dilute Aqueous Solution by Activated Carbon. *Water Research*, 11: 673-688.



- Huang, C.P., et al. (1985) The Removal of Cobalt (II) from Water by Activated Carbon. *AIChE Symposium Series, Separation of Heavy Metals*, 81, 243: 85-98.
- Jagiello, J., Badosz, T.J., and Schwarz, J.A. (1992) Inverse Gas Chromatographic Study of Activated Carbons: The Effect of Controlled Oxidation on Microstructure and Surface Chemical Functionality. *Journal of Colloid and Interface Science*, 151: 433-445.
- Jaroniec, M. (1975) Adsorption on Heterogeneous Surfaces: The Exponential Equation for the Overall Adsorption Isotherm. *Surface Science*, 50: 553-564.
- Jodellah, A.M. (1985) "Removal of Humic Substances and THM Precursors by Activated Carbon: Effects of Heterogeneity, Chemical Pretreatment, and System Characteristics", Ph.D. Thesis, University of Michigan, Ann Arbor.
- Jodellah, A.M., and Weber, W.J. Jr. (1985) Controlling Trihalomethane Formation Potential by Chemical Treatment and Adsorption. *Journal AWWA*, 77: 95-100.
- Juhola, A.J. (1975) Iodine Adsorption and Structure of Activated Carbons. *Carbon*, 13: 437-442.
- Kilduff, J.E., and Weber, W.J., Jr. (1992) Transport and Separation of Organic Macromolecules in Ultrafiltration Processes. *Environmental Science and Technology*, 26: 569-577.
- Knuutinen, J., Virkki, L., Mannila, P., Mikkelsen, P., Paasivirta, J., and Herve, S. (1983) High-Performance Liquid Chromatographic Study of Dissolved Organic Matter in Natural Waters. *Water Research*, 22: 985-990.
- Komorita, J.D. and Snoeyink, V.L. (1985) Technical Note: Monochloramine Removal from Water by Activated Carbon. *Journal AWWA*, 77: 62-64
- Koopal, L. (1981) The Effect of Polymer Polydispersity on the Adsorption Isotherm. *Journal of Colloid and Interface Science*, 83: 116-129.
- Kwak, J.C.T., and Nelson, R.W.P. (1977) Ultrafiltration of Fulvic and Humic Acids, a Comparison of Stirred Cell and Hollow Fiber Techniques. *Geochimica et Cosmochimica Acta*, 41: 993-996.
- Ladd, J.N. (1969) The Extinction Coefficients of Soil Humic Acids Fractionated by Sephadex Gel Filtration. *Soil Science*, 107: 303-306.
- Lafrance, P., and Mazet, M. (1989) Adsorption of Humics Substances in the Presence of Sodium Salts. *Journal AWWA*, 81: 155-162
- Laine, J-M., Clark, M.M., Mallevalle, J. (1990) Ultrafiltration of Lake Water: Effect of Pretreatment on the Partitioning of Organics, THM Formation Potential, and Flux. *Journal AWWA*, 82: 82-87.
- Lakshminarayanaiah, N. (1965) Transport Phenomena in Artificial Membranes. *Chemical Reviews*, 65: 491-557.

- Lebrun, R.E., Bouchard, C.R., Rollin, A.L., Matsuura, T., and Sourirajan, S. (1989) Computer Simulation of Membrane Separation Processes. *Chemical Engineering Science*, 44: 313-320.
- Lee, M.C., Crittenden, J.C., Snoeyink, V.L., and Ari, M. (1983) Design of Carbon Beds to Remove Humic Substances. *Journal of the Environmental Engineering Division, Proceedings of the ASCE*, 109: 631.
- Lee, M.C., Snoeyink, V.L., and Crittenden, J.C. (1981) Activated Carbon Adsorption of Humic Substances. *Journal AWWA*, 73: 440-446.
- Liao, W. et al. (1982) Structural Characterization of Aquatic Humic Material. *Environmental Science and Technology*, 16:403-410.
- Lippens, B.C., et al. (1964) Studies on Pore Systems in Catalysts, I. The Adsorption of Nitrogen; Apparatus and Calculation. *Journal of Catalysis*, 3: 32-37.
- Liu, K.T., and Weber, W.J., Jr. (1981) Characterization of Mass Transfer Parameters for Adsorber Modeling and Design. *Journal of the Water Pollution Control Federation*, 53: 1541-1550.
- Logan, B.E., and Jiang, Q. (1990) Molecular Size Determination of Dissolved Organic Matter. *Journal of Environmental Engineering*, 116: 1046-1062.
- Lykins, B.W., Jr., Clark, R.M., and Adams, J.Q. (1988) Granular Activated Carbon for Controlling THMs. *Journal AWWA*, 80: 85-92
- Ma, R.P., Gooding, C.H., and Alexander, W.K. (1985) A Dynamic Model for Low-Pressure, Hollow-Fiber Ultrafiltration. *AIChE Journal*, 31:1728-1732
- Macko, C., Maier, W.J., Eisenreich, S.J., and Hoffman, M.R. (1979) Ultrafiltration Characterization of Aquatic Organics. *AIChE Symposium Series*, 75: 162-169
- Malcolm, R.L. and MacCarthy, P. (1986) Limitations in the Use of Commercial Humic Acids in Water and Soil Research. *Environmental Science and Technology*, 20: 904-911.
- Malcolm, R.L. (1990) The Uniqueness of Humic Substances in Each of Soil Stream and Marine Environments. *Analytica Chimica Acta*, 232: 19-30.
- Mansour, A., et al. (1982) Numerical solution of Liquid Phase Multicomponent Adsorption in Fixed Beds. *American Institute of Chemical Engineers Journal*, 28: 765-772.
- Mathuthu, A.S., and Ephriam, J.H. (1993) Calcium Binding by Fulvic Acids Studied by an Ion Selective Electrode and an Ultrafiltration Method. *Talanta*, 40: 521-526.
- Mattson, J.S., and Mark, H.B. (1971) *Activated Carbon*, Marcel Dekker, Inc., New York.
- Mattson, J.S., H.B. Mark, Jr., Malbin, M.D., Weber, W.J., Jr., and Crittenden, J.C. (1969) Surface Chemistry of Active Carbon: Specific Adsorption of Phenols. *Journal of Colloid and Interface Science*, 31:116.

- Mazet, M., Yaacoubi, A. and Lafrance, P. (1988) The Influence of Metal Ions Released by an Activated Carbon on the Adsorption of Organics: The Role of Calcium Ions. *Water Research*, 22: 1321-1329.
- McCarthy, J.F., and Jimenez, B.D. (1985) Interactions Between Polycyclic Aromatic Hydrocarbons and Dissolved Organic Matter. *Environmental Science and Technology*, 19: 1072-1076.
- McCreary, J.J., and Snoeyink, V.L. (1980) Characterization and Activated Carbon Adsorption of Several Humic Substances. *Water Research*, 14: 151-160.
- McGinley, P.M., L.E. Katz, and W.J. Weber, Jr. (1993) A Distributed Reactivity Model for Sorption by Soils and Sediments: II. Competitive Sorption of Hydrophobic Compounds. *Environmental Science and Technology*, 27: 1524-1531.
- Metcalf and Eddy, Inc. (1972) *Wastewater Engineering: Treatment, Disposal, Reuse*. Second Edition, Rev. George Tchobanoglous. McGraw Hill, New York, pp. 203-204.
- Micheals, A.S. (1968) New Separation Technique for the CPI. *Chemical Engineering Progress*, 64: 31-43.
- Micheals, A.S. (1968) *Ultrafiltration*, Amicon Corporation, Lexington, MA.
- Miles, C.J., and Brezonik, P.L. (1983) High-performance Size Exclusion Chromatography of Aquatic Humus. *Journal of Chromatography*, 259, 499-503
- Misra, D.N. (1970) New Adsorption Isotherm for Heterogeneous Surfaces. *The Journal of Chemical Physics*, 52: 5499-5501.
- Moore, R.M., Burton, J.D., Williams, P.J., and Young, M.L. (1979) The Behavior of Dissolved Organic Material, Iron, and Manganese in Estuarine Mixing. *Geochimica et Cosmochimica Acta*, 43, 919-926.
- Morel, F.M.M. (1983) *Principles of Aquatic Chemistry*. John Wiley, New York.
- Muller, G., Radke, C. J., and Prausnitz, J. M. (1985) Adsorption of Weak Organic Electrolytes from Dilute Aqueous Solution onto Activated Carbon. *Journal of Colloid and Interface Chemistry*, 103: 466-483.
- Muller, G., Radke, C. J., and Prausnitz, J. M. (1980) Adsorption of Weak Organic Electrolytes from Aqueous Solution on Activated Carbon. Effect of pH. *Journal of Physical Chemistry*, 84: 369-376.
- Neretnieks, I. (1976) Adsorption in Finite Bath and Countercurrent Flow with Systems Having a Nonlinear Isotherm. *Chemical Engineering Science*, 31: 107-114.
- Nkedi Kizza, P, Rao, P.S.C., and Hornsby, A.G. (1985) Influence of Organic Cosolvents on Sorption of Hydrophobic Organic Chemicals by Soils. *Environmental Science and Technology*, 19: 975-979
- Ogino, K., Yukihiro, K., Minoura, T., Agui, W., and Abe, M. (1988) Removal of Humic Substances Dissolved in Water. *Journal of Colloid and Interface Science*, 121: 161-169.

- Ogura, N. (1974) Molecular Weight Fractionation of Dissolved Organic Matter in Coastal Seawater by Ultrafiltration. *Marine Biology*, 24: 305-312.
- Ohashi, H., Sugawara, T., Kikuchi, K., and Konno, H. (1981) Correlation of Liquid-Side Mass Transfer Coefficient for Single Particles and Fixed Beds. *Journal of Chemical Engineering of Japan*, 14: 433-438.
- Olmstead, K.P., and Weber, W.J., Jr. (1990) Statistical Analysis of Mass Transfer Parameters for Sorption Processes and Models. *Environmental Science and Technology*, 24: 1693.
- Opong, W.S. and Zydney, A.L. (1991) Diffusive and Convective Protein Transport through Asymmetric Membranes. *AIChE Journal*, 37:1497-1510.
- Papenhuijzen, J., Fleer, G.J., and Bijsterbosch, B.H. (1985a) Adsorption of Polystyrene Sulfonate on Polyoxymethylene Single Crystals at High Ionic Strength. *Journal of Colloid and Interface Science*, 104: 530.
- Papenhuijzen, J. Van Der Schee, H.A. and Fleer, G.J. (1985b) Polyelectrolyte Adsorption, I. A New Lattice Theory. *Journal of Colloid and Interface Science*, 104: 540-552.
- Pefferkorn, E., Dejardin, P., and Varoqui, R. (1978) Derivation by Hydrodynamics of the Structural Characteristics of Adsorbed Polymers at Liquid-Solid Interfaces. *Journal of Colloid and Interface Science*, 63: 353-361.
- Pierce, C. (1959) Effects of Interparticle Condensation on Heats of Adsorption and Isotherms of Powder Samples. *Journal of Physical Chemistry*, 63: 1076-1079.
- Pirbazari, M.P., and Weber, W.J. Jr. (1984a) Removal of Dieldrin from Water by Activated Carbon. *Journal of Environmental Engineering*, 110: 656-669.
- Pirbazari, M.P., and Weber, W.J. Jr. (1984b) Technical Note: Adsorption of p-Dichlorobenzene from Water. *Journal AWWA*, 76: 82-84
- Pontius, F.W. (1990) Complying With the New Drinking Water Regulations. *Journal AWWA*, 82: 32-52.
- Porter, M.C., and Nelson, L. (1972) Ultrafiltration in the Chemical, Food-Processing, Pharmaceutical, and Medical Industries. In *Recent Developments in Separation Science*, Volume II, CRC Press, Cleveland, pp. 227-267.
- QuantaChrome Corporation, Autosorb-1 Operation Manual. QuantaChrome, Syosset, NY.
- Radke, C.J., and Prausnitz, J.M. (1972) Thermodynamics of Multi-Solute Adsorption from Dilute Liquid Solutions. *American Institute of Chemical Engineers Journal*, 18: 761-768.
- Ramachandran, R., and Somasundaran, P. (1987) Competitive Adsorption of Polyelectrolytes: A Size Exclusion Study. *Journal of Colloid and Interface Science*, 120: 184-188.
- Randtke, S.J. (1988) Organic Contaminant Removal by Coagulation and Related Process Combinations. *Journal AWWA*, 80: 40-56.

- Randtke, S.J., and Jepsen, C.P. (1982) Effects of Salts on Activated Carbon Adsorption of Fulvic Acids. *Journal AWWA*, 74: 84-93
- Randtke, S.J., and Snoeyink, V.L. (1983) Evaluating GAC Adsorptive Capacity. *Journal AWWA*, 75: 406-413
- Ranz, W.E., and Marshall, W.R. (1952) Evaporation from Drops. *Chemical Engineering Progress*, 48: 141.
- Rausa, R., Mazzolari, E., and Calemma, V. (1991) Determinations of Molecular Size Distributions of Humic Acids by High Performance Size Exclusion Chromatography. *Journal of Chromatography*, 541: 419-429.
- Reid, P.M., Wilkinson, A.E., Tipping, E., and Jones, M.N. (1990) Determination of Molecular Weights of Humic Substances by Analytical (UV Scanning) Ultracentrifugation. *Geochimica et Cosmochimica Acta*, 54: 131-138.
- Reinhard, M. (1984) Molecular Weight Distribution of Dissolved Organic Carbon and Dissolved Organic Halogen in Advanced Treated Wastewaters. *Environmental Science and Technology*, 18: 410-415.
- Reuter, J.H., and Perdue, E.M. (1981) Calculation of Molecular Weights of Humic Substances from Colligative Data: Application to Aquatic Humus and its Molecular Size Fractions. *Geochimica et Cosmochimica Acta*, 45: 2017-2022
- Roberts, P.V., Cornel, P., and Summers, R.S. (1985) External Mass-Transfer Rate in Fixed-Bed Adsorption. *Journal of Environmental Engineering*, 111: 891-905.
- Rossi, C., Bianchi, U., and Magnasco, V. (1958) Diffusion and Viscosity Measurements on Macromolecules in Solution. *Journal of Polymer Science*, 110: 175-186
- Safe Drinking Water Act Amendments of 1986 (June 1986), PL 99-339.
- Saito, Y., and Hayano, S. (1979) Application of High-Performance Aqueous Gel Permeation Chromatography to Humic Substances from Marine Sediment. *Journal of Chromatography*, 177: 390-392.
- Schlautman, M.A., and Morgan, J.J. (1994) Adsorption of Aquatic Humic Substances on Colloidal-size Aluminum Oxide Particles: Influence of Solution Chemistry. *Geochimica et Cosmochimica Acta*, 58:4293-4303.
- Schulten, H.R., and Schnitzer, M. (1993) A State of the Art Structural Concept for Humic Substances. *Naturwissenschaften*, 80: 29-30.
- Schnitzer, M. (1991) Soil Organic Matter -- The Next 75 Years. *Soil Science*, 151: 41-58.
- Seidel, A., and Carl, P.S. (1989) The Concentration Dependence of Surface Diffusion for Adsorption on Energetically Heterogeneous Adsorbents. *Chemical Engineering Science*, 44: 189-194.
- Semmens, M.J., and Staples, A.B. (1986) The Nature of Organics Removed During Treatment of Mississippi River Water. *Journal AWWA*, 78: 76-81

- Semmens, M.J., Norgaard, G.E., Hohenstein, G., and Staples, A.B. (1986) Influence of pH on the Removal of Organics by Granular Activated Carbon. *Journal AWWA*, 78: 89-93
- Sherwood, T.K., Pigford, R.L., and Wilke, C.R. (1975) , *Mass Transfer*, McGraw Hill, New York.
- Sips, R. (1948) On the Structure of a Catalyst Surface. *Journal of Chemical Physics*, 16: 490-495.
- Sips, R. (1950) On the Structure of a Catalyst Surface II. *Journal of Chemical Physics*, 18: 1024-1026.
- Skoog, D.A. (1985) *Principles of Instrumental Analysis*, Saunders College Publishing, New York.
- Smith, E.H. (1987), *Modeling the Adsorption of Hazardous Organic Compounds by Activated Carbon in the Presence of Background Dissolved Organic Matter*. PhD. Thesis, University of Michigan, Ann Arbor, MI.
- Smith, E.H., Tseng, S., and Weber, W.J. Jr. (1987) Modeling the Adsorption of Target Compounds by GAC in the Presence of Background Organic Matter. *Environmental Progress*, 6: 18-25
- Smith, E.H., and Weber, W.J. Jr. (1988) Modeling Activated Carbon Adsorption of Target Organic Compounds from Leachate-Contaminated Groundwaters. *Environmental Science and Technology*, 22: 313-321
- Smith, E.H., and Weber, W.J. Jr. (1989) Evaluation of Mass Transfer Parameters for Adsorption of Organic Compounds from Complex Organic Matrices. *Environmental Science and Technology*, 23: 713-722.
- Smith, E.H. (1991) Evaluation of Multicomponent Adsorption Equilibria for Organic Mixtures Onto Activated Carbon. *Water Research*, 25: 125-134.
- Snoeyink, V.L., Weber, W.J., Jr., and Mark, H.B., Jr. (1969) Sorption of Phenol and Nitrophenol by Active Carbon. *Environmental Science and Technology*, 3: 918.
- Snoeyink, V.L., and Weber, W.J. Jr. (1967) The Surface Chemistry of Active Carbon, A Discussion of Structure and Surface Functional Groups. *Environmental Science and Technology*, 1: 228-234.
- Soltanieh, M., and Gill, W.N. (1981) Review of Reverse Osmosis Membranes and Transport Models. *Chemical Engineering Communications*, 12: 279-363.
- Sontheimer, H., Crittenden, J.C., and Summers, R.S. (1989) *Activated Carbon for Water Treatment*. Second Edition. DVGW-Forschungsstelle, FRG.
- Speth, T.F. (1991) Evaluating Capacities of GAC Preloaded with Natural Water. *Journal of Environmental Engineering*, 117: 66-79.
- Speth, T.F., and Miltner, R.J. (1989) Effect of Preloading on the Scale-Up of GAC Microcolumns. *Journal AWWA*, 81: 141-148.

- Spiteller, M., and Schnitzer, M. (1983) A Comparison of the Structural Characteristics of Polymaleic Acid and a Soil Fulvic Acid. *Journal of Soil Science*, 34: 525-537.
- Starek, J., Zukal, A., and Rathousky, J. (1994) Comparison of the Adsorption of Humic Acids from Aqueous Solutions on Active Carbon and Activated Charcoal Cloths. *Carbon*, 32: 207-211.
- Steelink, C. (1977) Humates and Other Organic Substances in the Aquatic Environment. *Journal of Chemical Education*, 54: 599-603
- Steenberg, B. (1944) *Adsorption and Exchange of Ions on Activated Charcoal*, Almquist and Wiksell, Uppsala, Sweden.
- Stewart, A.J., and Wetzel, R.G. (1981) Asymmetric Relationships Between Absorbance, Fluorescence, and Dissolved Organic Carbon. *Limnology and Oceanography*, 26: 590-597.
- Stumm, W.S., and Morgan, J.J. (1981) *Aquatic Chemistry*, John Wiley and Sons, New York.
- Summers, R.S., and Roberts, P.V. (1988a) Activated Carbon Adsorption of Humic Substances, I. Heterodisperse Mixtures and Desorption. *Journal of Colloid and Interface Science*, 122: 367-381.
- Summers, R.S., and Roberts, P.V. (1988b) Activated Carbon Adsorption of Humic Substances, II. Size Exclusion and Electrostatic Interactions. *Journal of Colloid and Interface Science*, 122: 382-397.
- Summers, R.S., Cummings, L., et al. (1992) *Standardized Protocol for the Evaluation of GAC*. American Water Works Association Research Foundation, Denver, CO.
- Summers, R.S., Haist, B., Koehler, J., Ritz, J., and Zimmer, G. (1989) The Influence of Background Organic Matter on GAC Adsorption. *Journal AWWA*, 81: 66-74
- Suzuki, M., and Kawazoe, K. (1974) Batch Measurement of Adsorption Rate in an Agitated Tank -- Pore Diffusion Kinetics with Irreversible Isotherm. *Journal of Chemical Engineering of Japan*, 7: 346-350.
- Suzuki, M., and Kawazoe, K. (1975) Effective Surface Diffusion Coefficients of Volatile Organics on Activated Carbon During Adsorption from Aqueous Solution. *Journal of Chemical Engineering of Japan*, 8: 379-382.
- Suzuki, M., Kawai, T., and Kawazoe, K. (1976) Adsorption of Poly(oxyethylene) of Various Molecular Weights from Aqueous Solutions on Activated Carbon. *Journal of Chemical Engineering of Japan*, 9: 203-208.
- Swift, R.S. and Posner, A.M. (1972) Nitrogen, Phosphorus and Sulphur Contents of Humic Acids Fractionated with Respect to Molecular Weight. *Journal of Soil Science*, 23: 50-57
- Swift, R.S., Thornton, B.K., and Posner, A.M. (1970) Spectral Characteristics of a Humic Acid Fractionated with Respect to Molecular Weight Using an Agar Gel. *Soil Science*, 110: 93-99.

- Swift, R.S., Leonard, R.L., Newman, R.H., and Theng, B.K.G. (1992) Changes in Humic Acid Composition with Molecular Weight as Detected by  $^{13}\text{C}$ -Nuclear Magnetic Resonance Spectroscopy. *The Science of the Total Environment*, 117/118: 53-61.
- Tan, L., and Sudak, R. G. (1992) Removing Color From a Groundwater Source. *Journal AWWA*, 84:79-87.
- Thacker, W.E., Crittenden, J. C., and Snoeyink, V.L. (1984), Modeling of Adsorber Performance: Variable Influent Concentration and Comparison of Adsorbents. *Journal of the Water Pollution Control Federation*, 56: 243.
- Tipping, E. (1993) Modeling the Competition between Alkaline Earth Cations and Trace Metal Species for Binding by Humic Substances. *Environmental Science and Technology*, 27: 520-529.
- Tipping, E., Backes, C.A., and Hurley, M.A. (1988) The Complexation of Protons, Aluminum, and Calcium by Aquatic Humic Substances: A Model Incorporating Binding Site Heterogeneity and Macroionic Effects. *Water Research*, 22:597-611.
- Thurman, E.M., Wershaw, R.L., Malcolm, R.L., and Pinckney, D.J. (1982) Molecular Size of Aquatic Humic Substances. *Organic Geochemistry*, 4: 27-35
- Tóth, J., Rudzinski, W., Waksmundzki, A., Jaronic, M., and Sokolowski, S. (1974) *Acta Chem. Acad. Sci. Hung.* 82: 11.
- Tuschall, J.R., and Brezonik, P.L. (1980) Characterization of Organic Nitrogen in Natural Waters: Its Molecular Size, Protein Content, and Interactions With Heavy Metals. *Limnology and Oceanography*, 25: 495-504
- Urano, K., Koichi, Y., and Yamamoto, E. (1982) Equilibria for Adsorption of Organic Compounds on Activated Carbons in Aqueous Solutions, II. Generalization and a Prediction Method of Adsorption Isotherms. *Journal of Colloid and Interface Science*, 86: 43-50.
- Wauchope, R. D., Savage, K. E., and Koskinen, W. C. (1983) Adsorption Desorption Equilibria of Herbicides in Soil: Napthalene as a Model Compound for Entropy-Enthalpy Effects. *Weed Science*, 31: 744-751.
- Weber, T.W., and Chakravorti, R.K. (1974) Pore and Solid Diffusion Models for Fixed Bed Adsorbers. *AIChE Journal*, 20: 228-238.
- Weber, W.J. Jr. (1971) *Physicochemical Processes for Water Quality Control*, John Wiley and Sons, New York, pp. 330-335.
- Weber, W.J. Jr., Pirbazari, M., Long, J.B., and Barton, D.A. (1980) Potential Mechanisms of Removal of Humic Acids from Water by Activated Carbon. In *Activated Carbon Adsorption of Organics from the Aqueous Phase, Volume 1*, 317-336.
- Weber, W.J., Jr., and Liu, K.T. (1980) Determination of Mass Transport Parameters for Fixed-Bed Adsorbers. *Chemical Engineering Communications*, 6: 49-60.



- Weber, W.J., Jr., Pirbazari, M., Long, J.B., and Barton, D.A. (1980) Potential Mechanisms of Removal of Humic Acids from Water by Activated Carbon. In *Activated Carbon Adsorption of Organics from the Aqueous Phase, Volume 1*, 317-336.
- Weber, W.J., Jr., and Pirbazari, M. (1982) Adsorption of Toxic and Carcinogenic Compounds from Water. *Journal AWWA*, 74: 203-209.
- Weber, W.J., Jr., Voice, T.C., and Jodellah, A.M. (1983) Adsorption of Humic Substances: the Effects of Heterogeneity and System Characteristics. *Journal AWWA*, 75: 612-618
- Weber, W.J., Jr., and Jodellah, A.M. (1985) Removing Humic Substances by Chemical Treatment and Adsorption. *Journal AWWA*, 77(4): 132-137.
- Weber, W.J., Jr., and Liang, S. (1985) Parameter Evaluation for Modeling Multicomponent Mass Transfer in Fixed-Bed Adsorbers. *Chemical Engineering Communications*, 35: 49-61.
- Weber, W.J., Jr., and C. K. Wang (1987) A Microscale System for Estimation of Model Parameters for Fixed-Bed. *Environmental Science and Technology*, 21: 1096.
- Weber, W.J., Jr., and Smith, E.H. (1987) Simulation and Design Models for Adsorption Processes. *Environmental Science and Technology*, 21: 1040.
- Weber, W.J., Jr., McGinley, P. M., and Katz, L.E. (1991) Sorption Phenomena in Subsurface Systems: Concepts, Models, and Effects on Contaminant Fate and Transport. *Water Research*, 25: 499.
- Weber, W.J., Jr., P.M. McGinley, and Katz, L.E. (1992) A Distributed Reactivity Model for Sorption by Soils and Sediments: I. Conceptual Basis and Equilibrium Assessments. *Environmental Science and Technology*, 26: 1955-1962.
- Wheeler, J.R. (1976) Fractionation by Molecular Weight of Organic Substances in Georgia Coastal Water. *Limnology and Oceanography*, 21, 846-852
- Wiesner, M.R., and Chellam, S. (1992) Mass-Transport Considerations for Pressure-Driven Membrane Processes. *Journal AWWA*, 84: 88-95.
- Williamson, J.E., Bazaire, K.E., and Geankoplis, C.J. (1963) Liquid Mass Transfer at Very Low Reynolds Numbers in Packed Beds. *Industrial and Engineering Chemistry Fundamentals*, 2: 126-129.
- Wilmanski, K., and Van Breemen, A. N. (1990) Competitive Adsorption of Trichloroethylene and Humic Substances from Groundwater on Activated Carbon. *Water Research*, 24: 773.
- Wilson, E.J., and Geankoplis, C.J. (1966) Liquid Mass Transfer at Very Low Reynolds Numbers in Packed Beds. *Industrial and Engineering Chemistry Fundamentals*, 5: 9-14.
- Wilson, S.A., and Weber, J.H. (1977) A Comparative Study of Number-Averaged Dissociation-Corrected Molecular Weights of Fulvic Acid Isolated from Water. *Chemical Geology*, 19, 285-293

- Woerner, D.L., and McCarthy, J.L. (1986) The Effect of Manipulatable Variables on Fractionation by Ultrafiltration. *Proceedings of the AIChE Symposium Series, Industrial Membrane Processes*, Number 248: 77-86.
- W. R. Grace & Company (1987) *Technical Data, Spiral Membrane Ultrafiltration Cartridges*, Publication 744, Amicon Division, W. R. Grace, Danvers, MA.
- Yau, W.W., Kirkland, J.J., and Bly, D.D. (1979) *Modern Size Exclusion Chromatography*. Wiley Interscience, New York, pp. 318-326.
- Yonge, D.R., and Keinath, T.M. (1986) The Effects of Non-Ideal Competition on Multi-Component Adsorption Equilibria. *Journal Water Pollution Control Federation*, 58: 77-81.
- Zimmer, G., Crittenden, J.C., Sontheimer, H., and Hand, D.W. (1988) Design Considerations for Fixed-Bed Adsorbers that Remove Synthetic Organic Chemicals in the Presence of Natural Organic Matter. *Proceedings, American Water Works Association Annual Conference, Orlando, FL*.